UNIVERSITY OF Southampton

Linear stability of an interface between two miscible liquids

by

Abdesselem Khenien

Thesis submitted in partial fulfillment of
the requirements for the degree of
Doctor of Philosophy

Department of Engineering and the Environment

Energy Technology Research Group

University of Southampton

October 20, 2014

I would like to dedicate this thesis to my loving parents.

Acknowledgements

I would like to express my sincere gratitude to my supervisor for the continuous support of my Ph.D study and research, for his patience, motivation, enthusiasm, and immense knowledge. His guidance helped me in all the time of research and writing of this thesis, which would not have been completed without the constant advice and encouragement from my supervisor, Dr. Anatoliy Vorobev.

Abstract

The evolution of small disturbances to a horizontal interface separating two miscible liquids is examined. Initially, the liquid-liquid binary system is assumed to be out of its thermodynamic equilibrium, and hence, the system immediately starts moving towards its equilibrium state. The aim is to investigate whether the slow interface smearing is overrun by faster and more complex mixing. The study is based on the numerical solution of the linear stability of the phase boundary subjected to normal thermo- and hydro-dynamics perturbations.

It was found that the classical results for the stability of immiscible interfaces can be re-obtained through the phase-field approach provided that the wavelength, that defines the perturbation, is greater than the thickness of the interface. Additionally the system becomes thermodynamically unstable if the value of the interface thickness is greater than the value of the interface thickness that is defined at thermodynamic equilibrium, so the gravity waves may become unstable. It was also found that the interfacial mass transfer plays the role of additional dissipation, reducing the growth rate of the Rayleigh-Taylor instability and increasing the dissipation of the gravity waves, and the mutual action of diffusive and viscous effects completely suppresses the modes with shorter wavelengths.

The flow imposed along the interface adds the mechanisms of the Kelvin-Helmholtz and Holmboe instabilities. It was found that if the heavier liquid lies above the lighter liquid, then the interface is unconditionally unstable. Viscosity, diffusivity and capillarity reduce the growth of perturbations. In the opposite case of the heavier liquid underlying the lighter one, the interface can be stable. The stability boundaries are primarily defined by the strength of the density contrast and the intensity of the imposed flow. Thinner interfaces are usually more unstable (characterised by larger zones of instability), however, the thermodynamic instability identified for interfaces with thicknesses greater than the thickness of a thermodynamically equilibrium phase boundary makes such interfaces unconditionally unstable. Surprisingly, the diffusivity and capillarity effects were found to alter the behaviour of the interface in miscible liquids. However, the viscosity effect retains its stabilising role for both immiscible and miscible liquids.

Contents

List of Figures

Nomenclature

Roman Symbols

$\mathbf{n}$	the normal vector
$\overline{c}$	phase velocity
A	phase parameter
a	phenomenological parameter
a_0	the left bound of the domain
b	phenomenological parameter
b_0	the right bound of the domain
C	concentration
Ca	Capillary number
F	Chan-Hilliard free energy function
F_0	classical Landau free energy function
g	gravitational acceleration
Gr	Grashof Number
i	is an imaginary unit
k	the wave number

L length

M determinant

P pressure field

p perturbed pressure field

Pe Peclet Number

r scaling parameter

Re Reynolds number

T actual temperature of a system

T_c temperature of critical point

U base term of velocity

u the component of velocity in x-direction

v the component of velocity in y-direction

w the component of velocity in z-direction

$\overline{A}$ matrix

$\overline{B}$ matrix

Greek Symbols

α mobility coefficient

χ total error

χ_0 tolerated error

δ thickness of transition layer separating two liquids

δ_u thickness of shear layer

ϵ capillary parameter

η viscosity coefficient

γ normal vector of gravity

μ the chemical potential

ω the complex eigenvalue

σ the surface tension coefficient

ξ small distortion of surface

ϕ density contrast

ρ density

σ_K Korteweg stres

Superscripts

$\hat{}$ defines the perturbed terms

Subscripts

$*$ defines the parameters scale

0 defines the terms at the base state

1 references a parameter of liquid 1

2 references a parameter of liquid 2

i defines the real imaginary of a complex variable

r defines the real part of a complex variable

x defines a component in $x-$deriction

y defines a component in $y-$deriction

Acronyms

CCM Chebyshev collocation method

CMM compound matrix method

ESM explicit shooting method

FDM finite different method

GCW gravity capillary waves

HI Holmboe instability

KHI Kelvin-Helmholtz instability

RTI Rayleigh-Taylor instability

Chapter 1

Introduction

1.1 Motivation

The interaction of miscible liquids is an essential part of many industrial and natural processes, to the extent that the performance of the processes is ultimately dependent on the mixing rate, which can be affected by a number of physical factors such as viscosity, diffusion of mass, temperature, density variations, surface tension and geometry. The interest in miscible liquids is driven by various engineering applications, such as: oil extraction in the food industry [108, 127], soil remediation [82, 133], enhanced oil recovery [9, 37, 148] and drug delivery [36].

In oil extraction, the oil is removed by adding a relevant solvent (hexane, supercritical carbon dioxide) into the raw material which forms a porous medium. The solvent is separated from the solute by an evaporation technique at the end of the process [45, 127, 160]. Classically, the oil recovery process is based on injecting water into the pores filled with the remaining oil. Recent developments have shown that the efficiency of the oil recovery can be greatly improved by replacing water with a miscible solvent for which the capillary pressure and the viscosity are reduced. This, in particular, enhances the extraction of the oil from dead-end pores [82]. The solvents used for the miscible-injection technique are hydrocarbon gases [9] or carbon dioxide [37]. In soil remediation, the solvent is applied into an unconfined geometry where at the end of the process both the

contaminants and solvents are removed. The other application of miscible liquids is in the transportation and dissolution of the injected drugs in the tissues of the body that are regarded as a porous medium.

Despite the intensive works carried out, a comprehensive theory that one may rely on for the study of miscible liquid-liquid interfaces is still missing. As it was recently confirmed, miscible liquid-liquid interfaces are endowed with surface forces similar to the case of immiscible liquid-liquid interfaces. Therefore, for understanding the complexities that accompany the evolution of the flow generated between two miscible liquids, the surface tension has to be included in the governing equations, another key difference between the flow in immiscible and miscible liquids is that in miscible liquids the velocity field is not generally solenoidal due to the dependence of the mixture density and viscosity on the concentration [85]. Here, we use the phase-field approach in order to capture thermo- and hydrodynamic evolution of the miscible binary mixture which endows surface forces [99].

1.2 Objective

The mixing of miscible liquids ultimately occurs through the interfacial diffusion that should lead to enlarging the mixing region. However, we aim from this study to identify the influence of the other mechanisms on the evolution of the interface. In particular, we focus on understanding the effect of the hydrodynamic flow imposed along the interface. For this purpose, the phase-field approach is used to study the mixing of two slowly miscible liquids brought into contact.

Despite the fundamental importance of the liquid-liquid diffusion and of its seeming simplicity, its understanding is still missing [141, 142]. It is known that diffusion in liquid-liquid binary mixtures differs from diffusion in gaseous mixtures (where intermolecular forces are negligible), or from diffusion of a minor impurity dissolved in a liquid solvent. The diffusion in latter cases is well defined by the classical Fick's law in which the diffusion flux is linearly proportional to the concentration gradient. Fick's law, however, does not properly define the diffusion at liquid-liquid interfaces [141].

Complexities of the liquid-liquid interface diffusion stem from the difference in intermolecular forces in the continua of the neighbouring liquids leading to the capillary effect, which defines both the interface morphology and the interfacial diffusion. The molecules need to possess sufficient kinetic energy in order to overcome the interfacial potential barrier created by the intermolecular forces. In miscible liquids, the potential barrier at the interface can be gradually reduced, leading to the disappearance of the interface. Subsequently, the binary liquid may become homogeneous at the end of the diffusion process.

It becomes now clear that the effective surface tension may play a crucial role in determining the interface shape and the flow of motion within the interface driven by diffusion. Thus, the theoretical or numerical approaches that aim to study the interfacial diffusion between two miscible liquids must include the effect of the surface tension for accurate description.

1.3 Scope of the thesis

Linear stability theory is employed to study miscible binary mixtures with two different configurations; when the heavy liquid stands over the lighter one and in the opposite case in which the heavier liquid underlies the lighter one. We investigate the effects of viscosity, diffusivity, gravity, temperature and capillary forces on the behaviour of the interface separating two miscible liquids. Their base state can be either stationary or in relative shear motion.

1.4 Contribution

The following is the summary of the main contributions of this thesis, where it was shown that:

- the classical results for immiscible interfaces can be reproduced within the phase-field approach;
- when a heavier liquid stands over (or underlies) a lighter one, the diffusivity enforces additional dampening in similar manner to the effect of viscosity;

- the gravity waves are thermodynamically unstable if the interface thickness is larger than its thermodynamic equilibrium value;
- in the presence of a fluid motion imposed along the interface, the diffusivity retains its dampening role if the heavier liquid stands over the lighter one; and
- the diffusivity enlarges the zones of Kelvin-Helmholtz and reduce the zones of Holmboe instabilities if the heavier liquid underlies the lighter one.

1.5 Layout of the thesis

In Chapter 2, the physical and mathematical models are summarized and then reformulated in non-dimensional form. Linear theory is developed in Chapter 3, for two superposed miscible liquids. The ordinary differential equations are of the Orr-Sommerfeld type. They are of the eighth order and contain non-constant coefficients. Their solution require appropriate numerical methods as presented in Chapter 4. Four numerical methods are tested, with explicit shooting and compound matrix methods are compared in terms of accuracy and feasibility to the current problem. In addition, the disctretisation finite difference and Chebyshev collocation methods are also checked against accuracy and capability. Overall, explicit shooting and Chebyshev collocation methods are chosen due to their accuracy.

One of the characteristics of the phase-field approach is its capability to recover the sharp interface limits. This is also confirmed in the current study. In Chapter 5, the sharp interface method is explored to derive the eigenvalue equations for a general system presented by a simple plane layer that contains two superposed immiscible liquids. With two possible configurations, the lighter liquid underlies the heavier liquid and the inverse scenario. These results are used to validate the immiscible data obtained in the following chapters for miscible cases.

Rayleigh-Taylor instability and gravity-capillary waves are employed in Chapter 6 to investigate the behaviour of a diffuse interface separating two miscible liquids. A parametric study is conducted. In Section 6.1 the immiscible liquid-liquid interface is considered. The Phase-field method successfully recovers the

sharp interface limits if the mode wavelengths are much larger than the interface thicknesses. The thermodynamic stability is studied in Section 6.2, which reveals that the interface might become thermodynamically unstable if the interface thickness is greater than the equilibrium value. In Section 6.3, we consider two miscible liquids separated by a diffuse interface that is subjected to thermo and hydrodynamic effects. It is shown that the diffusivity is generally reduced to further dissipation of the perturbations through imitating the effect of viscosity.

In Chapter 7, an external shear motion is imposed along the interface separating two miscible liquids. Both configurations are also used in which the heavier liquid can be underneath or above the lighter one. Following the parametric analysis of Chapter 6, Section 7.1 is devoted to investigation of the case of an immiscible liquid-liquid interface. In Section 7.2 we study the effect of interfacial diffusion on the stability of miscible interface subjected to shear motion. The main conclusion is that the diffusion has the same dissipation effect as in the stationary case when the heavier liquid stands over the lighter one. However, in the inverse configuration, the diffusion enhances stationary instability if the interface is subjected to a shear motion.

Chapter 8 summarises the current work and gives recommendations for future work that can be conducted to aid further understanding of the behaviour of miscible free boundary. Finally, the remainder of the current Chapter is used for presenting the relevant literature review. In particular, we have summarized the experimental evidences of the surface tension existence when two slowly miscible liquids are brought into contact. In addition, the relevant literature in the main problems used for the current study are summarized.

1.6 Some peculiarities of miscible liquid/liquid interfaces

When immiscible liquids are brought into contact, they remain separated by a thin interface if there are no external factors imposed. At a macroscopic level, the capillary forces that prevent the co-diffusion of the liquids define the existence of the interface. In fact, these forces originate from the interaction of the molecules

of two liquids leading to construction of an energy barrier that prevents the molecules from moving from one liquid to the other. However, when bringing a binary system near its critical temperature, the thickness of the interface tends to infinity [53, 120, 151].

Van der Waals [151] assumed that the interface is a diffused region allowing the continuity of material and physical properties between the bulks of the two liquids. He proposed an isothermal model based on thermodynamics to study the state of a binary liquid at a critical point. It was found that the interface becomes infinite at a critical or supercritical temperature, which lowers the energy barrier that allows the diffusion of the liquids. Bosscha [89] reported experimental visualisation in which two miscible liquids are brought into contact. He suggested that the capillary forces may play an important role in generating the flow, as in the case of two immiscible liquids.

Based on the works of van der Waals and Bosscha, Korteweg [89] proposed his well-known model describing the stress forces that arise at the interface due to the strong concentration and density gradients. The model was revised and expressed in the following general form

$$\sigma_K = -\frac{1}{3}(\delta_1|\nabla C|^2) + \delta_2\nabla^2 C + \delta_1\nabla C \otimes \nabla^2 C + \delta_2\nabla C \otimes \nabla C. \tag{1.1}$$

Here σ_K is the Korteweg stress, δ_1 and δ_1 are two constants that do not depend on the concentration field C. The density of the simple mixture ρ is given by the equation of state for mixture

$$\rho(C) = \rho_1 + (\rho_2 - \rho_1)C = \rho_1(1 - \phi C), \tag{1.2}$$

where $\phi = \frac{(\rho_1 - \rho_2)}{\rho_1}$ is the density contrast and ρ_1 and ρ_2 are the densities of the two liquids.

For simple planar interface [21, 151] the surface tension σ_K can be expressed as follows

$$\sigma_K \propto \int_{-y_0}^{y_0} \left(\frac{\partial C}{\partial y}\right)^2 dy, \tag{1.3}$$

where y is the coordinate across the interface.

The earliest measurements of interfacial tension between miscible liquids were conducted by Quincke [123], where the values of surface tension were taken at an early time of contact. The author used ethyl alcohol in contact with miscible liquids, such as sulphates of zinc and copper. The values of surface tension were found to lie within the range 0.8×10^{-3} and 3×10^{-3}N/m. Freundlish [48] measured the interfacial tension between two immiscible liquids and also treated partially miscible liquids. Similarly, Smith et al. [134] estimated the interfacial tension coefficient by using $2000cs$ and $1cs$ of silicon oil mixture, the superficial interface value was 1×10^{-3}N/m.

The interfacial tension in immiscible liquids is static as the interface retains its shape even in the case of strong topological change. However, in the case of miscible liquids the static concept is no longer relevant, where the interface tension can be reduced with time due to the interfacial diffusion. Therefore, in miscible liquids the dynamic or transient (effective) surface tension is mostly used instead of static interfacial tension [72, 105, 129].

May and Maher [105] have measured the effective interfacial tension at the interface of a miscible mixture (isobutyric acid and water). Through the use of light scattering, the correlated effective surface tension expression (σ) was given as function of temperature through

$$\sigma(T,t) = F(T)/[\xi_0 + (D_{eff}\, t)^{1/2}], \tag{1.4}$$

where T is the system temperature, t is the time taken after the liquids are placed in contact, ξ_0 is the initial equilibrium correlation length at 30^oC, D_{eff} is the effective diffusion constant, $F(T)$ is constant for low temperature and $T = 26.085$ is the critical temperature of the mixture. The surface tension below the critical point was found to be $0.01\ ^{-3}$N/m and the upper critical point was 5.2×10^{-7}N/m.

Lacaze et al. [91] repeated the experiment of May and Mehar but the measurements were taken by quenching the temperature about the critical point. The authors found interfacial tension of order 10^{-8}N/m, which is much smaller than the values found by May and Maher [105]. The relaxation of the interfacial

tension in time was presented with the model defined by

$$\sigma^{+}(t) = \frac{\sigma_{fit}}{\sqrt{1 + \frac{4\pi D^{+}}{l_{i,fit}}(t - t_2)}}, \tag{1.5}$$

where $\sigma^{+}(t)$ is the relaxed surface tension at or above the critical point, σ_{fit} is the surface tension below the critical point T_c, D^{+} is the diffusion coefficient, $l_{i,fit}$ is the local thickness that increases with time, t_2 is the initial time and t is the time.

Pojman et al. [121] used the spinning-drop tensiometry (STD) method to measure the interfacial tension in a miscible IBA/water mixture. The values of surface tension were in the range of values measured by May and Maher [105], which were approximately 1.4×10^{-5}N/m and 5.2×10^{-5}N/m for temperature $T = 30^{o}C$. The STD technique was also used for measuring the effective surface tension coefficients of 1-butanol/water and polymer/monomer mixtures of dodecyl acrylate [121, 165]. For the former mixture, the surface tension mixture was in the range 10^{-5} N/m and 3×10^{-5} N/m while for the latter the surface tension was in the range of 2×10^{-6} N/m and 2×10^{-5} N/m. It was shown that the surface tension of dodecyl acrylate relaxes with increasing the temperature but increases with increasing the concentration of the monomer and polymer. The authors found no evidence of the dependence of surface tension on the rotation rate and the droplet volume.

Petitjeans and Maxworthy [119] used a glycerol/water mixture to measure the effective surface tension which was found approximately in the range of 0.4×10^{-3}N/m and 0.5×10^{-3}N/m. Stevar and Vorobev [141] conducted an experimental study on the evolution of the shapes of solute/solvent interfaces in horizontal capillaries with different cross-sections. For all the mixtures used (glycerol/water, soybean oil/hexane and IBA/water), the observations confirmed that the shape of the interface remains visible for a long time. It was reported that the values of the surface tension measured for glycerol/water mixture in [119] are overestimated and the estimation of the surface tension for soybean oil/hexane was around 0.1×10^{-3}N/m.

The dissolution process in a binary liquid mixture is described by the molec-

ular diffusion that results from the random and irregular movements of the molecules; the motion is caused by the thermal energy as well as by the gradients of pressure, temperature and concentration. For example in miscible liquids, the net diffusion flux depends on the strength of the concentration gradient such that the molecules move from the higher to lower concentration region until the system becomes uniform. However, the diffusion rate can be affected by strong viscosity gradient in the binary liquid mixture [13].

Fick [46] developed a phenomenological model describing the diffusion in the binary liquid mixture. The diffusion flux is linearly proportional to the gradient of the concentration such that the factor of proportionality is constant, which is also called the coefficient of diffusion. Maxwell [104] proposed another model to describe the diffusion in gases and later Standart et al. [139] extended it to binary liquid mixtures. Fick's and Maxwell-Stephon's models are related by the relation $D = \Gamma\bar{D}$, D is the Fick's diffusion coefficient, $\bar{D}$ is the Maxwell diffusion coefficient and Γ is the thermodynamic correction factor defined in terms of an excess Gibbs energy.

In miscible liquids, the relaxation of the interfacial tension is dependent on the intensity of interfacial diffusion that is driven by the concentration gradients of mixture components [89, 105, 151]. Due to its importance in engineering application, the mass transfer rate was measured in a binary system that can be either in thermodynamic equilibrium or out of equilibrium [54, 62, 80, 150]. Petitjeans and Maxworthy [119] measured the diffusion coefficient between the glycerol and water mixture for various temperature and different concentrations, at the room temperature the diffusion coefficient was found to be $D = 1.2 \times 10^{-10} m^2/s$. D′Errico el al. [32] showed that the interface diffusion coefficient linearly decreases to $1.2 \times 10^{-11} m^2/s$ for water-glycerol and pure water, the diffusion coefficient becomes null at critical temperature [27, 28, 87, 159]. But above the critical temperature the diffusion coefficient increases according to

$$D = D_0 \left(\frac{T - T_c}{T_c} \right)^v . \tag{1.6}$$

Here $v = 0.66$, $D_0 = 5.9 \times 10^{-10} m^2/s$ an T_c is the critical temperature. Thus, for temperature $T = 27^o C$ the diffusion coefficient is $D = 1.3 \times 10^{-11} m^2/s$ and for

$T = 30^oC$ the diffusion coefficient is $D = 2.8 \times 10^{-11} m^2/s$.

Antrim et al. [8] showed that the effective surface tension at the interface of dodecyl acrylate is determined by the speed of mass transfer within the mixing region. It was found that Fick's law is only valid at a late stage of diffusion while at the earlier stage of mass transfer the diffusion follows a non-Fickian law. Viner and Pojman [154] investigated the width of the mixing region of 1-butanol/water and IBA/water mixtures at the supercritical point. He showed that the mixing region width grows slowly into one of the component regions with speed proportional to $t^{0.06}$ and the phase boundary itself propagates towards unsaturated component with speed proportional to $t^{0.09}$. To confirm these findings, the same mixture was used but a tensiometer technique was used to measure the surface tension. For the monomer/polymer mixture, the phase boundary width increases with speed proportional to $t^{0.5}$, which is indicating the validity of Fick's law. However, for IAB/water and 1-butanol/water mixtures, they noted that there was no contribution of the barodiffusion process into non-Fick's law stage.

Petitjeans and Maxworthy [119] noted that the transition zone between glycerol and water slowly increased into the glycerol region. Dambrine et al. [30] also investigated the mutual diffusion between the water and 40% of glycerol/water in a microchannel. They observed that the phase boundary moves toward the glycerol region and the width of interface increases with the speed $(Dt)^{1/2}$. Stevar and Vorobev [141] conducted experimental work on the appearance of interface between miscible liquids. Although the binary mixtures glycerol/water and soybean oil/hexane are miscible in all proportions, the shape of the interface remained visible for a long time. They have noted that width of the phase boundaries increases slowly in comparison to their movement in the capillary tube. The speed of the phase boundaries was found to follow the expression given by

$$v \propto D^{1/3} t^{-2/3} d^2, \tag{1.7}$$

where D, t and d are the diffusion coefficient, time and capillary diameter, respectively. The authors claimed that these behaviours can not be explained on the basis of Fick's law; instead, the effect of barodiffusion is perhaps behind these observations.

Non-homogeneous density mixture can be generated either by the change in the concentration of gradients [121] or by variations in the temperature. Joseph and Renardy [84] noted that thermal plumes may exhibit surface tension effects. Also, Gandikota et al. [50] measured the effective surface tension of H_2 at supercritical temperatures $T_c+10\,mK$, $+100\,mK$ and $1\,K$. The corresponding effective surface tension values are respectively 10^{-8} N/m, 2×10^{-8} N/m and 4×10^{-8}N/m.

In miscible liquids, the surface tension depends on both the temperature and concentration of liquids component at the interface. When a strong surface tension gradients arises at the interface may lead to the interface dynamics that is driven by a Marangoni spreading process. The stability or instability of the interface, that is subjected to the effect of Marangoni, is usually promoted by the gradients of concentration, viscosity, diffusivity and temperature [5].

1.7 Stability of phase boundary separating two stationary liquids

Rayleigh-Taylor instability (RTI) occurs when a heavier fluid driven by gravity mixes with a lighter fluid. The configuration of the heavier liquid above the lighter one is always unstable to any infinitesimal perturbation. On the other hand, when a heavier liquid underlies a lighter one, gravity and capillary waves (GCW) develop, and so this configuration is always stable to small perturbations.

Taylor [144] developed a linear method to investigate the instability of the sharp interface separating two liquids, with the heavier liquid on the top. He showed that the interface is unstable to any initial small perturbations provided that the amplitude of these perturbations is sufficiently smaller than the wavelength. Rayleigh [126] separately investigated the same configuration [144], and showed that the change of amplitude of perturbations at the horizontal plane interface follows the expression $e^{\omega\,t}$, with ω being the growth rate. For inviscid-immiscible liquids, the dispersion relation is given by

$$\omega^2 = g\frac{\rho_2-\rho_1}{\rho_2+\rho_1}k - \frac{\sigma}{\rho_2+\rho_1}k^3. \tag{1.8}$$

Here, ρ_1 and ρ_2 are the densities of lighter and heavier liquids respectively, k is the wave number, g is the acceleration of gravity, and σ is the surface tension.

For RTI, the equation (1.8) indicates that the system is unstable ($\omega_i > 0$) for all wave numbers $k > 0$ if the surface tension is disregarded. However, when capillary forces are taken into account, the short wavelength can be stabilized. Bellman and Pennington [15] studied the effect of surface tension on RTI. The authors showed that the critical cut-off wave number k_c, which is independent of the viscous effects, takes the form

$$k_c^2 = g\frac{\rho_2 - \rho_1}{\sigma}, \tag{1.9}$$

where for $k > k_c$ the surface tension has stabilizing effect on the interface but if the $k < k_c$ the surface tension has no effect on the unstable RTI modes. The linear theory of the RTI has been experimentally proven [41, 96, 124].

Gravity-capillary waves develop under the effects of gravity and capillary forces, if a lighter liquid is placed on top of a heavy liquid. It is known that the effect of capillarity is limited to the short wavelengths, and its action is similar to the stretched membrane, while gravity forces mainly affect the long wavelengths [14]. The majority of the works on gravity capillary waves are concerned with a free boundary separating air and water. There are many works devoted to this kind of air-water interface, which are reviewed by Dias and Kharif [33], and Perlin and Schultz [118].

The dispersion relation for gravity-capillary waves generated between two immiscible-inviscid liquids is also given by the analytical expression (1.8). In the case of viscous-immiscible liquids, it was found that viscosity enhances the dissipation of gravity-capillary waves [15, 26, 93].

Recently a number of studies have focused on the use of RTI and GCW to validate the multiphase models. Antonio et al. [25] used RTI to show the capability of a phase-field approach to predict the development of instability in a binary immiscible system. In their work, the classical dispersion relation (1.8) was derived on the basis of phase-field method with zero interface thickness assumption. For instance, the authors [34, 79] showed that the results obtained through the phase-field method for zero interface thickness converge to the results

of sharp interface limit.

A few works have investigated the stability of miscible systems. Most have considered the Hele-Shaw system where the Navier-Stokes equations are reduced to Darcy's law [66]. Abid et al. [1] studied numerically the RTI instability using the capillary tube, without taking into account the Korteweg surface tension. On the bases of the Fick's equation law, Kurowski et al. [90] investigated analytically the instability of the interface between two semi-infinite miscible fluids. The author assumed that the perturbations grow faster than the interface spreading, where the base profile of concentration is defined as

$$C = \operatorname{erf}\left(\frac{z}{\sqrt{D\,t}}\right). \tag{1.10}$$

Here, C is the concentration and D is the coefficient of the diffusion and t is time. For inviscid liquids, the growth rate was expressed as follows

$$\omega \simeq \frac{gR}{4Dk}, \tag{1.11}$$

where g is the gravity, $R = \rho^{-1}\frac{d\rho}{dc}$ is the solutal expansion coefficient, D is the diffusion coefficient and k is the wave number.

Vanaparthy et al. [153] and Vanaparthy and Meiburg [152] investigated linear instability of RTI using two miscible liquids placed in a vertical capillary tube. Gaponenko and Shevtsova [51] studied the effect of vibrations on the dynamics of miscible interface. Hu and Joseph [73] also studied the fingering instability of miscible interface placed in Hele-Shaw cell. Riaz and Meiburg [128] conducted a linear stability analysis of miscible displacements in porous media. The governing equations were written in a form that makes them suitable for porous media. It was shown that the diffusivity has a stabilising effect on the modes with short wavelengths.

1.8 Shear layer: Kelvin-Helmholtz and Holmboe instabilities

The linear analysis of shear flow is very important to understand mixing and transition to turbulence that occur in atmosphere, oceans and separation processes (e.g., the separation between oil and water in the oil industry). In such phenomena, the flow occurs in density stratified media. Both shear flow and density stratification define the development of instability.

The homogenous shear flow is unstable owing to the Kelvin-Helmholtz instability (KHI), which is subjected to the criteria of Rayleigh [125] and Fjϕrtoft [47]. The Howard [70] condition must be satisfied in order for the KHI instability to exist in stratified flow. For continuous velocity base profile, KHI develops if the fluids are inviscid, however, strong viscous forces can minimize the instability of shear flow [17, 26, 39]. According to Carpenter et al. [24], the instability of homogenous shear flow is caused by interaction of two stationary waves mainly invoked by vorticity. If gravitational effects are included in the shear flow, then RTI and KHI simultaneously develop that is leading to a competition between the shear flow and gravitational effects. Therefore, the short wavelengths modes of RTI can be suppressed under the effect of shear flow [16, 59, 112, 164]. The interface thickness was found to have an effect on the instability of combined RTI-KHI; for thick interfaces the instability of the modes with long wavelengths increases whereas it decreases at short wavelengths decreases [157, 161].

The stratifaction of the flow is defined with the Richardson number $Ri = N^2/U'^2$, where U' is the local mean velocity and N is the Vaisala frequency given by

$$N(y) = \sqrt{\frac{g}{\rho}\frac{d\rho}{dy}}. \tag{1.12}$$

Here, ρ and g are the density and gravity.

Miles and Howard theorems showed that the stratified shear flow is stable for $Ri > 1/4$. Holmboe [65] showed that if the thickness of the stratified profile is much smaller than the shear layer thickness, then the flow is unstable despite the presence of high stratification. The Holmboe instability (HI) is triggered by

the interaction of the velocity profile (which induces vorticity waves) with the density profile (which induces gravity waves). There are two waves in HI, one wave propagates in one direction with respect to the centre of the mean flow and the other propagates in the opposite direction. The shear flow of sufficiently large amplitude makes the flow unstable through the Kelvin-Helmholtz and Holmboe instabilities [39].

The boundaries of the Kelvin-Helmholtz and Holmboe instabilities were later determined for various density and velocity profiles [10, 23, 38, 61, 71, 102]. Drazin [38] investigated stratified shear flow using a continuous velocity profile defined by $V = V_0 \tanh(y/\delta)$ and a density profile defined by $\exp(\beta y)$. He showed that a small amplitude disturbance is neutrally stable if the Richardson number $J = k^2d^2(1 - k^2d^2)$ or $J > J_c = \frac{1}{4}$, with d being the length scale which represents the width of the interface and J_c is the critical Richardson number. Maslowe et al. [102] considered various velocity and density profiles to study inviscid stratified flows. Baines et al. [10] used arbitrary but symmetric profiles of density and velocity to show that HI exists if the $R_i < \frac{1}{4}$ in a central interface of arbitrary small thickness. The mechanism responsible for this instability is the interaction between the two waves which is different from the mechanism of KHI. However, if $R_i > \frac{1}{4}$ everywhere, the flow is damped as the free waves are absorbed by the critical layer. Carpenter et al. [23] used continuous density and velocity profiles in the investigation of the development of both KHI and HI in the viscous stratified flows.

The non-symmetric configuration was also investigated [95, 130]. The effects of surface tension were investigated by Alabduljalil and Rangel [2] and the effect of larger density contrast was also investigated [3, 12], the effect of diffusion was considered in a number of works [60, 88, 136]. The existence of both Kelvin-Helmholtz and Holmboe instabilities were experimentally confirmed in [67, 146, 147].

Chapter 2

Mathematical and physical model

This chapter presents a short review of the main approaches used for solving multiphase systems with a focus on the phase-field model that is appropriate to describe the evolution of binary mixtures. The thermodynamic model is defined and the coupled Cahn-Hilliard and Navier-Stokes governing equations are also presented.

2.1 Tracking interface methods

The most challenging task in multiphase flows is how to model the interface between two or more phases, e.g. fluid-fluid, fluid-solid interfaces. In an attempt to study a simple planar interface configuration, Taylor [144] was the first to use a sharp interface model. He treated the interface between two immiscible fluids as an infinitely thin boundary endowed with physical properties. However, this method might be impractical for solving more complex flows, e.g., droplet breakup, coalescence and miscible liquids. A number of alternative diffuse-interface approaches were proposed in order to tackle real problems that occur in nature and industrial phenomena [126, 151]. The fundamental idea of the diffuse-interface approach is that the interface can experience steep and yet smooth transition of physical quantities between two bulks of fluids [103, 120]. This approach is based on the phase-field parameter which is presented with assigned function ϕ in level set method (LS), scalar function C in Volume of Fluid

method (VoF) and concentration (or density) in the phase-field method (PH). The LS method was developed by Osher and Sethian [114], it treats the interface as a zero level which is tracked by a signed distance function that is only needed near the interface.

The level set method naturally handles strong morphological and topological (coalescence and droplet break-up) changes very well [122]. However, the main drawback of the LS method is that mass conservation is not guaranteed [44]. Hirt and Nichols [64] developed the Volume of Fluid (VOF) method in which the interface is tracked through a scalar function C. Brackbill et al. [20, 35] added surface forces, represented by a continuum surface force (CSF) model to the VOF approach. Even though the mass is conserved in VOF, the scalar function is however arbitrary selected, which means that some accuracy can be lost. The LS and VoF methods are mainly used for immiscible liquids where the interface thickness does not grow significantly during the flow evolution.

Generally, LS and VOF methods become difficult to implement for systems near their critical points, i.e. the fluids may become miscible as the interface thickness tends to infinity [151]. Therefore, the natural choice is the phase-field approach which is based on the same idea as VOF and LS methods, however, the entire domain, including the interface, is implicitly presented by a concentration profile determined from the equations for species conservation [21]. In this work, as we are dealing with slowly miscible liquids, the phase-field method will be used.

The phase-field approach can be traced back to the work of Gibbs [53]. He mathematically presented a line separating the diffuse interface into two regions by what he called a dividing surface (or surface of discontinuity) which is defined by micro and macroscopic forces. The Gibbs model suffered from tremendous limitations in providing a mathematical description of these forces. Alternatively, Van der Waals [151] assumed that the interface is smooth and the evolution of the interface can still be determined through the thermodynamic characteristics. He determined the thickness of the interface of a binary liquid below the critical point and showed how this interface disappears at its critical point. After a century, Cahn-Hilliard [21] used the van der Waals smooth interface principle to reformulate a so-called modified Cahn-Hilliard model for investigation of spinodal

decomposition.

A number of authors have generalized Cahn-Hilliard's model to account for various problems of binary and multicomponent flows [7, 18, 58, 79, 81, 99, 140]. Antanovskii [7] developed a phase-field model for nonisothermal flow to investigate thermocapillary flow. In order to compute the interface thickness, he considered a binary flow with a simple planar interface with varying temperature. A thermocapillary flow was also investigated by Jasnow and Vinal [81] using a model developed for nonisothermal binary flows. They used the same model to investigate the spinodal decomposition of binary fluid in a varying temperature field. In a similar situation, Gurtin et al. [58] studied the spinodal decomposition of binary flow but they used the model for isothermal binary flow.

Jacqmin [79] developed an isothermal phase-field model for incompressible inviscid binary flow, where he derived the interfacial forces in terms of concentration gradients of a fluid component similar to the Korteweg stress. In his work, the model was used to investigate droplet breakup, wave breaking, sloshing and moving contact lines. Lowengrub and Truskinovsky [99] presented a diffuse-interface model that was verified through entropy production. It was used to show the difference between compressible and quasi-incompressible binary flow. In particular, for quasi-incompressible binary flow of different densities, the authors showed that the velocity flow in the diffuse-interface region is nonsolenoidal ($\vec{\nabla} \cdot \vec{v} \neq 0$). They stressed that Gibbs free energy function is the appropriate function that can be used for deriving chemical potential energy for quasi-incompressible binary flow. In this approach, the density is independent of the pressure which is determined from the Navier-Stokes equations. The authors also used the model to investigate the nucleation of both compressible and incompressible binary flows.

The phase-field models described above are particularly designed for the study of immiscible flows, however, they are still valid for studying miscible liquids on the same basis as the diffuse-interface concept. The phase-field approach in miscible liquids has great importance as a result of the way the surface tension between two miscible liquids is handled. In particular the surface tension that arise between two miscible liquids can be presented by the Korteweg model.

Joseph [85] studied miscible liquids using a classical diffusion equation (Fick's law) coupled with continuity, transport and temperature-based-diffusion equa-

tions. The transport equations were modified to account for Korteweg stress, which considers the surface tension that arises at the interface separating two miscible fluids. The density was assumed to be a function of concentration and temperature but is independent of the pressure. It was also shown that the flow at the interface may be non-solenoidal as a result of temperature and concentration variation within the interface. His numerical results were found to be consistent with the experimental data that was presented in the same work. Joseph et al. [86] reconsidered the model of Joseph [85] to show that the relaxation of interfacial tension (dynamical surface tension) between two miscible liquids is proportional to $1/\sqrt{t}$. The relaxation is also influenced by the Korteweg stresses and nonsolenoidal velocity at the diffuse region. The author identified a change of viscosity with concentration and found that there is no pressure jump resulting from Korteweg stress in a planar interface. The only change in pressure was found to be due to the hydrostatic pressure resulting in the interface relaxation with time. However, when the curvature of the interface is not zero, there is a jump in pressure at the interface caused by Korteweg forces and the nonsolenoidal velocity is proportional to the variation of viscosity.

The notions developed by Joseph [85] were adopted by Lowengrub and Truskinovisky [99] in order to derive governing equations for the flow evolution within the diffuse-interface approach. The equations include the continuity, momentum and diffusion equations. The diffusion equation is based on thermodynamic characteristics ensuring the dependence of density only on fluid components. Vorobev [156] further extended the model of Lowengrub and Truskinovisky [99] by deriving the Boussinesq approximation of the full equations. It was shown that by using the multiscale method, the fast quasi-compressible process can be separated from the convective and slow diffusion processes. The current study uses this approach to investigate the diffuse interface separating two slowly miscible liquids. Although the phase-field approach represents the stress gradients' distribution differently to the sharp interface approach, there are a number of studies that show the phase-field method converges to its sharp interface limit [7, 18, 81, 99, 109, 137].

2.2 Thermodynamic model

The phase-field method describes the interface between two liquids through the concentration (or density) field where the equilibrium state of the binary system is defined by its free-energy function. Cahn-Hilliard [21] proposed the free-energy function F as a function of density, concentration and concentration gradient, given by

$$F(c) = F_0(\rho, C) + \frac{\epsilon}{2}|\nabla C|^2, \tag{2.1}$$

where C is the concentration field, defined as the mass fraction of one of the components in the mixture, and the capillary coefficient ϵ is very small that makes the new term everywhere negligible in the domain with the exception at locations where there are a strong gradients of concentration, such as at interfaces. The term F_0 is the classical Landau expression of free energy function given by

$$F_0 = a(C - C_c)^2 + b(C - C_c)^4, \tag{2.2}$$

where a and b are constants defining the state of a system, and C_c is the concentration at the critical point.

The expression (2.2) was proposed as an approximation to define a system near its critical temperature. This expression should be then regarded as a model for a binary mixture with homogeneous and heterogeneous states with two phenomenological parameters a and b. It can be shown that parameter a is proportional to $T - T_c$, with T being the actual temperature of the system and T_c being the critical temperature. The parameter a is negative for temperatures below the critical point $T < T_c$ and positive for $T > T_c$. In the current work the evolution of systems both near and far from the critical point is studied.

If we assume that the binary system is incompressible in which the density ρ is a function of concentration but is independent of the pressure P, the chemical potential can be obtained from the free-energy function [78, 99]. The chemical potential μ is then given as follows

$$\mu = \mu_0(C) + \phi(\mathbf{g} \cdot \mathbf{r}) - \epsilon\nabla^2 C, \tag{2.3}$$

where $\mu_0 \equiv \frac{dF_0}{dC}$ is the classical chemical potential, $\phi(\mathbf{g} \cdot \mathbf{r})$ is the barodiffusion.

In this study, the evolution of miscible liquid-liquid interface within the framework of the Boussinesq approximation is investigated. The concentration and densities of a binary system are related by the following expression

$$\rho = \rho_2(1 - \phi C), \quad \phi \equiv \frac{\rho_2 - \rho_1}{\rho_1}, \tag{2.4}$$

where ρ_1 and ρ_2 stand for the density of two liquids, ϕ is the contrast of the density and C is the concentration.

2.3 Cahn-Hilliard-Navier-Stokes equations

The full set of the Cahn-Hilliard-Navier-Stokes equations that describe the thermo-hydrodynamic evolution of binary mixtures were first derived by Lowengrub and Truskinovsky [99]. One of the main features of these equations is quasi-compressibility: even if evolution of two immiscible liquids is studied, the full continuity equation should be used due to dependence of mixture density on concentration. This feature makes the full set of equations hardly feasible for numerical treatment, due the requirement of an extremely small time step needed for numerical time integration in order to resolve fast quasi-acoustic motion. It was later shown by Vorobev [156] that the full Cahn-Hilliard-Navier-Stokes equations could be simplified on the basis of the multiple-scale method by separating fast quasi-acoustic and slow diffusive and convective processes. It was shown that the slow evolution of binary mixtures is defined by the Boussinesq approximation, the approach is used in the current work. It is presented by the continuity equation (2.5), momentum equation (2.6) and diffusion equation (2.7) which are

$$\nabla \cdot \mathbf{u} = 0, \tag{2.5}$$

$$\rho\left(\frac{\partial \mathbf{u}}{\partial t} + (\mathbf{u} \cdot \nabla)\,\mathbf{u}\right) = -\nabla p + \eta \triangle \mathbf{u} - \epsilon \nabla^2 C \nabla C - \phi C \mathbf{g}, \tag{2.6}$$

$$\rho\left(\frac{\partial C}{\partial t} + (\mathbf{u} \cdot \nabla)\,C\right) = \alpha \nabla^2 \mu, \tag{2.7}$$

where ρ, p, $\mathbf{u}$, C are the density, pressure, velocity field and concentration. The parameters α and η are the diffusion and viscosity coefficients, and $\mathbf{g}$ is the gravity field. The momentum equation includes the so-called Korteweg force $\sigma_k = \epsilon \nabla^2 C \nabla C$, which models the effect of the surface tension on the interface morphology.

2.4 Boundary conditions

The current study is limited to the linear stability analysis applied to a system formed of two semi-infinite liquids. Hence the effect of boundaries can be neglected, with more details presented in the next chapter for an unbounded simple plane layer. However, it is important to present the appropriate boundary conditions that generally hold for the current phase-field approach. Then for the velocity field ($\mathbf{u}$) the standard no-slip conditions can be specified,

$$\mathbf{u} = 0. \tag{2.8}$$

The equations for the concentration field are fourth order accurate. To exclude the diffusive mass flux through the wall, the normal derivative of the chemical potential must be set zero,

$$\mathbf{n} \cdot \nabla \mu = 0, \tag{2.9}$$

where $\mathbf{n}$ is the unit normal to the wall. In addition, we impose the following condition on the wall,

$$\mathbf{n} \cdot \nabla C = 0. \tag{2.10}$$

This condition defines the wetting properties on the wall. Since we are not interested in what happens at the wall, the idealised form of these boundary conditions are accepted here, which simply signifies that the molecules of the wall are neutral to the molecules of the mixture components.

The set of governing equations and boundary conditions of the current work differ from the ones used in other studies, for example, see the references in [51, 73, 116], where the diffusive flux is defined through the classical Fick's law. Even though such an assumption simplifies the consideration of the equation with

lower order, some important effects then are lost.

2.5 Nondimensionalisation of the governing equations

In order to non-dimensionalize the governing equations we adopt the same scales used in [156], which are velocity, pressure, and specific free energy, defined as follows:

$$\tau_* = \frac{L_*}{V_*}, \quad V_* = \mu_*^{\frac{1}{2}}, \quad p_* = \rho_* \mu_*, \quad f_* = \mu_*. \tag{2.11}$$

In these formulae L_* stands for the typical length scale. For the typical density, ρ_*, and chemical potential, μ_*, we can accept the following values, $\rho_* = \rho_2$ and $\mu_* = b$. In non-dimensional form the governing equations then read

$$\frac{\partial \mathbf{u}}{\partial t} + (\mathbf{u} \cdot \nabla)\mathbf{u} = -\nabla P + \frac{1}{Re}\nabla^2 \mathbf{u} - Ca\nabla^2 C \nabla C - GrC\gamma, \tag{2.12}$$

$$\frac{\partial C}{\partial t} + (\mathbf{u} \cdot \nabla)C = \frac{1}{Pe}\nabla^2 \mu, \tag{2.13}$$

$$\mu = Gr(\gamma \cdot r) + 2AC + 4C^3 - Ca\nabla^2 C. \tag{2.14}$$

The non-dimensional parameters entering the above equations are the Peclet number,

$$Pe = \frac{\rho_* L_*}{\alpha \mu_*^{1/2}}; \tag{2.15}$$

the capillary number,

$$Ca = \frac{\epsilon}{\mu_* L_*^2}; \tag{2.16}$$

the Reynolds number,

$$Re = \frac{\rho_* \mu_*^{1/2} L_*}{\eta_*}; \tag{2.17}$$

and the Grashof number,

$$Gr = \phi \frac{g L_*}{\mu_*}. \tag{2.18}$$

The parameter $A = \frac{a}{\mu_*}$ defines the equilibrium states of the binary system (if

A is negative the system can be homogeneous or heterogeneous, for positive A the binary mixture is always homogeneous in equilibrium) and ϕ is the density contrast. The viscosities of mixture components are different and viscosity is in general a function of concentration. We however assume that this difference is small, so it does not affect the evolution of a mixture. In the definition of the Reynolds number, η_* can be chosen as the viscosity of one of the pure component, e.g. η_2.

Chapter 3

Linear stability analysis of heterogeneous miscible system

The objective of this chapter is to reduce the original governing equations into a set of linearized equations that might be used to form an eigenvalue problem. A short review of the methods mostly used in the linear stability is also presented. Using the normal modes method, the Orr-Somerfeld equations are derived and presented with respect to 2D perturbations.

3.1 Linear instability analysis

Modal analysis is the basis of linear stability analysis of hydrodynamical systems. Its foundation dates back to the 19^{th} Century, starting from the work of Rayleigh and Taylor who examined the stability of parallel shear flow. This method is specifically applied when the base flow varies in $1D$, such as base density (Rayleigh-Taylor instability and gravity capillary waves) and the base velocity in parallel shear flows (Kelvin-Helmholtz and Holmboe instabilities).

Huerre and Monkewitz [75] show that in weakly non-parallel, flows local instability analysis can also be applied because the change in the base flow occurs at a larger length scale than the wavelength of the perturbations. As an extended approach, Joseph [83] developed global linear instability analysis which is applied to flows with a highly non-parallel basic state. Theofilis [145] reviewed global lin-

ear instability analysis and provided the BiGlobal and TriGlobal terms in order to distinguish $2D$ and $3D$ highly non-parallel base flows.

The energy method is another type of linear stability analysis, used to identify the boundaries at which a transition occurs from linear to nonlinear instability [143]. In fact, such a transition is not possible to detect by the classical instability method [68, 69]. Hu and Joseph [74] extensively used the energy method to study the effects of interfacial tension, interfacial friction and Reynolds stress in the development of instabilities at an immiscible interfacial boundary.

Nonmodal analysis is an emerging approach as a complementary tool in linear stability analysis. In certain flows the transition from linear into nonlinear regime occur with critical characteristics that can not be identified by modal instability analysis. Barkley et al. [11] provide the evidence that the transient of the threshold of energy is beyond the scope of modal methods, particularly in spatially varying flows, such as in open flows. Schmid and Henningson [131] showed that the dynamics of these flows cannot be determined by modal analysis, i.e. the superposition of the stable modes may lead to energy amplification due to the non-orthogonality of eigenfunctions. Thus, the interactions between these functions may trigger the transition from a linear to a nonlinear regime.

In the current study, we use linear instability analysis where the method of normal modes is employed to derive the eigenvalue problem for miscible binary liquid.

3.2 Basic state of a plane layer

The current thermo-hydrodynamic linear instability analysis is concerned with the study of the evolution of random small amplitude disturbances. The system that is unstable under any type of small amplitude perturbations will experience spontaneous instability that will grow in time until it becomes non-linear.

The normal modes are added to the base state of the parallel shear flow for two miscible liquids with a basic configuration of the concentration and velocity profiles depicted in Figure 3.1. In this case, the base state is thermodynamically unstable and the free energy function has two minima for a binary mixture.

For a stationary plane layer, the concentration C_0 defines the whole system including the interface, presented by the equation

$$C_0 = \frac{1}{2}\tanh\left(\frac{y}{\delta}\right), \tag{3.1}$$

where δ is the thickness of the interface which is defined when the system is out of equilibrium.

Substituting the concentration profile in the equation (2.14), if the system is at equilibrium, we obtain

$$\mu(C_0) = 2AC_0 + 4C_0^3 - Ca\nabla^2 C_0 = 0. \tag{3.2}$$

By replacing the equation (3.1) in (3.2), the resulting equation is satisfied only for $A = \pm\frac{1}{2}$ and $\delta_0 = \sqrt{-\frac{Ca}{A}}$, presents the interface thickness at equilibrium.

The surface tension (σ) applied on the interface of a plane layer at equilibrium state [21, 151] is defined by the integral

$$\sigma = \frac{Ca}{2}\int_{-\infty}^{\infty}\left(\frac{dC_0}{dy}\right)^2 dy. \tag{3.3}$$

Inserting the basic state profile (3.1) in the equation (3.3), we find the magnitude of the surface tension, which is given by

$$\sigma = \frac{Ca}{3\delta_0}. \tag{3.4}$$

For steady parallel shear flow, in addition to the concentration profile the steady motion of the liquids is defined by the tangential velocity profile

$$U_x(y) = U_0\tanh(\frac{y}{\delta_u}), \tag{3.5}$$

where δ_u is the nondimensional thickness of shear motion and $U_0 = V_0/V_*$ is the nondimensionalised amplitude velocity of the liquids (V_0 is the dimensional basic flow).

As miscible liquids are being dealt with here, we have to show that the increase

of the interface thickness is slower than the perturbation growth. In Appendix 8.2, it is shown that the interface thickness is linearly growing in time as $\delta = \sqrt{D_0 t} \sim \sqrt{\frac{t}{Pe}}$. In this case, the time of concentration thickness diffusion is much slower than the exponential growth of linear perturbations in time. Thus, the linear stability analysis can be conducted on the assumption that the basic state of the interface is a frozen state.

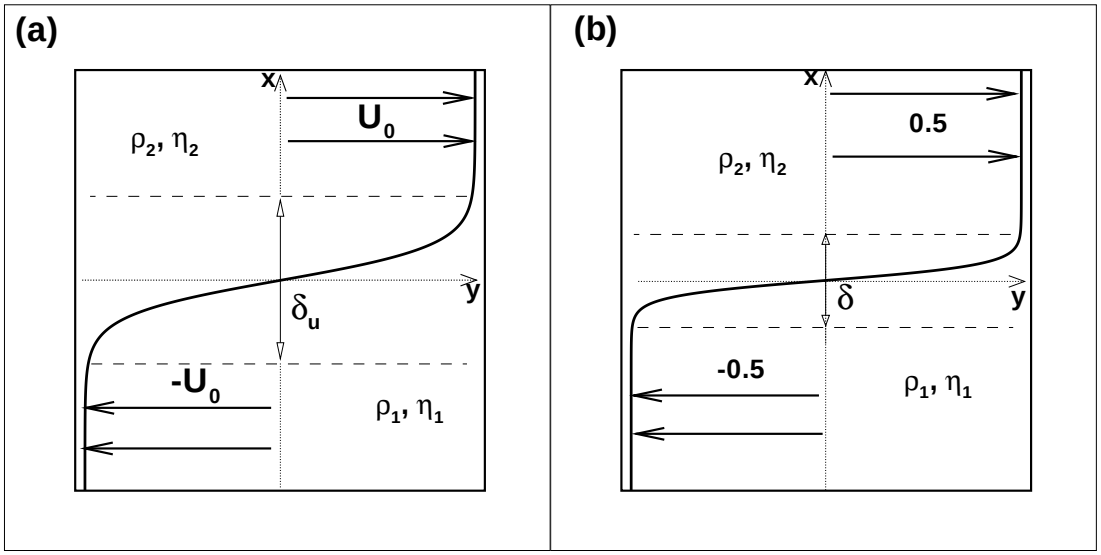

Figure 3.1: Basic profiles of velocity (a) and concentration (b). The binary mixture of two incompressible miscible liquids are of different densities ρ_1 and ρ_2 and viscosities, η_1 and η_2. Mixture components are separated by an interface with thickness δ, the shear flow thickness is represented by δ_u. The layer is assumed to be unbounded and the length L is chosen to be large enough to ignore its influence in the results.

3.3 Normal mode approach

In order to predict the fate of perturbations, the normal mode approach is used to study the linear stability of a phase boundary. In the case of stationary liquids in an equilibrium state, the flow can be described only by the concentration profile. For a parallel shear flow along the phase boundary, we assume that the flow is

in the x-direction and the system obeys the velocity and concentration profiles defined in Figure 3.1.

The small amplitude linear perturbations are proportional to $\sim \exp(ik_x + ik_z - i\omega t)$ which are superposed onto the base state. Thus, the components of velocity field (u, v, w), pressure P, concentration C and chemical potential μ describing the perturbed parallel shear flow are given by

$$u\,(x, y, z, t) = U_0(y) + \hat{u}(y)\exp(ik_x x + ik_z z - i\omega t), \tag{3.6}$$

$$v\,(x, y, z, t) = \hat{v}(y)\exp(ik_x x + ik_z z - i\omega t), \tag{3.7}$$

$$w\,(x, y, z, t) = \hat{w}(y)\exp(ik_x x + ik_z z - i\omega t), \tag{3.8}$$

$$P\,(x, y, z, t) = P_0(y) + \hat{P}(y)\exp\left(ik_x x + ik_z z - i\omega t\right), \tag{3.9}$$

$$C\,(x, y, z, t) = C_0(y) + \hat{C}(y)\exp\left(ik_x x + ik_z z - i\omega t\right), \tag{3.10}$$

$$\mu(x, y, z, t) = \mu_0(y) + \hat{\mu}(y)\exp\left(ik_x x + ik_z z - i\omega t\right), \tag{3.11}$$

where U_0, P_0, C_0 and μ_0 respectively are the basic velocity, pressure, concentration and chemical potential. The perturbations $(\hat{u}, \hat{v}, \hat{w})$ are the amplitudes of the velocity field; and $\hat{P}$, $\hat{C}$ and $\hat{\mu}$ are respectively the pressure, concentration and chemical potential amplitudes of the perturbed parts. Also, k_x and k_z are the wave numbers in the x and z-directions, and the total wave number k is written as

$$k = \sqrt{k_x^2 + k_z^2} \quad \text{and} \quad \lambda = \frac{2\pi}{k}, \tag{3.12}$$

with λ being the wavelength.

For stationary liquids, the basic velocity is $U_0 = 0$. The parameter $\omega = \omega_r + i\omega_i$ is composed of the real part ω_r that represents the phase speed, and the imaginary part ω_i that represents the growth/decay rate of the perturbations. If $\omega_i > 0$ the perturbations are unstable and grow exponentially in time. The perturbations are said to be neutrally stable only if $\omega_i = 0$. Additionally, if $\omega_i < 0$ the perturbations decay. The perturbations develop periodically when $\omega_r \neq 0$ or aperiodically if $\omega_r = 0$.

Rayleigh [125] developed the inflection point theory for homogenous shear flow. The flow is unstable if the velocity profile satisfies the inflection point condition $U_0''(y) < 0$ for the values of y in the domain of the flow. However,

the flow may become stable under the strong criterion of Fjortoft [47] theory, in which the inflection point occurs for such flow only if $U''(U - U_s) < 0$ where U_s is the mean velocity.

In the normal modes method, the temporal modes are the solutions that grow in time with ω being complex determined at a fixed real value of wavenumber k. In contrast, the spatial modes are the solutions that can be determined by considering ω real and the wave number k complex. Spatial modes are used in the study of linear evolutions of small amplitude perturbations that grow in space. Thus, the determination of spatial instability is based on the equations that are mathematically nonlinear in terms of the spatial growth (or decay) rate k. This may lead to further difficulties in solving the equations, particularly for higher order differential equations such as the equations used in the current study. According to Gaster [52], the spatial modes can be obtained from temporal modes.

The aim of using linear instability analysis was based on the assumption that transition from the linear regime to the turbulent regime is immediate. However, it is later shown that this is not true in most flows [94, 97, 143]. Despite the linear stability only being valid for a very short period of time, it correctly describes the onset and early evolution of small amplitude perturbations. Its importance in hydrodynamics is reflected in its capability to qualitatively and correctly predict the overall flow physics that is concluded from the instability of a flow analysis [92, 101, 131]. As an indication on its usefulness in detecting the physical growth mechanisms and the evolvement of the perturbations, there are a large number of studies devoted to the use and development of the linear stability theory, e.g., Langer [94], Lin [97], Stuart [143], Lamb [92], Chandrasekhar [26], Drazin [39], and Schmid and Henningson [131], as well as, review papers by Maslowe [101], Pellacani [117], Gage [49] and Carpenter et al. [24]

Having defined the basic state and the type of modes, now we can reduce the nonlinear partial differential equations (2.5), (2.6) and (2.7) into a system of linear ordinary differential equations with boundary conditions depending on the specific flow configuration.

3.4 Derivation of linear equations

In order to derive the linear differential equations of momentum, equations (3.6), (3.7) and (3.8) are substituted into the nonlinear differential equations (2.12)-(2.14), so that the nonlinear terms are filtered and similar terms are collected leading to the linear differential equations

$$ik_x\hat{u} + \frac{d\hat{v}}{dy} + ik_z\hat{w} = 0, \tag{3.13}$$

$$-i\omega\hat{u} + ik_xU_0\hat{u} + U_0'\hat{v} = -ik_x\hat{P} + \frac{1}{Re}\left(\frac{d^2\hat{u}}{dy^2} - k^2\hat{u}\right) - ik_xCaC_0''\hat{C}, \tag{3.14}$$

$$i(k_xU_0 - \omega)\hat{v} = -\frac{d\hat{P}}{dy} + \frac{1}{Re}\left(\frac{d^2\hat{v}}{dy^2} - k^2\hat{v}\right) - CaC_0'\left(\frac{d^2\hat{C}}{dy^2} - k^2\hat{C}\right) - CaC_0''\frac{d\hat{C}}{dy} - Gr\hat{C}, \tag{3.15}$$

$$-i\omega\hat{w} + ik_zU_0\hat{w} = -ik_z\hat{P} + \frac{1}{Re}\left(\frac{d^2\hat{w}}{dy^2} - k^2\hat{w}\right) - ik_zCaC_0''\hat{C}. \tag{3.16}$$

Making use of the continuity equation (3.13) in the equation $k_x \times$ (3.14) $+ k_z \times$ (3.16), to obtain

$$i\left(U_0k_x - \omega\right)\frac{id\hat{v}}{dy} + k_xU_0\hat{v} = -ik^2\hat{P} + \frac{1}{Re}\left(\frac{id^3\hat{v}}{dy^3} - k^2\frac{id\hat{v}}{dy}\right) - iCak^2C_0''\hat{C}. \tag{3.17}$$

By derivation of the latter equation in respect to the variable y, and with some algebraic simplifications we may obtain

$$i\left(U_0k_x - \omega\right)\frac{d^2\hat{v}}{dy^2} - ik_xU_0''\hat{v} = -k^2\frac{\hat{P}}{dy} + \frac{1}{Re}\left(\frac{d^4\hat{v}}{dy^4} - k^2\frac{d^2\hat{v}}{dy^2}\right) - Cak^2C_0'''\hat{C} - Cak^2C_0''\frac{d\hat{C}}{dy}. \tag{3.18}$$

Subtracting equation (3.18) from $k^2 \times$ (3.15) allows us to reduce the momentum equations into a single linear differential equation. And, by applying normal modes to nonlinear diffusion and chemical potential equations (2.13) and (2.14),

we obtain the set of ordinary linear differential equations

$$i\left(U_0 k_x-\omega\right)\left(\hat{v}''-k^2\hat{v}\right)-ik_xU_0''\hat{v}=\frac{1}{Re}\left(\hat{v}^{iv}-2k^2\hat{v}''+k^4\hat{v}\right)+ Cak^2\left(\left[\hat{C}''-k^2\hat{C}\right]C_0'-C_0'''\hat{C}\right)+Grk^2\hat{C}, \tag{3.19}$$

$$i\left(U_0k_x-\omega\right)\hat{C}+\hat{v}C_0'=\frac{1}{Pe}\left(\frac{d^2\hat{\mu}}{dy^2}-k^2\hat{\mu}\right), \tag{3.20}$$

$$\hat{\mu}=2A\hat{C}+12C_0^2\hat{C}-Ca\left(\frac{d^2\hat{C}}{dy^2}-k^2\hat{C}\right). \tag{3.21}$$

Here $\hat{v}(y)$, $\hat{C}(y)$, and $\hat{\mu}(y)$ represent the amplitudes of the v velocity, concentration C, and chemical potential μ respectively.

These are the Orr-Sommerfeld kind equations of eighth order, defining development of perturbations at the shear flow. The linear differential equations for interface between two stationary liquids can be obtained by enforcing $U_0 = 0$.

3.5 Three or two-dimensional instability

Squire [138] studied the stability of a viscous and incompressible flow between parallel walls. He showed that each unstable three-dimensional perturbation is accompanied by a more unstable two-dimensional perturbation with a smaller critical value of the Reynolds number. This is known as Squire's theorem.

Yih [163] used Squire's theorem to study the fluid flow between two parallel walls allowing the density and viscosity to vary. Pearlstein [77] extended Squire's theorem to investigate flows with varying temperature and solute concentration. Yiantsios and Higgins [162] used linear stability analysis to investigate the plane Poiseuille flow of two superposed fluids with different viscosity, where the capillary forces were taken into account. They showed that Squire's theorem holds only for $n > \sqrt{m}$, with n being the ratio of thickness and m the viscosity ratio. Moreover, Koppel [88] showed that Squire's theorem holds only for parallel shear flow between two fluids with the same densities. Smyth and Peltier [135] also showed that, for Holmboe instability, the flow is initially unstable to three-dimensional disturbances for smaller values of Reynolds number.

Chen and Fried [158] studied the Rayleigh-Taylor instability with phase transition. They showed that the Squire's theorem holds, so the flow is initially unstable to two-dimensional disturbance for small values of Weber, Froude, Voronkov and Gurtin numbers. Similar to the Squire's theorem, Koppel [88] provided a general theory for miscible liquids, she showed that a $3D$-dimensional perturbations is equivalent to solve $2D$-dimensional highly stratified flow for smaller Reynolds and Prandtl numbers but higher Richardson number.

For the current system, we are not able to apply the Squire's theorem without investigating whether $3D$ perturbations are the most dangerous for given values of the parameters Pe, Re, Gr, A and Ca. Since the present data is validated against the classical pure RT and KH instabilities, which are initially subjected to $2D$ perturbations, the current analysis is limited to the stability study in respect of $2D$ perturbations.

In stationary binary mixture ($U_0 = 0$), the amplitude equations (3.19), (3.20) and (3.21) become independent from the x-component of the wave number. The dispersion relation is determined by the expression

$$\omega = \omega(Re, Pe, Gr, Ca, A, k). \tag{3.22}$$

This is the same form of the eigenvalue problem resulting from two-dimensional disturbances. This allows us to assume that the interface is initially unstable to two-dimensional perturbation and the instability of the flow can be determined by solving a $2D$ system. As the liquids are incompressible and the flow is irrotational, one can use the velocity in the $y-$direction ($\hat{v}$) and $x-$direction ($\hat{u}$) in linear differential equations (3.19) and (3.20) to obtain the new system of differential equations in terms of the streamfunction as follows

$$u = \frac{d\psi}{dy} \quad \text{and} \quad v = -\frac{d\psi}{dx} \quad \text{where} \quad \nabla^2\psi = 0.$$

The equations (3.19), (3.20) and (3.21) can be modified to the following form

used for numerical calculations

$$-i\omega\left(\psi''-k^2\psi\right)=\frac{1}{Re}\left(\psi^{iv}-2k^2\psi''+k^4\psi\right)+ ikCa\left(\left[\hat{C}''-k^2\hat{C}\right]C_0'-C_0'''\hat{C}\right)+ikGr\hat{C}, \tag{3.23}$$

$$-i\omega\hat{C}-ikC_0'\psi=\frac{1}{Pe}\left(\frac{d^2\hat{\mu}}{dy^2}-k^2\hat{\mu}\right), \tag{3.24}$$

$$\hat{\mu}=2A\hat{C}+12C_0^2\hat{C}-Ca\left(\frac{d^2\hat{C}}{dy^2}-k^2\hat{C}\right). \tag{3.25}$$

This form is the Orr-Sommerfeld equation type that will be used for analysing the stability of the interface separating two stationary miscible liquids. For shear flow we similarly assume that the perturbations initially are two-dimensional when viscosity, diffusion and capillary forces are included. Accounting for the effect of the shear motion, then the equations (3.23) and (3.24) become

$$i(U_0k-\omega)\left(\psi''-k^2\psi\right)-ikU_0''\psi=\frac{1}{Re}\left(\psi^{iv}-2k^2\psi''+k^4\psi\right)+ ikCa\left(\left[\hat{C}''-k^2\hat{C}\right]C_0'-C_0'''\hat{C}\right)+ikGr\hat{C}, \tag{3.26}$$

$$i(U_0k-\omega)\hat{C}-ikC_0'\psi=\frac{1}{Pe}\left(\frac{d^2\hat{\mu}}{dy^2}-k^2\hat{\mu}\right), \tag{3.27}$$

In light of the above differential equations, we can see that solving the complete set of linear equations is not a trivial task. Generally, one is not necessarily required to determine v (or ψ), C and μ to obtain a clear understanding of the flow instability mechanisms. In reality, the linear stability theory is frequently used for determination of the dependence of the complex values of ω on the wave number k. This dependency usually describes the dispersion relation, which is easy to determine by means of an analytical approach if the system has a simple configuration. Otherwise, numerical and asymptotic methods have to be used for more complicated systems. The main concern of these methods is to identify the type of stability or instability and its limits.

The determination of the values of ω are not straightforward because of the complexity of the differential equations so there is a need for an appropriate

numerical approach. The next chapter is used to develop the relevant numerical methods from which we select the appropriate methods capable of tackling the stiffness of the current system of equations.

Chapter 4

Numerical methods for linear stability analysis

The objective of this chapter is to present the commonly used numerical methods to solve linear stability problems. To obtain the spectral properties of the linear stability is not straightforward, as in most cases including the current problem, the differential equations are stiff. To overcome this issue there are robust and sophisticated numerical methods including: the shooting, compound matrix, Chebyshev collocation and finite difference methods. They are compared and two of them are chosen for use in the next chapters.

4.1 Numerical methods to solve equations of the Orr-Sommerfeld type

In hydrodynamic linear stability theory, numerical approaches are concerned with the determination of the most unstable modes through solving the linear differential equations. The solution cannot be obtained in a straightforward manner as the equations themselves are naturally stiff for some values of the parameters. Also, due to a variety of factors, the solutions might become prone to lose their orthogonality which is very important for the numerical stability and hence the accuracy [39, 131]. The numerical methods can be classified into two main categories:

1. Direct integration method (local methods): explicit shooting method (ESM) [17, 106, 149] and compound matrix method [4, 76, 111] (CMM),

2. Spectral methods and direct disctritization [6, 55, 63] (global methods): finite difference (FDM) and Chebyshev collocation methods (CCM).

In the direct integration methods[1], the ESM method can be used to solve higher and lower order differential equations. The method of CMM is sufficient only for solving differential equations up to the sixth order. The method of ESM was the first approach used for solving the inviscid Rayleigh equations [106]. The CMM method was developed by Ng and Reid [111] for solving differential equations of the fourth and then extended to the differential equations of the sixth order. The advantage of the CMM method over ESM is that CMM preserves the analyticity where the non-orthogonality issue can be removed as a result of reducing the original system of equations into a new system, which has a single solution at each boundary. This new system is then solved in a similar way to the ESM method, but the integration is initialized with a single solution as will be shown later.

The disadvantage of the CMM method is that the size of the system becomes larger with the increasing order of the differential equation. That is, to solve a differential equation of the eight order we need to solve a modified matrix of very large size, which is not an easy task. The ESM method is used widely for solving linear problems of hydrodynamic stability in bounded and unbounded domains [19, 98]. It is often combined with an orthogonalization scheme such as the Gram–Schmidt algorithm, which is very efficient in maintaining the solutions orthogonality, and hence, ensuring that these solutions also remain linearly independent during the integration process [29, 100, 149].

FDM and CCM methods are also used widely in solving boundary value problems in hydrodynamics [98, 155]. These methods are easy to implement; but the FDM method is known to produce oscillatory solutions at particular boundary conditions. The CCM method is mainly used for solving bounded shear flows.

[1] The reader needs to be aware that both the ESM and CMM methods using shooting procedure, however, they don't solve the same equations as it will be shown later in this chapter.

Orszag [113] used the Chebyshev tau method to find the linear instability of Poiseuille flow. The author showed that the Chebyshev approximation method can be superior to the FDM method, as it provides a higher order of accuracy and resolution. In particular, it requires less time and computational resources. Voiget et al. [155] developed a spectral approach for solving ordinary and partial differential equations. They have provided a detailed derivation of expressions for CCM derivatives. Furthermore, the CCM method was used for solving unbounded inviscid shear flow where algebraic mapping was required [40, 57, 98]. In the current study, as we are dealing with an unbounded flow domain, it is convenient to use one of these mapping techniques.

4.2 Shooting method for boundary-value problems

Here, we present the essentials of the boundary value problems that are relevant to the current study. Let a general differential equation have the form

$$y^{(n)} = f(x, y, y^{'}, ..., y^{n-1}) \quad \text{for} \quad a \leq x \leq b \tag{4.1}$$

with the boundary conditions

$$\begin{aligned}(y(a), y^{'}(a), ..., y^{(n-1)}(a))^T &= (\alpha_1, ..., \alpha_{n-1})^T \\ (y(b), y^{'}(b), ..., y^{(n-1)}(b))^T &= (\beta_1, ..., \beta_{n-1})^T.\end{aligned} \tag{4.2}$$

In order to illustrate the method of solution, we use a homogeneous ordinary differential equation of order n that is given by a general formula

$$y^{(n)}(x) + Q_1(x, \lambda, \omega)y^{(n-1)}(x, \lambda, \omega) + ... + Q_{n-1}(x, \lambda, \omega)y(x) = 0, \quad x\epsilon[a, b], \tag{4.3}$$

where $Q_1(x, \lambda)$,.., $Q_{n-1}(x, \lambda)$ are the coefficients which can be real or complex, k is the real wave number and ω is the eigenvalue, and the boundaries of the domain a and b are the real constants. The boundary conditions of the boundary

value problem are written as

$$y_i(a,\lambda,\omega) = y_i^{a,k,\omega}, \quad i = 1,2,...,q \tag{4.4}$$

$$y_i(b,\lambda,\omega) = y_i^{b,k,\omega}, \quad i = q+1,q+2,...,n, \tag{4.5}$$

where i and q are integers.

The solutions of the ordinary differential equation (4.3) can be determined by solving the system of first order differential equations of the form

$$\frac{d\mathbf{y}}{dx} = \mathbf{f}(x,\mathbf{y},k,\omega), \tag{4.6}$$

where the vector $\mathbf{y}$ is given as

$$\mathbf{y} = \begin{pmatrix} y_1 \\ y_2 \\ y_3 \\ \vdots \\ y_n \end{pmatrix} \equiv \begin{pmatrix} y \\ y' \\ y'' \\ \vdots \\ y^{(n-1)} \end{pmatrix}. \tag{4.7}$$

As in most cases of boundary value problems, some boundary conditions are not known and in order to obtain the solution, the shooting procedure is frequently used. In the current work the boundary-value problems (3.23)-(3.25) yield asymptotic solutions; which are used with the shooting method and a root finding scheme to determine the eigenvalues.

4.2.1 Discretization

The main domain is divided into the two sub-domains $[a_0, m_0]$ and $[m_0, b_0]$, where m_0 is the middle point of the domain $[a_0, b_0]$. Each sub-domain is discretized into n points, the number of which depends on the adaptive process that may lead to the desired accuracy of the solution. The sub-domains are discretized with an unequispaced grid. The solutions at a_0 and b_0 for the boundary value problem (4.3) are given by $y^{a_0}(k,\omega)$ and $y^{b_0}(k,\omega)$.

4.2.2 Integrator

The main part of the shooting method is the integration that can be performed through a highly accurate scheme such as Runge-Kutta. Here, the five-stage Runge-Kutta method that is fourth order accurate is used, the solution is given by

$$\mathbf{y}_n = \mathbf{y}_{n-1} + \frac{1}{2}(\mathbf{k}_1 + 4\mathbf{k}_4 + \mathbf{k}_5), \tag{4.8}$$

which is determined through the scheme defined by the following system of equations

$$\begin{cases} \mathbf{k}_1 = \frac{h}{3}\mathbf{f}(x + \frac{h}{3}, \mathbf{y}, k, \omega) \\ \mathbf{k}_2 = \frac{h}{3}\mathbf{f}(x + \frac{h}{3}, \mathbf{y} + \mathbf{k}_1, k, \omega) \\ \mathbf{k}_3 = \frac{h}{3}\mathbf{f}(x + \frac{h}{3}, \mathbf{y} + \frac{1}{2}(\mathbf{k}_1 + \mathbf{k}_2), k, \omega) \\ \mathbf{k}_4 = \frac{h}{3}\mathbf{f}(x + \frac{h}{2}, \mathbf{y} + \frac{3}{8}k_1 + \frac{9}{8}\mathbf{k}_3, k, \omega) \\ \mathbf{k}_5 = \frac{h}{3}\mathbf{f}(x + h, \mathbf{y} + \frac{3}{2}\mathbf{k}_1 - \frac{9}{2}\mathbf{k}_3 + 6\mathbf{k}_4, k, \omega) \end{cases} \tag{4.9}$$

The errors that may result from the calculations are given by

$$\mathbf{e} = \frac{1}{5}(\mathbf{k}_1 - \frac{9}{2}\mathbf{k}_3 + 4\mathbf{k}_4 + \frac{1}{2}\mathbf{k}_5), \tag{4.10}$$

The main error (χ) can be determined through the expression

$$\chi = \sqrt{e_1^2 + e_2^2 + \ldots + e_n^2}. \tag{4.11}$$

The initial step size h_0 is then adapted at each step of integration as follows

$$\begin{aligned} \text{if} \quad (\chi \leq \chi_0 \quad \text{and} \quad \chi \geq 3.125 \times 10^{-2}\,\chi_0) \quad \text{then} \quad h = h_0, \\ \text{if} \quad (\chi < 3.125 \times 10^{-2}\,\chi_0) \quad \text{then} \quad h = 2h_0, \\ \text{if} \quad (\chi > \chi_0) \quad \text{then} \quad h = \frac{1}{2}h_0, \end{aligned}$$

where h is the adapted steps size and χ_0 is the tolerated error.

The current scheme provides an adaptive marching step size h with a wide region of numerical stability. In order to plot the contours in which Runge-Kutta methods are numerically stable, we assume that $Z = f(x, y, s, k, \omega) = s\,\omega$, where

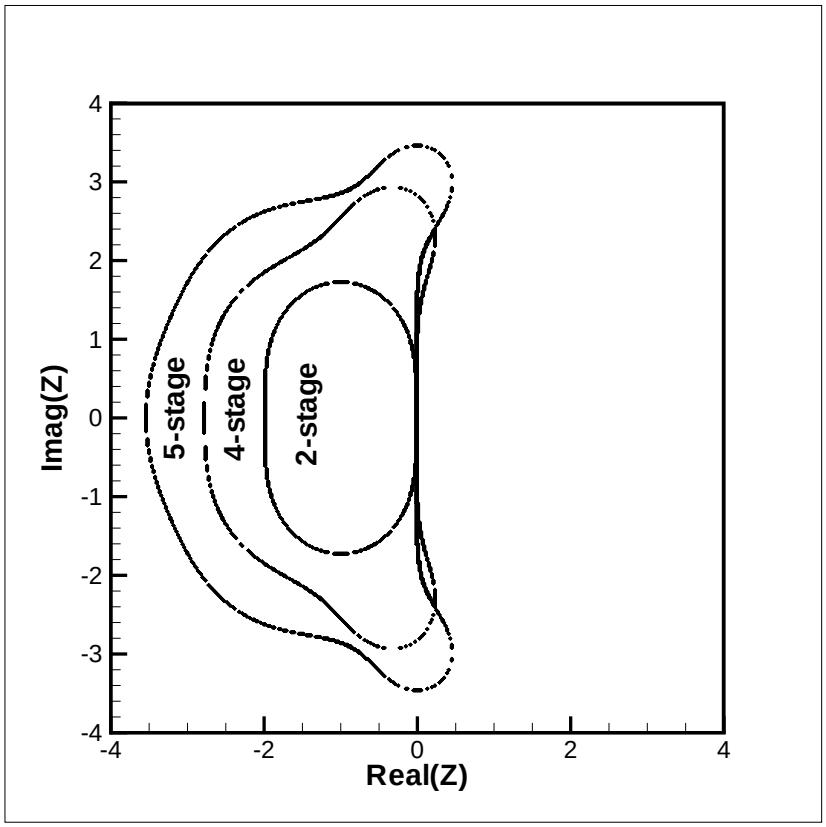

Figure 4.1: Stability regions for 2-stage, 4-stage and 5-stage Runge-Kutta algorithms, where each method is stable within its own boundaries. The method that is used for determining the shapes of stability can be found in the book of Canuto et al. [22].

s is any real number and ω is the eigenvalues: Z can be complex for higher order systems. Figure 4.1 illustrates the regions of numerical stability of various Runge-Kutta schemes.

In fact the solution of equation (4.3) is the linear combination of many solutions that satisfy both the equation and the boundary conditions. Assuming that the system is symmetric and the solutions that satisfy the boundary conditions at the boundary $x = a$ are y_i with $i = 1, ..., q$, and at $x = b$ are y_j with $j = q + 1, ..., n$ with i and q are integers. Thus, the matrix of these solutions at

the middle ($x = 0$) is

$$M = \begin{bmatrix} y_1(x,k,\omega) & \dots & y_q(x,k,\omega) & y_{q+1}(x,k,\omega) & \dots & y_n(x,\lambda,\omega) \\ \frac{\partial y_1(x,k,\omega)}{\partial x} & \dots & \frac{\partial y_q(x,\lambda,\omega)}{\partial x} & \frac{\partial y_{q+1}(x,q,\omega)}{\partial x} & \dots & \frac{\partial y_n(x,k,\omega)}{\partial x} \\ \frac{\partial^2 y_1(x,k,\omega)}{\partial x^2} & \dots & \frac{\partial^2 y_q(x,k,\omega)}{\partial x^2} & \frac{\partial^2 y_{q+1}(x,k,\omega)}{\partial x^2} & \dots & \frac{\partial^2 y_n(x,k,\omega)}{\partial x^2} \\ \vdots & \vdots & \vdots & \ddots & \vdots & \vdots \\ \frac{\partial^n y_1(x,k,\omega)}{\partial x^n} & \dots & \frac{\partial^n y_q(x,k,\omega)}{\partial x^n} & \frac{\partial^n y_{q+1}(x,k,\omega)}{\partial x^2} & \dots & \frac{\partial^n y_n(x,k,\omega)}{\partial x^n} \end{bmatrix}$$

For higher order differential equations, it is convenient to diagonalize the matrix so the determinant of the eigenvalue problem is simply the product of the diagonal elements. The eigenvalues are then obtained through solving the following expression

$$\phi(k,\omega) = M_{1,1}(k,\omega)\, M_{2,2}(k,\omega) \dots M_{n,n}(k,\omega) = 0, \tag{4.12}$$

where $M_{1,1}(k,\omega), M_{2,2}(k,\omega), \dots, M_{n,n}(k,\omega)$ are the diagonal elements of the diagonalized matrix M.

When solving higher order differential equations, the solutions can be non-orthogonal for some parameters and to ensure the orthogonality the Gram–Schmidt method is usually used.

The eigenvalues ω can then be calculated through a shooting method in conjunction with a root finding method, which is applied at the middle point satisfying the condition $\phi(\lambda,\omega) = 0$.

4.2.3 Orthonormalization technique

The solutions y_i, where $i = 1, ..., n$, are not always linearly independent, which can lead to numerical instability. As a remedy, the Gram–Schmidt [56, 132] or pseudo-orthogonalization [107] methods are introduced in order to enforce the orthogonality between the base solution during the integration process.

In the current study, we use the Gram–Schmidt orthonormalization technique. Following the method of Conte [29], the main domain $[a, b]$ is subdivided into m equal width h sub-domains, so that at the mesh points $x_i = i\,h$ we apply the Range-Kutta scheme to obtain the base solutions $Y = [y_1, ..., y_n]$. We examine

these base solutions at each grid point and when the base solution go beyond the given nonorthogonality criterion we orthonormalize the base solutions. The criterion is given as follows

$$\min_{(i,j)} \cos^{-1} \left| \frac{y_i \cdot y_j}{(y_i \cdot y_i)(y_j \cdot y_j)} \right| < \alpha, \quad i, j = 1, \ldots, k, i \neq j. \tag{4.13}$$

The angle α can vary between $0°$ and $90°$. If $\alpha = 0°$ no orthogonalisation is performed; if $\alpha = 90°$ the orthogonalisation is required. Let x_i be any point in the domain $[a, b]$ where orthogonality criterion is exceeded. The base solutions of the equation (4.3) are orthonormalized by the multiplication of $q \times q$ matrices as follows

$$Z(x_i) = Y(x_i)P_i, \tag{4.14}$$

where $Z(x_i)$ is the orthogonalisation base solution, $Y(x_i)$ is the base solution and $\overline{P}_i$ is the matrix used for orthonormalization given as

$$\overline{P}_i = \begin{pmatrix} \overline{P}_{11} & \overline{P}_{12} & \ldots & \overline{P}_{1q} \\ 0 & \overline{P}_{22} & \ldots & \overline{P}_{2q} \\ & & \ldots & \\ 0 & 0 & 0 & \overline{P}_{qq} \end{pmatrix}. \tag{4.15}$$

From the matrix of base solutions $Y(x)$ we can determine the elements $\overline{P}_{ij}$ of the matrix $P(x)$ as follows, q positive integer.

$$\overline{P}_{ij} = \begin{cases} -(z_i \cdot y_i)/(w_{ii} \cdot w_{jj}), & \text{if} \quad i < j \\ 0, & \text{if} \quad i > j \\ 1/w_{jj}, & \text{if} \quad i = j, \end{cases} \tag{4.16}$$

where z and w are determined from the Gram-Schmidt recursion formulas for orthonormalizing a set of solutions $[y_1, ..., y_q]$, we use

$$
\begin{aligned}
w_{11} = \sqrt{y_1 \cdot y_1}, \quad z_1 = y_1/w_{11}, \\
t_2 = y_2 - (y_2 \cdot z_1)z_1, \quad w_{22} = \sqrt{t_2 \cdot t_2}, z_1 = t_2/w_{22}, \\
\vdots \\
t_j = y_j - (y_j \cdot z_1)z_1 - \ldots - (y_j \cdot z_{j-1})z_{j-1}, \\
w_{jj} = \sqrt{y_j \cdot y_j}, \quad z_j = t_j/w_{jj}, \quad j = 1, \ldots, k.
\end{aligned}
$$

These are the main steps that can be followed when using explicit shooting method in solving a linear boundary value problem. Despite the fact that the shooting method is known to produce accurate results, when solving boundary value problems, it's main drawback is the stiffness (which can be overcome through a direct discretization methods).

4.3 Direct discretization methods

The equations of the Orr-Sommerfeld type can also be solved through the use of direct discretization methods, the finite difference and spectral collocation method [31, 113, 115]. Both Chebychev tau (CTM) and CCM methods are used in the solution of linear stability problems. The CCM method is however more popular in numerical treatment of Navier-Stokes equations. The accuracy of CTM is based on the number of Chebyshev polynomials and the treatment of boundary conditions. The CCM method is simple and similar to the FDM method in the sense of discretisation of a continuous function on a finite interval. Its accuracy is dependent on the number of grid points. In particular, it is proven to be an accurate and numerically stable approach.

The fundamental idea of FDM and CCM methods for solving an eigenvalue problem is to approximate the solutions using extrapolation, so that the solutions must satisfy the eigenvalue problem at specific grid points. In the FDM method, the grid points are the points in the domain separated by a fixed step size h. While in the CCM method, the grid points are the points defined by the Chebychev-Gauss-Lobatto formulae.

The accuracy and convergence of both FDM and CCM methods are dependent on the number of grid points and the length of the plane layer. In order to remove the influence of the length L on the results, the variable $y\epsilon[-L, L]$ is mapped into the variable $x\epsilon[-1, 1]$ in which Chebyshev polynomials are continuous and orthogonal. We have adopted the mapping formulae used by Liou and Morris [98], which is given by

$$y = \frac{x}{\sqrt{r^2 - x^2}}, \tag{4.17}$$

where r is the scaling factor and $x\epsilon[-1, 1]$.

Then, the metric $m = \frac{dx}{dy}$ can be obtained from the equation (4.17), we obtain

$$m = \frac{(1 - x^2)^{3/2}}{r}. \tag{4.18}$$

For better illustration of how these methods are used, a relevant example is presented in the next section.

4.4 Implementation of the methods

It is convenient to use a relevant example in order to explain the CCM, FDM and CCM methods. We have therefore chosen the well established parallel shear flow problem. The flow is described by the Orr-Sommerfeld equation derived by Betchov and Szewczyk [17]. The same assumptions are used as in the original work; the liquids are immiscible-viscous with matched densities and they occupy a sufficiently large $2D$ plane layer. For unbounded shear flow, the velocity profile is presented by the equation $U_0(y) = \tanh(\frac{y}{\delta})$. The Orr-Sommerfeld equation is given by

$$(kU_0 - \omega)(v'' - k^2 v) - U_0'' v = -\frac{1}{Re}\left(v^{iv} - 2k^2 v'' + k^4 v\right), \tag{4.19}$$

where U is the velocity profile, Re is the Reynolds number, k is the wave number and v is small amplitude of the perturbed vertical velocity. The boundary conditions are $v = 0$ and $U_0(y) = \pm 1$ and $U_0'(y) = 0$ at $y = \pm L_\infty$, where L_∞ is the

length of the semi-infinite plane layer width. The plane layer is assumed to be large enough that the boundary has no influence on the results. Prime ($'$) stands for the $y-$derivative.

4.4.1 Explicit shooting and compound matrix methods

At $y = \pm L_\infty$, the differential equation (4.19) has four exact solutions,

$$\exp(\pm ky), \exp(q_1 y) \quad \text{and} \quad \exp(q_2 y),$$

where k is the real number and q_1 and q_2 are the roots of the characteristic equation of (4.19) at $\pm L_\infty$, which are given as follows

$$q_1 = \sqrt{k^2 - (k + iRe\omega)} \quad \text{and} \quad q_2 = \sqrt{k^2 + k - iRe\omega}.$$

The solutions are subjected to the boundary conditions, with only two valid solutions at each boundary.

Explicit shooting method (ESM)

For the ESM method the eigenvalue problem (4.19) is solved by following the steps described in the sections (4.2). At $y \to \pm\infty$, the asymptotic solutions of the equation (4.19) are used as the boundary conditions. Thus, at $y \to -\infty$, the boundary conditions are

$$\mathbf{f} = \begin{pmatrix} 1 \\ k \\ k^2 \\ k^3 \end{pmatrix} \exp(ky) \quad \text{and} \quad \mathbf{f} = \begin{pmatrix} 1 \\ q_1 \\ q_1^2 \\ q_1^3 \end{pmatrix} \exp(q_1 y), \tag{4.20}$$

and the boundary conditions at $y \to +\infty$ are given by

$$\mathbf{f} = \begin{pmatrix} 1 \\ -k \\ k^2 \\ -k^3 \end{pmatrix} \exp(-ky) \quad \text{and} \quad \mathbf{f} = \begin{pmatrix} 1 \\ -q_2 \\ q_2^2 \\ -q_2^3 \end{pmatrix} \exp(-q_2 y). \tag{4.21}$$

For simplicity, the boundary value problem can be converted to the matrix form given by the following expression

$$\frac{d\mathbf{f}}{dy} = \overline{A}\mathbf{f}, \tag{4.22}$$

where $\mathbf{f} = (v_0, v_1, v_2, v_3)^T = (v, v', v'', v''')^T$ and the matrix A is given by

$$\overline{A} = \begin{pmatrix} 0 & 1 & 0 & 0 \\ 0 & 0 & 1 & 0 \\ 0 & 0 & 0 & 1 \\ \overline{A}_{41} & 0 & \overline{A}_{43} & 0 \end{pmatrix}, \tag{4.23}$$

with $\overline{A}_{41} = -(ik^2 Re(U_0 k - \omega) + U'' Re + k^4)$ and $\overline{A}_{43} = 2k^2 + iRe(U_0 k - \omega)$.

By making use of these equations and the Range-Kutta methods given above, we can obtain the determinant that allows us to find the eigenvalues of the Orr-Sommerfeld problem. It is given by

$$D = \begin{vmatrix} v_{1,-L} & v_{2,-L} & v_{1,L} & v_{2,L} \\ v'_{1,-L} & v'_{2,-L} & v'_{1,L} & v'_{2,L} \\ v''_{1,-L} & v''_{2,-L} & v''_{1,L} & v''_{2,L} \\ v'''_{1,-L} & v'''_{2,-L} & v'''_{1,L} & v'''_{2,L} \end{vmatrix}. \tag{4.24}$$

In conjunction with Muller's method, the eigenvalues can be determined for various values of Re. Here, it was noticed that the exact solutions of the equation (4.19) at $\pm L_\infty$ are orthogonal over the interval $[-L_\infty, L_\infty]$ during the integration process. Thus, there was no need for orthonormalization scheme. However, for some problems this issue may arise as shown in the next chapters.

Compound matrix method (CMM)

The Compound matrix method (CMM) was developed by Ng [110] in order to overcome the issue of dependent eigenfunctions that are usually common in ESM. In its essence, the original linearised governing equations are modified to a new boundary value problem with a single vector at each boundary. The integration process, however, is the same as in ESM.

The new system used with the CMM method, is given by

$$\overline{A}\psi = \overline{B}\phi. \tag{4.25}$$

Here, ϕ is a column vector and B is a 6×6 matrix with the elements formed from the matrix $\overline{A}$ defined in (4.23). The matrix $\overline{A}$ is

$$\overline{B} = \begin{pmatrix} \overline{A}_{11} + \overline{A}_{22} & \overline{A}_{23} & \overline{A}_{24} & -\overline{A}_{13} & -\overline{A}_{14} & 0 \\ \overline{A}_{32} & \overline{A}_{11} + \overline{A}_{33} & \overline{A}_{34} & \overline{A}_{12} & 0 & -\overline{A}_{14} \\ \overline{A}_{42} & \overline{A}_{43} & \overline{A}_{11} + \overline{A}_{44} & 0 & \overline{A}_{14} & \overline{A}_{13} \\ -\overline{A}_{31} & \overline{A}_{21} & 0 & \overline{A}_{22} + A_{33} & \overline{A}_{34} & -\overline{A}_{24} \\ -\overline{A}_{41} & 0 & \overline{A}_{21} & \overline{A}_{43} & \overline{A}_{22} + \overline{A}_{44} & \overline{A}_{23} \\ 0 & 0 & -\overline{A}_{41} & A_{31} & -\overline{A}_{42} & \overline{A}_{33} + \overline{A}_{44} \end{pmatrix}.$$

Using the asymptotic solution, the modified initial conditions are given as

$$\phi^{\pm L} = (\phi_0^{\pm L}, \phi_1^{\pm L}, \phi_2^{\pm L}, \phi_3^{\pm L}, \phi_4^{\pm L}, \phi_5^{\pm L})^T. \tag{4.26}$$

Here

$$\phi_0^{\pm L} = \begin{vmatrix} v_{1,\pm L} & v_{2,\pm L} \\ v'_{1,\pm L} & v'_{2,\pm L} \end{vmatrix} = (q \pm k), \quad \phi_1^{\pm L} = \begin{vmatrix} v_{1,\pm L} & v_{2,\pm L} \\ v'_{1,\pm L} & v'_{2,\pm L} \end{vmatrix} = q^2 - k^2,$$

$$\phi_2^{\pm L} = \begin{vmatrix} v_{1,\pm L} & v_{2,\pm L} \\ v''_{1,\pm L} & v''_{2,\pm L} \end{vmatrix} = \pm q^3 \pm k^3, \quad \phi_3^{\pm L} = \begin{vmatrix} v_{1,\pm L} & v_{2,\pm L} \\ v'''_{1,\pm L} & v'''_{2,\pm L} \end{vmatrix} = kq^2 \pm qk^2,$$

$$\phi_4^{\pm L} = \begin{vmatrix} v'_{1,\pm L} & v'_{2,\pm L} \\ v''_{1,\pm L} & v''_{2,\pm L} \end{vmatrix} = kq^3 - qk^3, \quad \phi_5^{\pm L} = \begin{vmatrix} v''_{1,\pm L} & v''_{2,\pm L} \\ v'''_{1,\pm L} & v'''_{2,\pm L} \end{vmatrix} = \pm k^2 q^3 \pm q^2 k^3.$$

The expression of eigenvalue $D(k, \omega)$ is given by the Evans function [42, 43]

$$Det(k, \omega) = \phi_0^- \phi_5^+ - \phi_1^- \phi_4^+ + \phi_2^- \phi_3^+ + \phi_3^- \phi_2^+ - \phi_4^- \phi_1^+ + \phi_5^- \phi_0^+, \tag{4.27}$$

where ϕ^- and ϕ^+ are the vectors obtained after integration from the left and right sides towards the middle of the plane layer. A root finding algorithm is used in order to find the eigenvalues ω versus the wave number values k. This method is efficient for solving the system of equations of up to sixth order.

4.4.2 Finite difference and Chebyshev collocation methods

For numerical implementation, the Orr-Sommerfeld equation can be modified to the following expression

$$(D^2 - k^2)(D^2 - k^2)v + iReU_0''v - Re\, iU_0(D^2 - k^2)v = \overline{c}(D^2 - k^2)v, \tag{4.28}$$

where $D^2 = \frac{d^2}{dy^2}$ is the second derivative and $\overline{c} = \omega/k$ is the eigenvalue. The mapped form of the equation (4.28) in the domain $[-1, 1]$ is

$$(m^2 G^{(2)} + m' m G^{(1)} - k^2 v)(m^2 G^{(2)} + m' m G^{(1)} - k^2 v) + iReU_0''v - iReU_0(m^2 G^{(2)} + m' m G^{(1)} - k^2 v) = \lambda((m^2 G^{(2)} + m' m G^{(1)} - k^2 v). \tag{4.29}$$

Here, $(\cdot)' = \frac{d}{dx}$, $G^{(1)}$ is the discretization of the first derivative $\frac{dv}{dx}$, G^2 is the discretization of the second derivative $\frac{d^2v}{dx^2}$ and $G^{(4)}$ is the discretization of the fourth derivative $\frac{d^4v}{dx^4}$. These terms will be presented in the next subsections accordingly to the methods of discretization CCM or FDM.

The eigenvalue problem then can be written as follows

$$\overline{A}v = \overline{CB}v. \tag{4.30}$$

Where A and B are the matrices that can be determined using either FDM or CCM, $\overline{C}$ contains the eigenvalues and v is the vector of the eigenfunctions of the system. The equation (4.30) is a well known form of the generalized eigenvalue problem and can be solved through the algorithm QR of LAPACK library, which is available in both Fortran and MATLAB.

Finite difference method (FDM)

In the case of the FDM method, the derivatives in equation (4.19) are approximated by using the finite difference analogues of the second order

$$G^{(1)} = \frac{v_{j+1} - v_{j-1}}{2h}, \tag{4.31}$$

$$G^{(2)} = \frac{v_{j+1} - 2v_j + v_{j-1}}{h^2}, \tag{4.32}$$

$$G^{(4)} = \frac{v_{j+2} - 4v_{j+1} + 6v_j - 4v_{j-1} + v_{j-2}}{h^4}, \tag{4.33}$$

where $h = \frac{2}{N}$ is the step size and $j = 1, ..., N$ with N being a positive integer representing the number of grid points in the domain $[-1, 1]$.

Chebyshev collocation method (CCM)

The CCM method is similar to the FDM method, however there is a key difference in determining the matrices in each method. The matrix obtained from the FDM method is filled only by the elements near the diagonal while the matrix obtained from the CCM method consists of all non-zero entries. In the CCM method, the grid points are defined by the Chebyshev-Gauss-Lobatto quadrature formula

given by

$$x_i = \cos\left(\frac{2j\pi}{N}\right), \tag{4.34}$$

where $j = 0, 1, ..., N$ where N is a positive integer.

The solutions are just the interpolant $v(x) = v$ presented by the unique Lagrange polynomial of degree N, given by

$$v(x) = \sum_{j=1}^{N} \frac{\prod_{k=0,k\neq j}^{N}(x - x_k)}{\prod_{k=0,k\neq j}^{N}(x_j - x_k)} v_j, \tag{4.35}$$

where v is evaluated only at the grid points, and hence, the derivatives must be evaluated also at the same grid points in terms of the grid values of the functions v_j. Thus, the q^{th} derivative of v is given by

$$v^{(q)} = \sum_{j=0}^{N} G_{k,j}^{(q)} v(x_j), \quad j = 0, ..., N \tag{4.36}$$

where $G^{(q)} = \frac{d^q v}{dx^q}$, so the first derivative $G^{(1)}$ can be obtained from the differentiation of the interpolation polynomial (4.35) q times, written as

$$G_{k,j}^{(1)} = \frac{c_k(-1)^{k+j}}{c_j(x_k - x_j)}, \tag{4.37}$$

$$G_{k,k}^{(1)} = \frac{x_k}{2(1 - x_k^2)}, \tag{4.38}$$

$$G_{0,0}^{(1)} = -G_{N,N}^{(1)} = \frac{2N^2 + 1}{6}, \tag{4.39}$$

where $c_0 = c_N = 2, \quad c_j = 1, \quad j = 1, ..., N - 1.$

Omitting complicated calculations, the elements of matrices of the second order $G^{(2)}$ and forth order $G^{(4)}$ derivatives can be calculated simply using expressions (4.37), (4.38) and (4.39), we obtain the following

$$G_{j,k}^{(2)} = \sum_{k=0}^{N} G_{j,k}^{(1)} G_{k,j}^{(1)}, \quad j = 0, ..., N, \tag{4.40}$$

$$G_{j,k}^{(4)} = \sum_{k=0}^{N} G_{j,k}^{(2)} G_{k,j}^{(2)}, \quad j = 0, ..., N. \tag{4.41}$$

N	ω_i of FDM r=1	ω_i of CCM r=1	ω_i of FDM r=2.5	ω_i of CCM r=2
16	0.16584751	0.16121641	0.16139561	0.16177449
32	0.16665203	0.16176490	0.16157402	0.16172146
64	0.16350713	0.16172150	0.16168631	0.16172162
80	0.16282323	0.16172169	0.16170001	0.16172162
128	0.16204974	0.16172162	0.16171238	0.16172162

Table 4.1: Convergence of maximum growth rate ω_i dependent on the number of grid points N and scale ratio r. The data is obtained through Finite difference (FDM) and Chebyshev collocation (CCM) for $k = 0.45$ and $Re = 50$. The values obtained by using ESM and CMM methods respectively are $\omega_i = 0.16177427$ and $\omega_i = 0.16172162$.

It is easy to note that after applying the mapping equations, the same form of the eigenvalue problem (4.29) is obtained which leads to the same generalized eigenvalue problem (4.30). Hence, it follows the same procedure to calculate the eigenvalues and eigenfunctions. Also, it can be noted that the advantage of FDM and CCM is that the eigenfunctions v are orthogonal and obtained simultaneously with eigenvalues c.

4.5 Validation of the methods

The aim is now to identify the capability and limits of the numerical methods described above. Based on accuracy and numerical stability, the appropriate methods will be chosen for conducting calculations in the next chapters.

Both the FDM and CCM methods are dependent on the effect of the scaling factor r and the number of grid points N. We conduct a comparison study in order to determine the one that performs better. The effect of the scaling parameter r had already been investigated by Liou and Morris [98] through the second order differential equation (Rayleigh equation), the values of r are presented in the table 4.2. Here, we attempt to check whether their values of r can still generate accurate results when the technique is applied to the fourth order differential equation.

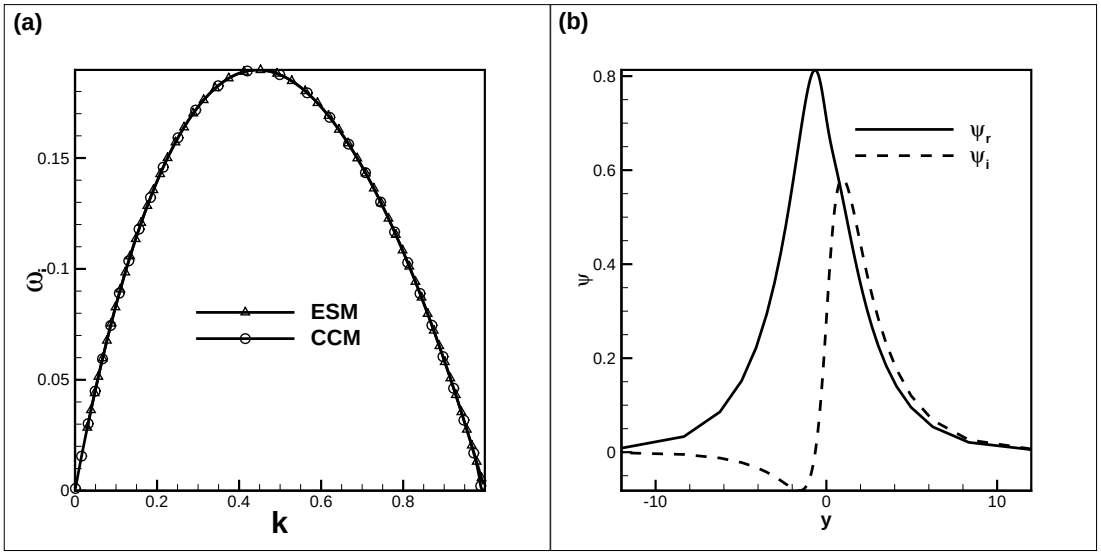

Figure 4.2: (a) illustrates the spectra curves of most unstable modes of inviscid parallel shear flow. (b) presents the eigenfunctions of small amplitude perturbations that grow at the parallel shear layer $\omega_i = 0.1897$ and wave number $k = 0.45$.

Table 4.1 illustrates the data obtained for FDM and CCM methods and their dependency on the number of grid points N and scaling factor r. The data produced from ESM and CMM also are compared. One may note that, when $r = 1$, the most unstable mode converges at $N \sim 80$ if CCM is used and a higher number of grid points if FDM is used. The situations can be improved for CCM when $r = 2$, for which the growth rate of the most unstable mode converges at a lower number of grid points about $N \sim 32$, whereas the value of ω_i of FDM converges for $N > 128$.

Based on these observations, we choose the CCM and ESM methods to conduct the calculations in the next chapters. In particular, for differential equations of the eight order, ESM becomes more complicated to use. In addition, it fails to produce results for small or large values of some parameters (e.g., large Re, Pe and small value of Ca). With both CCM and ESM in hand, we will be able to obtain more reliable results.

Figure 4.2 (a) presents the spectra of shear flow instability obtained through using both CCM and ESM methods. It is showing that they are capable of

accurately producing spectra of most unstable modes. The results for ESM are obtained for inviscid liquids presented by the second order differential equation. The reduction of the order of the equation is required in order to obtain solutions of inviscid liquids because when dealing with viscous liquids we have to solve a fourth order differential equation in which the SEM method is unable to produce the results for $Re > 80$. For this value the solutions are far away from converging to the inviscid case. However, the CCM method does not suffer from the issue of stiffness when solving the differential equation of fourth order. The data obtained from the CCM method converges to inviscid results for $Re \sim 500$. Figure 4.2 (b) shows the eigenfunction of the unstable mode of KHI. The curves are the vectors v obtained from solving the eigenvalue problem (4.30).

The numerical issues confronted when solving the equations developed in Chapter 3, are related to the value of capillary number Ca and phase parameter A. When using the ESM method, the singularity (floating point) develops if the capillarity parameter $Ca = 0$ and phase parameter $A < 0$. This particular issue was overcome through the use of the Taylor expansion. However, a significant loss of accuracy can be incurred if attention is not paid to a particular degree of the series. It was found that the SEM performs better than CCM for small values of the interface thickness $\delta \leq 0.01$.

The main drawback of ESM is that it cannot solve the boundary value problem for larger values of Pe, Re or very small values of Ca. Hence, the solutions are obtained through the parametrization approach, i.e. the order of boundary value problem can be reduced if the liquids are inviscid or immiscible. In the case of the CCM method, we are able to solve the boundary value problem without a need for parametrization. However, this method is unable to produce accurate solutions for $\delta \leq 0.01$.

Chapter 5

Sharp interface approach

In this chapter, we introduce the sharp interface method through studying some of the classical problems. The focus here is on writing the dispersion relations in terms of phase-field parameters. These expressions will be used for validation in the next chapters.

In sharp interface method, the phase boundary is presented by an infinitely thin interface separating two fluids. Its basic idea is that the Navier-Stokes equations can be solved separately for each fluid and then the solutions must satisfy the boundary conditions at the interface.

5.1 Linear instability of a thin planar interface

The linear stability analysis is used to derive the dispersion relation for normal modes that grow or decay at the sharp interface. A generic case is represented by a simple plane layer with two superposed liquids which are in relative shear motion. In the first instant the small amplitude linear equations will be derived, after which the Rayleigh-Taylor (RTI), Kelvin-Helmholtz (KHI) instabilities and the gravity-capillary waves (GCW) problems will be used to reproduce the classical results [15, 26, 93]. Here, the results are obtained within the frame work of the Boussinesq approximation.

The liquids are presumed to be immiscible and incompressible separated by a sharp interface. The upper liquid 1 of constant density ρ_1 and viscosity coefficient

η_1 stands over liquid 2 of constant density ρ_2 and viscosity coefficient η_2. Furthermore, the liquids are assumed to have the same constant kinematic viscosity ν. The liquids are also assumed to be in parallel shear motion where the upper liquid moves with the speed (U_0) and the liquid underneath flows in opposite direction with $(-U_0)$. Small amplitude perturbations $\sim \exp(i\,k_x x + i\,k_y y - \omega\,t)$ are introduced to the base state of the flow in order to linearise the equations of motion. The equations of motion describe incompressible viscous binary mixtures are given by

$$\rho\left[\frac{\partial \mathbf{u}}{\partial t} + (\mathbf{u}\cdot\nabla)\mathbf{u}\right] = -\nabla P + \eta\nabla^2\mathbf{u} + g\rho\,\gamma, \tag{5.1}$$

$$\nabla\cdot\mathbf{u} = 0. \tag{5.2}$$

Here $\mathbf{u}$, η, g, P, ρ and γ are the velocity field, viscosity coefficient, acceleration of the gravity, pressure, density and the normal in z-direction respectively.

The momentum and continuity equations (5.1) and (5.2) can be rewritten in Cartesian coordinates as follows

$$\rho\left(\frac{\partial u}{\partial t} + U_0\frac{\partial u}{\partial x}\right) = -\frac{\partial p}{\partial x} + \eta\nabla^2 u, \tag{5.3}$$

$$\rho\left(\frac{\partial v}{\partial t} + U_0\frac{\partial v}{\partial x}\right) = -\frac{\partial p}{\partial x} + \eta\nabla^2 v, \tag{5.4}$$

$$\rho\left(\frac{\partial w}{\partial t} + U_0\frac{\partial w}{\partial x}\right) = -\frac{\partial p}{\partial z} + \eta\nabla^2 w - g\,\rho, \tag{5.5}$$

$$\frac{\partial u}{\partial x} + \frac{\partial v}{\partial y} + \frac{\partial w}{\partial z} = 0, \tag{5.6}$$

where u, v and w are the velocities in the x, y and the z-directions respectively, and η is the viscosity coefficient.

Substituting the normal modes $(\exp(k_x x + k_y y) - i\omega t))$ in equations (5.3), (5.4), (5.5) and (5.6), we obtain the linearized differential equations given by

$$ik_x p' = -i(U_0 k_x - \omega)\rho u + \eta\left(\frac{\partial^2 u}{\partial z^2} - (k_x^2 + k_y^2)u\right), \tag{5.7}$$

$$ik_y p' = -i(U_0 k_x - \omega)\rho v + \eta\left(\frac{\partial^2 v}{\partial z^2} - (k_x^2 + k_y^2)v\right), \tag{5.8}$$

$$i(U_0 k_x - \omega)\rho w = -\frac{\partial p'}{\partial z} + \eta \left(\frac{\partial^2 w}{\partial z^2} - (k_x^2 + k_y^2) w \right), \tag{5.9}$$

$$i\, k_x\, u + i\, k_y\, v = -\frac{\partial w}{\partial z}. \tag{5.10}$$

Combining the equations (5.7)-(5.10), we obtain the pressure perturbation p', which is given by

$$\frac{p'}{\rho} = i\, \frac{(U_0 k_x - \omega)}{k^2} \frac{\partial w}{\partial z} + \frac{\nu}{k^2} \left(-k^2 \frac{\partial w}{\partial z} + \frac{\partial^3 w}{\partial z^3} \right). \tag{5.11}$$

In order to get rid of the pressure term p', we insert the equation (5.11) into the equation (5.9), then we obtain the fourth order differential equation expressed as

$$i(U_0 k_x - \omega)\, w = \nu \left(\frac{\partial^2 w}{\partial z^2} - k^2 w \right) - i\, \frac{(U_0 k_x - \omega)}{k^2} \frac{d^2 w}{dz^2} - \frac{\nu}{k^2} \left(\frac{\partial^4 w}{\partial z^4} - k^2 \frac{\partial^2 w}{\partial z^2} \right) \tag{5.12}$$

The solution of equation (5.12) is the linear combination of the fundamental solutions

$$\exp(-k\, z) \quad \text{and} \quad \exp(-q_1\, z) \quad \text{for} \quad z > 0, \tag{5.13}$$

$$\exp(k\, z) \quad \text{and} \quad \exp(q_2\, z) \quad \text{for} \quad z < 0, \tag{5.14}$$

where

$$q_1 = \sqrt{k^2 + i(U_0 k_x - \omega)/\nu} \quad \text{and} \quad q_2 = \sqrt{k^2 - i(U_0 k_x + \omega)/\nu}.$$

5.2 Boundary conditions

At the sharp interface the boundary conditions are given by

$$\mathbf{u}_1 = \mathbf{u}_2, \tag{5.15}$$

$$(p_1 - p_2) n_i = (\tau_{1,ij} - \tau_{2,ij}) n_j + \sigma \left(\frac{1}{R_1} + \frac{1}{R_2} \right), \tag{5.16}$$

where $\mathbf{u}$ is the velocity field, p_1 and p_2 are the total pressures at the sides of the interface, τ_1 and τ_2 are the shear or normal stresses. Here, $i, j = 1 \ldots 3$ and n_i is the unit vector normal to the interface.

Since the small amplitudes are only dependent on z, then the coordinate of normal vector is $n = (0, 0, 1)$. By projecting the boundary conditions, we obtain

$$w_1 = w_2, \quad u_1 = u_2 \quad \text{and} \quad v_1 = v_2, \tag{5.17}$$

$$\tau_{zx,1} = \tau_{zx,2} \quad \text{and} \quad \tau_{zy,1} = \tau_{zy,2}, \tag{5.18}$$

$$-p_1 + 2\,\eta_1 \frac{\partial w_1}{\partial z} = -p_2 + 2\,\eta_2 \frac{\partial w_2}{\partial z} - g\rho' + \sigma \left(\frac{1}{R_1} + \frac{1}{R_2} \right). \tag{5.19}$$

Using the continuity equation and normal modes, the boundary conditions can be written as follows

$$w_1 = w_2, \tag{5.20}$$

$$\frac{\partial w_1}{\partial z} = \frac{\partial w_2}{\partial z}, \tag{5.21}$$

$$\eta_1 (\frac{\partial^2}{\partial z^2} + k^2) w_1 = \eta_2 (\frac{\partial^2}{\partial z^2} + k^2) w_2. \tag{5.22}$$

However, as the distortion of the shape of the interface ξ is small, $\left(\frac{1}{R_1} + \frac{1}{R_2} \right)$ can be approximated as $\left(\frac{\partial^2 \xi}{\partial x^2} + \frac{\partial^2 \xi}{\partial y^2} \right)$. Thus, equation (5.19) becomes

$$-p_1' + \rho_1 g\,\xi + 2\,\eta_1 \frac{\partial w_1}{\partial z} = -p_2' + \rho_2 g \xi + 2\,\eta_2 \frac{\partial w_2}{\partial z} - \sigma \left(k_x^2 + k_y^2 \right) \xi, \tag{5.23}$$

where $\rho_{1,2}$ and $p_{1,2}'$ are the densities and perturbed pressures of the liquids 1 and 2 at the interface.

The liquids are in realtive shear motion and the velocity U exprience a sharp change from one liquid to the other one. The continuity of matter presumes that the following equation must be satisfied at the interface [26],

$$\frac{\partial \xi}{\partial t} + U \frac{\partial \xi}{\partial x} = w_s \tag{5.24}$$

where w_s is the velocity of the interface and U is either U_0 or $-U_0$. This equation

allows us to write the following expression for ξ as

$$\xi = \frac{1}{2}\left[\frac{w_1}{U_0 k_x - \omega} + \frac{w_2}{-U_0 k_x - \omega}\right] \tag{5.25}$$

5.3 Stationary, inviscid and immiscible liquids

We now consider two superposed inviscid liquids that are initially stationary ($U_0 = 0$). Within a liquid domain at a point far from the interface, the equation (5.12) can be reduced to

$$\left(\frac{\partial^2 w}{\partial z^2} - k^2 w\right) = 0, \tag{5.26}$$

which yields the solution

$$w = A\exp(-kz) + B\exp(kz), \tag{5.27}$$

where A and B are arbitrary constants. The solution must vanish at $z \to \pm\infty$ which can be satisfied by making the appropriate choice of A and B giving the following solutions

$$w_1 = B\exp(kz) \quad z \to -\infty, \tag{5.28}$$

$$w_2 = A\exp(-kz) \quad z \to +\infty. \tag{5.29}$$

Matching these solutions at the phase boundary and making use of the equation (5.23), we obtain the following analytical dispersion expression

$$\omega = \sqrt{gk\frac{\rho_1 - \rho_2}{\rho_2 + \rho_1} - \frac{k^3\sigma}{\rho_2 + \rho_1}}. \tag{5.30}$$

The non-dimensionalisation process is shown in Appendix B. 1. The equation in non-dimensional form is then given by

$$\omega^2 = \frac{1}{2}Grk + \frac{Ca}{6\delta}k^3, \tag{5.31}$$

where Gr is the Grashof number, k is the wave number, Ca is the capillary number and δ is the thickness of the interface. Here, we presume that that Ca and δ tend to 0.

Expression (5.31) is the dispersion relation, indicating that, when the heavier liquid is superposed on the lighter one with $Gr < 0$, the sharp interface is always unstable, while the capillary forces stabilize the modes with short wavelengths. In the case where a heavier liquid underlies a lighter one ($Gr > 0$), the sharp interface is always stable and exhibits gravity-capillary waves propagating with a phase speed ω_r/k.

5.4 Stationary, viscous and immiscible liquids

Here again we assume that the liquids are initially assumed stationary ($U_0 = 0$) and the viscosity is important. Because the kinematic viscosity ν of liquids is the same, so that, far from the interface the equation (5.12) becomes

$$\left[1 + i\frac{\nu}{\omega}\left(\frac{\partial^2}{\partial z^2} - k^2\right)\right]\left(\frac{\partial^2}{\partial z^2} - k^2\right) w = 0, \tag{5.32}$$

which satisfys the following fundamental solutions

$$w_1(z) = A_1 \exp(-kz) + B_1 \exp(-qz) \quad \texttt{for} \quad z > 0, \tag{5.33}$$

$$w_2(z) = A_2 \exp(kz) + B_2 \exp(qz) \quad \texttt{for} \quad z < 0, \tag{5.34}$$

where A_1, A_2, B_1 and B_2 are the constants of integration.

Substituting the last two equations in the boundary equations (5.20), (5.21), (5.22) and (5.23), we obtain the system of linear equations

$$A_1 + B_1 = A_2 + B_2, \tag{5.35}$$

$$k\,A_1 + q\,B_1 = -k\,A_2 - q\,B_2, \tag{5.36}$$

$$2k^2 A_1 + (q^2 + k^2)B_1 = 2k^2 A_2 + (q^2 + k^2)B_2. \tag{5.37}$$

As $U_0 = 0$, the equation (5.23) can be simplified to

$$\left\{\left[\rho_2 - i\frac{\eta_2}{\omega}\left(\frac{\partial^2}{\partial z^2} - k^2\right)\right]\frac{\partial w_2}{\partial z}\right\}_{z=0} - \left\{\left[\rho_1 - i\frac{\eta_1}{\omega}\left(\frac{\partial^2}{\partial z^2} - k^2\right)\right]\frac{\partial w_1}{\partial z}\right\}_{z=0} + \frac{2i}{\omega}\left(\eta_2\frac{\partial w_2}{\partial z} - \eta_1\frac{\partial w_1}{\partial z}\right) = -\frac{k^2}{\omega^2}\left\{g\left(\rho_1 - \rho_2\right) + k^2\sigma\right\}\left(w_1 + w_2\right) \tag{5.38}$$

Inserting the solutions w_1 and w_2 in (5.38) and dividing it by $\rho_1 + \rho_2$, we obtain

$$k\frac{\rho_2}{\rho_1+\rho_2}A_2 - k\frac{\rho_1}{\rho_1+\rho_2}A_1 = \frac{gk^2}{2\omega^2}\left(\frac{\rho_1-\rho_2}{\rho_1+\rho_2} + \frac{k^2\sigma}{g}\right)(A_1 + B_1 + A_2 + B2) + \frac{k^2\nu}{\omega}\frac{\rho_1-\rho_2}{\rho_1+\rho_2}(k\,A_1 + q\,B_1 - k\,A_2 - q\,B_2). \tag{5.39}$$

The latter equation can be rearranged to

$$\left(\frac{R_0}{2} - Q - i\omega\right)A_1 + \left(\frac{R_0}{2} - Q - \frac{q}{k}\right)B_1 = \left(-\frac{R_0}{2} - Q + i\omega\right)A_2 + \left(\frac{R_0}{2} - Q - \frac{q}{k}\right)B_2, \tag{5.40}$$

where $R_0 = -\frac{gk}{2i\omega}\left(\frac{\phi}{2} - \frac{\sigma k^2}{(\rho_1+\rho_2)}\right)$, $Q = -k^2\nu\phi/2$ with $\frac{\rho_1}{\rho_1+\rho_2} \sim \frac{1}{2}(1-\phi/2)$ and $\frac{\rho_2}{\rho_1+\rho_2} \sim \frac{1}{2}(1+\phi/2)$.

The equations (5.35)-(5.37) and (5.40) constitute a system of homogeneous algebraic equations with four unknown constants A_1, A_2, B_1 and B_2. The non-trivial solution of this system exists only if the determinant of the resulting matrix equals zero

$$\left(R_0 + \nu(q^2 - k^2)\right)(q+k) - \nu^2(1+\phi/2)(1-\phi/2)(q-k)(q+k)k = 0, \tag{5.41}$$

where $q = \sqrt{k^2 + i\omega/\nu}$.

The non-dimensionalisation process is shown in Appendix B. 2. Thus the equation in non-dimensional form is given by

$$-\frac{q(q+k)(q-k)^2}{Re^2} = \frac{1}{2}Grk + \frac{Ca}{6\delta_c}k^3, \tag{5.42}$$

where the root q becomes $q = \sqrt{k^2 + iRe\omega}$, and Ca, Re and Gr are defined in (2.16)-(2.18).

Muller's method is used to obtain the roots ω of the equation (5.42) as a function of the wave number k. The results are presented in the next two subsections for both the Rayleigh-Taylor instability and gravity-capillary waves.

5.4.1 A heavier liquid set on top of a lighter one: $Gr < 0$

The data presented in Figure 5.1 are obtained from the dispersion relations (5.31) and (5.42). In this case, the liquids at the base state are motionless and satisfy the Rayleigh-Taylor instability (RTI) if $Gr < 0$ (the heavier liquid stands over the lighter one). As expected, the eigenvalues ω are purely positive imaginary indicating that the interface is unconditionally unstable. This also shows that the growth rate ω_i decreases by decreasing the values of Gr, there no RTI modes exist when the densities of the liquids are matched ($Gr = 0$).

In addition, the viscous forces may significantly reduce the instability of the interface at short wavelengths. The viscous effect alone cannot make the interface completely stable as indicated in Figure 5.1 (a). Figure 5.1 (b) shows that the capillary forces are capable of stabilizing the growth of modes. The cutoff wave number for which the inviscid interface becomes stable ($\omega_i \leq 0$) can be worked out from equation (5.31)

$$k_c = \sqrt{\frac{-3\delta Gr}{Ca}}, \tag{5.43}$$

where $Gr < 0$.

The expression (5.43) agrees with the data shown in Figure 5.1(b). In particular, it shows that the cutoff wave number k_c is independent of the Reynolds number Re that is at fixed $Ca = 0.01$. For $Re = 10$ and $R = \infty$, the cutt-off values k_c are identical.

The eigenfunctions are presented in Figures 5.1 (c) and (d) show the effects of Re and Ca, where the curves are plotted for $k = 1.5$. The solutions are purely real and normalised by their maximum values. One may note that the width y of the amplitude v_r in inviscid liquids is larger than in viscous liquids.

A heavier liquid underlying a lighter one: $Gr > 0$

Figures 5.2 and 5.3 present the dispersion relations obtained from the equations (5.31) and (5.42) for gravity-capillary waves ($Gr > 0$). The perturbations develop into stable waves if the liquids are inviscid. Viscosity introduces dissipation leading to the decay of waves (Figure 5.2 (a,b)). The short waves decay aperiodically ($\omega_r = 0$) with two different ways of decay, the viscous (fast) and the creeping (slow) modes.

Figure 5.2 (c,d) illustrates the effect of capillarity on the immiscible viscous interface. The data reveals that the capillarity retards the appearance of the aperiodically decaying modes to short wavelengths that are then replaced by capillary waves. Figure 5.3 (a,b) also shows that the development of the gravity waves depends on the strength of gravity forces so that no gravity waves can exist if $Gr = 0$.

The eigenfunctions are illusrated in Figures 5.3 (c,d) presenting the decay of the periodic and aperiodic waves, where they are normalised by their maximum values. Figure 5.3 (c) illustrates how an aperiodic mode ($k = 2.9$) decays. Figure 5.3 (d) illustrates the effect of Gr on the amplitude functions for the mode $k = 0.5$. It shows that the imaginary part decreases and the real part increases with increasing values of Gr.

5.5 Parallel shear flow of two inviscid liquids

Now we consider the shear motion of two inviscid miscible liquids. The velocity of the shear motion is continuous, so equation (5.23) can be reduced to the expression

$$-(U_0\,k_x+\omega)^2\frac{\rho_2}{\rho_1+\rho_2}-(U_0\,k_x-\omega)^2\frac{\rho_1}{\rho_1+\rho_2}=\frac{-gk}{2}\left(\frac{\rho_2-\rho_1}{\rho_1+\rho_2}-\frac{\sigma\,k^2}{(\rho_2+\rho_1)}\right). \tag{5.44}$$

This is a quadratic equation and it is easy to obtain its roots, which are given by

$$\omega=-\frac{1}{2}k_xU_0\phi\mp\sqrt{\frac{1}{2}g\,k\phi+\sigma\,k^2/(g(\rho_1+\rho_2))-k_x^2U_0^2(1-\frac{\phi}{2})(1+\frac{\phi}{2})}. \tag{5.45}$$

Knowing that $\phi << 1$ and making use of the phase-field scaling parameters, the equation (5.45) becomes

$$\omega = \sqrt{\frac{1}{2}Gr\,k + \frac{Ca\,k^3}{6\delta} - k_x^2 U_0^2}. \tag{5.46}$$

The expression (5.46) indicates that the growth rate is purely imaginary for $Gr < 0$ provided that $Ca = 0$. However, when $Ca \neq 0$, the interface can be completely stabilized if the following condition fulfilled

$$U_0 < \left(\frac{CaGr}{3\delta}\right)^{1/4}. \tag{5.47}$$

5.6 Parallel shear flow of two viscous liquids

Finally, the dispersion relation describing the growth or the decay of small amplitude perturbations can be determined from the boundary conditions (5.20), (5.21), (5.22), (5.23) and (5.25). They are written in terms of the perturbation parameters as follows

$$A_1 + B_1 = A_2 + B_2, \tag{5.48}$$

$$-kA_1 - q_1 B_1 = kA_2 - q_2 B_2, \tag{5.49}$$

$$(1 - \frac{\phi}{2})(k^2 A_1 + (k^2 + q_1^2)B_1) = (1 + \frac{\phi}{2})(k^2 A_2 + (k^2 + q_2^2)), \tag{5.50}$$

$$\begin{aligned}(\frac{R_1}{2} + i(U_0 k_x - \omega) - Q)A_1 + (\frac{R_1}{2} - \frac{q_1}{k} - Q)B_1 = \\ (-\frac{R_2}{2} - Q + i(U_0 k_x + \omega) - Q)A_2 + (\frac{R_1}{2} - \frac{q_2}{k} - Q)B_2,\end{aligned} \tag{5.51}$$

where $A_1, B_1, A_2,\ B_2$ are constants and $Q = -\frac{1}{2}\phi k^2 \nu$. The terms R_1 and R_2 respectively are

$$R_1 = -\frac{gk}{2}\left(\frac{1}{2}\phi - \frac{\sigma k^2}{g(\rho_1 + \rho_2)}\right)\frac{1}{i(U_0 k - \omega)}, \tag{5.52}$$

$$R_1 = \frac{gk}{2}\left(\frac{1}{2}\phi - \frac{\sigma k^2}{g(\rho_1 + \rho_2)}\right)\frac{1}{i(U_0 k + \omega)}. \tag{5.53}$$

The determinant of the linear system of the equations (5.48), (5.49), (5.50) and (5.51) must vanish. Using the fact that $\phi \to 0$, the expression of the dispersion relation becomes

$$\begin{aligned}\left(R_1 + R_2 + \nu(q_1^2 - k^2) + \nu(q_2^2 - k^2)\right)\left(\nu(q_2 + k)\right) \\ +2\nu^{-2}(q_1 + k)(q_2 + k)k = 0,\end{aligned} \tag{5.54}$$

Substituting the terms R_1 and R_2 and the scaling parameters (2.11) in equation (5.54), the dispersion relation in nondimensional form becomes

$$\begin{aligned}-\frac{(q_1^2 - k^2)(q_2^2 - k^2)}{Re^2}\left(\frac{4(q_1 + k)(q_2 + k)k}{(q_1 + q_2 + 2k)(q_1^2 + q_2^2 - 2k^2)} + 1\right) = \\ \frac{1}{2}Grk + \frac{Cak^3}{2\delta}.\end{aligned} \tag{5.55}$$

One may note that equation (5.55) converges to one of the previous expressions for the limiting values of Re and U_0. In particular for the interface between two inviscid immiscible liquids ($R \to \infty$ and $U_0 = 0$), the dispersion relation (5.31) is recovered. Similarly, for finite Re and $U_0 = 0$ the equation (5.42) for a viscous-immiscible plane layer is also recovered. Also, when $Re \to \infty$ but $U_0 > 0$, the equation (5.55) can be reduced to a quadratic equation that allows us to work out the dispersion relation (5.46).

The solutions of equation (5.55) are shown in Figures 5.4. It shows how viscosity and capillarity affect the instability of the sharp interface subject to shear motion. One may note that the interface is unconditionally unstable as long as $Ca = 0$ and $Gr < 0$. In contrast to the case of the stationary base flow ($U_0 = 0$), the viscosity just slightly reduces the instability of the sharp interface. However, the interface becomes stable if inequality (5.47) is satisfied.

When the sharp interface between two liquids is subjected to shear motion with the heavier liquid underlies a lighter one, both KHI amd HI instabilities may develop. The data of these type of instabilities are often presented by neutral curves. Here, we are not able to produce the neutral stability curves as the

interface is always unstable at short and long wavelengths. We will therefore conduct our analysis on data presented by the growth rates of modes similar to stationary liquids.

Figures 5.4 illustrates the effects of viscosity and shear motion. It is showing that both types of Kelvin-Helmholtz (KHI) and Holmboe (HI) instabilities develop if the sharp interface is subjected to shear motion. In the case of inviscid liquids, the KHI modes only develop at the interface as indicated in Figure 5.4 (a,b). However, the short wavelengths of KHI can be transformed into the Holmboe instability if the viscosity effect is introduced (Figure 5.5 (a,b)). Figures 5.5 (c,d) show the dependency of the KHI and HI on the values of the base velocity U_0. It is showing that the instability increases by increasing the value of velocity of the shear flow.

5.7 Conclusion

We reproduced the classical results for sharp interfaces separating two immiscible liquids through the use of the Laplacian approach and linear instability analysis. Gravity-capillary waves, Rayleigh-Taylor and Kelvin-Helmholtz instabilities were investigated.

The interface is always unconditionally unstable when the immiscible inviscid heavier liquid stands over the lighter one. The capillarity stabilises the modes that develop at short wavelengths. Also, the instability of the interface can be significantly reduced if the liquids are viscous. If the heavier liquid underlies the lighter one, the interface is always unconditionally stable with the development of gravity-capillary waves. The waves may decay monotonically if the liquids are viscous.

We also investigated the effect of shear motion on the instability of the sharp interface separating two superposed immiscible liquids. We found that the combination of Rayleigh-Taylor and Kelvin-Helmholtz instabilities leads to increasing the instability of the sharp interface, indicating that the induced vorticity waves can be enhanced by the effects of gravitational forces. These multiple effects make the effect of viscosity negligible. However, the capillary forces are able to

completely dampen the short wavelengths. The interface with an unconditionally stable configuration (in the no flow case) is no longer stable if it is subjected to shear motion. In this case, the interface is subjected to the Kelvin-Helmholtz instability. We found that the capillarity enhances the instability of the interface. Furthermore, it was shown that the Holmboe instability develops only in the case of viscous liquids. In particular, it was shown that Holmboe instability occurs at short wavelengths while the Kelvin-Helmholtz instability occurs at long wavelengths.

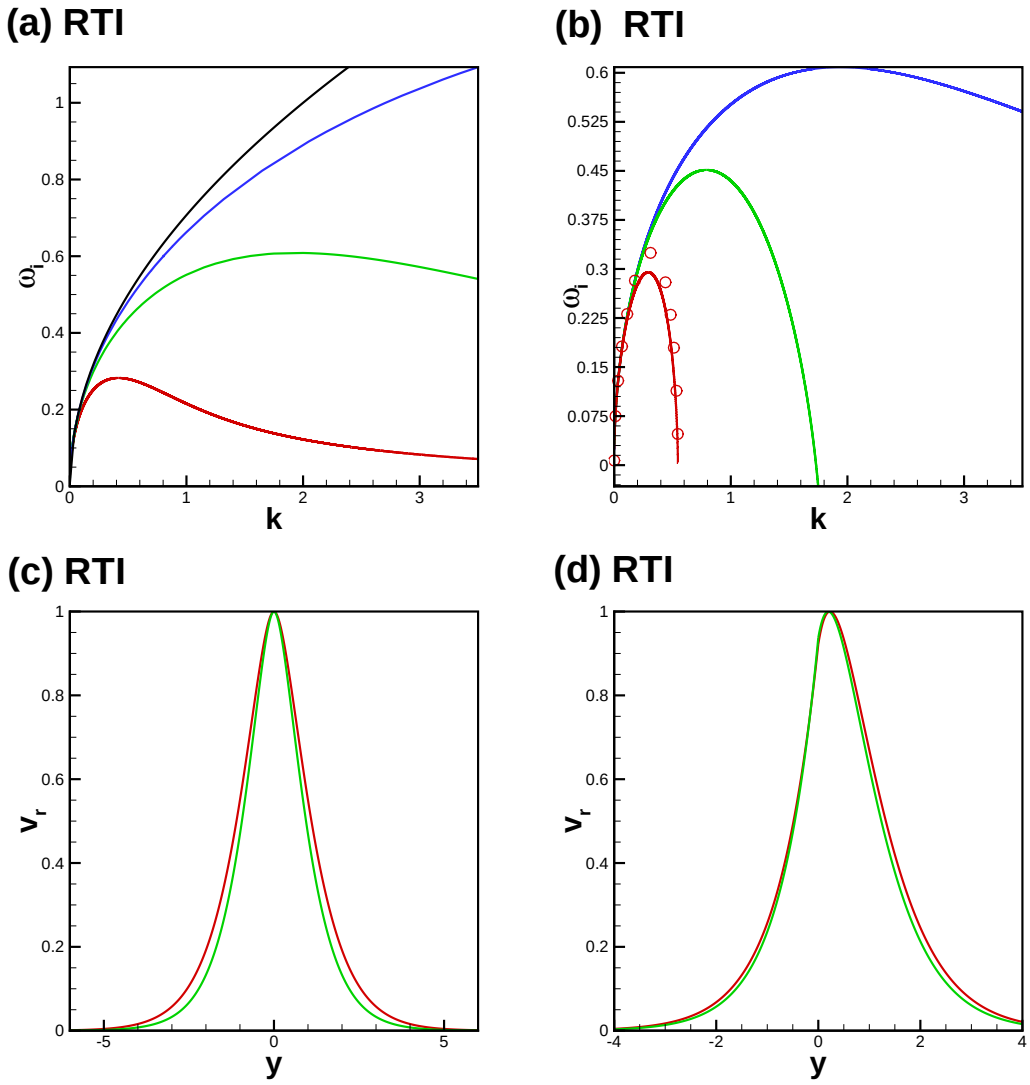

Figure 5.1: Dependence of growth rate ω_i on the wave number k for Rayleigh-Taylor instability (a) and (b). (a) the data is obtained for $Gr = -1$, $Ca = 0$ and different values of Re: $Re = \infty$ (black line), $Re = 100$ (blue line), $Re = 10$ (green line) and $Re = 1$ (red line). (b) data is obtained for $Gr = -1$, $Re = 10$ and different values of Ca: $Ca = 0$ (blue line), $Ca = 0.001$ (green line) and $Ca = 0.01$ (red line); the symbol $\circ$ presents the inviscid data. (c,d) the eigenfunctions of velocity v_r are plotted for $Gr = -1$ and $k = 1.5$ and (c) $Ca = 0$, $Re = 10$ with $\omega_i = 0.48$ (red line); and $Re = 1$ with $\omega_i = 0.14$ (green line). (d) $Re = 10$, $Ca = 0$ with $\omega_i = 0.16$ (green line) and $Ca = 0.001$ with $\omega_i = 0.041$ (red line). V_r is the real part of velocity.

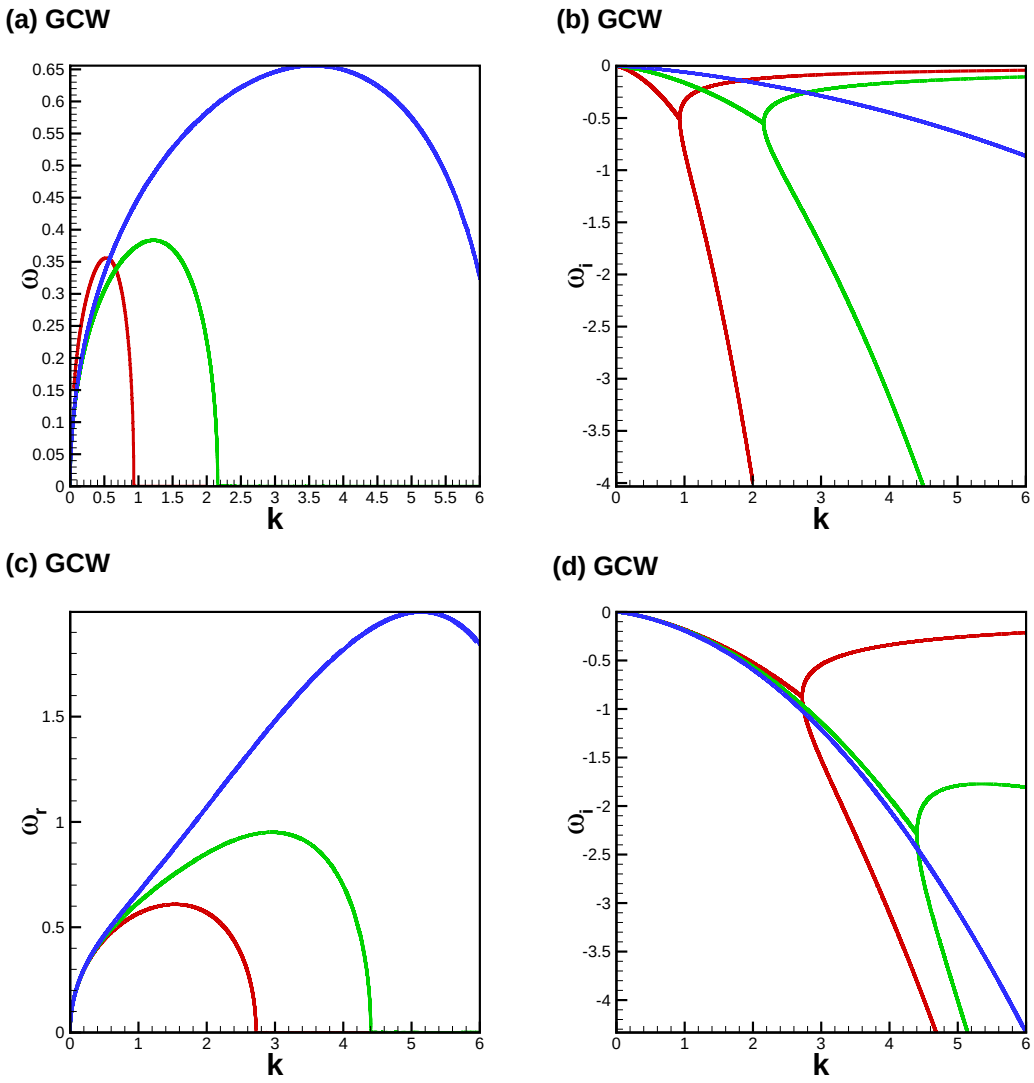

Figure 5.2: (a,b) dependence of ω on the wave number k for gravity-capillary waves (GCW) at immiscible sharp interface. The data are obtained for $Gr = 1$, $Ca = 0$ and different values of Re: $Re = 1$ (red line), $Re = 5$ (green line) and $Re = 25$ (blue line)). (c,d) data are obtained for $Re = 5$, $Gr = 1$ and different values of Ca: $Ca = 0$ (red line), $Ca = 0.0005$ (green line) and $Ca = 0.001$ (blue line).

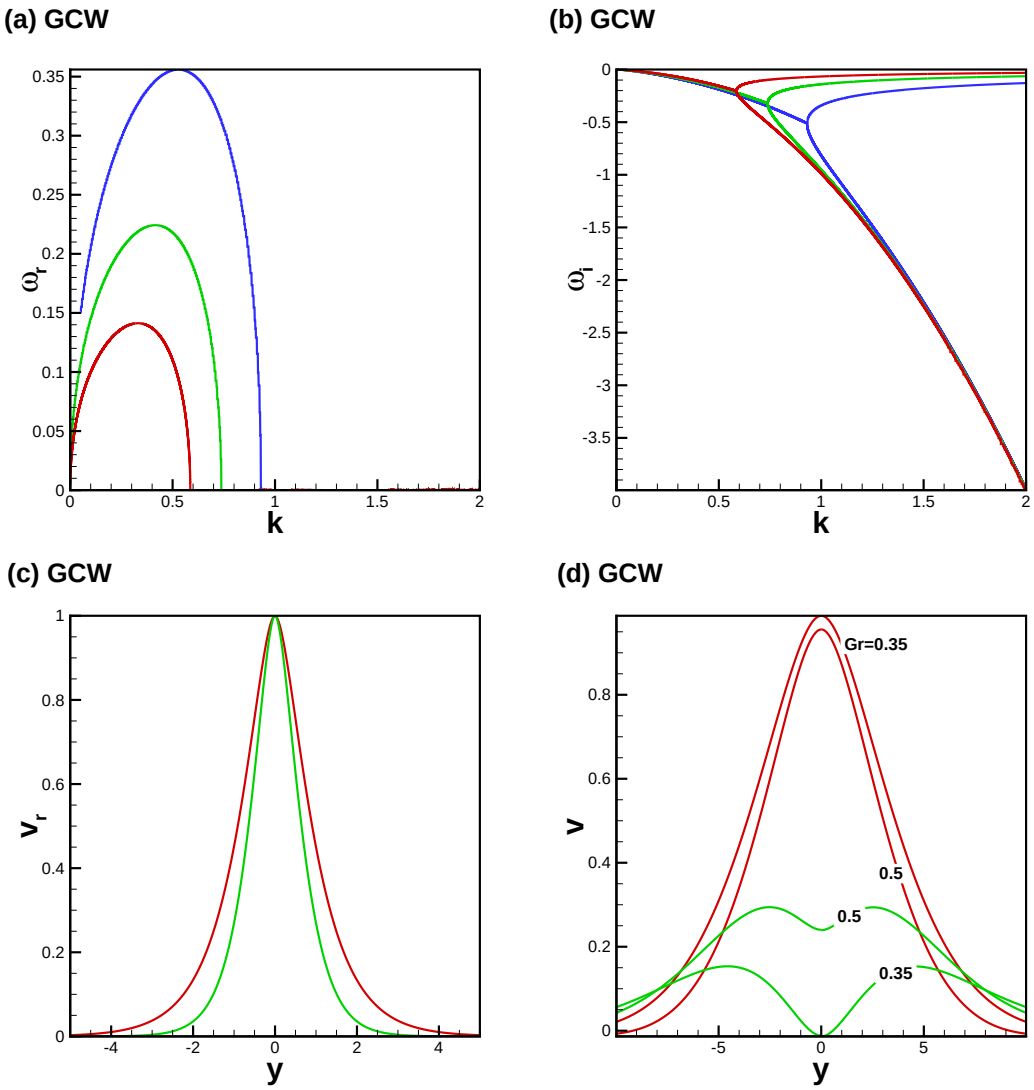

Figure 5.3: Dependence of ω on the wave number k for gravity-capillary waves (GCW) at immiscible sharp interface. (a,b) the data are obtained for $Re = 1$, $Ca = 0$ and different values of Gr: $Gr = 1$ (blue line), $Gr = 0.5$ (green) and $Gr = 0.25$ (red line). (c and d) the eigenfunctions of of gravity-capillary waves (GCW) developed at immiscible sharp interface. (c) profiles of creeping velocity v_{cr} (green line) with ($\omega_i = -0.60$) and viscous velocity v_{vis} with $\omega_i = -1.35$ (red line), the data is plotted for $Gr = -1$, $Re = 5$ and $k = 2.9$. (d) the profiles of the imaginary part v_i (red line) and real part v_r (green line) are plotted for $Re = 1$, $Ca = 0$, $k = 0.5$, the data is plotted for $Gr = -0.5$ with $\omega = (0.218, -0.17)$ and $Gr = -0.35$ with $\omega = (0.16, -0.162)$.

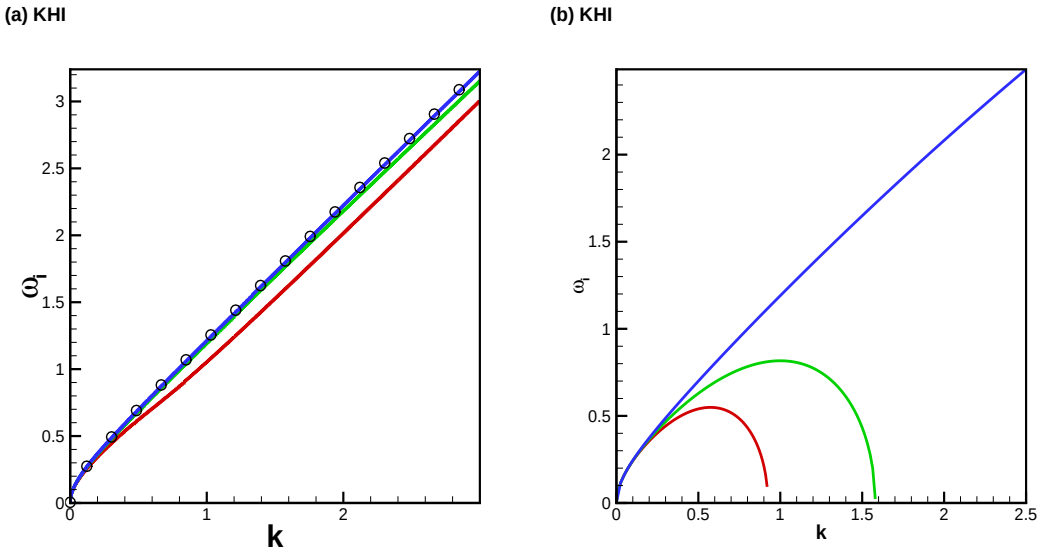

Figure 5.4: Dependence of ω_i on the wave number k for two immiscible liquids in relative shear motion, the lighter liquids underlies the heavier one (KHI and RTI are combined). (a) data is obtained for $Gr = -1$, $Ca = 0$, $U_0 = 1$ and different values of Re: $Re = 1$ (red line), $Re = 10$ (green line), $Re = 100$ (blue line) and $Re = \infty$ (symbol $\circ$). (b) curves are plotted for $Re = 10$, $Gr = -1$ and different values of Ca: $Ca = 0$ (blue line), $Ca = 0.005$ (green line) and $Ca = 0.01$ (red line).

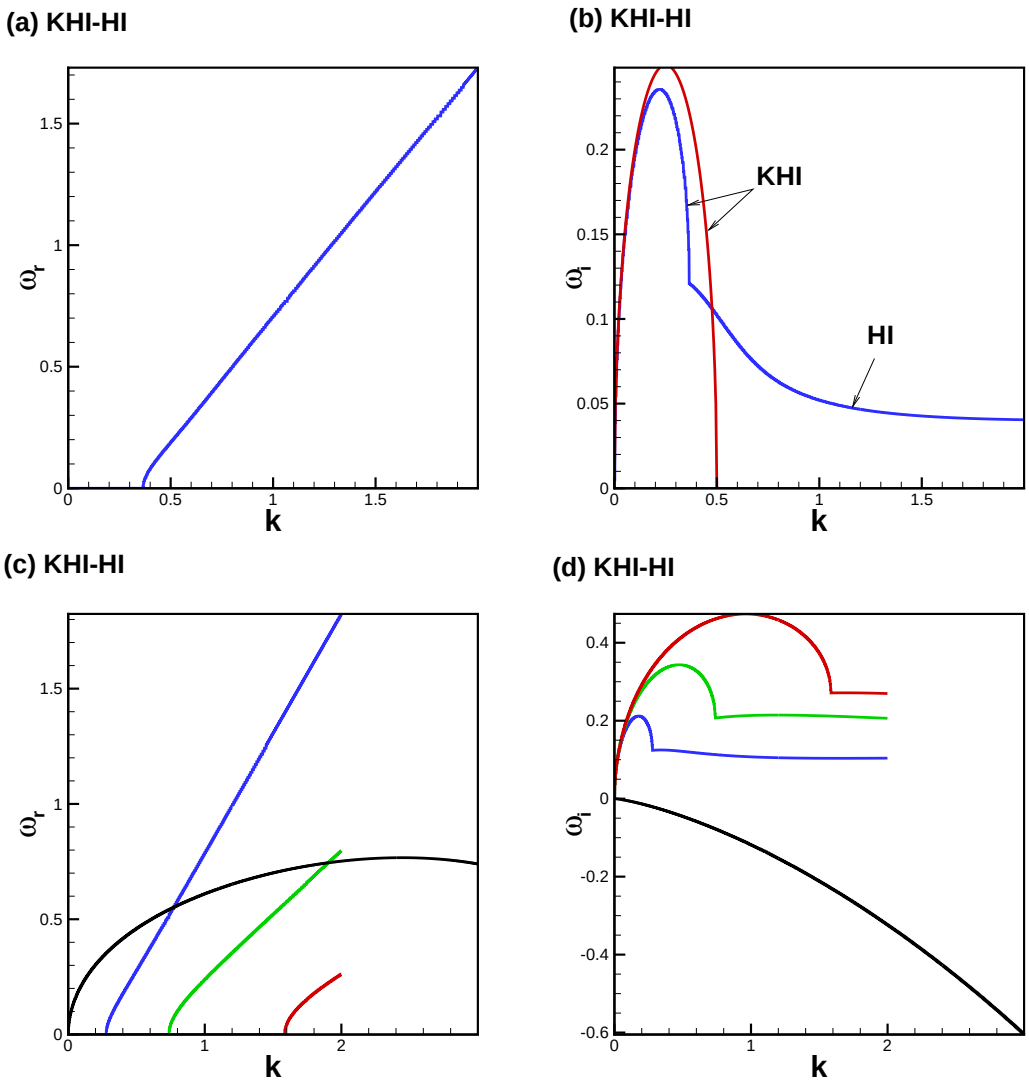

Figure 5.5: Dispersion relations for the Kelvin-Helmholtz and Holmboe instabilities develop at the sharp interface of a immiscible-viscous binary liquid. (a,b) data are obtained for $Ca = 0$, $Gr = 1$, $U_0 = 1$ and different values of Re: $Re = 100$ (blue line) and $Re = \infty$ (red line). (c,d) data is obtained for $Gr = 1$, $Re = 10$, $Ca = 0$ and different values of U_0: U_0=1 (red line), U_0=0.5 (green line), U_0=0.25 (blue line) and U_0=0 (black line).

Chapter 6

Stationary miscible liquids

The objective of this chapter is to study the evolution of an interface separating two miscible liquids, with base velocity of zero. The calculation of the data is based on the linearised governing equations developed in Chapter 3. For the purpose of validation, the case of immiscible liquids is firstly considered. Then, by removing the hydrodynamic terms, the pure thermodynamic stability is investigated. The last section is devoted to conduct a parametric analysis of miscible liquid-liquid interface through the RTI and GCW problems.

6.1 Immiscible interface of finite thickness subject to hydrodynamic effect

For two immiscible and viscous liquids, the amplitude equations (3.21)-(3.23) are reduced to the fourth order differential equation given by

$$-i\omega(\psi'' - k^2\psi) = \frac{1}{Re}(\psi^{iv} - 2k^2\psi'' + k^4\psi) - i\frac{k^2}{\omega}CaC_0'(2C_0''\psi' - C_0'(\psi'' - k^2\psi)) - i\frac{k^2}{\omega}GrC_0'\psi. \tag{6.1}$$

The numerical solution of equation (6.1) can be obtained using either ESM or CCM methods (see Chapter 4). At infinity ($L \sim \pm\infty$), the equation (6.1) is simplified to a fourth order differential equation with the following asymptotic

solutions

$$y \to -\infty : \quad \psi = A_1 \exp(ky) + A_3 \exp(qy), \tag{6.2}$$

$$y \to \infty : \quad \psi = A_2 \exp(-ky) + A_4 \exp(-qy), \tag{6.3}$$

where $q \equiv \sqrt{k^2 - i\omega Re}$.

Formulae (6.2) and (6.3) are used in the ESM method to initialize the integration as in Chapter 4. For immiscible inviscid liquids the equation (6.1) can be reduced into the following eigenvalue problem

$$\frac{d\mathbf{f}}{dy} = \begin{pmatrix} 0 & 1 \\ A_{21} & A_{22} \end{pmatrix} \mathbf{f} \tag{6.4}$$

where $\mathbf{f} = (\psi_0, \psi_1)^T = (\psi, \psi')^T$, and the elements of the matrix are

$$A_{21} = k^2(1 - iGrC_0'/(\omega^2 - k^2 CaC_0^{2'})),$$
$$A_{22} = -ik^2 CaC_0'/(\omega^2 - k^2 CaC_0^{2'}).$$

In order to ensure that the current results are accurate and reliable, both ESM and CCM methods are used in the calculation of eigenvalues. Then, the eigenvalue problem generated by the CCM method is given by

$$\begin{pmatrix} (D^{(4)} - 2k^2 G^{(2)} + k^4)/Re & B - iGrkI \\ -iC_0' kI & Z \end{pmatrix} V = i\omega \begin{pmatrix} Re(D^{(2)} - k^2 I) & Z \\ Z & I \end{pmatrix} V. \tag{6.5}$$

Here $B \equiv -iCak[(D^{(2)} - k^2 I)C_0' - C_0''' I$, where $D^{(2)} = m^2 G^{(2)} + m' G^{(1)}$ and $D^{(4)} = D^{(2)} D^{(2)}$ are the second and fourth order derivatives respectively, $G^{(1)}$ and $G^{(2)}$ are given in Chapter 4 by the expressions (4.37) and (4.40). Also, Z and I are the zero and identity matrices, ω is the eigenvalue and eigenfunctions are given by the vector $V = (\psi_1, ..., \psi_N, c_1, ..., c_N)^T$.

Exploring the ESM method, the integrations of the system of equations (6.4) are initiated from each boundary and carried out towards the middle of the domain. The conditions of the linear independency of the equation $D(Re, Gr, Ca, k, \omega) = 0$ presents the eigenvalue problem. For particular values of the parameters Re,

Gr, and Ca the eigenvalues ω are determined against the values of the wavenumber k through using the the root finding Muller's method. When using the CCM method, the eigenvalues and eigenfunctions can be obtained in straightforward manner through the QR algorithm.

For validation, the numerical results are compared against the analytical expressions (5.31) and (5.42) developed in Chapter 5. They define the dispersion relations for both the RTI and GCW problems according to the sign of the Grashof number. For $Gr > 0$, with a heavier liquid underlying a lighter one, $\rho_1 > \rho_2$, which, with small amplitude perturbations, stimulates the development of the gravity-capillary waves (GCW).

In pure gravity waves and inviscid liquids, the eigenvalues ω are purely real. This indicates that the gravity waves are stable and propagating with the frequency ω_r/k. Since $\omega_i = 0$, the waves do not grow or decay. In immiscible viscous liquids, the eigenvalue ω is complex, defining oscillatory decaying gravity waves. The aperiodic decaying modes defined by purely imaginary negative eigenvalues ω_i exist at some wave numbers corresponding to $\omega_r = 0$.

In the opposite case, $Gr < 0$, the interface is subject to the Rayleigh-Taylor instability (RTI) in which the eigenvalues ω are always purely positive imaginary, indicating that the perturbations are monotonically growing. The viscous force can be stabilising.

The numerical data for the Rayleigh-Taylor instability, obtained on the basis of the current phase-field approach, is plotted in Figure 6.1 for the interfaces separating two inviscid (Figure 6.1 (a-d)) and two viscous liquids (Figure 6.2 (a,c)). The results are shown against the curves obtained from the classical formulae (5.31) and (5.42). All classical observations for the Rayleigh-Taylor instability can be reproduced. In particular, we observe that the amplitudes of all modes grow monotonically. The growth rates are lower for more diffuse interfaces (Figures 6.1 (a) and 6.2 (a)). The capillary forces dampen the development of the short-wavelength modes, which is illustrated by Figure 6.1 (b). The surface tension effect reduces the range of the unstable modes by the cut-off value $k_c = \sqrt{3\delta Gr/Ca}$.

Dependencies on the interface thickness differ for the cases of zero and non-zero capillary numbers. If the capillary forces can be disregarded, i.e. $Ca = 0$,

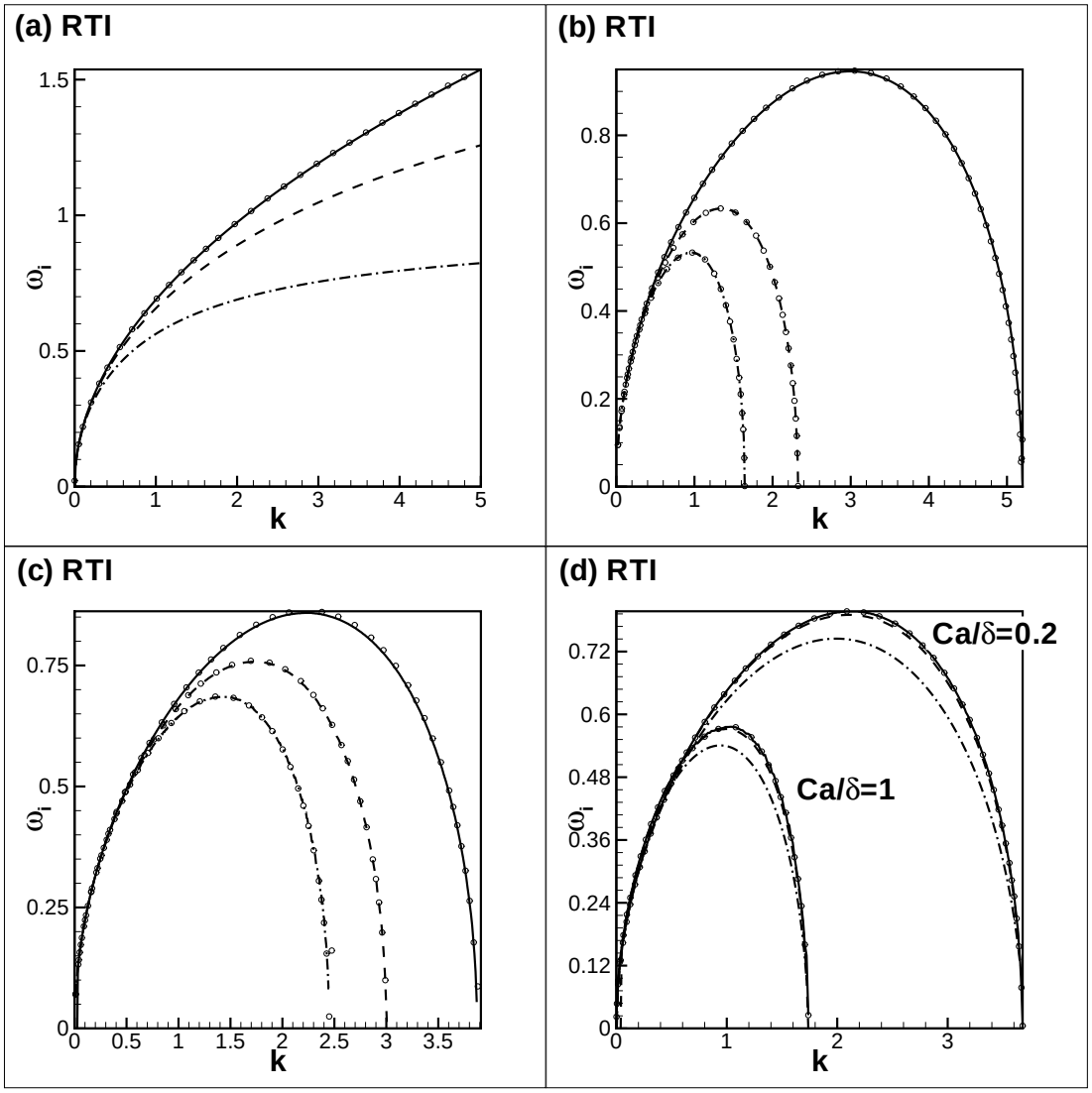

Figure 6.1: Rayleigh-Taylor instability at an immiscible interface. The growth rate ω_i versus the wavenumber k is shown for $Gr = -1$, and (a) $Ca = 0$ and various interface thicknesses: $\delta = 0.5$ (dash-dot line), $\delta = 0.1$ (dash line), $\delta = 0.001$(solid line). (b) $\delta = 0.001$ and various capillary numbers: $Ca = 0.001$ (dash-dot line), $Ca = 0.0005$ (dashed line), $Ca = 0.0001$ (solid line). (c) $Ca = 0.005$ and various δ: $\delta = 0.001$ (dash-dot line), $\delta = 0.0015$ (dash line), $\delta = 0.0025$ (solid line). (d) various Ca and δ under constant ratio; for the ration $Ca/\delta = 0.2$: $Ca = 10^{-4}$ and $\delta = 5 \cdot 10^{-4}$ (solid line), $Ca = 0.001$ and $\delta = 0.005$ (dash line), and $Ca = 0.01$ and $\delta = 0.05$ (dash-dot line); while for the ratio $Ca/\delta = 1$: $Ca = \delta = 0.001$ (solid line), $Ca = \delta = 0.01$ (dash line), $Ca = \delta = 0.1$ (dash-dot line). (a-d) depict inviscid results. Symbol '$\circ$' refers to the sharp-interface results.

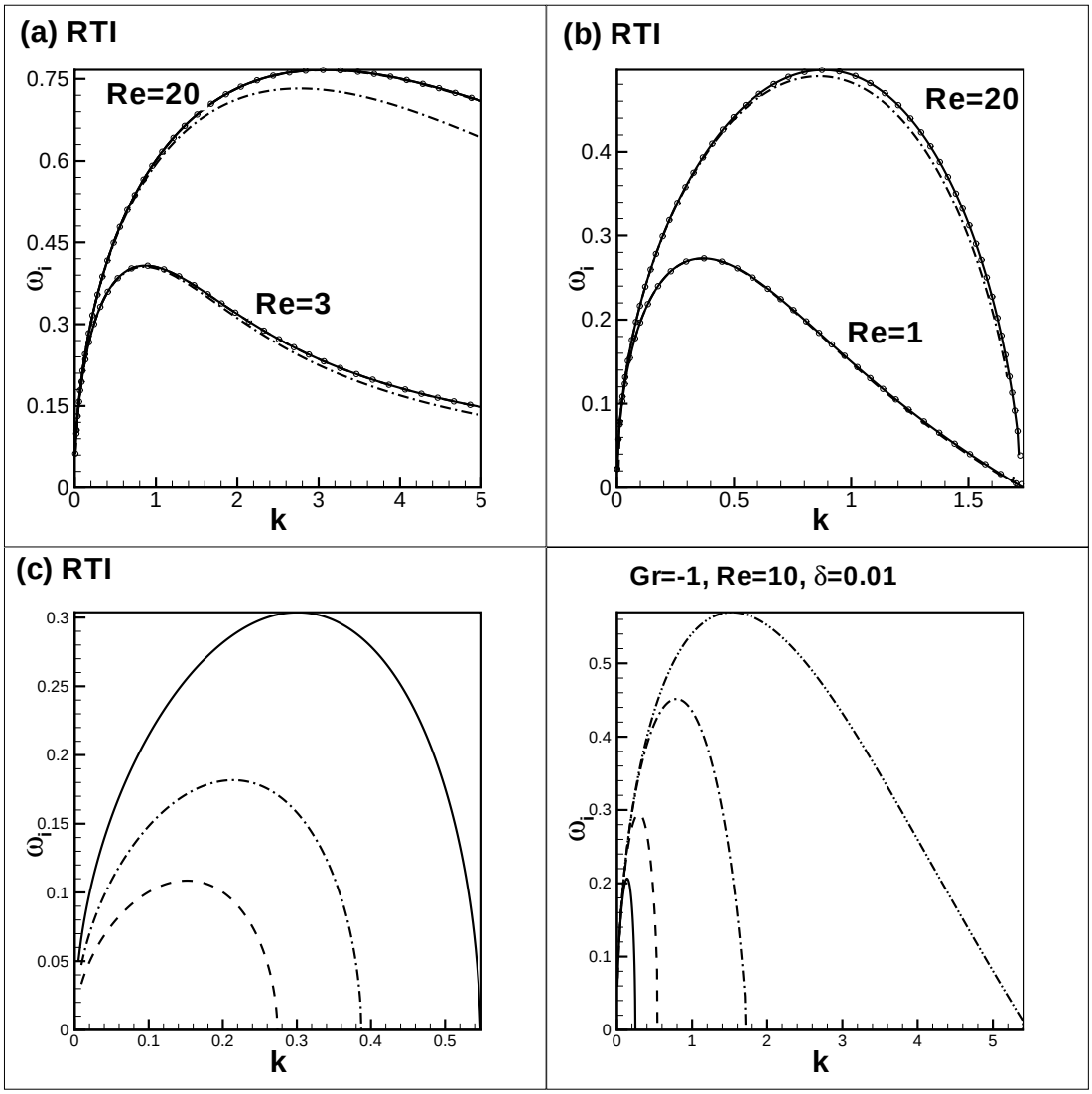

Figure 6.2: Rayleigh-Taylor instability (RTI) at an immiscible interface, the growth rate ω_i versus the wavenumber k is shown (a-c). (a) $Gr = -1$, $Re = 3$, $Re = 20$, $Ca = 0$ and different values of δ: $\delta = 0.1$ (dash-dot line); $\delta = 0.01$ (dash line), $\delta = 0.001$ (solid line). (b) $Gr = -1$, $Re = 1$, $Re = 20$ and different Ca and δ under constant ratio $Ca/\delta = 1$: $Ca = \delta = 0.1$ (dash-dot line), $Ca = \delta = 0.01$ (dash line), $Ca = \delta = 0.001$ (solid line). (c) $Re = 10$, $Ca = 0.01$, $\delta = 0.01$ and different values of Gr: $Gr = -0.25$ (dash line), $Gr = -0.5$ (dash-dot line), $Gr = -1$ (solid line). (d) $Re = 10$, $\delta = 0.01$ $Gr = -1$ and different values of Ca: $Ca = 0.5$ (solid line), $Ca = 0.1$ (dash line), $Ca = 0.01$ (dash-dot line) and $Ca = 0.001$ (dash-dot-dot line).

the curves obtained for the gradually decreasing values of the interface thickness converge to the sharp-interface results (Figure 6.1 (a)). When $Ca \neq 0$, i.e. the capillary effects are taken into account, a sole reduction of the interface thickness does not produce the behaviour of a sharp interface. This can be easily explained by the fact that the surface tension is defined as the ratio between the capillary number and the interface thickness as defined in the equation (3.4). Hence by decreasing the interface thickness, the capillary effect is also increased, which is revealed by stronger dampening of the short-wavelength modes (Figure 6.1 (c)). In order to obtain the sharp-interface behaviour, the capillary number and the interface thickness must be simultaneously decreased, which is done in Figures 6.1 (d) and 6.2 (b).

The dependence of the Rayleigh-Taylor instability (RTI) on Grashof number is shown in Figure 6.2 (c). As expected, when $Gr < 0$ (where a heavier liquid stands over lighter one), the instability of the phase boundary decreases if $Gr \to 0$, such that no instability appears if $Gr = 0$. For a fixed value of sharp thickness, Figure 6.2 (d) shows the effect of the capillarity on the RTI modes, where for strong capillarity the instability of sharp interface disappears.

For the gravity-capillary waves (GCW) developing at an interface separating two viscous liquids both real and imaginary parts of ω are different from zero as shown in Figure 6.3. Again, all classical properties of the gravity-capillary waves can be reproduced. It can be shown that in the inviscid limit the phase speed is proportional to $k^{-1/2}$, i.e. longer modes propagate faster. The waves are dampened by the viscous effect: some modes start dissipating monotonically (with appearance of the creeping and viscous modes, totally similar to the waves at a sharp interface [26]), and hence they lose their wave-like behaviour. One also sees that the capillarity primarily affects the development of the modes with shorter wavelengths.

Figure 6.4 depicts the eigenfunctions, i.e. the streamfunction profiles for the Rayleigh-Taylor instability and gravity-capillary waves. In the case of the Rayleigh-Taylor instability, the streamfunction is always purely real, and in the case of the waves, the eigenfunction is real in the inviscid case and has both real and imaginary parts in the viscous case. The streamfunctions are continuous, but their derivatives are discontinuous if the viscous effect is not considered. In the

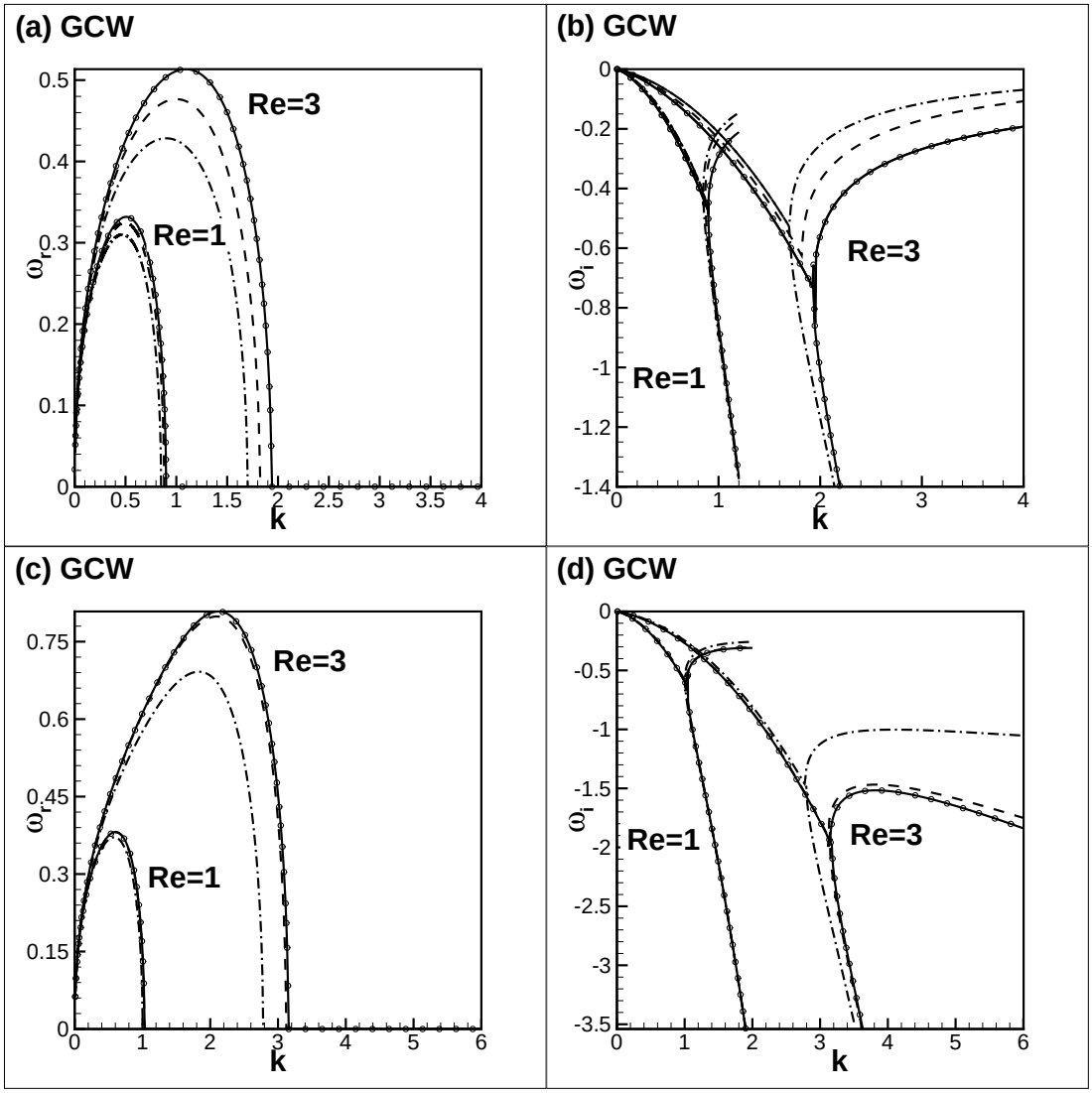

Figure 6.3: Gravity-capillary waves at an immiscible interface. The real and imaginary parts of the frequency ω versus the wavenumber k are shown for $Gr = 0.9$ and $Re = 1$ and $Re = 3$, and (a,b) $Ca = 0$ and various interface thicknesses: $\delta = 1$ (dash-dot line), $\delta = 0.5$ (dash line), and $\delta = 0.01$ (solid line). (c,d) for a constant ratio $Ca/\delta = 1$: $Ca = \delta = 0.5$ (dash-dot line), $Ca = \delta = 0.1$ (dash line), and $Ca = \delta = 0.01$ (solid line). Symbol '$\circ$' marks the sharp-interface results.

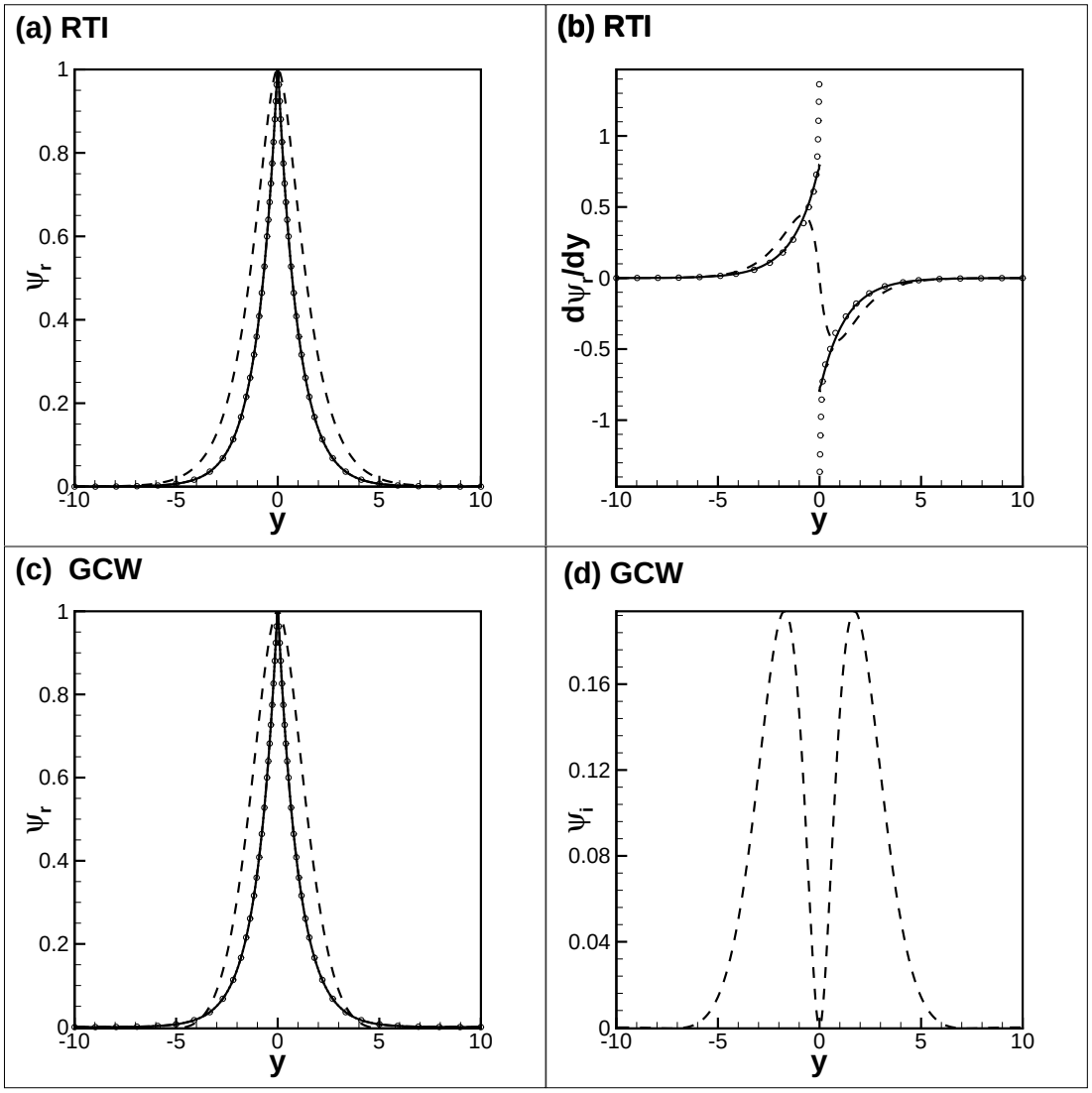

Figure 6.4: Typical shapes of perturbations (eigenfunctions) induced at an immiscible interface at $k = 1$. (a,b) The real parts of the streamfunction and their first derivative are shown for the Rayleigh-Taylor instability (the imaginary part of the streamfunction is zero in this case). For $Ca = 0$, the growth rate is 0.740 (inviscid mode) and 0.405 (viscous mode); for $Ca = 0.05$, the growth rate is 0.630 (inviscid case). (c,d) The real (c) and imaginary (d) parts of the streamfunction are plotted for the gravity waves. For $Ca = 0$, the eigenvalue is $\omega = (0, -0.74)$ (inviscid case) and $\omega = (0.511, -0.256)$ (viscous case); for $Ca = 0.05$, the eigenvalue is $\omega = (0, -0.630)$ (inviscid case). The eigenfunctions are plotted for $Gr = \pm 1$, $\delta = 0.01$, $Ca = 0$ for inviscid (solid lines) and viscous ($Re = 3$, dash lines) cases, and another eigenfunction for $Ca = 0.05$, inviscid case is marked by '$\circ$' symbols.

viscous case, both streamfunction and derivative are continuous. One can also note that the thickness of the eigenfunction is of the order of 10, independent of to the thickness of the interface (which is 0.01 for the shown results), and is only slightly different for the inviscid and viscous cases. The eigenfunction profiles do not depend on the value of the capillary number.

We wish now to discuss the applicability of the phase-field approach. The interface is smeared and the new length scale, the interface thickness δ, is introduced within this approach. Nevertheless, the thickness of a real phase boundary is usually very small, just several molecular layers, and hence the limit of a sharp-interface is of paramount importance for the results of the phase-field theory. We found that perfect agreement between the results obtained for the diffusive and sharp interfaces is restricted by the inequality $k\delta << 1$. In Figure 6.1 (a), the numerical data obtained for the diffuse interfaces and the analytical data for a sharp boundary coincide while the wavenumber remains small, and such a matching deteriorates for larger k. For thin interfaces, e.g. with $\delta = 0.001$, the numerical results closely follow the analytical curve. However, this remains true only within the shown range of the wavenumbers.

In order to obtain accurate results with the use of the phase-field approach, the interface thickness δ should be smaller than all other length scales, including the wavelength of perturbations $\lambda = 2\pi/k$, which one cannot guarantee for arbitrary perturbations. The surface tension and viscous effects introduce the cut-off wavenumber, k_c, limiting the range of the unstable modes in the case of the Rayleigh-Taylor instability and the range of the modes with the periodic wave-like behaviour in the case of the gravity-capillary waves. In this case, the condition on δ becomes $k_c\delta << 1$, and the accurate eigenvalue spectra may be obtained for interface thicknesses of order $\delta \sim 0.1 \div 0.01$.

6.2 Thermodynamic stability of an interface separating two liquids

We now consider the opposite situation neglecting hydrodynamic flows and hence with the mass transfer driven purely by diffusion. The full set of amplitude equa-

tions (3.19)-(3.21) is reduced to an equation written in terms of the concentration field,

$$Ca\hat{C}^{iv} - \left(D_0 + 2Cak^2\right)\hat{C}'' - 2D_0'\hat{C}' + \left(k^2\left(D_0 + Cak^2\right) - D_0'' - i\omega Pe\right)\hat{C} = 0, \tag{6.6}$$

where $D_0 \equiv 2A+12C_0^2$ is the diffusion coefficient. When $y \to \pm\infty$, the asymptotic solutions of this equation are given by

$$y = -\infty : \quad \hat{C} = A_1 \exp(q_1 y) + A_3 \exp(q_2 y), \tag{6.7}$$

$$y = \infty : \quad \hat{C} = A_2 \exp(-q_1 y) + A_4 \exp(-q_2 y), \tag{6.8}$$

where

$$q_1 = \sqrt{0.5(k^2 + D_1/Ca) - 0.5\sqrt{D_1^2/Ca^2 + 4iPe\,\omega/Ca}}, \tag{6.9}$$

$$q_2 = \sqrt{0.5(k^2 + D_1/Ca) + 0.5\sqrt{D_1^2/Ca^2 + 4iPe\,\omega/Ca}}, \tag{6.10}$$

with $D_1 = 2A + 3$ being the diffusion coefficient for $y \to \pm\infty$. The above asymptotic solution are used to determine the boundary conditions used with the system of first order differential equations given by

$$\hat{\mathbf{C}}' = \begin{pmatrix} 0 & 1 & 0 & 0 \\ 0 & 0 & 1 & 0 \\ 0 & 0 & 0 & 1 \\ A_{41} & A_{42} & A_{A3} & 0 \end{pmatrix} \hat{\mathbf{C}} \tag{6.11}$$

where $\hat{\mathbf{C}} = (\hat{C}_0, \hat{C}_1, \hat{C}_2, \hat{C}_3)^T = (\hat{C}, \hat{C}', \hat{C}'', \hat{C}''')^T$ and

$$A_{4,3} = D_0/Ca + 2k^2, \quad A_{4,2} = 2D_0'/Ca,$$
$$A_{4,1} = [k^2(D_0 + Cak^2) - D_0'' - iPe\,\omega]/Ca.$$

The system solved in CCM method is

$$CaD^{(4)} - (D_0 + 2k^2)D^{(2)} - 2D_0'D^{(1)} + [k^2(D_0 + Cak^2 - D_0'']I = \lambda PeI, \quad (6.12)$$

where $D^{(1)} = \frac{d\hat{C}}{dy}$, $D^{(2)} = \frac{d^2\hat{C}}{dy^2}$, $D^{(4)} = \frac{d^4\hat{C}}{dy^4}$, where the scaled expressions are given in Chapter 4, and the diffusion coefficient is $D_0 = 2A + 12C_0^2$.

We use the equation (6.11) or (6.12), which are respectively corresponding to the ESM and CCM, to investigate the linear instability of a heterogeneous miscible system with respect to thermodynamic perturbations.

The results of the numerical solution of eigenvalue problem (6.6) are depicted in Figures 6.5 and 6.6. All eigenvalues were found to be purely imaginary. We note that the interface is always stable (all normal perturbations decay) for $A > 0$. The stability is increased (the decay rates grow) for greater values of A and smaller thicknesses δ. If however $A < 0$, the layer may be either stable or unstable which is determined by the interface thickness. Namely, all perturbations monotonically decay if the interface thickness is less than or equal to the equilibrium value, $\delta \leq \delta_0$, but the long wavelength instability is observed if the interface thickness is greater than δ_0, which is illustrated in Figure 6.5 (a). We also confirmed that when $\delta = \delta_0$, the decay rate follows the k^3 dependence for small values of k (and one sees that for $\delta < \delta_0$ the decay rate changes even faster). The effect of the capillarity on the growth rates is shown in Figure 6.5 (b), where one sees that the modes with long wavelengths remain virtually unaffected, but the modes with shorter wavelengths decay faster if the value of Ca is larger.

The instability decreases as the values of A approach the critical point, so there is no instability observed for $A \geq 0$. On the other hand, one may note that the instability of the interface is reduced dramatically for $\delta > \delta_0$ and $Ca \neq 0$. In particular, the short wavelengths can be completely cut-off (Figure 6.6 (a)).

One can also note, that the results in Figures 6.5 and 6.6 are plotted in terms of the product $\omega_i Pe$, and hence the decay/growth rates of pure thermodynamic perturbations would be rather small for larger Pe numbers.

Figures 6.5 (c,d) depict the typical shapes of the eigenfunctions, $C_r(z)$ (the imaginary part was found to be zero). The eigenfunctions shown are normalized by their maximum values, located in the middle of the layer. Figure 6.5 (c) shows

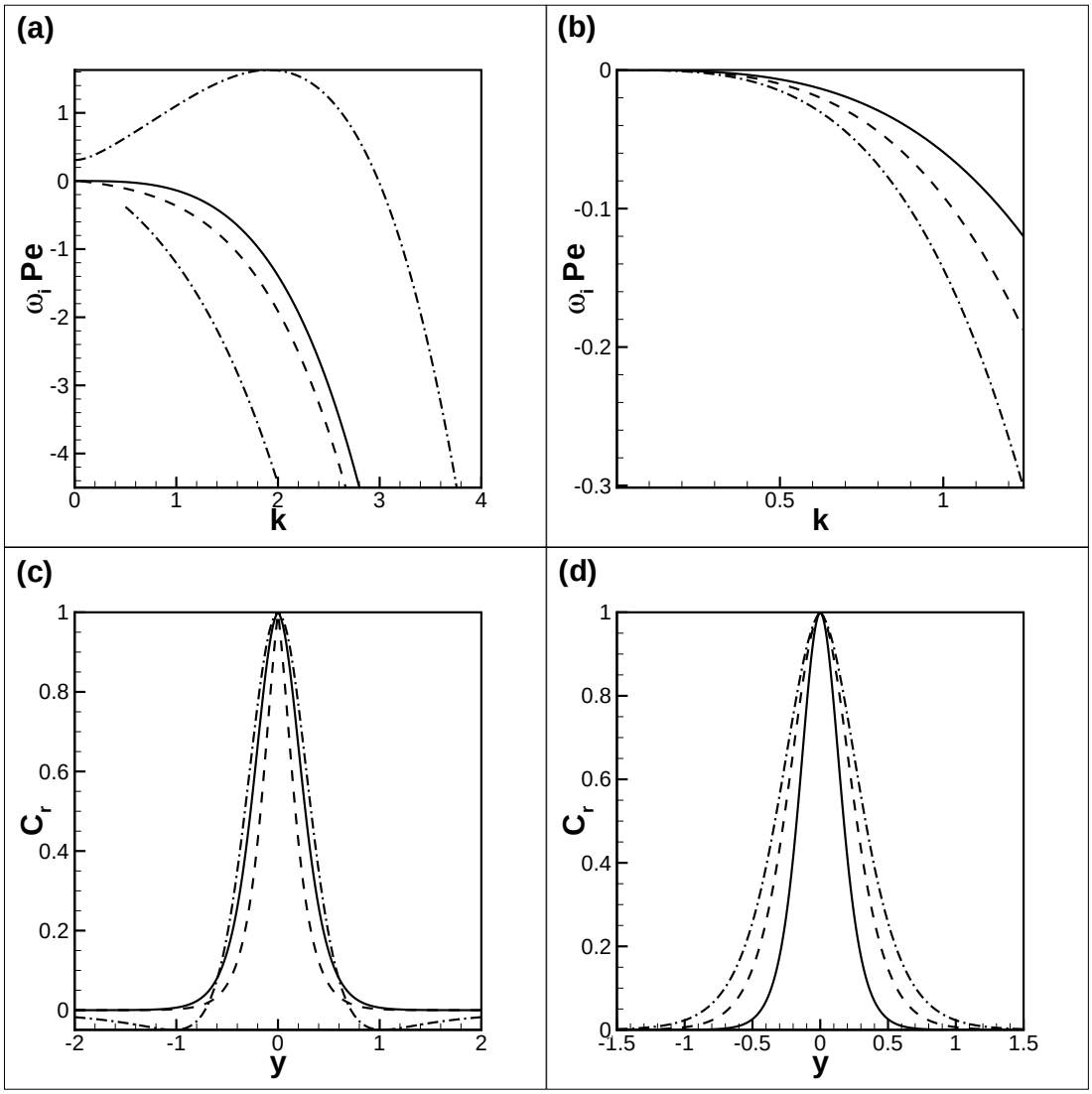

Figure 6.5: (a-b) Eigenspectra are plotted for interfaces subject to thermodynamic disturbances. (a) $Ca = 0.05$, $A = -0.5$, and various δ: $\delta = \delta_0 = 0.316$ (solid line); $\delta = 2\delta_0$ (dash-dot-dot line), $0.8\delta_0$ (dash line), $0.6\delta_0$ (dash-dot line). (b) $A = -0.4$, $\delta = \delta_0$ and various Ca: $Ca = 0.07$ (dash-dot line), 0.035 (dash line), and 0.01 (solid line). (c,d) Eigenfunctions are plotted for $k = 1$, $A = -0.5$, (c) $Ca = 0.05$ and various δ: $\delta = 2\delta_0$ (dash-dot line) ($\omega_i = 0.633$), $\delta = \delta_0$ (solid line) ($\omega_i = -0.155$), and $\delta = 0.5\delta_0$ (dash line) ($\omega_i = -0.436$)). (d) $\delta = \delta_0$ and various Ca: $Ca = 0.02$ (solid line) ($\omega_i = -0.186$), $Ca = 0.05$ (dash line) ($\omega_i = -0.079$), and $Ca = 0.08$ (dash-dot line) ($\omega_i = -0.053$)). All eigenfunctions in (e,f) are purely real and normalized by their maximum values.

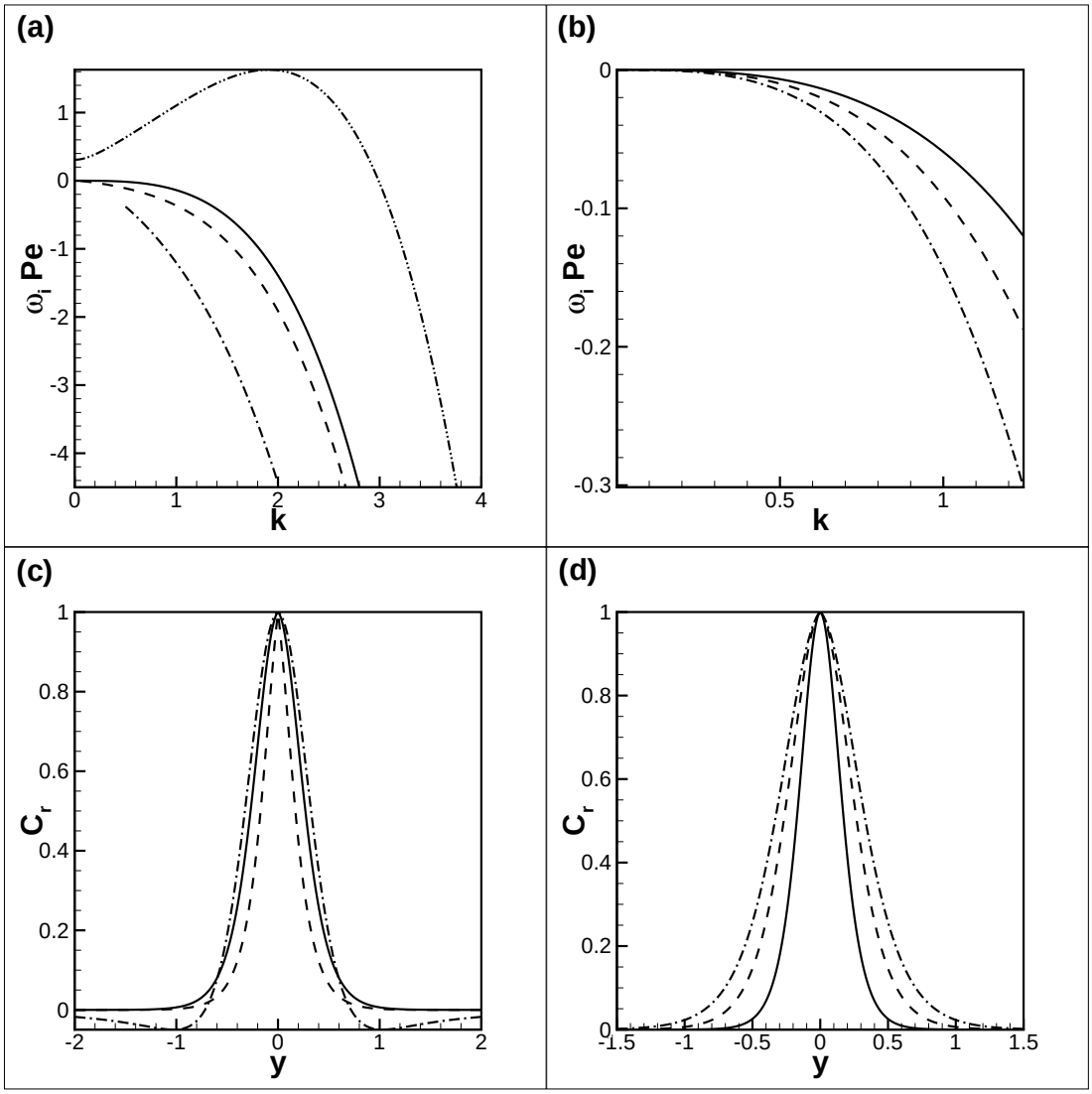

Figure 6.6: (a-c) Eigenspectra are plotted for interfaces subject to thermodynamic disturbances. (a) data obtained for $\delta = 1.25\delta_0$, $A = -0.5$ and various Ca: $Ca = 0.001$ (solid line), $Ca = 0.01$ (dash line) and $Ca = 0.1$ (dash-dot line). (b) the curves plotted for $Ca = 0.05$, $\delta = 1$ and various $A > 0$: $A = 0.5$ (solid line), $A = 0.3$ (dash line), and $A = 0.1$ (dash-dot line); and for $\delta = 0.5$: $A = 0.5$ (solid line with symbols) and $A = 0.3$ (dash line with symbols). (c) $\delta = \delta_0$, $Ca = 0.05$, and various $A < 0$: $A = -0.1$ (dash-dot line), $A = -0.3$ (dash line), $A = -0.5$ (solid line) and thick solid line represents $-k^3$ curve).

the eigenfunctions for $A < 0$. One sees that the thickness of the eigenfunction diminishes for smaller values of δ. The widths of the eigenfunction depicted in Figure 6.5 (d) are considerably smaller (by an order) compared to the widths of the purely hydrodynamic modes shown in Figure 6.4. One can also notice in Figure 6.5 (d) that the widths of the eigenfunctions depicted in Figure 6.5 (d) diminishes if Ca becomes smaller.

6.3 Stability of a miscible interface subject to both thermo- and hydrodynamic perturbations

Here the objective is to show how to calculate eigenvalues using the boundary value problem that was presented in Chapter 3 and given by equations (3.23), (3.24) and (3.25). We are dealing with higher order differential equations which are dependent on various parameters that might make them stiff to solve if one uses the ESM method. In order to understand how diffusivity and capillarity affect the behaviour of the interface, we conduct a parametric study in which the order of the differential equations can be reduced according to the considered case. In the case of inviscid miscible liquids and neglecting the effect of capillarity, we solve the fourth order differential equation as shown in Appendix C. 3. If however the capillarity effect is not neglected, we solve the sixth order differential equation (more details of which are presented in Appendix C. 4). In the case of viscous miscible liquids neglecting the effect of capillarity, we solve the sixth order differential equations that are presented in Appendix C. 5. However, when accounting for capillarity we solve the eighth order differential equations, which is presented in the current section.

When using the ESM method, parametrization is required because the full boundary value problem cannot be used. In this case we just consider very large values for Re and sufficiently small values for Ca in order to obtain the eigenvalues of the case of miscible inviscid liquids without accounting for capillarity. It was found that the ESM method is unable to produce results for sufficiently large

Re and small Ca. In particular, if $Ca \to 0$ the characteristic roots presented by equations (6.9) and (6.10) tend to $\pm\infty$, the asymptotic solutions also tend to ∞, which deteriorates the boundary conditions that are required for the perturbations to decay at ∞. Meanwhile, when using CCM, the reduction of the order of the full boundary problem is not needed as collocation methods are reliable in solving stiff problems. In this section we use the eigenvalue problem (6.12).

Following the steps used for the ESM method in Chapter 4, we show how the eigenvalues can be generally obtained by solving the full boundary problem, which is presented by equations (3.23), (3.24) and (3.25).

At $y \to \pm\infty$, the asymptotic solutions are used to define the boundary conditions used to initialize the system of the first order differential equations

$$\mathbf{f}' = A\mathbf{f} \tag{6.13}$$

where $\mathbf{f} = (f_0, f_1, f_2, f_3, f_4, f_5, f_6, f_7)^T = (\psi, \psi', \psi'', \psi''', \hat{C}, \hat{C}', \hat{C}'', \hat{C}''')^T$ and

$$A = \begin{pmatrix} 0 & 1 & 0 & 0 & 0 & 0 & 0 & 0 \\ 0 & 0 & 1 & 0 & 0 & 0 & 0 & 0 \\ 0 & 0 & 0 & 1 & 0 & 0 & 0 & 0 \\ A_{41} & 0 & A_{43} & 0 & A_{45} & 0 & A_{47} & 0 \\ 0 & 0 & 0 & 0 & 0 & 1 & 0 & 0 \\ 0 & 0 & 0 & 0 & 0 & 0 & 1 & 0 \\ 0 & 0 & 0 & 0 & 0 & 0 & 0 & 1 \\ A_{81} & 0 & 0 & 0 & A_{85} & A_{86} & A_{87} & 0 \end{pmatrix},$$

with the following elements

$$A_{41} = -k^2(k^2 - iRe\omega), \quad A_{43} = 2k^2 - iRe\omega, \quad A_{45} = ikCaReC_0',$$
$$A_{47} = ikRe(Gr - Ca(C''' - k^2C_0')), \quad A_{81} = \frac{iPekC_0'}{Ca},$$
$$A_{85} = \frac{D_0'' - k^2D_0 - k^4Ca + iPe\omega}{Ca}, \quad A_{86} = 2D_0'/Ca, \quad A_{87} = \frac{2k^2Ca + D_0}{Ca}.$$

The boundary conditions are given by

$$\begin{aligned}
\mathbf{f}_1 &= (1, \pm k, k^2, \pm k^3, 0, 0, 0, 0)^T \exp(\pm ky), \\
\mathbf{f}_2 &= (1, \pm q, q^2, \pm q^3, 0, 0, 0, 0)^T \exp(\pm ky), \\
\mathbf{f}_3 &= (\beta_1, \pm\beta_1 q_1, \beta_1 q_1^2, \pm\beta_1 q_1^3, 1, \pm q_1, q_1^2, \pm q_1^3)^T \exp(\pm q_1 y), \\
\mathbf{f}_4 &= (\beta_2, \pm\beta_2 q_2, \beta_2 q_2^2, \pm\beta_2 q_2^3, 1, \pm q_2, q_2^2, \pm q_2^3)^T \exp(\pm q_2 y),
\end{aligned}$$

where q_1 and q_2 are given by the equations (6.9) and (6.10) respectively and

$$\beta_{1,2} = -\frac{ikGrRe}{(q_{1,2}^2 - q^2)(q_{1,2}^2 - k^2)}. \tag{6.14}$$

6.3.1 Rayleigh-Taylor instability

Here, we investigate the simultaneous action of the small hydro- and thermodynamic perturbations on the stability of an interface, where the eigenvalues were obtained using both ESM and CCM methods.

We saw in Section 6.1 that the sharp interface behaviour could be revealed by simple gradual reduction of the interface thickness. In addition we found that the unstable thermodynamic modes exist if the capillarity effects are important and $A < 0$. We wish now to investigate the effects of diffusivity and capillarity on the behaviour of the interface separating two miscible superposed liquids, where the heavier liquids stands over the lighter one.

The case of miscible liquids without accounting for capillarity effect ($Ca = 0$)

The eigenvalue spectra obtained for the Rayleigh-Taylor instability in the case of neglected capillarity effects are shown in Figures 6.7 and 6.8. The data is obtained using the differential equations defining the cases of inviscid and viscous miscible liquids for negligible capillarity ($Ca = 0$). One can notice that the role of diffusion is reduced to additional dissipation (see Figure 6.7 (a)) and, in many ways, is similar to the effect exerted by viscosity. The similarity between the

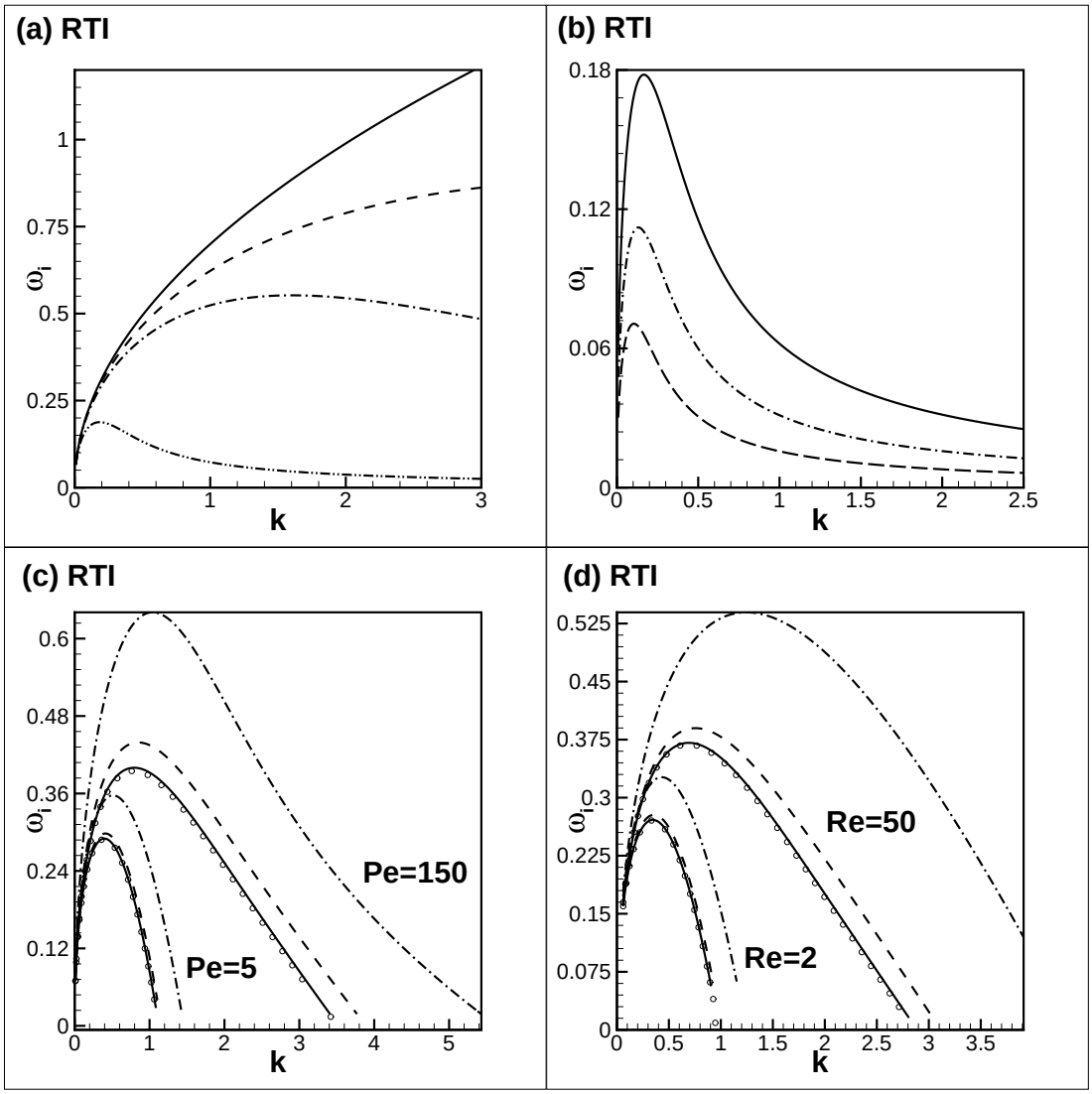

Figure 6.7: Rayleigh-Taylor instability at a miscible interface between two inviscid (a-b) and viscous (c,d) liquids. Capillary effects are disregarded. The growth rate ω_i versus the wavenumber k for (a) $Gr = -0.9$, $A = 0.2$ and $\delta = 0.001$, and various Peclet number Pe: $Pe = \infty$ (solid line), $Pe = 100$ (dash line), $Pe = 25$ (dash-dot line) and $Pe = 1$ (dash-dot-dot line). and (b) $Pe = 1$, $A = 0.5$, $\delta = 0.001$, and various Grashof numbers: $Gr = -1$ (solid line), $Gr = -0.5$ (dash line) $Gr = -0.25$ (dash-dot line). (c) $Gr = -1$, $A = -0.5$, $Re = 3$, $Pe = 5$ and $Pe = 150$ and various thickness δ: $\delta = 0.1$ (dash line), $\delta = 0.001$ (solid line), $\circ$ marks $\delta = 0.0001$). (d) $Gr = -1$, $A = -0.5$, $Pe = 5$, $Re = 2$ and $Re = 50$ and various δ (as in (c)).

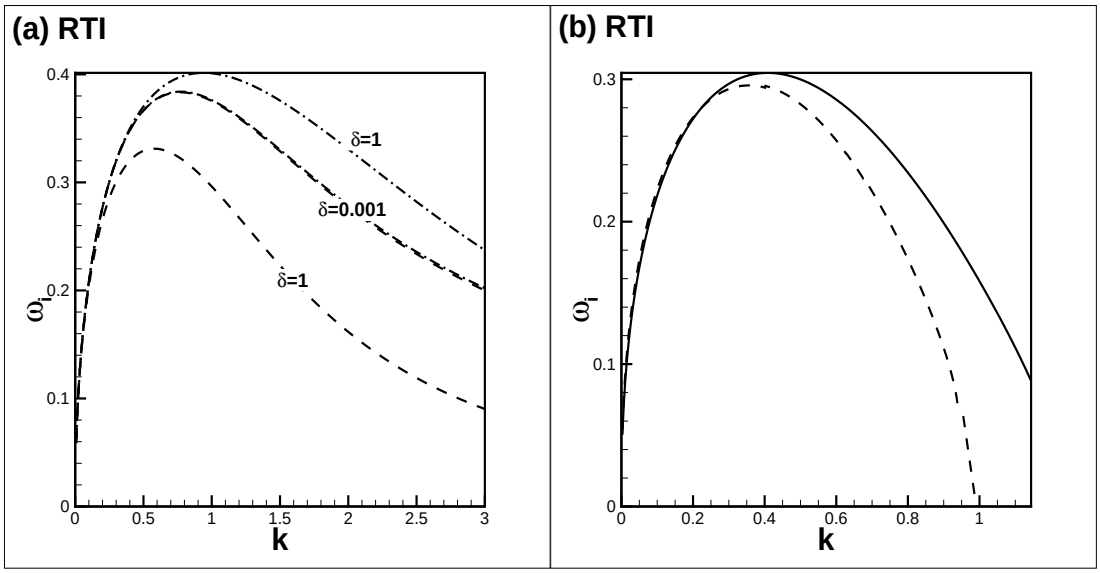

Figure 6.8: Rayleigh-Taylor instability at a miscible interface. Data is obtained for $Ca = 0$, $Gr = -1$ and $A = 0.5$; (a) comparing diffusivity and viscosity effects for $Pe = 10$ and $Re = \infty$ (dash-dot lines) and $Re = 2.5$ and $Pe = \infty$ (dash lines); (b) data is obtained for viscous miscible liquids, $Re = \frac{Pe}{D_0} = 2.5$ and two different values of interface thickness, which are the same as in (a): $\delta = 1$ (solid line) and $\delta = 0.001$ (dash line).

viscous and diffusive effects can be deduced from the amplitude equations (6.1) and (28) that can be reduced at infinity to the following

$$\psi^{iv} - (2k^2 - iRe\omega)\psi'' + k^2(k^2 - iRe\omega)\psi = 0, \tag{6.15}$$

$$\psi^{iv} - (2k^2 - \frac{i\omega Pe}{D_0})\psi'' + k^2(k^2 - \frac{iPe\omega}{D_0})\psi = 0. \tag{6.16}$$

One may note that viscosity is related to diffusivity by the expression $Re = Pe/D_0$. We also found that the results of immiscible interfaces are recovered for very large Peclet numbers. Subsequently, the cumulative action of viscosity and diffusivity is able to completely stabilize the growth of the modes of shorter wavelengths (Figure 6.7 (c,d)). However, neither viscosity alone (Figure 6.1 (f)) nor diffusivity alone (Figure 6.7 (a)) were capable of doing this.

In the case of $Ca = 0$, we found that the variation of the parameter A does not lead to any qualitative changes in the stability results, and the increase in A simply results in stronger damping. Figure 6.7 (b) shows how the growth rates of perturbations depend on the Grashof number, as one sees the instability is increased as Gr increases. However, the positions of the fastest growing modes remain almost unchanged.

Figure 6.7 (c,d) show how the growth rate of perturbations depends on the value of the interface thickness, illustrating that the curves converge to the limit of a sharp interface when δ tends to zero. Similar to immiscible interfaces, the convergence is perfect for the shown range of k but may deteriorate for the modes with larger wavenumbers. The stabilization of the short wavelength modes by the combined actions of viscosity and diffusivity relaxes the restriction on the value of the interface thickness. If one is interested in the unstable part of the eigenspectrum, or in the fastest growing modes, then the thickness of the interface can be taken as $\delta k_c(Re, Pe) << 1$ and the instability of a sharp interface will be accurately reproduced.

Furthermore, Figure 6.8 (a,b) illustrates the effect of diffusivity and viscosity when acting independently (Figure 6.8 (a)) and simultaneously (Figure 6.8 (b)). Figure 6.8 (a) shows that, in immiscible viscous liquids, perturbations developed at thick interfaces grow slower than the perturbations developed at sharp interfaces. In contrast, in inviscid miscible liquids, perturbations developed at sharp

interfaces grow slower than the ones developed at thick interfaces. In addition, it shows that viscosity and diffusivity effects become identical if the interface is sufficiently sharp and $\delta(Re = Pe/D_0) < \lambda$. In fact this can be concluded from equations (6.15) and (6.16), where $C_0 = \pm 1/2$ and $C_0' = 0$ for $\delta \to 0$. This is utilised to further investigate what behaviour the interface exhibits when the effects of viscosity and diffusivity are simultaneously applied. The corresponding data is shown in Figure 6.8 (b). Surprisingly, the simultaneous action of diffusivity and viscosity action results in behaviour similar to what was observed for inviscid miscible liquids. This observation indicates that viscosity can be reduced to further enhancement of diffusive dissipation. In addition, one may use sensitivity of the interface to the thickness δ in order to determine the values of the Peclet (Pe) (or Reynolds (Re)) number for which the diffusivity (or viscosity) can be neglected.

The case of miscible liquids with accounting for capillarity effect ($Ca \neq 0$)

The eigenvalue spectra are also obtained for Rayleigh-Taylor instability using both the full small amplitude equations, defining all physical effects, and the inviscid miscible liquids with accounting for capillarity effects.

The obtained numerical solution first allows us to confirm that the viscous force introduces the dissipation as usual, which is illustrated in Figure 6.9 (a,b). The inviscid result can be recovered by taking the Reynolds number to be large enough. The effect of diffusivity is also reduced to dissipation as illustrated in Figure 6.9 (c,d).

The capillary forces are also known to suppress the growth of the short wavelength modes. The strength of the capillary effect is defined by both the capillary number and the interface thickness. Figure 6.10 shows how the results depend on the capillary number. One sees that the increase of the capillary force results in an expectable reduction of the range of unstable modes and reduces the growth rates, which generally coincide with our earlier observations for immiscible interfaces.

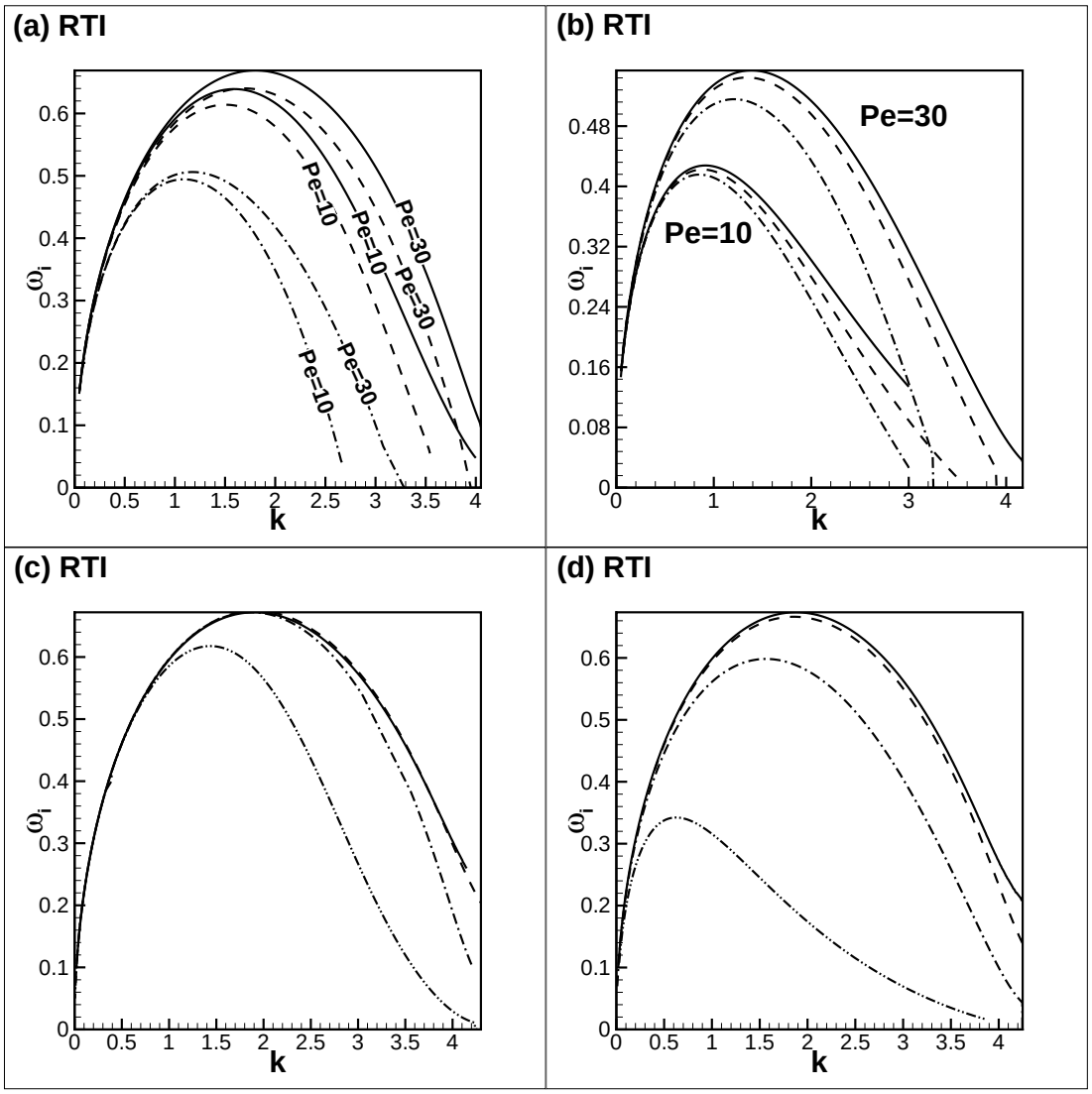

Figure 6.9: Rayleigh-Taylor instability at a miscible interface. The growth rate ω_i versus the wavenumber k is depicted for $Gr = -1$, $Ca = 0.05$, $\delta = 0.3$, (a) $A = -0.5$, $Pe = 10$ and $Pe = 30$, and various Re: inviscid result (solid line), $Re = 250$ (dash line), $Re = 50$ (dash-dot line). (b) $A = 0.5$, $Pe = 10$ and $Pe = 30$, and various Re: (lines as in (c)). (c) $A = -0.5$, $Re = 10$, and various Pe: immiscible case (solid line), $Pe = 100$ (dash line), $Pe = 10$ (dash-dot line), $Pe = 1$ (dash-dot-dot line). (d) $A = 0.5$, $Re = 10$, and various Pe: immiscible case (solid line), $Pe = 250$ (dash line), $Pe = 50$ (dash-dot line) and $Pe = 10$ (dash-dot-dot line);

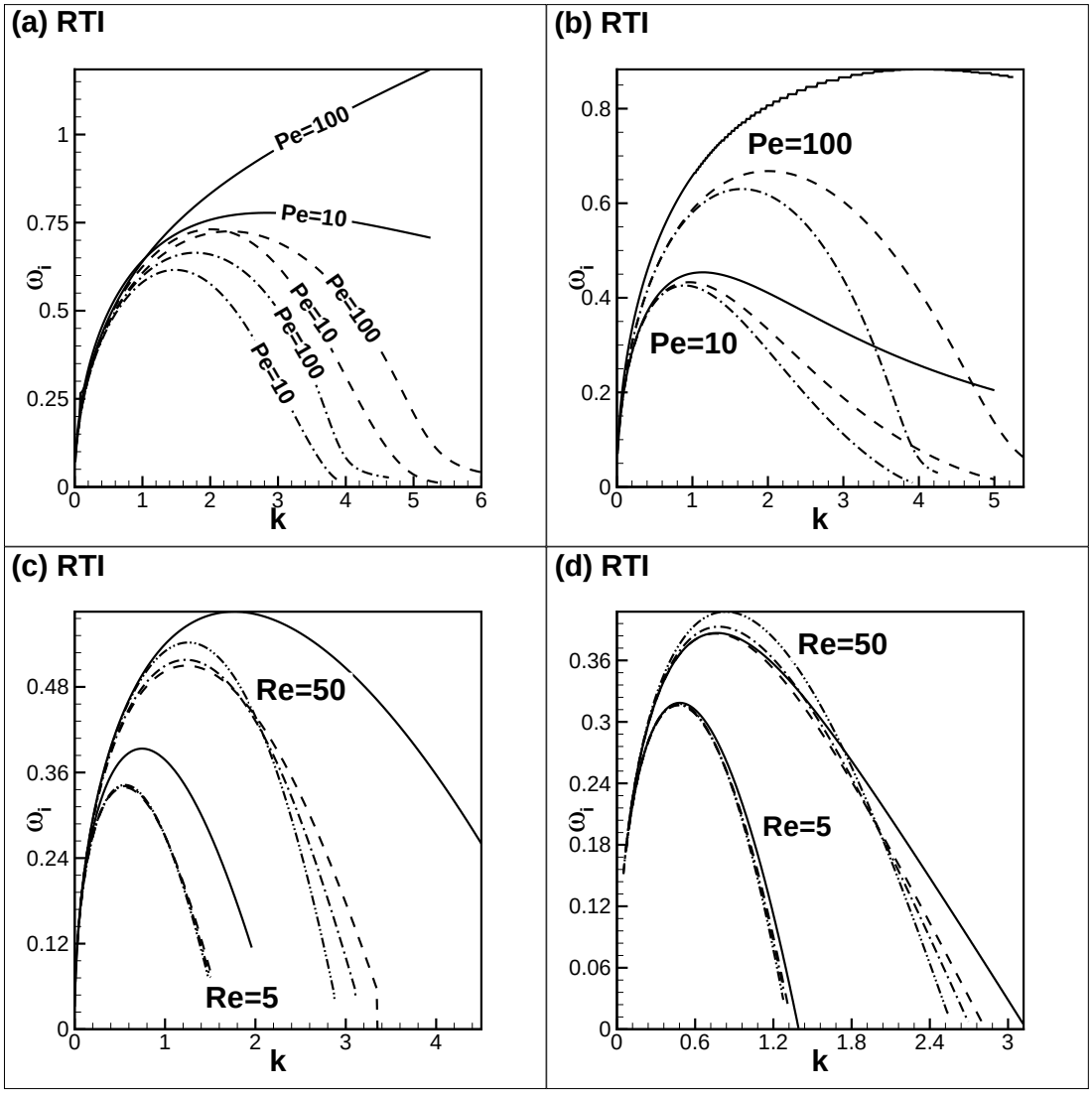

Figure 6.10: Rayleigh-Taylor instability at a miscible interface. The growth rate ω_i versus the wavenumber k is depicted for $Gr = -1$. (a) $Pe = 10$ and $Pe = 100$, $A = -0.5$, $\delta = 0.3$ and various capillary numbers: $Ca = 0$ (solid line), $Ca = 0.03$ (dash line), $Ca = 0.06$ (dash-dot line). (b) $Pe = 10$ and $Pe = 100$, $A = 0.5$, $\delta = 0.3$ (lines as in (a)). (c) $Pe = 10$, $A = -0.5$, $\delta = 0.05$ and various Ca: $Ca = 0$ (solid line), $Ca = 0.02$ (dash line), $Ca = 0.04$ (dash-dot line), and $Ca = 0.08$ (dash-dot-dot line). (d) $Pe = 10$, $A = 0.5$, $\delta = 0.05$ (lines as in (c)). (a) and (b) depict the inviscid results; (c) and (d) depict the viscous results for $Re = 5$ and $Re = 50$.

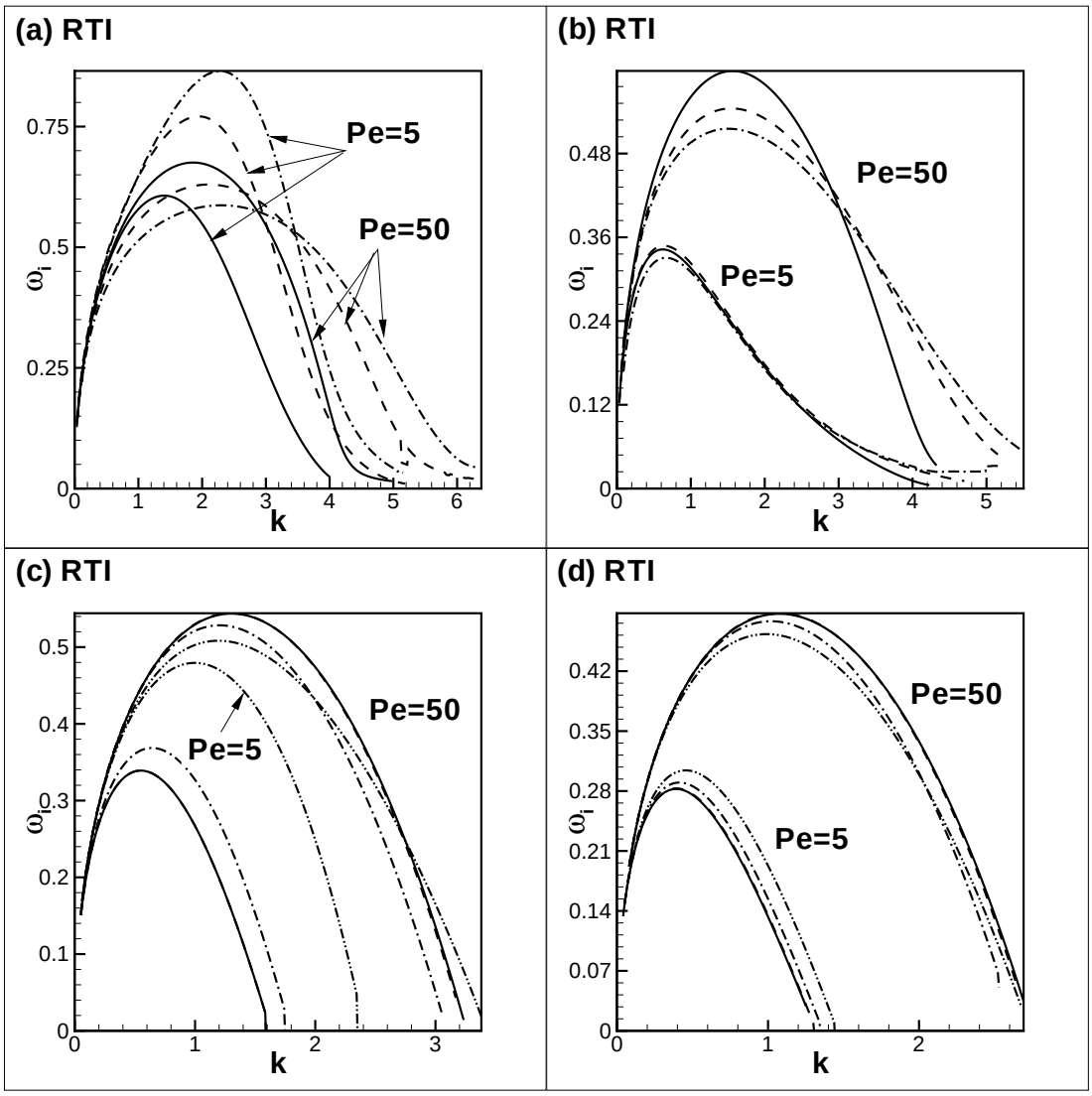

Figure 6.11: Rayleigh-Taylor instability at a miscible interface. The growth rate ω_i versus the wavenumber k is depicted for $Gr = -1$, $Ca = 0.05$, $Pe = 5$ and $Pe = 50$ (a) $A = -0.5$ and various interface thicknesses: $\delta = 0.9$ (dash-dot line), $\delta = 0.6$ (dash line), $\delta = 0.3$ (solid line). (b) $A = 0.5$ (lines as in (a)); (c) $A = -0.5$, $Re = 10$ and various δ: $\delta = 0.001$ (solid line), $\delta = 0.01$ (dash line) $\delta = 0.1$ (dash-dot line) and $\delta = 0.3$ (dash-dot-dot line). (d) $A = 0.5$, $Re = 10$ (lines as in (c)). (a,b) depict the inviscid results.

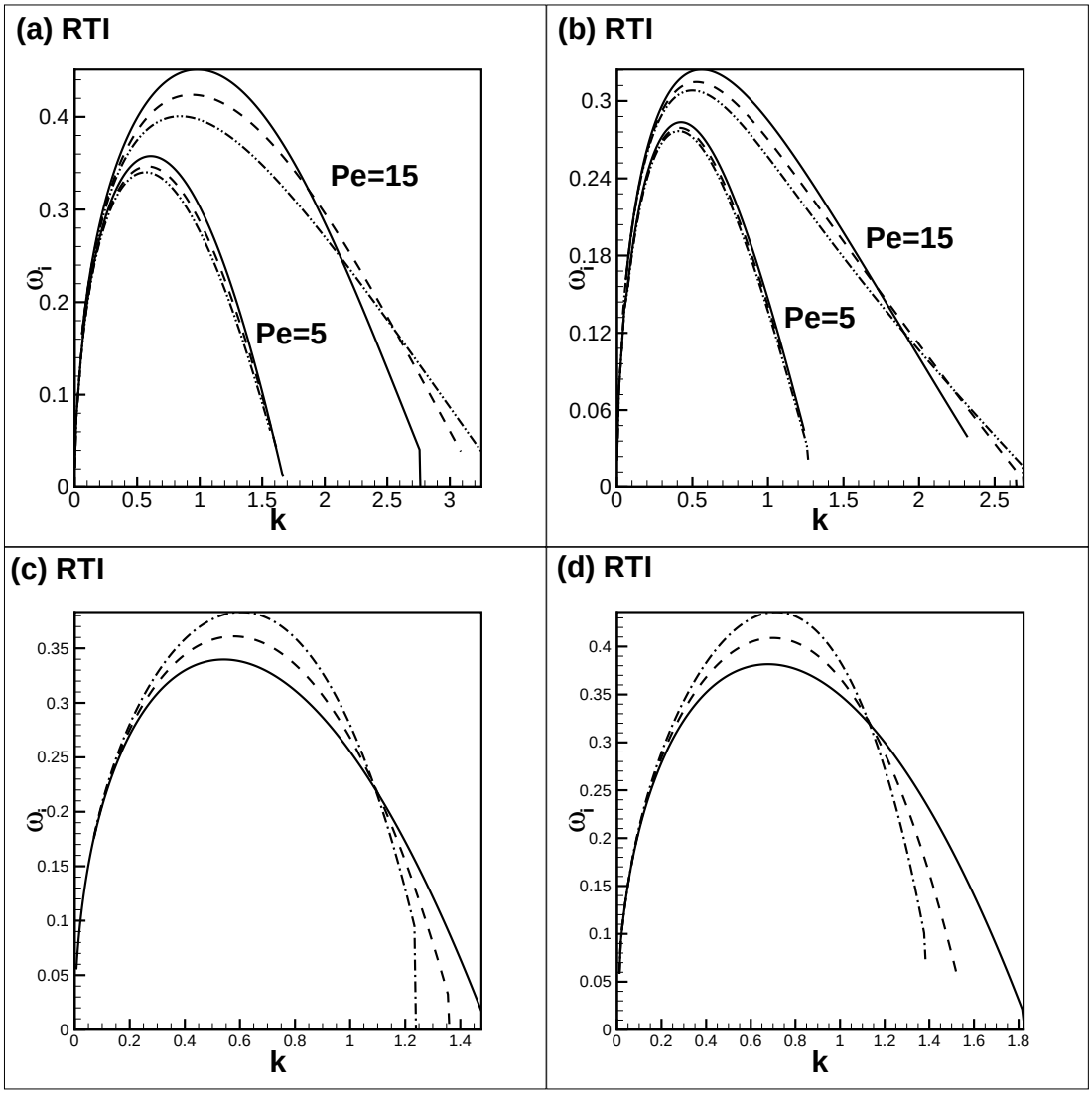

Figure 6.12: Rayleigh-Taylor instability at a miscible interface. The growth rate ω_i versus the wavenumber k is depicted for $Gr = -1$, $Ca = 0.05$, $Pe = 5$ and $Pe = 15$, $Re = 10$ and $Gr = -1$ (a,b) a) $A = -0.5$ (b) $A = 0.5$, and different capillary numbers and interface thicknesses for $Ca/\delta = 1$: (a) $Ca = \delta = 0.08$ (solid line), $Ca = \delta = 0.04$ (dash line) and $Ca = \delta = 0.02$ (dash-dot-dot line). (c) $Re = 5$, $Pe = 15$, $\delta = 0.001$, $A = 0.5$ and various Ca: $Ca = 0.05$ (solid line), $Ca = 0.5$ (dash line) and $Ca = 1$ (dash-dot line). (d) the data obtained for the same values and the corresponding lines in (c) but $A = -0.5$.

Figures 6.11 and 6.12 (a,b) illustrate the eigenspectra for the interfaces of different thicknesses. The curves are obtained for the inviscid and viscous cases at two different Peclet numbers. Here the effects of viscosity, diffusivity, and capillarity interact. In particular, the combined action of the viscous and diffusive damping can make the capillary action on the interface stability negligible. One can notice that the decrease in the interface thickness (hence the increase in the surface tension) does not always give us the expected suppression of the modes with shorter wavelengths. This means that the efficiencies of the viscous, diffusive and capillary mechanisms all depend on the interface thickness. As these three dependencies are different, the change in the interface thickness can sometimes lead to unexpected behaviour.

Figures 6.12 (a,b) show the curves obtained for the different capillary numbers and interface thicknesses that are changed so the ratio Ca/δ remains constant. We see that the convergence to the limiting sharp-interface behaviour can be achieved this way. To verify whether strong capillary forces are capable to stabilise a miscible interface as in the case of the immiscible interface (Figure 6.2 (d)), Figure 6.12 (c,d) shows the dependencies of growth rate ω_i on the capillary number for $A = 0.5$ and $A = -0.5$. The data show that, in miscible liquids, the capillarity effects are able to exceptionally dampen the short wavelengths, in contrast, it increases the instability of the most unstable modes.

The typical shapes of eigenfunctions are depicted in Figure 6.13 for both cases of $Ca = 0$ and $Ca \neq 0$. The plotted eigenfunctions have very different y-widths. In the case of $Ca = 0$, the typical thickness of the eigenfunction is of order 10, irrelevant to the thickness of the interface itself, and just slightly dependent on the values of the Reynolds number. In the case of $Ca \neq 0$, one notices that the perturbation of the y-profile becomes more compact. In the former case ($Ca = 0$) the eigenfunction profile is more similar to the one depicted in Figure 6.4, i.e. to the purely hydrodynamic mode. In the latter case ($Ca \neq 0$), however, the eigenfunction looks similar to Figure 6.5 (c,d), i.e. to the purely thermodynamic modes. These observations confirm that the evolution is driven by hydrodynamic modes in the case of $Ca = 0$, and thermodynamic effects become dominating for $Ca \neq 0$.

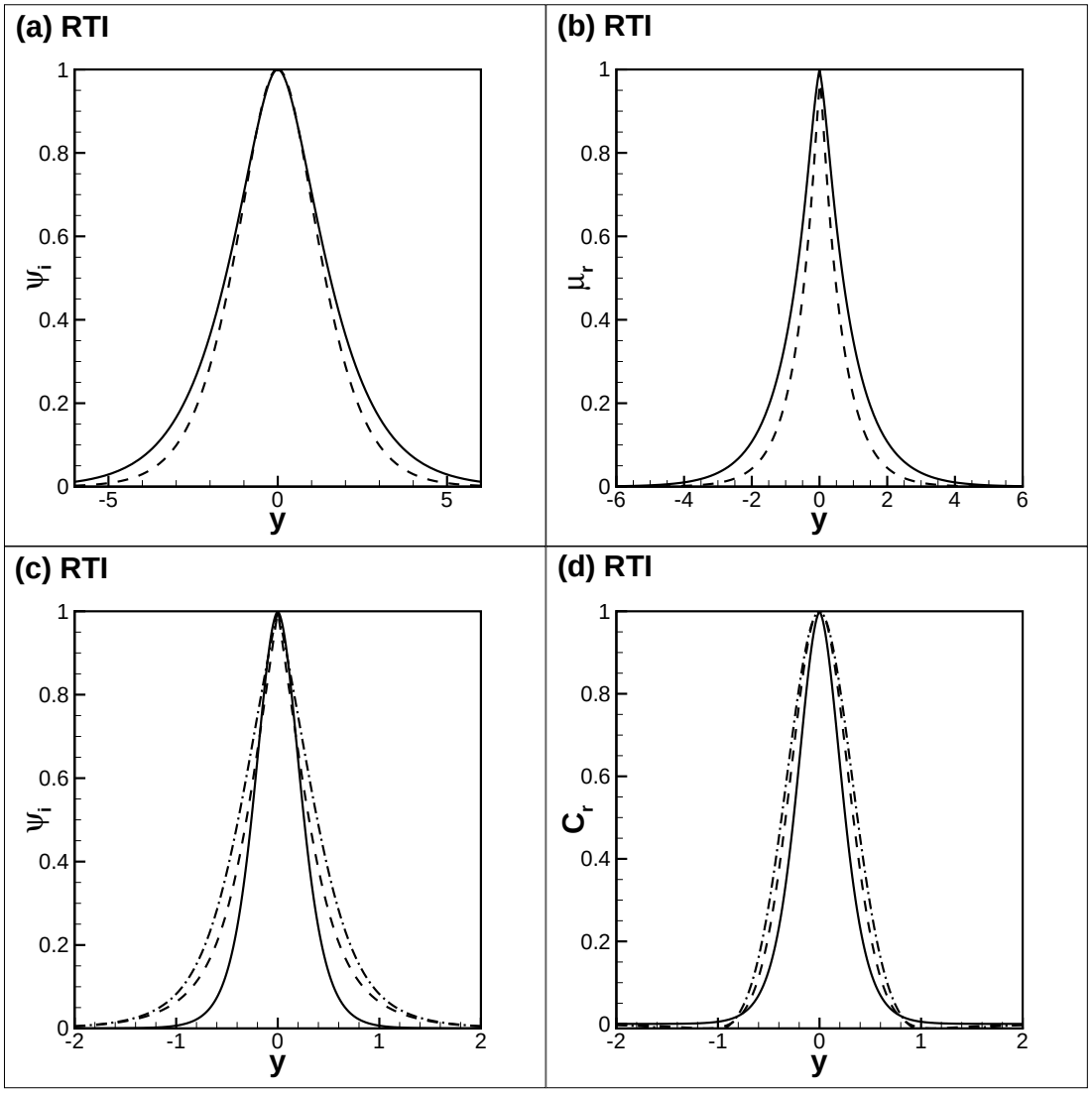

Figure 6.13: The eigenfunctions for the Rayleigh-Taylor instability developed at a miscible interface. (a,b) $Ca = 0$, profiles of the streamfunction (a) and chemical potential (b) are shown for the inviscid (solid lines) and viscous ($Re = 10$, dash lines) cases. The results are shown for $Gr = -1$, $k = 1$, $Pe = 5$, $\delta = 0.1$ and $A = 0.5$. The growth rate is $\omega_i = 0.306$ in the inviscid case and $\omega_i = 0.176$ in the viscous case. (c,d) $Ca = 0.05$, profiles of the imaginary part of streamfunction (c) and the real part of concentration (d) are shown for the interfaces between two inviscid liquids; the interface thicknesses are 0.3 (solid line), 0.6 (dash line), and 0.9 (dash-dot line), other parameters are $Gr = -1$, $Pe = 10$, $A = -0.5$, $k = 2$. The growth rates are $\omega_i = 0.778$ ($\delta = 0.9$), $\omega_i = 0.770$ ($\delta = 0.6$), and $\omega_i = 0.548$ ($\delta = 0.3$).

6.3.2 Gravity-capillary waves

In this case, I follow the same parametric study used in the previous section. In addition, we use both ESM and CCM methods to calculate the eigenvalues the boundary value problems presenting each cases. Firstly, pure gravity waves are considered then it is followed by considering gravity capillary waves.

Pure gravity waves

Similar to the previous section, our analysis for the behaviour of the interface separation two miscible liquids, the heavier liquid underlies the lighter one, starts from the case of the pure gravity waves, i.e. when $Ca = 0$. Figures 6.14 (a,b) illustrate the similarity of the effect exerted by diffusion to the viscous damping. Diffusivity introduces an additional dissipation mechanism, and similar to the viscosity effect, a cut-off wavenumber appears that limits the range of the modes exhibiting the wave-like behaviour. The solution for the larger wavenumbers becomes not unique, as the eigenvalues have two possible imaginary parts. At the point of bifurcation, the real part of the eigenvalue becomes equal to zero, hence these solutions describe quickly and monotonically dissipating perturbations. We also notice that the results for immiscible interfaces can be recovered by taking very large Peclet numbers, and, in the limit of small wavenumbers, the phase speed of the perturbations follow the classical $k^{-1/2}$ dependence.

Figures 6.14 (c,d) show that the increase in the value of the Grashoff number results in the increase of the phase-speed of perturbations, however the damping rate remains almost unaffected. Without the capillary terms, the waves are purely driven by the gravity force, and hence disappear when Gr tends to zero. In the case $Ca = 0$, an increase in the value of the parameter A leads to an increase in the diffusion coefficient and hence to a stronger damping of the waves. Figure 6.15 (a,b) show that the curves quickly converge to a sharp-interface limit if the interface thickness δ tends to zero. A comparison between the effects of diffusivity and viscosity acting separately on an unconditionally stable phase boundary is shown in Figure 6.15 (c,d). It was shown in Section 6.3.1 that the diffusivity and viscosity overlap each other when $L \to \infty$ such that $Re = Pe/D_0$, which is also

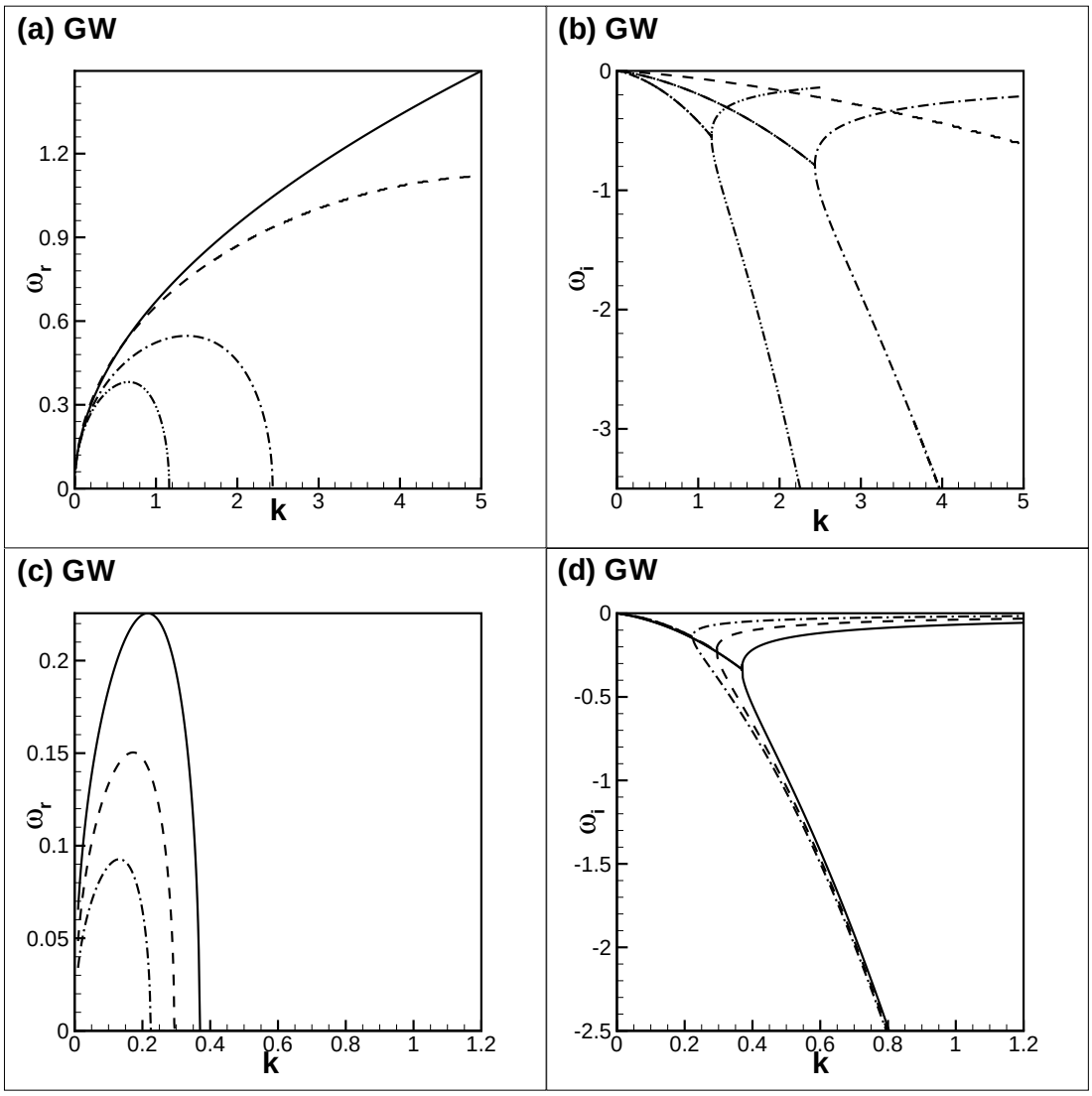

Figure 6.14: Dispersion relations and decay rates for the gravity waves on a miscible interface between two inviscid liquids. Capillary terms are neglected. The data are shown for (a,b) $Gr = 0.9$, $A = 0.2$, $\delta = 0.001$ and various Peclet numbers: $Pe = 5$ (dash-dot-dot line), $Pe = 15$ (dash-dot line), $Pe = 100$ (dash line) and immiscible case (solid line). (c,d) $Pe = 1$, $A = 0.2$, $\delta = 0.001$, and various Grashof numbers: $Gr = 0.9$ (solid line), $Gr = 0.5$ (dash line), $Gr = 0.25$ (dash-dot line).

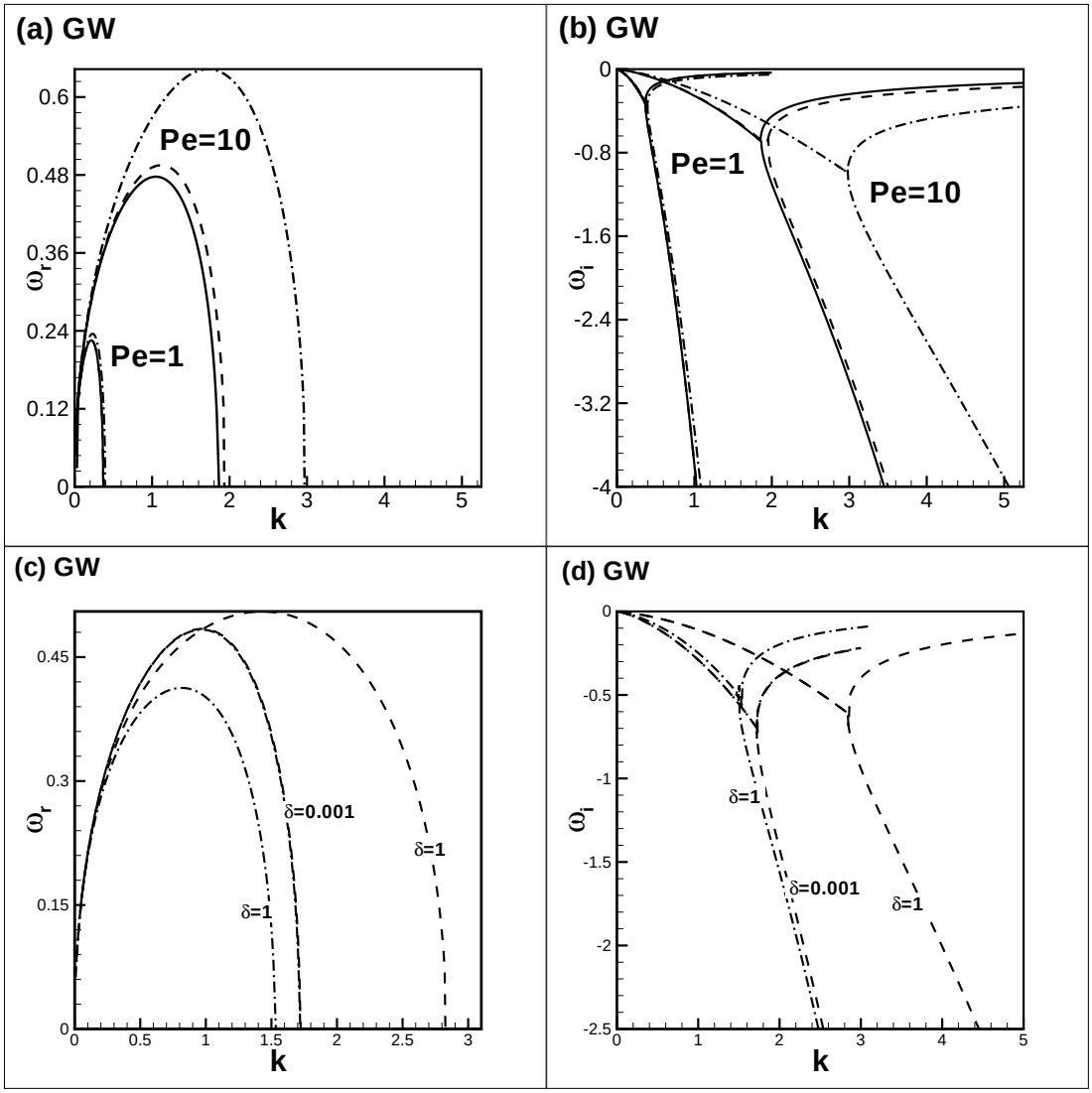

Figure 6.15: Dispersion relations and decay rates for the gravity waves, capillary terms are neglected. Miscible-inviscid (a,b), the data is shown for $A = 0.2$, $Pe = 1$ and $Pe = 10$, $Gr = 0.9$, and various interface thicknesses: $\delta = 0.05$ (dash-dot line), $\delta = 0.01$ (dash line) and $\delta = 0.001$ (solid line). (c,d) results are shown for miscible-inviscid liquids with $A = 0.5$ and $Pe = 10$ (dash lines); and for immiscible-viscous liquids $Re = Pe/D_0 = 2.5$ (dash-dot lines).

true for $\delta \to 0$ and $Gr > 0$ (Figure 6.15 (c,d)). However, the effect of viscosity is more significant than the effect of diffusivity in speeding up the decay of the gravity waves for a thicker interface. Figures 6.19 (c,d) illustrate the sensitivity of the interface stability to the diffusivity and the interface thickness. For a thicker interface, the diffusivity dissipates gravity waves slower than in the the case of a sharper interface.

Gravity-capillary waves

Here we discuss the dispersion relations obtained for gravity-capillary waves defined by both the full amplitude equations (3.21)-(3.23) and the sixth order differential equations for the case of inviscid miscible liquids with $Ca = 0$. We start from Figure 6.16 which confirms that viscosity generally continues to play its classical dissipative role. However, one also sees that when $A < 0$ and $\delta > \delta_0$ (Figure 6.16 (a,b)), the long wavelength instability appears, obviously driven by the thermodynamic instability described in Section 6.2. The longwave instability disappears if $\delta < \delta_0$, as seen in Figure 6.16 (c,d). Figure 6.17 shows that the inclusion of diffusivity also introduces an additional damping to the system.

Figures 6.18 (a,b) and 6.19 (a,b) show the changes in the dispersion relations associated with the variations of the interface thickness. The dependencies differ for the positive and negative values of A, and again the most interesting results are observed for $A < 0$, when the dynamics of thicker interfaces (with $\delta > \delta_0$) exhibits the development of the longwave instability. This effect is illustrated in more detail in Figures 6.18 (c,d). Furthermore, Figures 6.18(a,b) and 6.19 (a,b) also show that the thinner interfaces are obviously characterised with stronger interfacial tensions, and hence exhibit stronger suppression of the short wavelength modes. Figures 6.19 (c,d) show that the instability of waves can be reduced significantly with increasing the values of Ca even though $\delta = 2\delta_0$. This means that the capillary forces are more efficient in dampening the instability of waves for larger δ.

Figures 6.20 show the dispersion relations for the gravity-capillary waves for the various values of the capillary number also for the positive and negative values

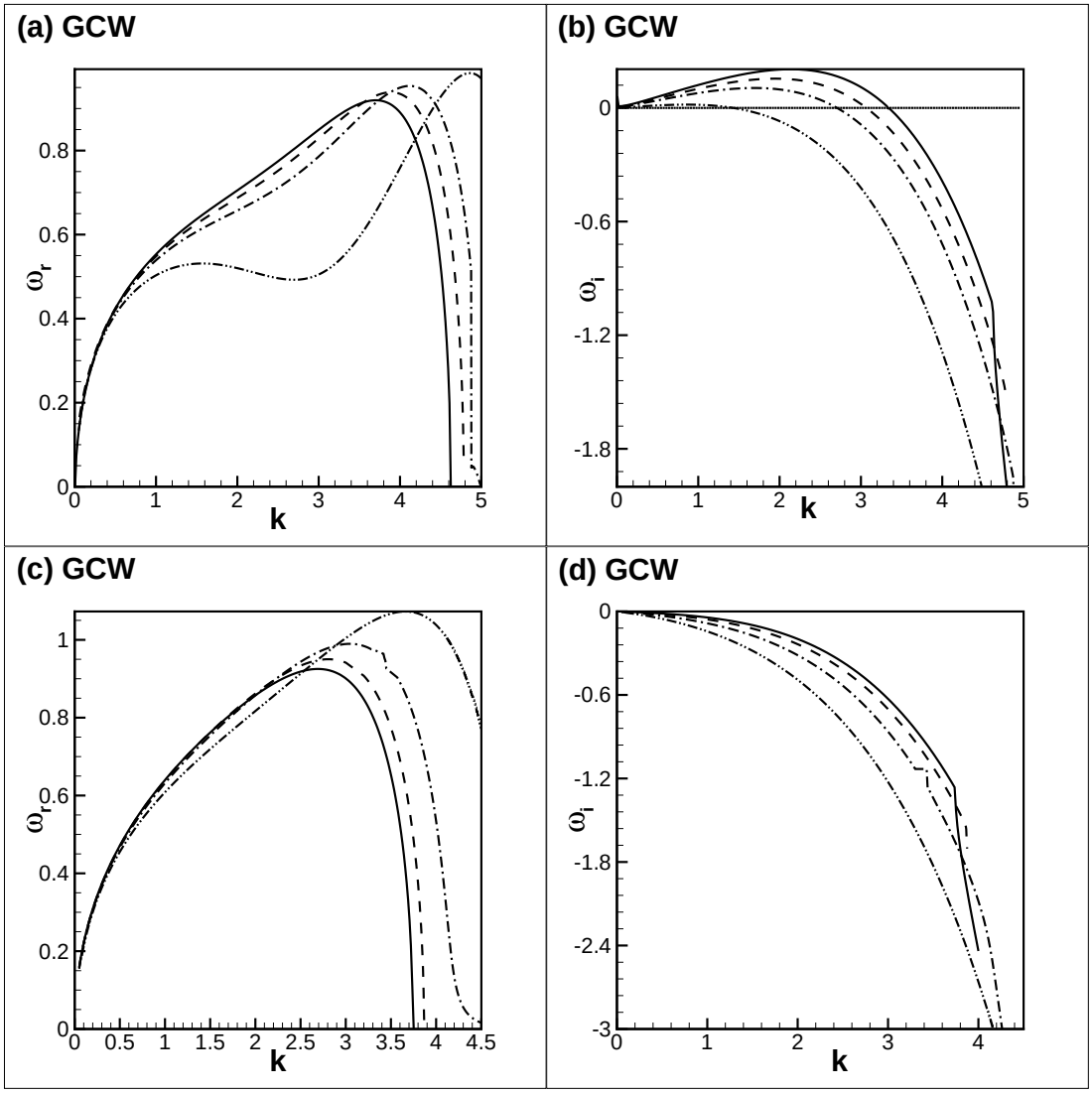

Figure 6.16: Dispersion relations and decay rates for the gravity-capillary waves on a miscible interface. The curves are obtained for $Gr = 1$, $Ca = 0.04$, $Pe = 10$, $A = -0.5$ (a,b) $\delta = 2\delta_0 \approx 0.57$: inviscid case (solid line), $Re = 100$ (dash line), $Re = 30$ (dash-dot line), $Re = 10$ (dash-dot-dot line). And (c,d) $\delta = 0.25$ and various Re: inviscid case (solid line), $Re = 70$ (dash line), $Re = 30$ (dash-dot line), $Re = 10$ (dash-dot-dot line).

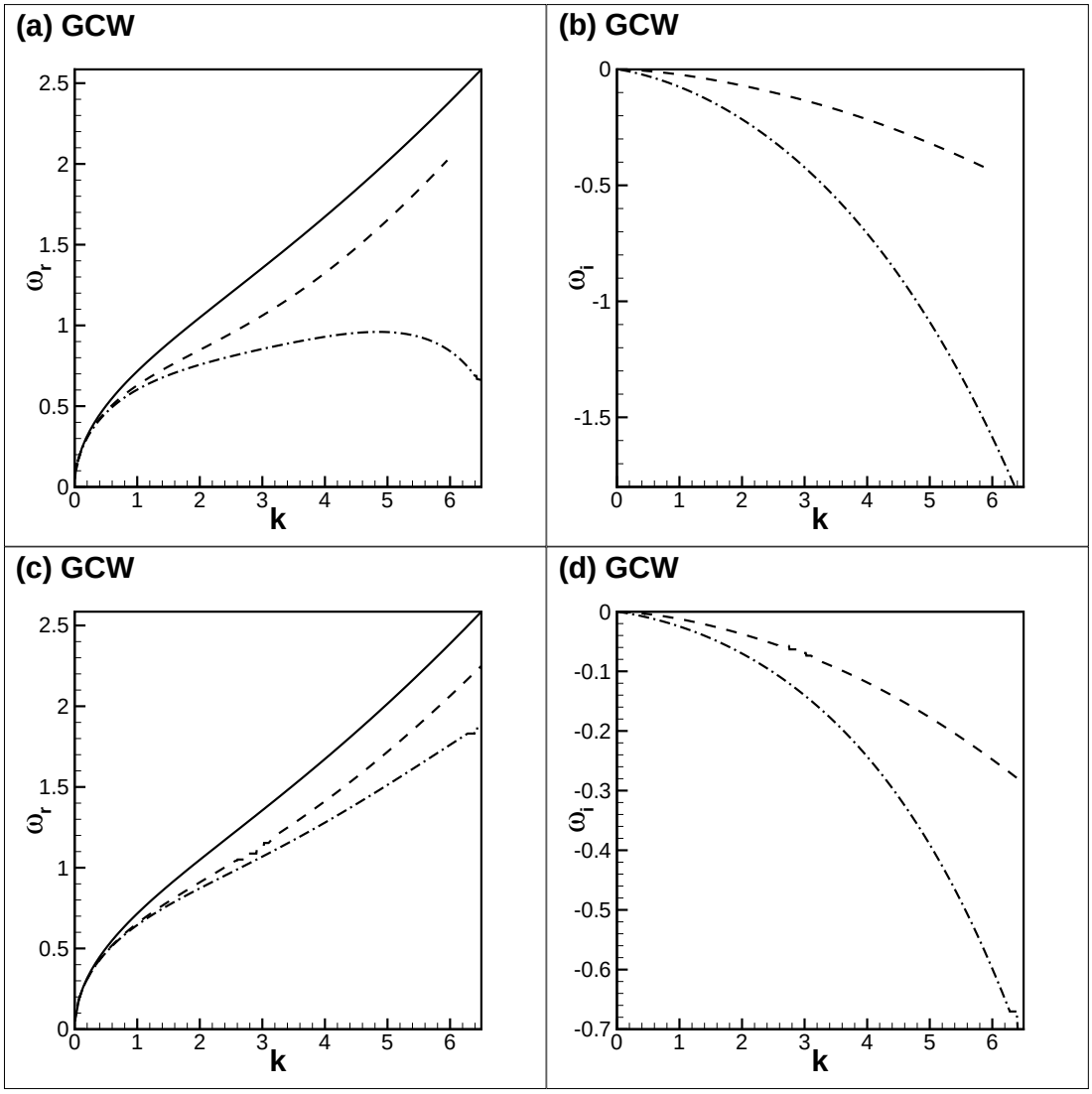

Figure 6.17: Dispersion relations and decay rates for the gravity-capillary waves on the surface of a miscible interface separating two inviscid liquids are shown for various Peclet numbers: immiscible case ($Re = \infty$) (solid line), $Pe = 500$ (dash line), and $Pe = 50$ (dash-dot line). The results are shown for $Gr = 1$, $Ca = 0.015$, $\delta = 0.1$ (a,b) $A = -0.5$ and (c,d) $A = 0.5$.

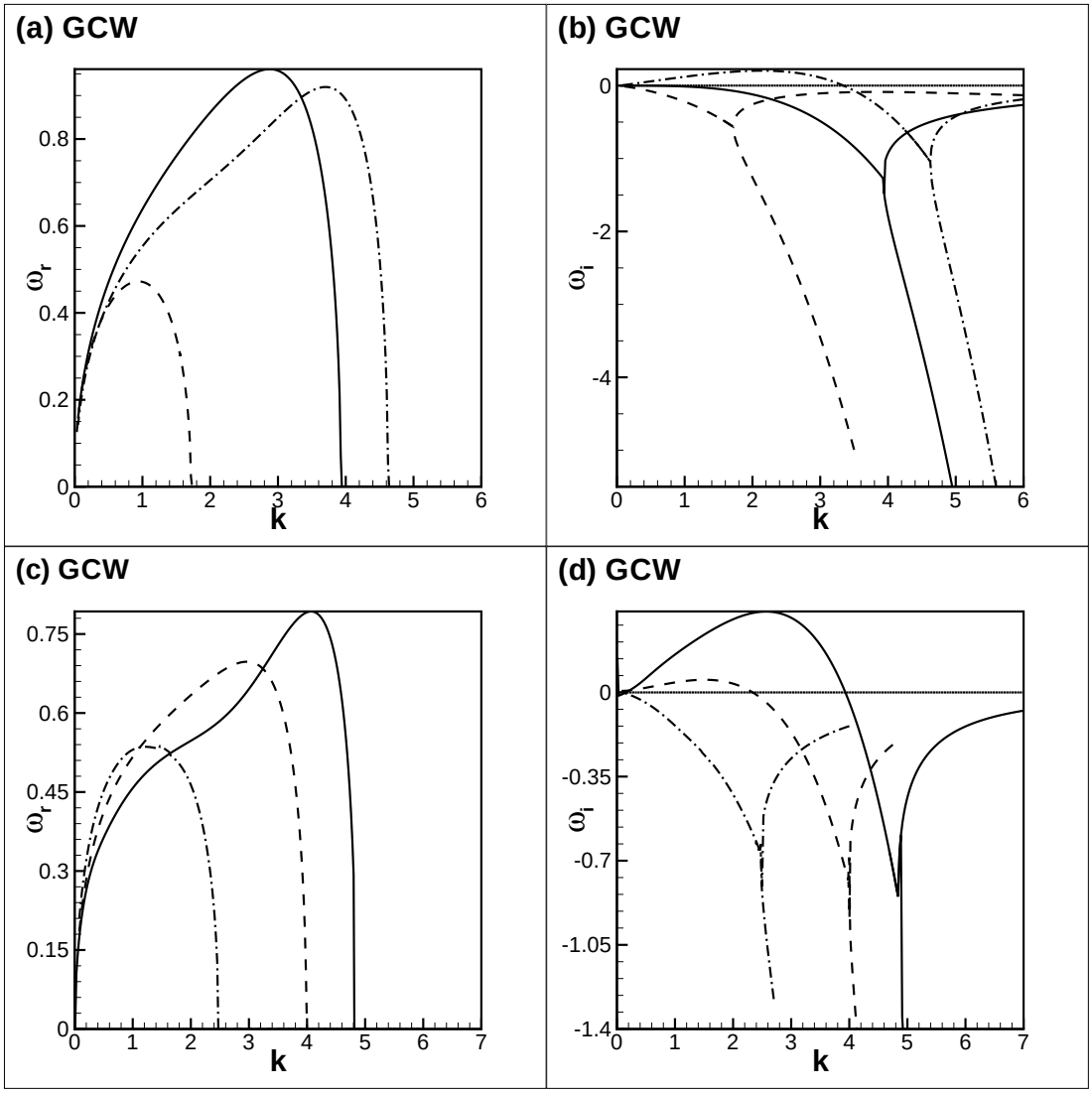

Figure 6.18: Dispersion relations and decay rates for the gravity-capillary waves on the surface of a miscible interface. The results are shown for $Gr = 1$, $Ca = 0.04$, $Pe = 10$. (a,b) $A = -0.5$ and various interface thicknesses: $\delta = \delta_0/3$ (dash line), $\delta = \delta_0$ (sold line) and $\delta = 2\delta_0$ (dash-dot line). And (c,d) The results are shown for $Gr = 1$, $Pe = 5$, $Ca = 0.04$, $\delta = 0.85$ and $A = -0.5$ (solid line), $A = -0.3$ (dash line), and $A = -0.1$ (dash-dot line).

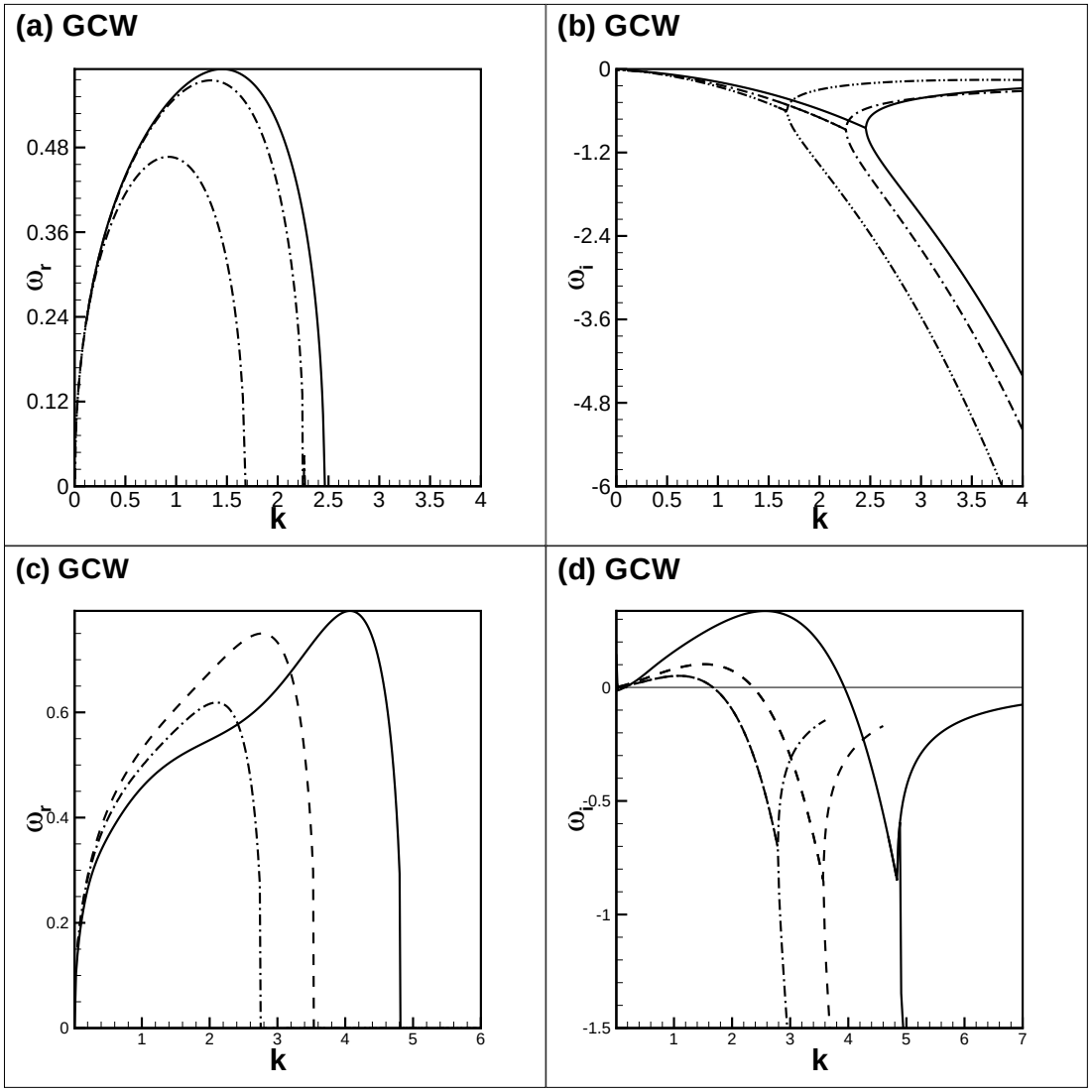

Figure 6.19: Dispersion relations and decay rates for the gravity-capillary waves on the surface of a miscible interface. The results are shown for $Gr = 1$, $Ca = 0.04$, $Pe = 10$ (a,b) $A = 0.5$ and various δ: $\delta = 0.1$ (solid line), $\delta = 0.2$ (dash line) and $\delta = 0.4$ (dash-dot line). (c,d) results are shown for $Gr = 1$, $Pe = 5$, $A = 0.5$, $\delta = 2\delta_0$ and various Ca: $Ca = 0.04$ (solid line), $Ca = 0.08$ (dash line) and $Ca = 0.16$ (dash-dot line).

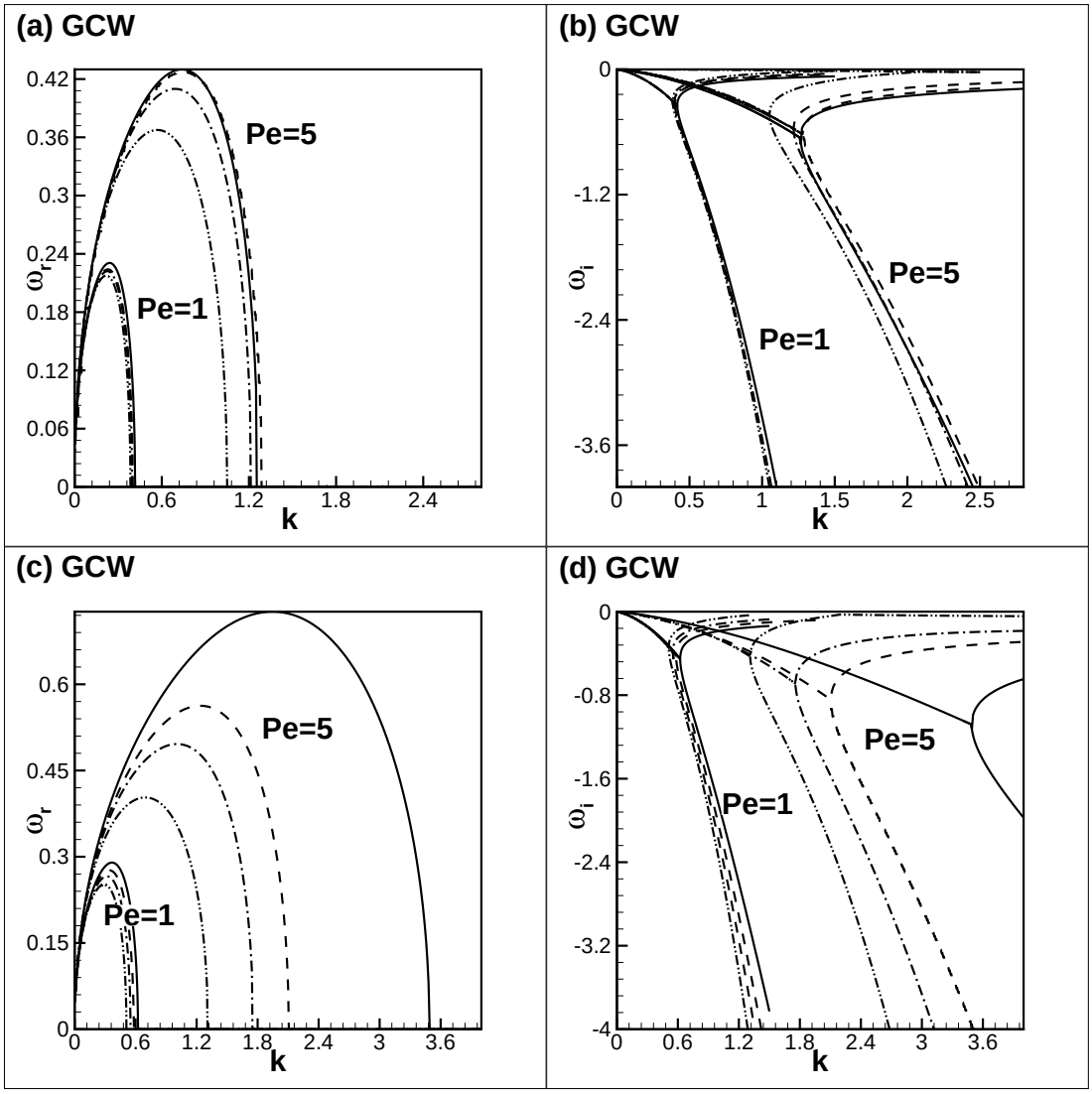

Figure 6.20: Dispersion relations and decay rates for the gravity-capillary waves on a miscible interface separating two inviscid liquids. The results are shown for $Gr = 0.9$, $\delta = 0.1$, $Pe = 1$ and $Pe = 5$ (a,b) $A = 0.3$; (c,d) $A = -0.3$. The curves are plotted for different Ca numbers: $Ca = 0$ (solid line) $Ca = 0.015$ (dash line), $Ca = 0.03$ (dash-dot line) and $Ca = 0.09$ (dash-dot-dot line).

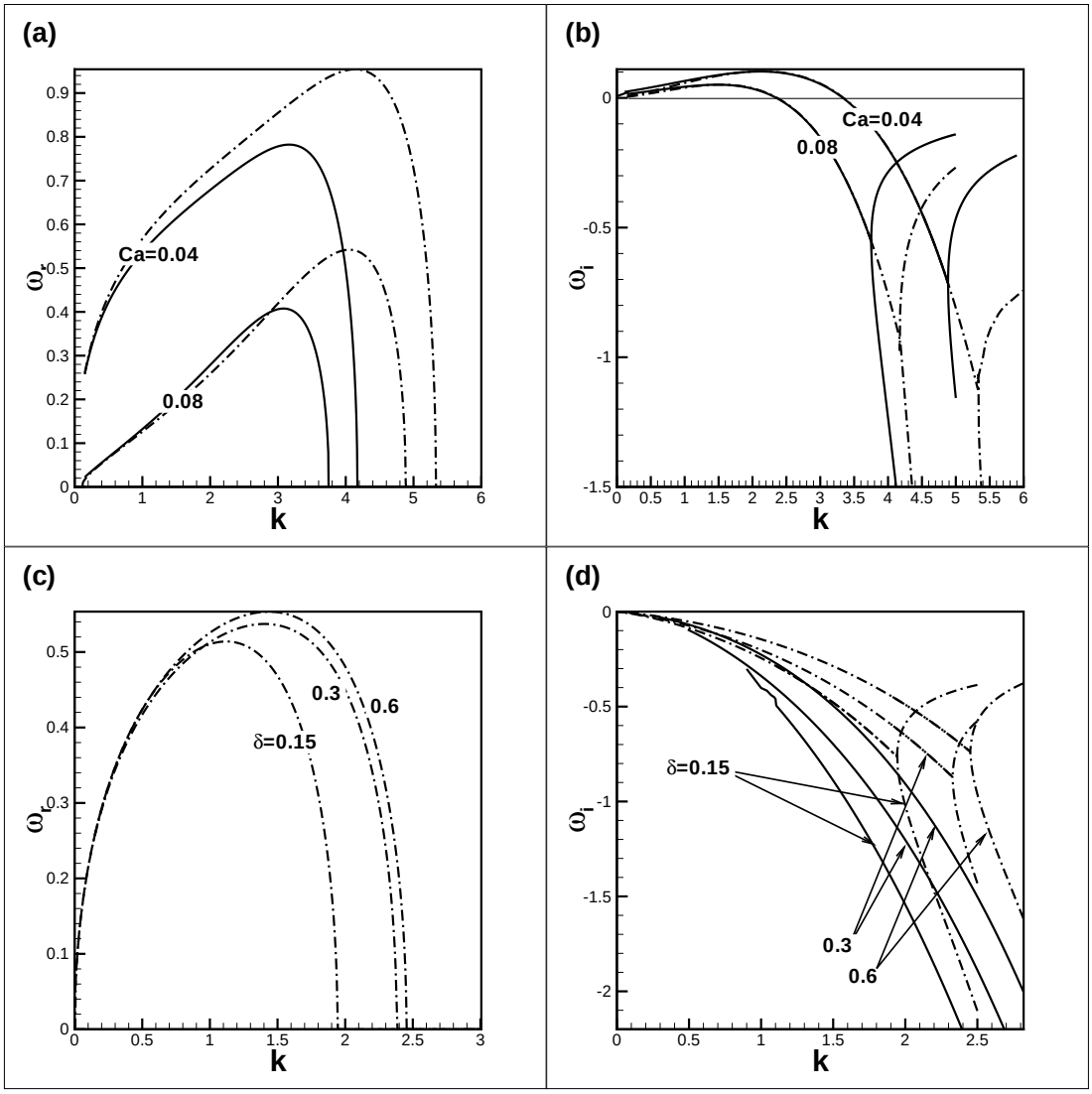

Figure 6.21: Dispersion relations and decay rates for the gravity-capillary waves on the surface that is separating two inviscid miscible liquids. (a,b) the curves are plotted for $A = -0.5$, $\delta = 2\delta_0$, $Pe = 10$, $Gr = 0$ (solid lines) and $Gr = 1$ (dash-dot lines). (c,d) the curves are plotted for $A = 0.5$, $Pe = 10$, $Ca = 0.06$ and two different values of Gr: $Gr = 0$ (solid lines), $Gr = 1$ (dash-dot lines).

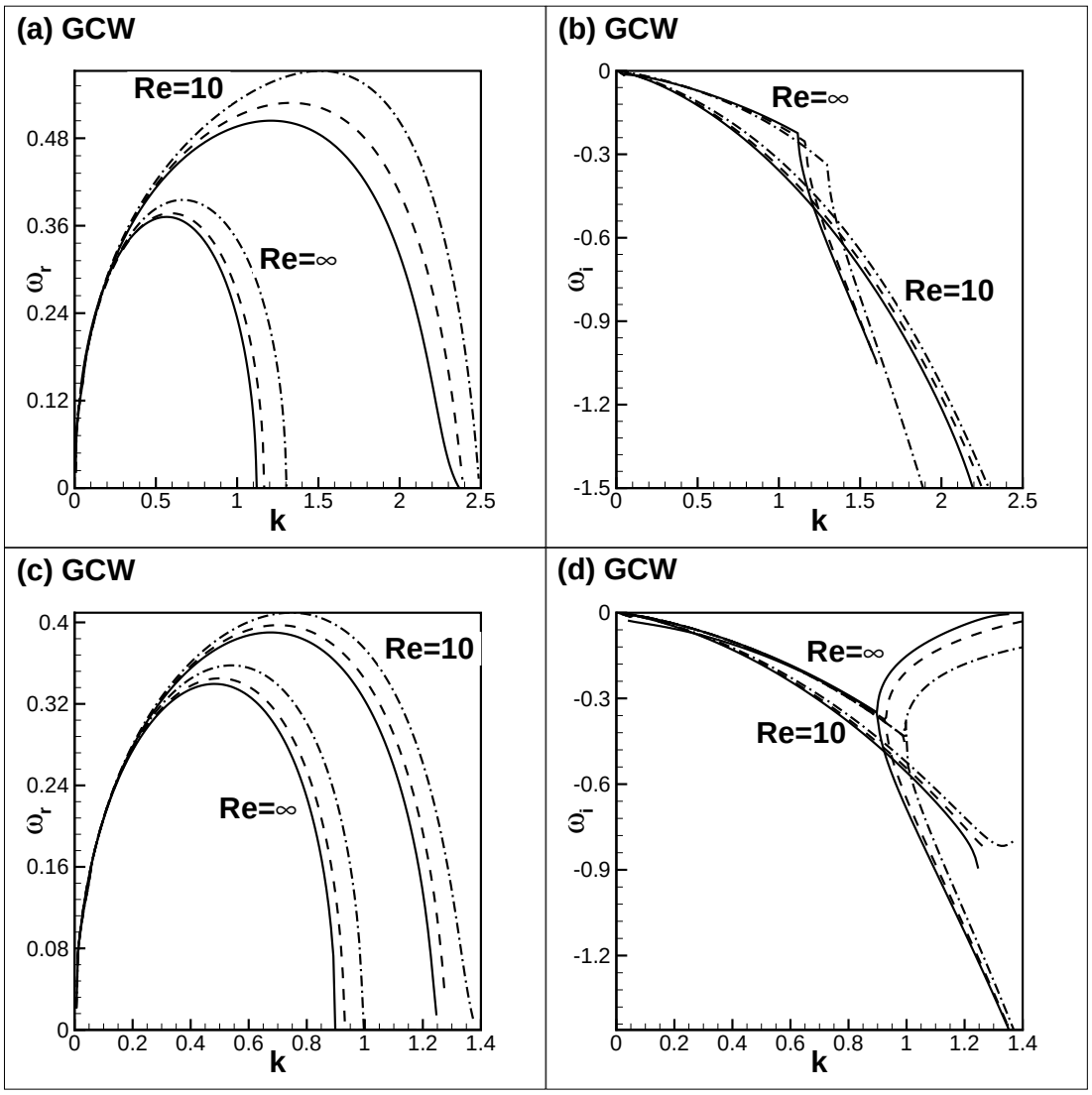

Figure 6.22: Dispersion relations and decay rates for the gravity-capillary waves on the surface of a miscible interface for the fixed ratio $Ca/\delta = 1$. The results are shown for $Gr = 1$, $Pe = 5$, for the inviscid and viscous ($Re = 10$) cases, (a,b) $A = -0.5$ and various Ca and δ: $Ca = \delta = 0.02$ (solid line), $Ca = \delta = 0.04$ (dash line), $Ca = \delta = 0.08$ (dash-dot line). (c,d) $A = 0.5$ and various Ca and δ: $Ca = \delta = 0.03$ (solid line), $Ca = \delta = 0.06$ (dash line), $Ca = \delta = 0.12$ (dash-dot line).

of A. One sees that the increase in the surface tension reduces the range of the modes with the wave-like behaviour (i.e. the modes showing oscillatory decay). This results in the waves with shorter wavelengths being suppressed. However, the damping rates of other waves are just slightly affected by the increase of the capillary terms.

Figure 6.21 illustrates the existence of gravity and capillary waves at interfaces endowed with strong and weak diffusion, which correspond to $A = 0.5$ and $A = -0.5$ respectively. In the latter case both gravity and capillary waves develop where the unstable waves occur at long wavelengths. The decay rate of the perturbations is the same for both types of waves. However, the gravity waves propagate faster than capillary waves. In the case of strong diffusion ($A = 0.5$), gravity waves develop but capillary waves cease to exist; i.e. If $Gr = 0$ the perturbations decay aperiodically as indicated in Figure 6.21 (c,d).

In Figure 6.18 we saw that the properties of the interface are changed by varying the interface thickness, and the gradual reduction of the interface thickness does not produce the sharp interface behaviour. Such limiting behaviour can however be obtained by the simultaneous reduction of the capillary number and interface thickness, so that the ratio Ca/δ remains constant, which is illustrated in Figure 6.22.

Figure 6.23 shows the typical shapes of perturbations. The profiles are just slightly dependent on the value of the Reynolds and Peclet numbers. The widths of the eigenfunctions obtained for $Ca = 0$ (Figure 6.23 (a,b)) point out their similarity to the purely hydrodynamic modes of Figure 6.4, and hence the development of such perturbations is driven by the hydrodynamic terms. In the case of $Ca \neq 0$, the y-width of eigenfunctions depends on the interface thickness δ, so for thicker interfaces the thickness of the eigenfunction increases. Nevertheless, the widths of the shown eigenfunctions point out their similarity to the thermodynamic modes depicted in Figure 6.5 (e,f), which means that the evolution in this case is dominated by the thermodynamic effects.

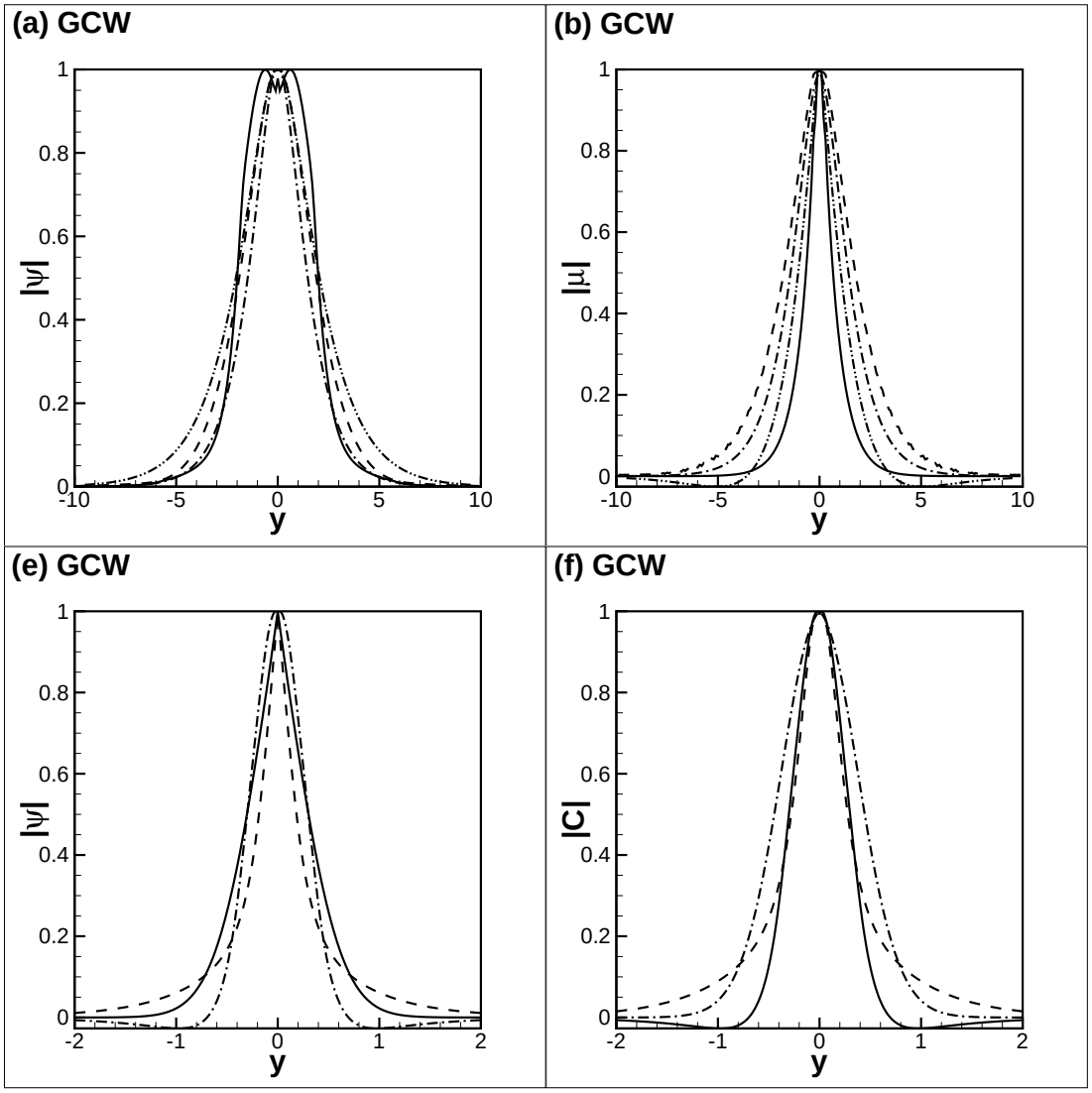

Figure 6.23: The eigenfunctions are plotted for the gravity-capillary waves at a miscible interface. (a,b) The capillary effects are disregarded. The moduli of the streamfunction (a) and chemical potential (b) are shown for $k = 2$, $Gr = 1$, $A = 0.5$, $\delta = 0.1$, for the inviscid and viscous cases. Solid line depicts the results for $Pe = 15$, inviscid case; dash line for $Pe = 5$, inviscid case; dash-dot line for $Pe = 15$ and $Re = 10$; and dash-dot-dot line for $Pe = 5$ and $Re = 10$. The eigenvalues are $\omega = (0.407, -0.542)$ ($Pe = 5$) and $\omega = (0.561, -0.275)$ ($Pe = 15$) for the viscous case and $\omega = (0.382, -0.444)$ ($Pe = 5$) and $\omega = (0.592, -0.187)$ ($Re = 15$) for the inviscid case. (c,d) The moduli of streamfunction (c) and concentration (d) are plotted for $k = 1.75$, $Pe = 5$, $Gr = -1$, $Ca = 0.04$, $A = -0.3$, and for $\delta = 3\delta_0$ (dash-dot line), $\delta = \delta_0$ (solid line), and $\delta = \delta_0/2$ (dash line). The eigenfunctions correspond to the eigenvalues of $\omega = (0.61, 0.005)$; ($\delta = 3\delta_0$), $\omega = (0.752, -0.193)$ ($\delta = \delta_0$), and $\omega = (0.61, -0.435)$ ($\delta = \delta_0/2$). The functions are normalized by the maximum values of the moduli.

6.4 Conclusions

We have investigated the linear evolution of the small normal disturbances to a flat horizontal phase boundary separating two slowly miscible liquids. The phase-field approach was employed to model the thermo- and hydrodynamic evolution of the binary mixture. The Boussinesq approximation of the full Cahn-Hilliard-Navier-Stokes equations was used to define the equations for the small normal disturbances. We were interested in the binary mixtures with the upper critical point, where the diffusivity is stronger. The thermodynamic states of the binary mixture were defined by the Landau free energy function, with the main phenomenological parameter A, which is negative for the subcritical temperatures and positive for the temperatures above the critical point.

Two primary aims pursued by this part of work were to understand the limits of the phase-field approach and to understand the effects of interfacial diffusion on the dynamics of the Rayleigh-Taylor instability and on the dispersion and dissipation of the gravity-capillary waves.

The work was fulfilled in three main steps. Firstly, we considered the pure hydrodynamic evolution (under the condition that $Pe \to \infty$) of a smeared interface. The results were validated through the use of the classical formulae obtained for sharp interfaces. We found that all classical expectations for the Rayleigh-Taylor instability and for the waves can be observed. In the case of the Rayleigh-Taylor instability (where a heavier liquid overlays a lighter one), all perturbations monotonically grow. The growth rates are reduced by the viscous and capillary forces. In the opposite configuration of a lighter liquid overlaying a heavier one, the gravity-capillary waves are developed, with the phase speed proportional to $k^{-1/2}$. The damping is defined by the viscous and capillary effects, reducing the range of the modes that exhibit the wave-like behaviour.

The sharp-interface results can be reproduced for thinner interfaces, but the situation is however different for $Ca = 0$ and $Ca \neq 0$. In the former case, the sharp interface results are achieved by a simple gradual reduction of the interface thickness. In the latter case, the interface thickness should be decreased simultaneously with the capillary number, keeping the ratio Ca/δ (which is proportional to the surface tension coefficient) constant. Such procedures allow ac-

curate reproduction of the eigenvalue spectrum of a sharp interface for the range of wavenumbers limited by $k\delta << 1$. For example, in order to reproduce the eigenvalue spectrum for $k \leq 5$, the interface thickness must be at least $\delta = 0.001$. This condition can however be relaxed on the basis of the following reasons. To describe the development of the Rayleigh-Taylor instability we may need to define accurately only the fastest growing mode, so the condition becomes $k_{max}\delta << 1$, or only the unstable modes, that are limited by the cut-off value $k_c = \sqrt{3\delta Gr/Ca}$ due to the capillary action, and the condition becomes $k_c\delta << 1$. In the case of the gravity-capillary waves, we may either be interested in the wave of a particular wavelength or in the modes that exhibit the wave-like behaviour, which are limited by the bifurcation point.

Next, we considered the pure thermodynamic instability of a diffuse interface. Contrary to the research results currently available in the literature, we treated Ca and δ as two independent parameters (in other works the stability of the kink solution, with $\delta_0 = \sqrt{-Ca/A}$, i.e. existent for $A < 0$, was investigated). We found that, for $A < 0$, all thermodynamic perturbations monotonically decay for thin interfaces, when $\delta \leq \delta_0$, and, for $A > 0$, all perturbations unconditionally decay. If however $A < 0$ and $\delta > \delta_0$, the longwave instability develops.

Finally, we considered the stability of miscible interfaces with respect to both thermo- and hydrodynamic perturbations. We found that the diffusivity introduces an additional dissipation, and its influence is very similar to the effects produced by the viscous force. The introduction of diffusivity slows the growth of the Rayleigh-Taylor instability and also reduces the propagation speeds of the gravity-capillary waves and increases the damping of the waves.

In general, the effects of viscosity, diffusivity and capillarity, dampen perturbations. However, these effects interplay and hence can emphasize or suppress each other. The cumulative viscous and diffusive damping is able to completely suppress the growth of the short wavelength modes, which is not observed when these effects act separately. The strong viscous or diffusive damping can make the effect of capillarity non-existent. That means that the use of the phase-field approach as a numerical method for describing the evolution of immiscible interfaces, should in general take into account the correlations between the Reynolds, Peclet, capillary numbers, and the interface thickness.

We also found the qualitative difference in the results obtained for $Ca = 0$ and $Ca \neq 0$. For the case of negligible capillary effects, the evolution of small perturbations is totally determined by hydrodynamics. The diffusion is included by the diffusive flux defined by the Fickian law, but we found that the concentration field in this case mostly adjusts the variations of the velocity field. If however $Ca \neq 0$, then the evolution of perturbations is dominated by the thermodynamic part of the mathematical problem. The difference in the results is even stronger for the gravity-capillary waves, when in the case of non-negligible capillary effects and when $A < 0$ and $\delta > \delta_0$, the thermodynamic longwave instability makes the layer unstable even if the lighter liquid overlays the heavier one.

Chapter 7

Shear flow along the interface between two miscible liquids

The objective of this chapter is to investigate the phase boundary separating two miscible liquids, which are in relative shear motion. Similar to the steps that were taken in Chapter 6, we carry on parametric linear stability analysis through the phase-field method. Kelvin-Helmholtz and Holmboe instabilities are added by imposing the flow along the interface.

7.1 Immiscible liquids

First, we study the instability of the interface separating two immiscible liquids ($Pe \to \infty$) that are in relative shear motion. For this purpose, the governing equations in linearised form (3.25), (3.26) and (3.27) can be simplified to

$$\begin{aligned} -i(\omega_i - kU_x)(\psi'' - k^2\psi) - ikU_x''\psi = \frac{1}{Re}\left(\psi^{vi} - 2k^2\psi + k^4\psi\right) +, \\ ikCa(\beta C_0'\psi'' + 2\beta' C_0'\psi' + (C_0'(\beta'' - k^2\beta) + C_0'''\beta)\psi) - \beta ikGr\psi, \end{aligned} \tag{7.1}$$

where the equation (7.1) describes the terms dependent on the effect of capillary number Ca and Grashof number Gr. The parameter β is given by

$$\beta = \frac{ikC_0'\psi}{kU_x - \omega}, \tag{7.2}$$

where its derivatives, presented by β' and β'', are easy to obtain.

For immiscible inviscid liquids, equation (7.1) can be reduced to a second order ordinary differential equation given by

$$\begin{aligned}(U_x k - \omega - kCa\beta C_0')\psi'' = 2k\beta'\, Ca\, C_0'\psi' \\ +k\left[k(kU_x-\omega) + U'' + Ca\left((\beta''-k^2\beta)C_0' - C'''\beta\right) + \beta Gr\right]\psi \end{aligned} \tag{7.3}$$

The dispersion relations of a sharp interface between two inviscid and viscous immiscible liquids were obtained in Chapter 5 for both $Gr < 0$ (where the heavier liquid stands over the lighter one) and $Gr > 0$ (the heavier liquid underlies the lighter one). These results are obtained based on the assumptions that both the shear interface thickness δ_u and concentration (density) thickness δ are infinitely thin.

However, in stratified flow, the interface thickness is smeared and prone to Holmboe instability if $Gr > 0$. For diffuse interface and no capillary effect, the linear differential equation (7.3) reduces to the classical Taylor-Goldstein equation given by

$$\psi'' - \left(k^2 - \frac{kU_x''}{\omega - kU_x} + \frac{k^2 J(y)}{(\omega - kU_x)^2}\right) = 0, \tag{7.4}$$

where $J(y) = C_0' Gr$ is the squared Brunt-Vaisala frequency.

The stability analysis of this equation was conducted for various density and velocity profiles. It was found that the interface is stable if the global Richardson number

$$Ri(y) = \frac{J(y)}{[U_x']^2} = \frac{C_0' Gr}{[U_x']^2} = \frac{Gr\delta_u^2}{2\delta}\frac{\cosh^4(y/\delta_u)}{\cosh^2(y/\delta)}, \tag{7.5}$$

is everywhere greater than 1/4. If in any circumstances $Ri(y) \leq 1/4$ then the instability is likely to occur but this not guaranteed. If this is the case, then a stability analysis is required for a definite answer.

For the basic profiles (3.1) and (3.5), the expression 7.5 indicates that the stability is determined by the Grashof number Gr and the thickness ratio δ_u/δ. In this case, we assume that $\delta_u > \delta$, so we expect that Holmboe instability develops for $\delta < \delta_u/2$ and $Gr > 0$.

The solution of the equations (7.1) and (7.3) are obtained through the ESM

or CCM methods as explained in the Chapter 4. Following the ESM method, where at $L \sim \pm L_\infty$ the asymptotic solutions are given as

$$y \to \infty : \quad \psi = A_1 \exp(-ky) + A_3 \exp(-q_1 y), \tag{7.6}$$

$$y \to \infty : \quad \psi = A_2 \exp(ky) + A_4 \exp(q_2 y), \tag{7.7}$$

where $q_1 \equiv \sqrt{k^2 - (k + i\omega Re)}$, $q_2 \equiv \sqrt{k^2 + (k - i\omega Re)}$, and A_1, A_2, A_3 and A_4 are arbitrary constants.

For immiscible inviscid liquids, the system of the ordinary differential equations of the first order (7.3) becomes

$$\mathbf{f}' = \begin{pmatrix} 0 & 1 \\ A_{21} & A_{22} \end{pmatrix} \mathbf{f}, \tag{7.8}$$

where $\mathbf{f} = (\psi_0, \psi_1)^T = (\psi, \psi')^T$ and the elements of the matrix are

$$A_{21} = \frac{k(k(kU_x - \omega) - U_x'' + CaC_0'\beta'')}{kU_x - \omega - kCa\beta C_0'} + \frac{k(Ca(kC_0' + C''') - Gr)}{kU_x - \omega - kCa\beta C_0'},$$

$$A_{22} = \frac{2kCa\beta' C_0'}{kU_x - \omega - kCa\beta C_0'}.$$

7.1.1 $Gr < 0$: the heavier liquid is on top of the lighter one

If $Gr < 0$, a horizontal phase boundary is always unstable due to the Rayleigh-Taylor instability. If in addition, the neighbouring liquids participate in a relative motion, the Rayleigh-Taylor instability competes with the Kelvin-Helmholtz instability. This is illustrated in Figure 7.1 (a), where the increase in the intensity of the imposed flow leads to a stronger growth of the modes with the longer wavelengths, and to a weaker growth of the modes with the shorter wavelengths. Thus, the instabilities do not sum up, as some modes develop slower, but this result agrees well with the simple analytic formula (5.46) for sharp interfaces and also with the earlier studies, [39, 164] in which the stability of smeared interfaces was previously examined. Figure 7.1 (a) also depicts the data for the inviscid and viscous liquids, showing the dissipative role of the viscous force.

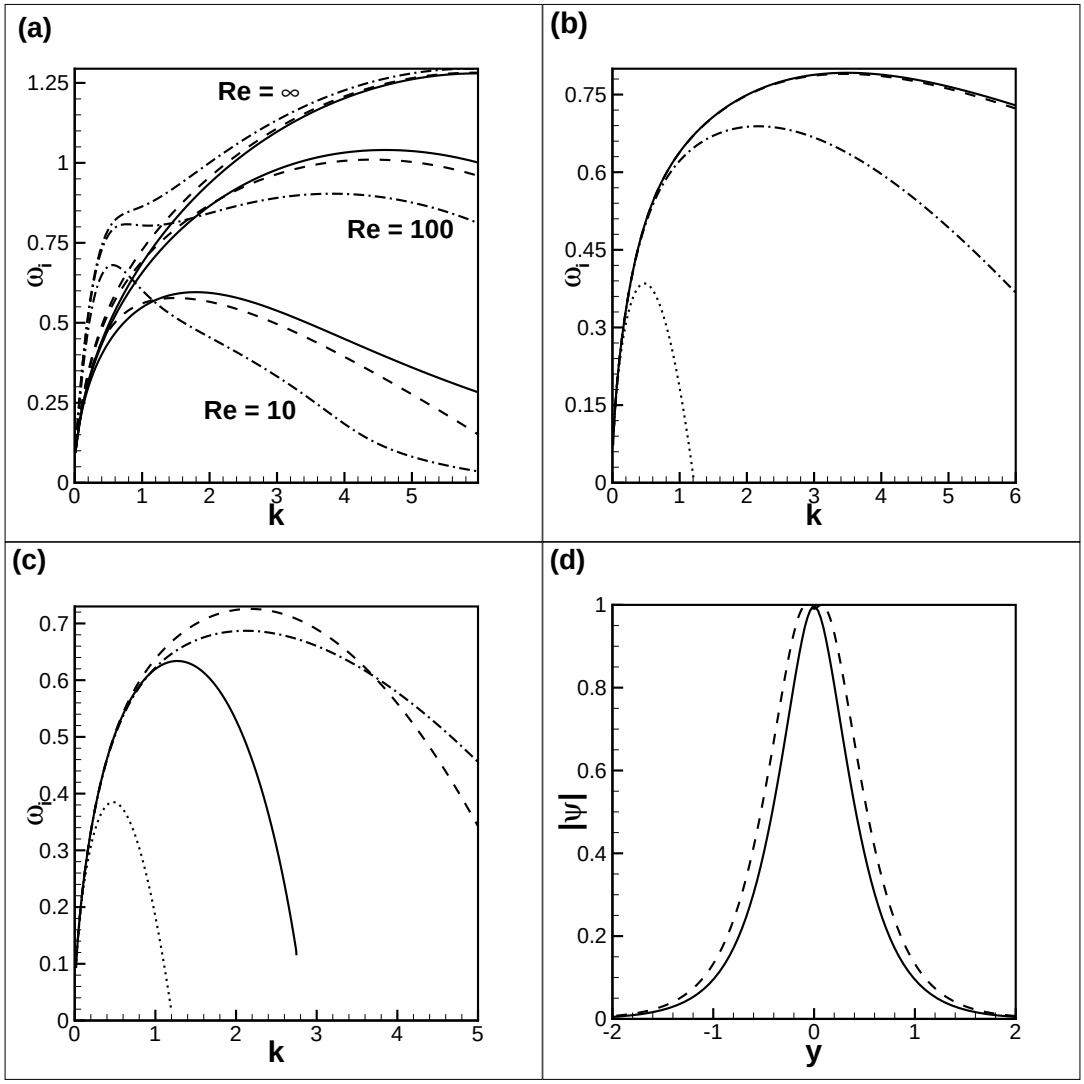

Figure 7.1: (a-c) The eigenspectra are plotted for an immiscible interface that separates the heavier liquid lying over the lighter liquid. The curves are plotted for $Gr = -1$, $\delta_u = 1$ and (a) $Ca = 0.001$, $\delta = 0.05$, $U_0 = 0$ (solid lines), $U_0 = 1$ (dashed lines), and $U_0 = 3$ (dash-dot lines) for three different Reynolds numbers: $Re = 1$, $Re = 100$, and $Re = 10$; (b) $Ca = 0$, $Re = 25$, $U_0 = 1$ and different values of δ: $\delta = 0.001$ (solid line), $\delta = 0.01$ (dash line), $\delta = 0.1$ (dash-dot line), and $\delta = 1$ (dot line); (c) $Ca = 0.001$, $Re = 25$, $U_0 = 1$, and different δ (lines as in (b)). (d) The eigenfunctions, namely the moduli of the stream functions, are plotted for $k = 3$, $Gr = -1$, $Re = 25$, $U_0 = 1$, $\delta = 0.01$, $Ca = 0$ (solid line) and $Ca = 0.01$ (dash line). The eigenvalues are $\omega = (0, 0.750)$ for $Ca = 0$, and $\omega = (0, 0.531)$ for $Ca = 0.01$.

Figures 7.1 (b,c) show the growth rates for perturbations developing at the interfaces of different thicknesses for the cases of $Ca = 0$ (Figure 7.1 b) and $Ca = 0.001$ (Figure 7.1 (c)). The results are similar to what we earlier observed in Chapter 6 for the case of pure Rayleigh-Taylor instability. Namely, for $Ca = 0$, we observe convergence to the sharp interface behaviour. If however the capillary effects are non-neglected, a simple reduction in the interface thickness leads to the growth of the surface tension (which is proportional to Ca/δ, see (3.4) and (5.46)) and to the strong damping of the short wavelength modes. For the pure Rayleigh-Taylor instability it was shown that the sharp interface behaviour can be revealed by simultaneous decrease of the interface thickness and capillary number. This however was not observed in the presence of the shearing flow.

Figure 7.1 (d) shows the shapes of the eigenfunctions, i.e. the ψ profiles of the stream functions for two cases of $Ca = 0$ and $Ca = 0.001$. In terms of the eigenfunctions, the difference between the cases of zero and non-zero capillary effects is not very strong. The eigenfunctions plotted for the interfaces of different thicknesses were also found to be almost coincident.

7.1.2 $Gr > 0$: the lighter liquid superposes the heavier one

The configuration with the heavier liquid lying underneath the lighter liquid would obviously be stable without externally imposed flow, and the flow could make this configuration unstable. The stability diagrams are depicted in Figure 7.2, where one sees that the flow makes the interface unstable towards the Kelvin-Helmholtz and Holmboe instabilities. The Kelvin-Helmholtz instability is limited to the lower Grashof numbers (smaller density contrasts), while the evolution at the higher Grashof numbers is dominated by the Holmboe instability. The zone of the Holmboe instability is usually large (in comparison to the zone of the Kelvin-Helmholtz instability), and even remains unclosed from the top for immiscible interfaces between inviscid liquids, when the growth of unstable modes is not stabilised even by the strong gravity force. Similar stability diagrams were earlier reported in other works [71, 141].

Figure 7.2 (a) shows the stability diagrams for the capillary forces of different

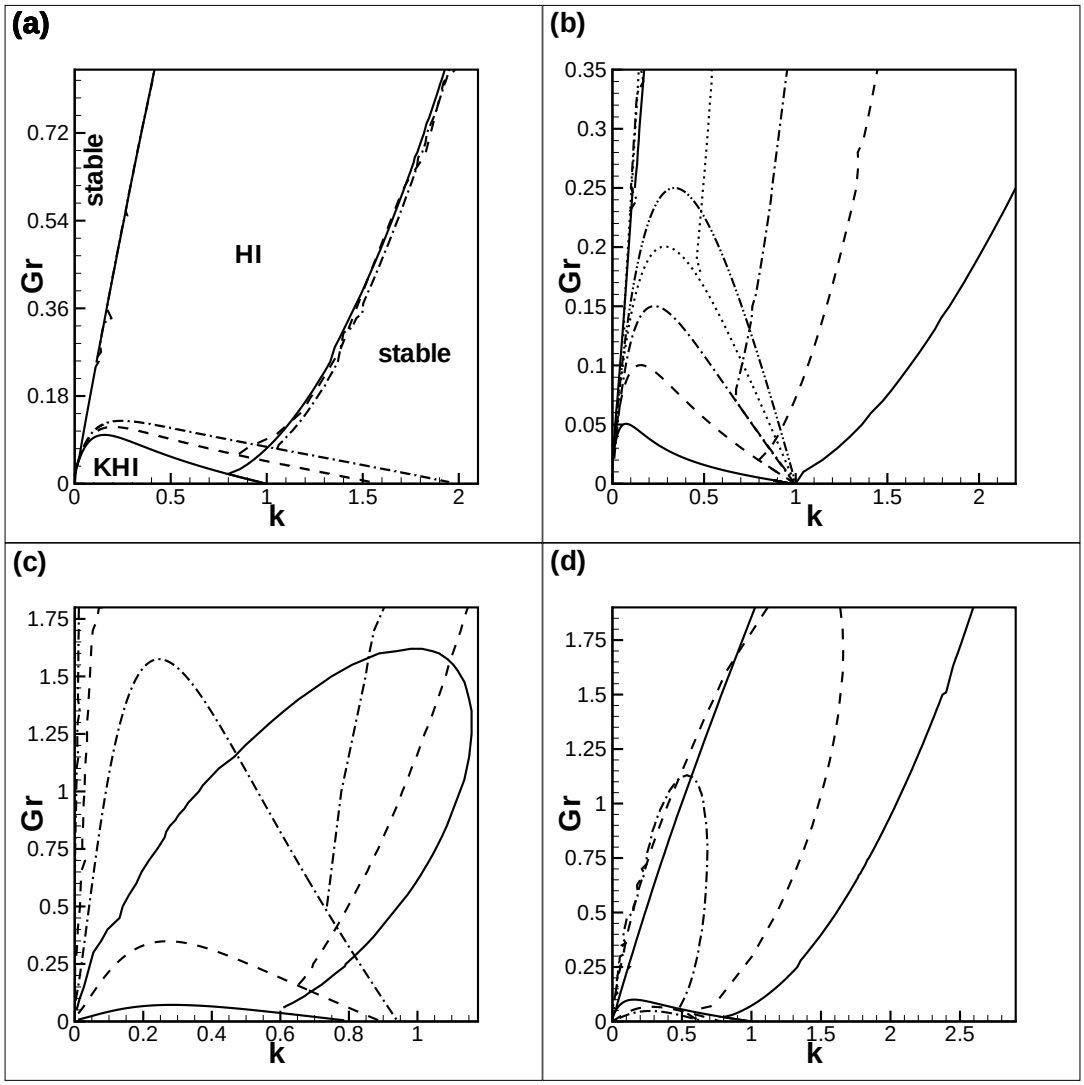

Figure 7.2: The neutral curves defining the zones of the Kelvin-Helmholtz (KHI) and Holmboe (HI) instabilities. The results are obtained for an immiscible ($Pe = 1$) horizontal interface separating two liquids with the heavier liquid at the bottom. The parameters are (a) $\delta = 0.2$, $U_0 = 1$, $Re = \infty$ and different values of Ca: $Ca = 0$ (solid line), $Ca = 0.0005$ (dash line), and $Ca = 0.001$ (dash-dot line); (b) $Re = 1$, $U_0 = 1$ and different values of δ: $\delta = 0.1$ (solid line), $\delta = 0.2$ (dash line), $\delta = 0.3$ (dash-dot line), $\delta = 0.4$ (dot line), and $\delta = 0.5$ (dash-dot-dot line); (c) $\delta = 0.2$, $Re = 20$ and different values of U_0: $U_0 = 1$ (solid line), $U_0 = 2$ (dash line), and $U_0 = 4$ (dash-dot line); (d) $\delta = 0.2$, $U_0 = 1$ and different values of Re: $Re = \infty$ (solid line), $Re = 50$ (dash line), and $Re = 10$ (dash-dot line). $\delta_u = 1$ for all plots.

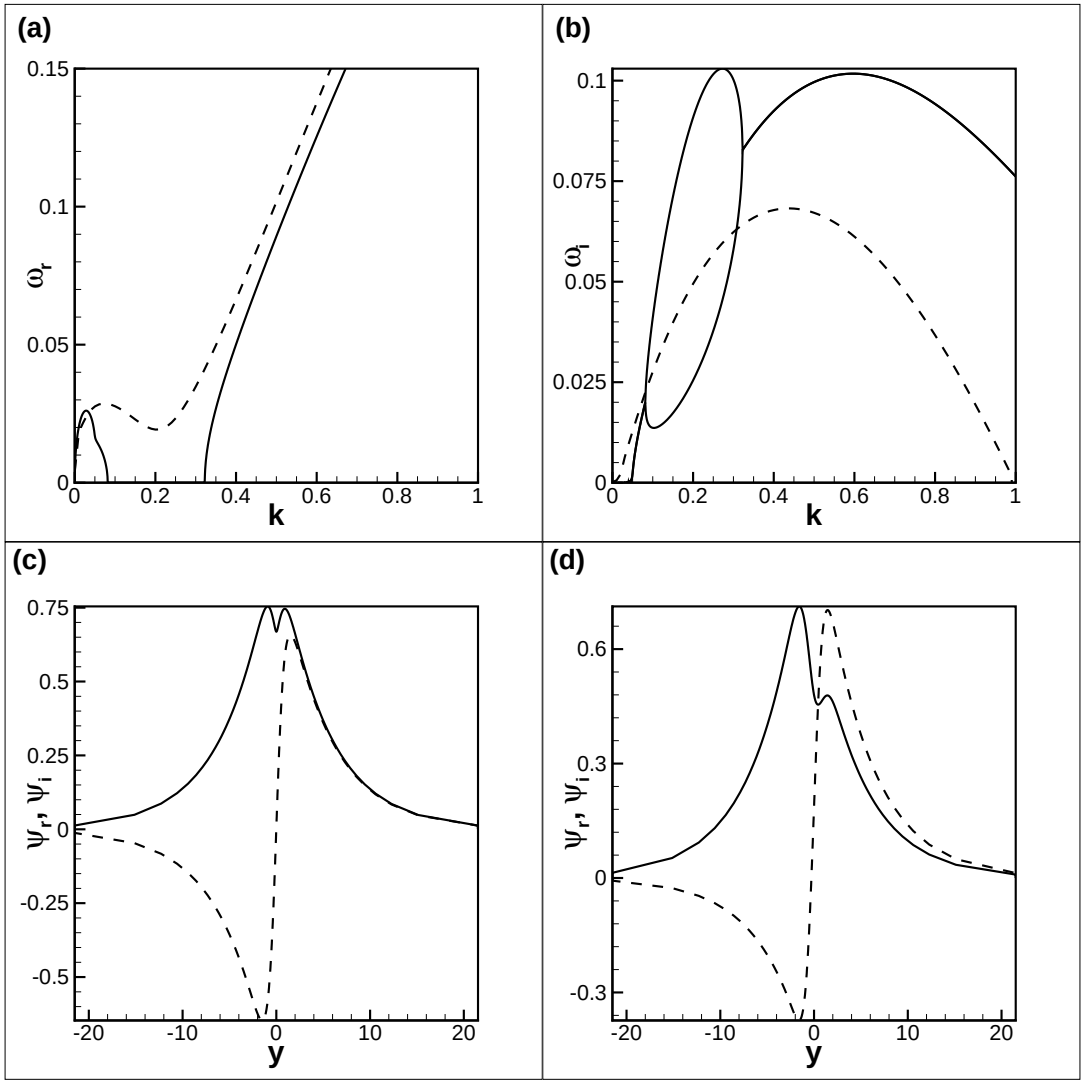

Figure 7.3: (a,b) The eigenspectra for the perturbations developing at an immiscible ($Pe = 1$) horizontal interface with the heavier liquid underneath the lighter one. The curves are shown $Gr = 0.1$, $Ca = 0$, $\delta = 0.1$ and different values of Re: $Re = 1$ (solid lines) and $Re = 50$ (dash lines). (a) shows ω_r and (b) shows ω_i. (c,d) The eigenfunctions, namely, the real (solid lines) and imaginary (dashed lines) parts of the stream function, are plotted for $k = 0.2$, $Gr = 0.1$, $Ca = 0$, $\delta = 0.1$, and (c) $Re = 1$, the eigenvalue is $\omega = (0, 0.092)$; and (d) $Re = 50$, $\omega = (0.022, 0.049)$. $\delta = 1$ for all plots.

strengths. Surprisingly, the increase in surface tension does not make the interface more stable. On the contrary, the capillary forces extend the range of the Kelvin-Helmholtz instability to the modes with shorter wavelengths and slightly widen the zone of the Holmboe instability.

Figure 7.2 (b) depicts the neutral curves for the interfaces of different thicknesses. Thicker interfaces are more sensitive to the Kelvin-Helmholtz instability. The range of Holmboe instability is however decreased for such interfaces, and, for the case of $Ca = 0$ and $U_0 = 1$, the Holmboe modes cease to exist if $\delta > 0.417$. In the opposite limit of thinner thicknesses, the Kelvin-Helmholtz instability becomes strongly suppressed and the instability is primarily defined by the Holmboe modes.

Figure 7.2 (c) shows how the increase in the amplitude of the imposed flow affects the shapes of the neutral curves. As expected, the zones of both Kelvin-Helmholtz and Holmboe instabilities increase. The curves are plotted for the finite value of the Reynolds number and by making comparison against Figure 7.2 (a), one notices that viscosity closes up the zones of the Holmboe instability, so the instability is suppressed by stronger gravity. Figure 7.2 (d) defines the stability diagrams for the different strengths of the viscous forces, additionally illustrating that viscosity reduces the range of unstable modes.

The typical eigenspectra are depicted in Figures 7.3 (a,b). The results are shown for the parameters of Figure 7.2 (b), for $Gr = 0.1$, and for the inviscid and viscous cases. In these plots, one sees that there is a short range of stable modes closer to $k = 0$, then there is a range of unstable modes (for which ω_i is positive), and again the instability is reinstated at larger wave numbers. The Kelvin-Helmholtz modes have zero wave speeds ($\omega_r = 0$), and the Holmboe modes are characterised by non-zero speeds (the positive branch of ω_r is only shown, and there is another symmetric branch with negative ω_r defining the wave travelling in the opposite direction). The development of the Kelvin-Helmholtz modes can be suppressed by viscosity (like that is shown in Figure 7.3 (b)), nevertheless, the modes remain unstable in respect to the Holmboe instability.

Figures 7.3 (c,d) depict the typical shapes of eigenfunctions. Figure 7.3 (c) depicts the Holmboe mode and Figure 7.3 (d) depicts the Kelvin-Helmholtz mode, the shapes of which are however not substantially different. The eigenfunctions

are much wider in comparison to the similar functions plotted for the gravitationally unstable configuration (Figure 7.1 (d)). In addition, there appears some non-symmetry about the middle point.

7.2 Miscible liquids

The objective of this section is to investigate the coupling of the thermodynamic and hydrodynamic effects on miscible displacements. The general case of the system of equations is given as follows

$$\begin{aligned} i(U_x k-\omega)(\psi''-k^2\psi)-ikU_x'' = \frac{1}{Re}(\psi^{iv}-2k^2\psi''-k^4\psi)+ \\ Cak[(C''-k^2C)C_0'-C_0'''C]-ikGrC, \end{aligned} \tag{7.9}$$

$$\begin{aligned} CaC^{iv}-\left(D_0+2Cak^2\right)C''-2D_0'C'+ \\ \left(k^2\left(D_0+Cak^2\right)-D_0''-iPe(U_xk-\omega)\right)C=-ikPeC'\psi, \end{aligned} \tag{7.10}$$

Similarly to the steps in Chapter 4, the asymptotic solutions at $y \to \pm\infty$ are used to defined the boundary conditions used to initialize the system of the first order differential equations

$$\mathbf{f}' = A\mathbf{f}, \tag{7.11}$$

where $\mathbf{f} = (f_0, f_1, f_2, f_3, f_4, f_5, f_6, f_7)^T = (\psi, \psi', \psi'', \psi''', \hat{C}, \hat{C}', \hat{C}'', \hat{C}''')^T$ and

$$A = \begin{pmatrix} 0 & 1 & 0 & 0 & 0 & 0 & 0 & 0 \\ 0 & 0 & 1 & 0 & 0 & 0 & 0 & 0 \\ 0 & 0 & 0 & 1 & 0 & 0 & 0 & 0 \\ A_{41} & 0 & A_{43} & 0 & A_{45} & 0 & A_{47} & 0 \\ 0 & 0 & 0 & 0 & 0 & 1 & 0 & 0 \\ 0 & 0 & 0 & 0 & 0 & 0 & 1 & 0 \\ 0 & 0 & 0 & 0 & 0 & 0 & 0 & 1 \\ A_{81} & 0 & 0 & 0 & A_{85} & A_{86} & A_{87} & 0 \end{pmatrix},$$

with the elements of matrix given as

$$A_{41} = -k^2(k^2 + (U_x k - iRe\omega) + iReU_x''), \quad A_{43} = 2k^2 + iRe(U_x k - \omega),$$
$$A_{45} = ikRe((k^2 C_0' + C''')Ca - Gr), \quad A_{47} = -ikReCaC_0', \quad A_{81} = \frac{iPekC_0'}{Ca},$$
$$A_{85} = \frac{D_0'' - k^2 D_0 - k^4 Ca - iPe(U_x k - \omega)}{Ca}, \quad A_{86} = 2D_0'/Ca, \quad A_{87} = \frac{2k^2 Ca + D_0}{Ca}.$$

The boundary conditions at $y \to \pm L_\infty$ are given by

$$\mathbf{f}_1 = (1, \pm k, k^2, \pm k^3, 0, 0, 0, 0)^T \exp(\pm ky), \tag{7.12}$$
$$\mathbf{f}_2 = (1, \pm q_{1,2}, q_{1,2}^2, \pm q_{1,2}^3, 0, 0, 0, 0)^T \exp(\pm ky), \tag{7.13}$$
$$\mathbf{f}_3 = (\beta_{1,2}, \pm\beta_{1,2}p_{1,2}, \beta_{1,2}p_{1,2}^2, \pm\beta_{1,2}p_{1,2}^3, 1, \pm p_{1,2}, p_{1,2}^2, \pm p_{1,2}^3)^T \exp(\pm p_{1,2} y), \tag{7.14}$$
$$\mathbf{f}_4 = (\beta_{3,4}, \pm\beta_{3,4}p_{3,4}, \beta_{3,4}p_{3,4}^2, \pm\beta_{3,4}p_{4,3}^3, 1, \pm p_{3,4}, p_{3,4}^2, \pm p_{3,4}^3)^T \exp(\pm p_{3,4} L), \tag{7.15}$$

where

$$p_{1,2} = \sqrt{\frac{1}{2}(2k^2 + D_0/Ca) \pm \frac{1}{2}\sqrt{D_0^2/Ca^2 - 4iPe(U_0 k - \omega)/Ca}}, \tag{7.16}$$
$$p_{3,4} = \sqrt{\frac{1}{2}(2k^2 + D_0/Ca) \pm \frac{1}{2}\sqrt{(D_0^2/Ca^2 + 4i\,Pe(U_0 k + \omega)/Ca)}}, \tag{7.17}$$
$$q_{1,2} = \sqrt{k^2 + iRe(U_{1,2}k - \omega)}, \tag{7.18}$$
$$\beta_{1,2} = -\frac{iGrkRe}{(p_{1,2}^2 - q_{1,2}^2)(p_{1,2}^2 - k^2)}, \tag{7.19}$$
$$\beta_{3,4} = -\frac{iGrkRe}{(p_{3,4}^2 - q_{1,2}^2)(p_{3,4}^2 - k^2)}. \tag{7.20}$$

For the CCM method, the eigenvalues λ can be obtained from the system of equations

$$\begin{pmatrix} (F^{(4)} - 2k^2 G^{(2)} + k^4)/Re & M - iGrkI \\ -iC_0' kI & \frac{1}{kPe}(iU_0'' I + T) \end{pmatrix} V = \lambda \begin{pmatrix} (F^{(2)} - k^2 I) & Z \\ Z & I \end{pmatrix} V. \tag{7.21}$$

Where

$$F^{(1)} = mG^{(1)}, \tag{7.22}$$

$$F^{(2)} = m^2 G^{(2)} + m' G^{(1)} - k^2 I, \tag{7.23}$$

$$F^{(4)} = F^{(2)}\, F^{(2)}, \tag{7.24}$$

$$M = -iCak[(F^{(2)} - k^2 I)C_0' - C_0''' I], \tag{7.25}$$

$$T = 2D_0' F^{(1)} + D_0 F^{(2)} - Ca\, F^{(4)}, \tag{7.26}$$

where m, $G^{(1)}$, $G^{(2)}$ are defined in Chapter 4.

Since the current part is based on the parametric study, the equations used for the calculation of the solutions of the other cases of inviscid and viscous miscible liquids for $Ca = 0$ and $Ca \neq 0$, are given in appendix B. 2.

7.2.1 Heavier liquid stands over the lighter one: $Gr < 0$

For miscible liquids, the configuration with the heavier liquid on top of the lighter liquid remains unconditionally unstable. Figure 7.4 to Figure 7.8 show the growth rates as functions of the wavenumber for various values of the non-dimensional parameters. Figures 7.4 and 7.5 depict the results obtained for $Ca = 0$, and Figures 7.6 and 7.7 illustrate the changes in the eigenspectra enforced by the capillary terms. In general, we may conclude that the effect of capillarity is mostly reduced to damping of the shortwave modes.

Figure 7.4 (a) shows that diffusion slows down the growth of perturbations. The viscosity also plays the dissipating role, which is illustrated in Figures 7.4 (c) and 7.7 (a).

Figures 7.4 (b) and 7.6 (a,b) show the growth rates for the perturbations developing at interfaces of different thicknesses. In Section 6.3.1, it was shown that the interface instability is sensitive to the thickness δ in both immiscible viscous liquids and miscible inviscid liquids. If the interface is subjected to shear motion, Figure 7.5 (c) shows that the interface keeps the same influence on the instability for immiscible viscous liquids as in stationary liquids. While in the case of miscible inviscid liquids, the interface responses to the perturbations differently than in the case of stationary liquids for sharp and thick interfaces. There are

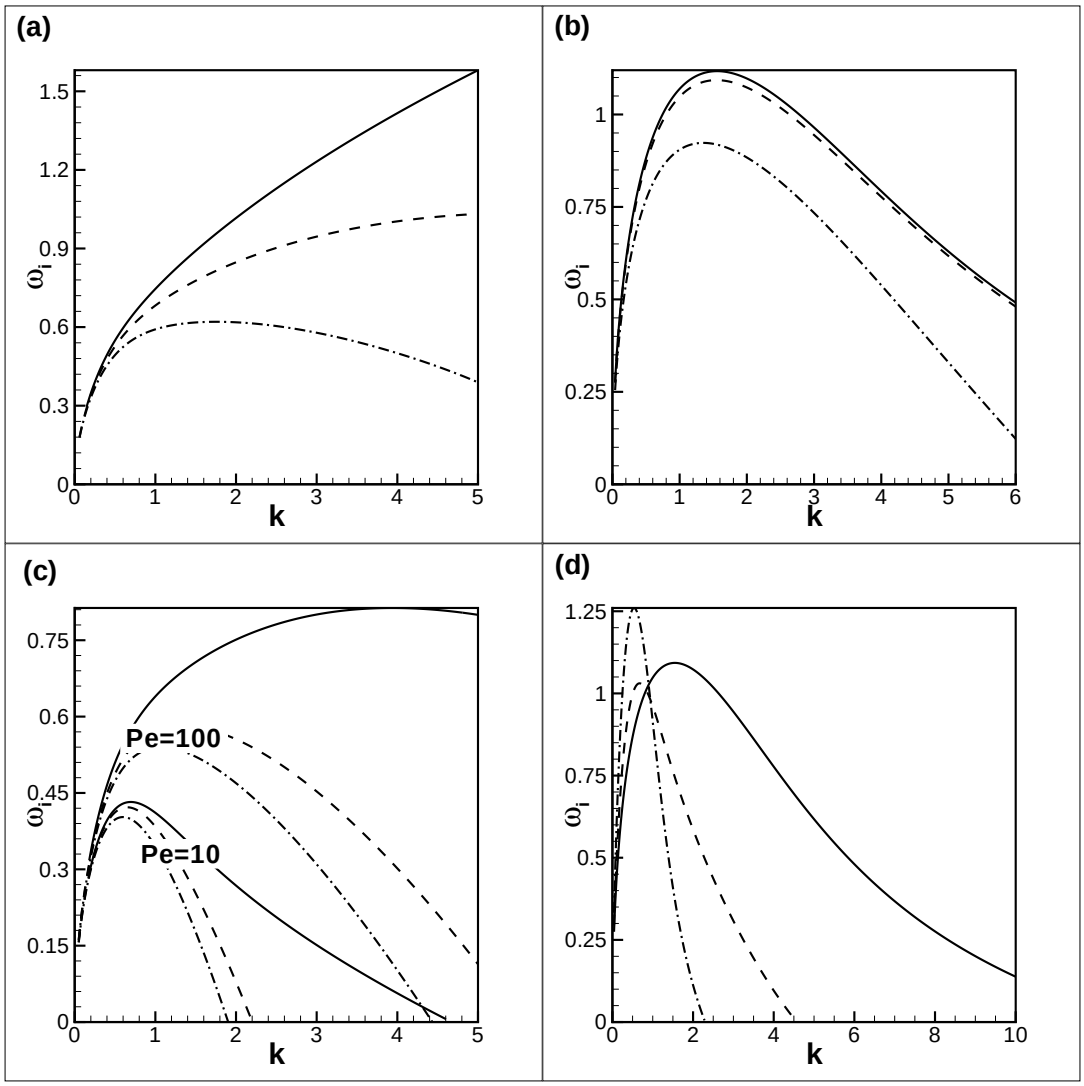

Figure 7.4: The eigenspectra for a miscible interface separating two liquids with the lighter liquid at the bottom. The curves are plotted for $Ca = 0$, $\delta_u = 1$ and (a) $Gr = 1$, $\delta = 0.1$, $Re = \infty$, $A = 0.5$, $U_0 = 1$, and different values of Pe: $Pe = \infty$ (solid line), $Pe = 250$ (dash line), and $Pe = 50$ (dash-dot line). (b) $Gr = -1$, $Pe = 20$, $Re = \infty$, $A = 0.5$, $U_0 = 1$ and different values of δ: $\delta = 0.001$ (solid line), $\delta = 0.01$ (dash line), and $\delta = 0.1$ (dash-dot line). (c) $A = 0.5$, $Gr = 1$, $U_0 = 1$, $\delta = 0.1$, $Pe = 10$ and $Pe = 100$ and different values of Re: $Re = \infty$ (solid lines), $Re = 50$ (dash lines), and $Re = 25$ (dash-dot lines). (d) $Gr = -1$, $\delta = 0.01$, $Pe = 20$, $Re = \infty$ and different values of U_0: $U_0 = 1$ (solid line), $U_0 = 3$ (dash line), and $U_0 = 5$ (dash-dot line).

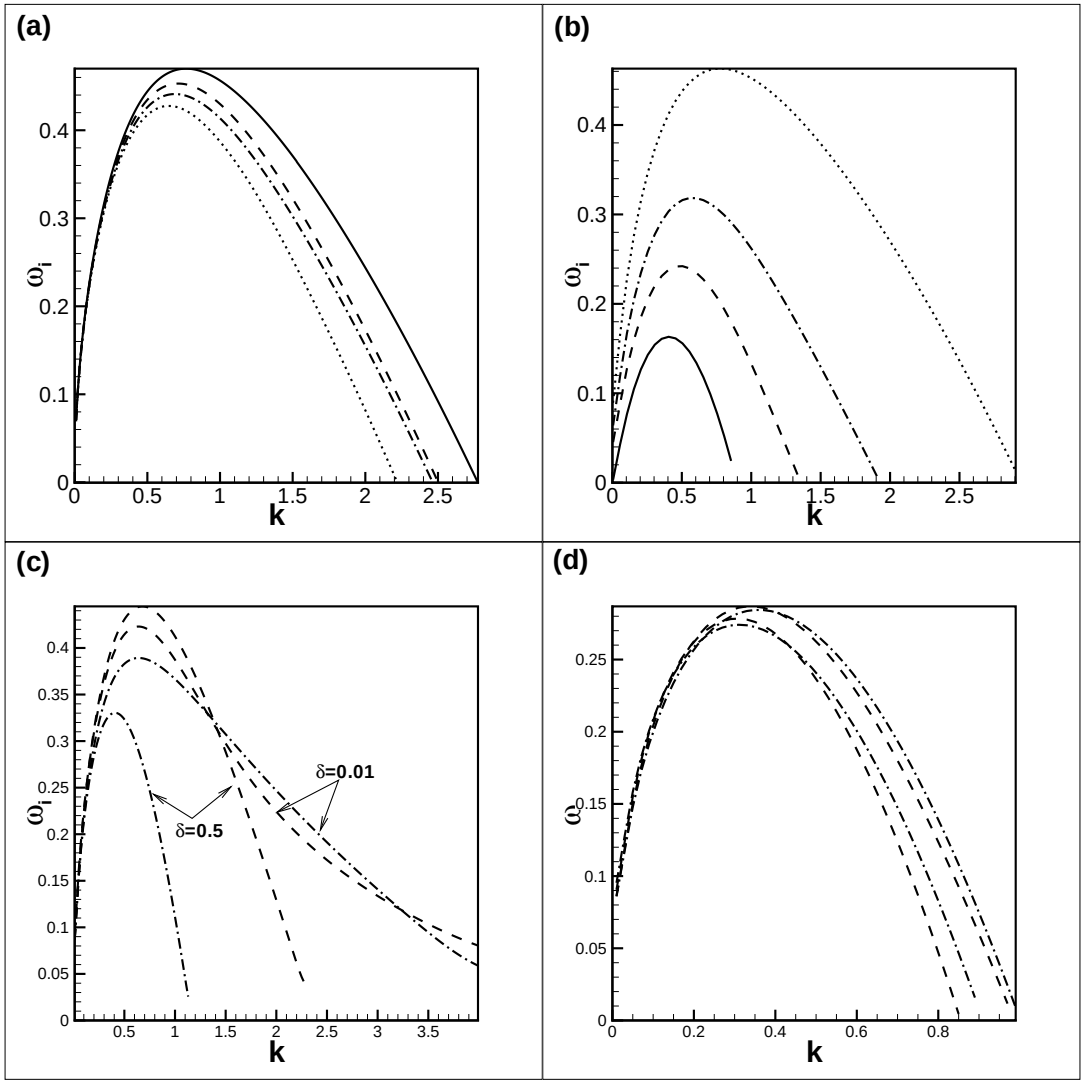

Figure 7.5: The eigenspectra for a miscible interface separating two liquids with the lighter liquid at the bottom. The curves are plotted for $U_0 = 1$, $Ca = 0$, $\delta_u = 1$. (a) $Gr = 1$, $\delta = 0.01$, $Pe = 20$, $Re = 50$, and $A = -0.5$ (solid line), $A = -0.25$ (dash line), $A = 0.25$ (dash-dot line), and $A = 0.5$ (dotted line). (b) $Pe = 20$, $Re = 50$, $A = 0.5$, $\delta = 0.1$, and $Gr = 0$ (solid line), $Gr = -0.25$ (dash line), $Gr = -0.5$ (dash-dot line), and $Gr = 1$ (dot line). (c) $Gr = -1$, $Pe = 10$ and $Re = \infty$ (dash lines), $Re = 2.5$ and $Pe = \infty$ (dash-dot lines). (d) $A = 0.5$, $Pe = 10$ and $Re = 2.5$ (dash lines), $Re = 10$ and $Pe = 2.5$ (dash-dot lines)

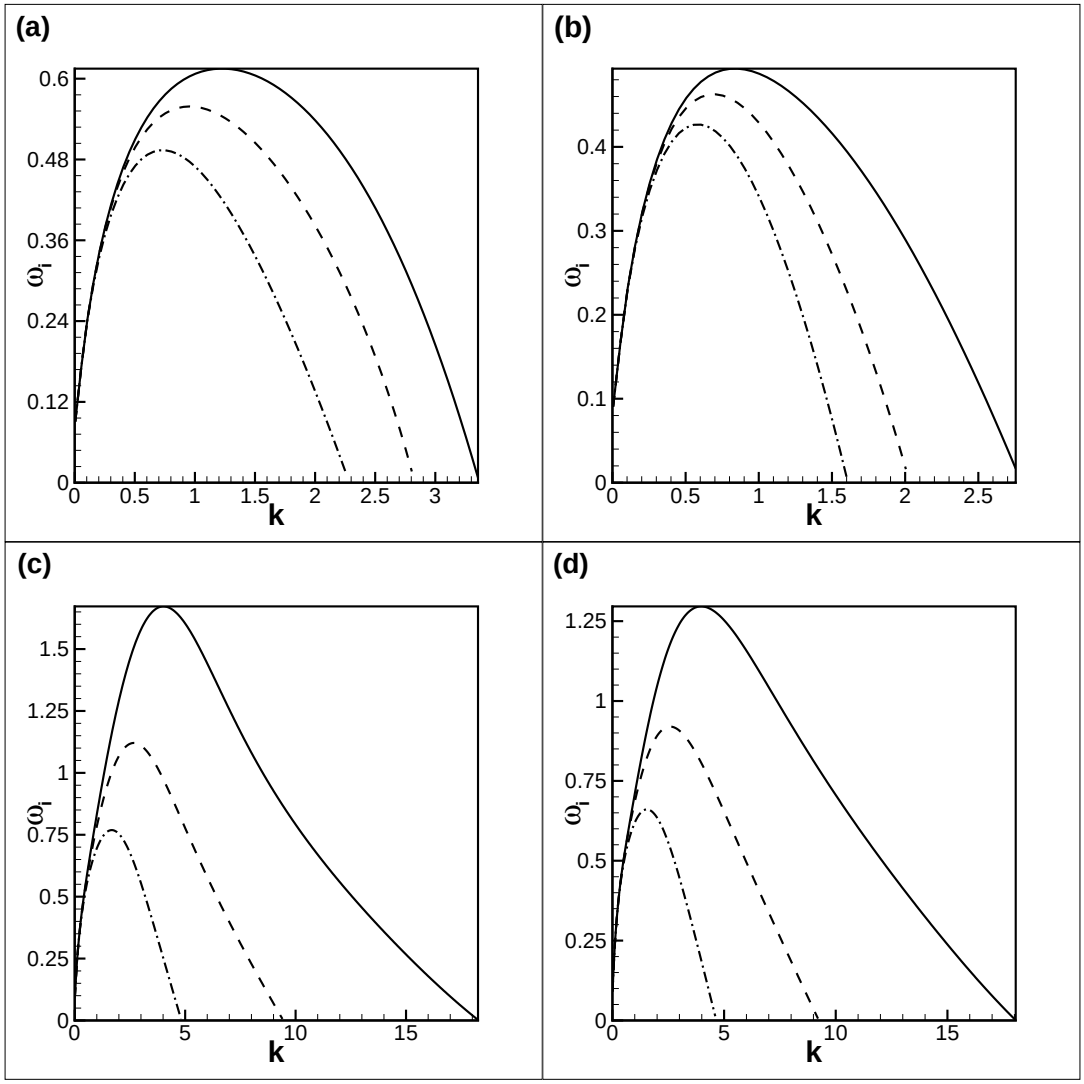

Figure 7.6: The eigenspectra for a miscible interface between two liquids with the lighter liquid at the bottom. The curves are plotted for $\delta_u = 1$, $Gr = -1$, $U_0 = 1$, $Pe = 20$. (a) $Ca = 0.05$, $Re = \infty$, $A = -0.5$ and different values of δ: $\delta = 0.3$ (solid line), $\delta = 0.5$ (dash line), and $\delta = 0.8$ (dash-dot line). (b) $Re = \infty$, $Ca = 0.05$, $A = 0.5$ and for different δ (lines named as in (a)). (c) $Re = 20$, $A = -0.5$, and $Ca = \delta = 0.05$ (solid line), $Ca = \delta = 0.1$ (dash line), $Ca = \delta = 0.2$ (dash-dot line). (d) $Re = 20$, $A = -0.5$, and the values of Ca and δ, and lines are named as in (c).

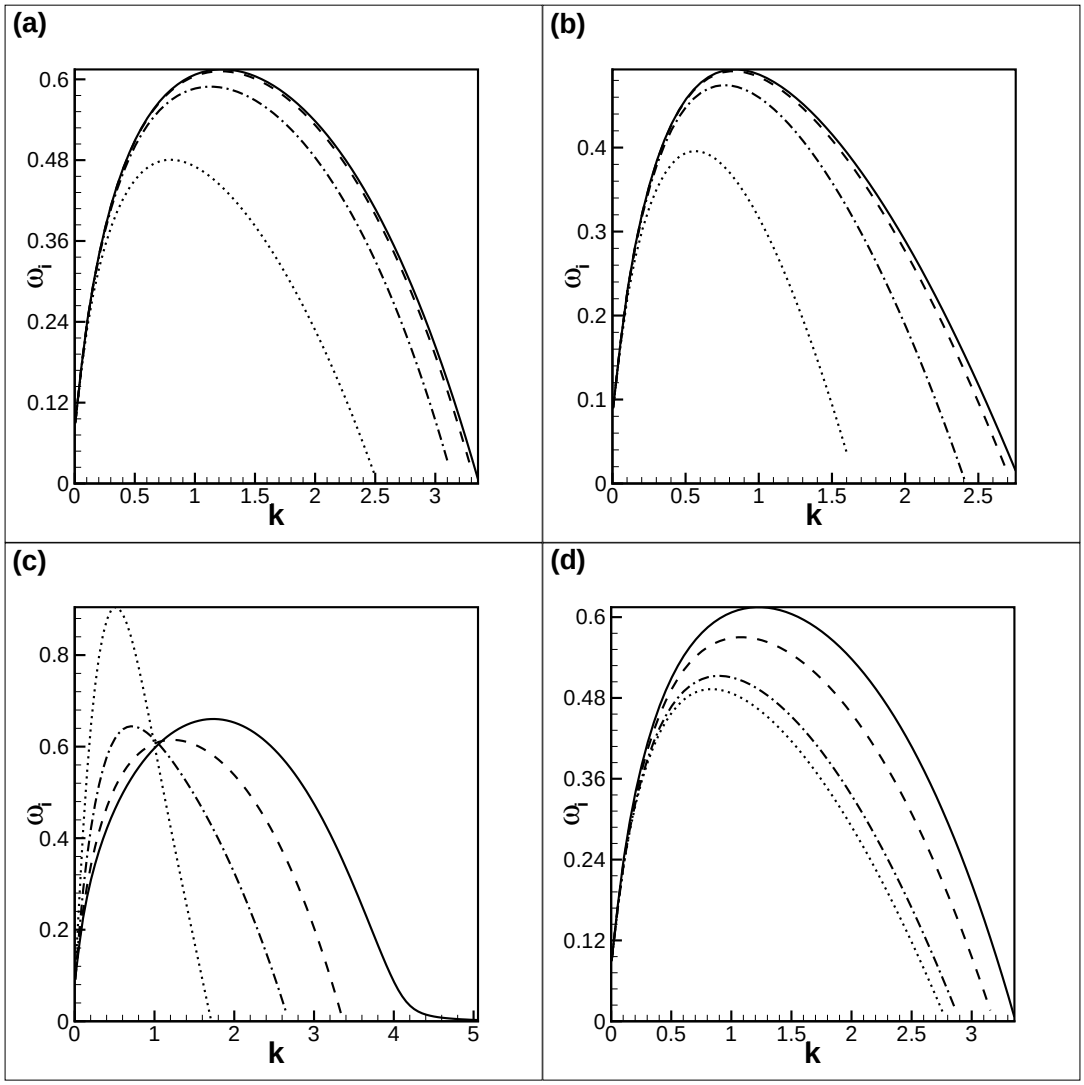

Figure 7.7: The eigenspectra for a miscible interface between two liquids with the lighter liquid at the bottom. The curves are plotted for $Gr = 1$, $Pe = 20$, $Ca = 0.05$, $\delta = 0.3$, $\delta_u = 1$. (a) $A = -0.5$, $U_0 = 1$ and different values of Re: $Re = \infty$ (solid line), $Re = 1000$ (dashed line), $Re = 100$ (dash-dot line), and $Re = 10$ (dot line). (b) $A = 0.5$, $U_0 = 1$, and different Re (lines as in (a)). (c) $Re = \infty$, $A = 0.5$ and different values of U_0: $U_0 = 0$ (solid line), $U_0 = 1$ (dash line), $U_0 = 2$ (dash-dot line), $U_0 = 4$ (dot line). (d) $U_0 = 1$, $Re = \infty$ and different values of A: $A = -0.5$ (solid line), $A = -0.25$ (dash line), $A = 0.25$ (dash-dot line), and $A = 0.5$ (dot line).

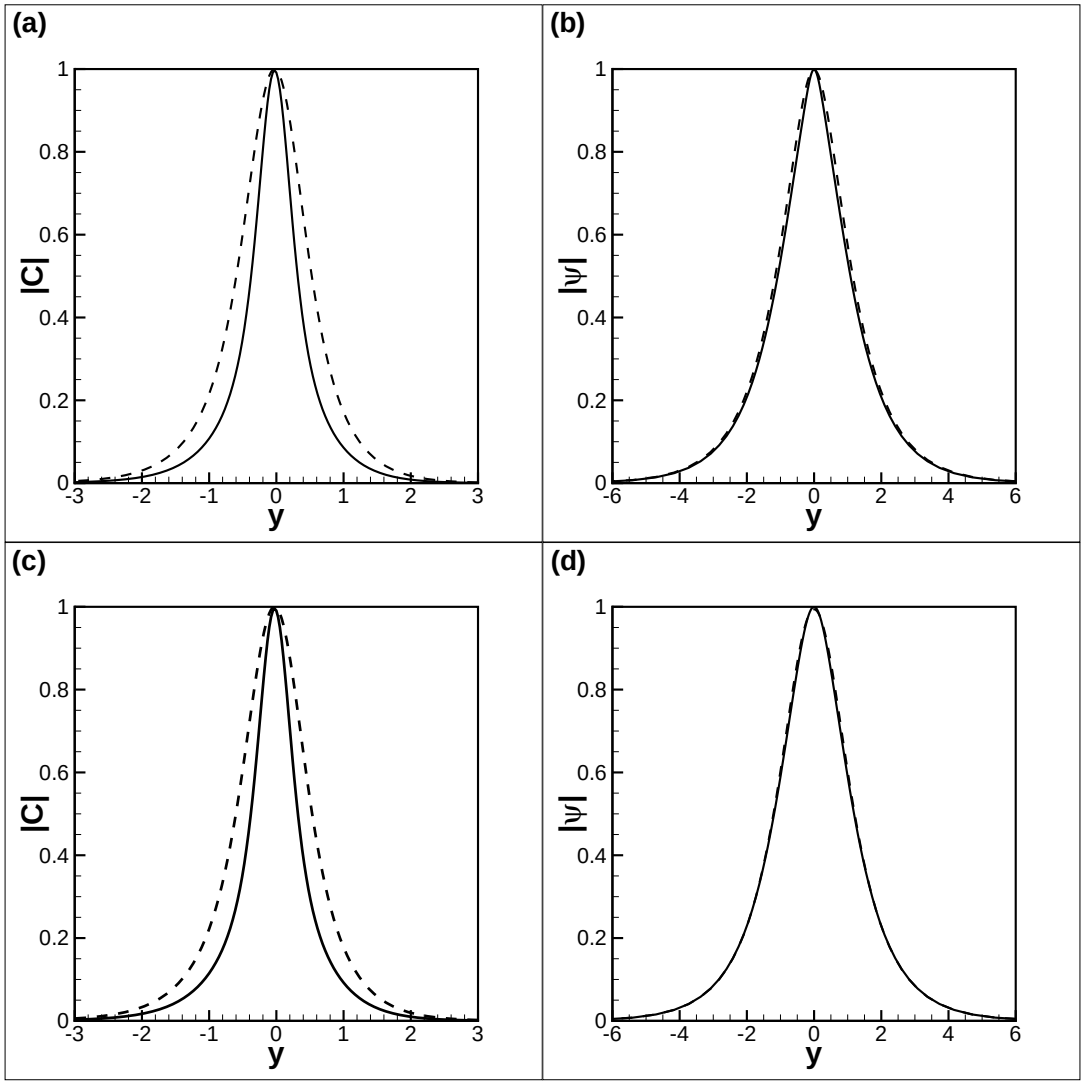

Figure 7.8: The eigenfunctions, namely the moduli of the concentration (a,c) and streamfunction (b,d) are shown for $k = 1$, $Gr = 1$, $Pe = 20$, $Ca = 0.05$, $\delta_u = 1$, $U_0 = 1$, $Re = \infty$, $\delta = 0.3$ (solid lines) and $\delta = 0.8$ (dash lines). The results are plotted for $A = -0.5$ (a,b) and $A = 0.5$ (c,d). The eigenvalues are (a,b) $\omega_i = 0.607$ ($\delta = 0.3$), $\omega_i = 0.469$ ($\delta = 0.8$) and (c,d) $\omega_i = 0.487$ ($\delta = 0.3$), $\omega_i = 0.341$ ($\delta = 0.8$).

two ranges of least and most unstable modes that are interchanged for thick and sharp interfaces.

Figure 7.5 (d) illustrates the cumulative effects of viscosity and diffusivity on sharp and thick interfaces. Interestingly, the interface shows similar behavior to the case of immiscible viscous liquid-liquid interface indicating that the interface is controlled by shear viscosity and shear motion that has similar effect as diffusivity. Thus, the role of the diffusivity and viscosity remains to reduce the instability of the interface, as in the case of stationary liquids.

In the case of negligible capillary effects (Figure 7.4 (b)) the results could be obtained for very small values of interface thickness, indicating convergence of the curves defining the sharp interface limit. If however the capillarity is important (Figures 7.6 (a,b)), only the curves for much thicker interfaces could be obtained, and convergence to the sharp interface behaviour was not revealed. In addition, we plotted the curves for the different values of Ca and δ, so that their values are simultaneously reduced (Figures 7.6 (c,d)). In these plots, the limiting behaviour of the sharp interface was not revealed either. As already mentioned above, the ratio Ca/δ defines the surface tension coefficient, and the simultaneous changes in these two parameters allowed us to obtain the behaviour of a sharp interface in the case of the pure Rayleigh-Taylor instability ($U_0 = 0$). The flow imposed along the interface obviously makes the dependence of the eigenspectrum on Ca and δ more complex.

Figures 7.4 (d) and 7.7(c) show how the flow amplitude affects the eigenspectrum. Similar to the immiscible case, the growth of the modes with long wavelengths is intensified, and the growth of the modes with the shorter wavelengths is reduced.

Figure 7.5 (b) shows the role of the gravity force on the growth rates. In the presence of the flow, the instability is obviously observed even for $Gr = 0$, when the phase boundary is subject to the pure Kelvin-Helmholtz instability. The range of the unstable modes and the maximum growth rates are increased if the Grashof number Gr is increased and hence the Rayleigh-Taylor instability is intensified. Figures 7.5 (a) and 7.7 (d) show that the value of the parameter A does not introduce any qualitative changes to the eigenvalue spectrum. This parameter defines the effective diffusion coefficient, $D_0 = 2A + 12C_0^2$, and hence,

the larger values of A correspond to stronger diffusion, and, consequently, to stronger damping of the growth.

Figures 7.8 depicts the typical shapes of the eigenfunctions, namely, the moduli of concentration and stream function. The eigenfunctions are shown for two values of parameter A and for two different thicknesses δ. The concentration profiles are noticeably narrower and become even more narrower if the interface thickness is reduced. The streamfunction profiles remain virtually unaffected by the changes in A and δ, but we saw that the streamfunction profiles become however narrower for lower values of the Reynolds numbers (stronger viscosity).

7.2.2 Heavier liquid underlies a lighter one: $Gr > 0$

Figures 7.9 to 7.13 depict the neutral curves that define the zones of the Kelvin-Helmholtz and Holmboe instabilities obtained for interfaces separating two miscible liquids. Figures 7.9 show the results for $Ca = 0$. Figure 7.9 (a,b) are obtained for a rather thin interface with and without interfacial diffusion. In the immiscible case, the zone of the Kelvin-Helmholtz instability is small, but the layer is almost unconditionally unstable to the Holmboe modes, which agrees with the observations made from Figure 7.2 (b) plotted for the immiscible interfaces of different thicknesses. An introduction of interfacial diffusion changes the stability boundaries: the zone of the Kelvin-Helmholtz instability is enlarged, while the zone of the Holmboe instability becomes narrower. Thus, in the case of strong interfacial diffusion (Figures 7.9 (c,d)), the thinner interfaces are more unstable. In these figures, the zones of the Holmboe instability are unclosed, with the left boundaries virtually coincident with the axis $k = 0$.

Figure 7.10 depicts the typical eigenspectra. Both the real and imaginary parts of the eigenvalues are plotted. The imaginary part defines the growth or decay rates of perturbations, so that its positive values signify instability. One may notice a thin region near $k = 0$, where the perturbations decay, then, there is a region of the Kelvin-Helmholtz ($\omega_r = 0$) or Holmboe ($\omega_r \neq 0$) instabilities, and the shortwave modes decay again. The results are shown for the viscous and inviscid cases, and one sees that the instability region is reduced with the added viscous effect. In addition, the Kelvin-Helmholtz instability can be observed for

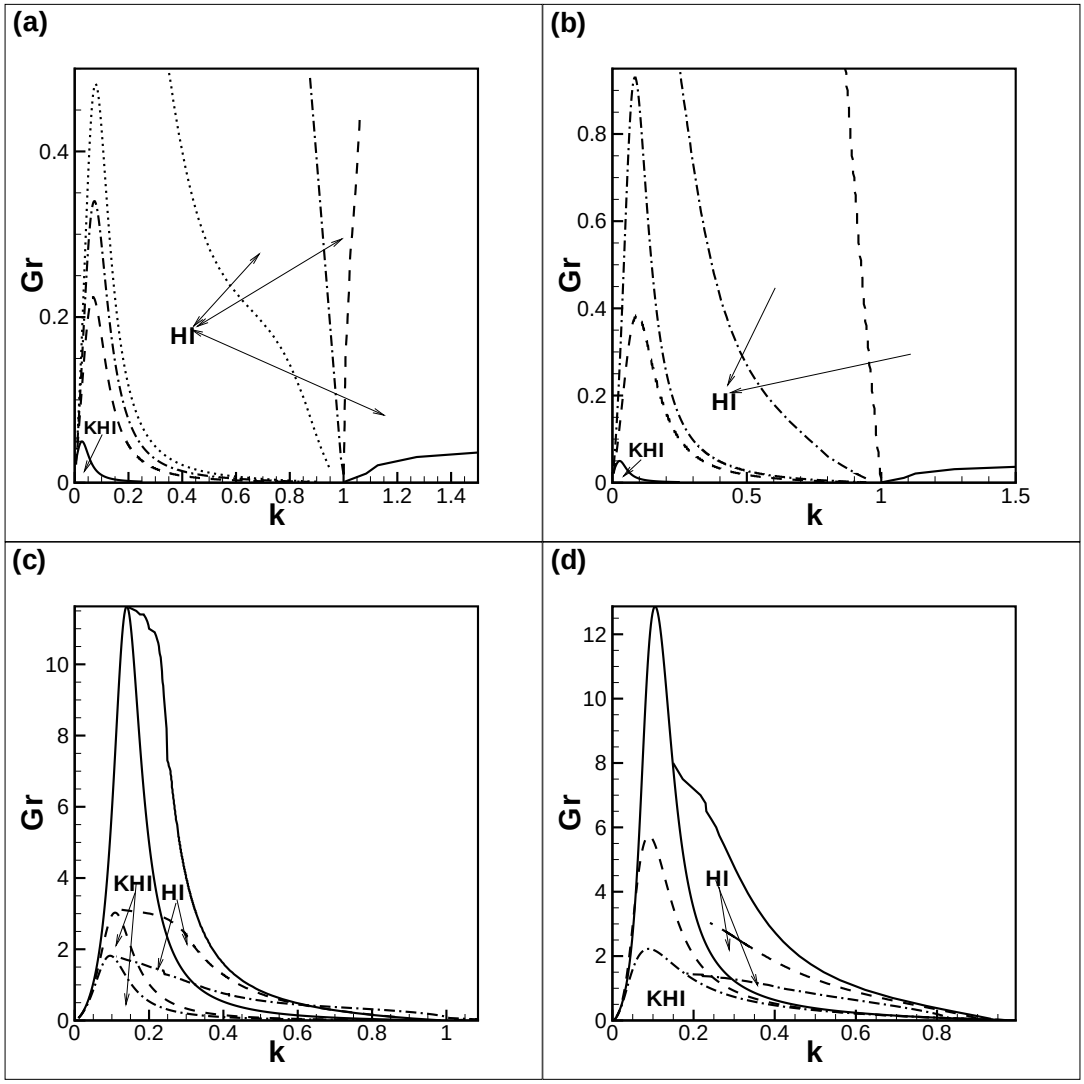

Figure 7.9: The neutral curves are plotted for a miscible interface between two inviscid liquids ($Re = \infty$) with the heavier liquid underneath the lighter one. The data are calculated for $Ca = 0$ and $\delta_u = 1$, $U_0 = 1$. (a) $A = -0.5$, $\delta = 0.01$, $Pe = \infty$ (solid line), $Pe = 1000$ (dash line), $Pe = 400$ (dash-dot line), and $Pe = 200$ (dot line). (b) $A = 0.5$, $\delta = 0.01$, $Pe = \infty$ (solid line), $Pe = 2500$ (dash line), $Pe = 100$ (dash-dot line). (c) $Pe = 20$, $A = -0.5$, $\delta = 0.001$ (solid line), $\delta = 0.005$ (dash line), $\delta = 0.01$ (dash-dot line). (d) $Pe = 10$, $A = 0.5$, $\delta = 0.05$ (solid line), $\delta = 0.1$ (dash line), and $\delta = 0.2$ (dash-dot line).

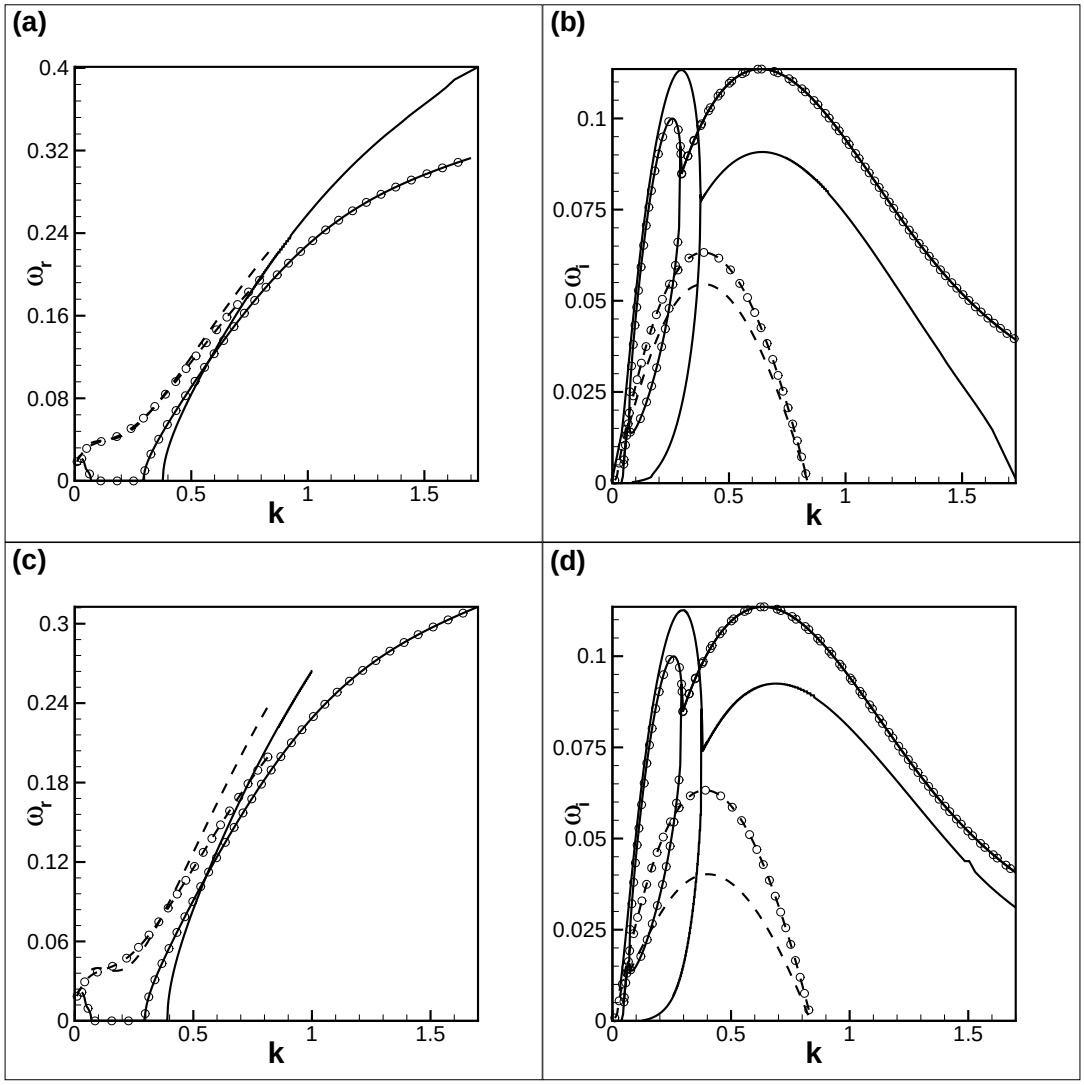

Figure 7.10: The eigenspectra are shown for the perturbations developing at a miscible interface that separates two liquids with the heavier liquid underneath. The two sets of curves are plotted for $Re = 20$ (dash lines) and $Re = \infty$ (solid lines) and $Gr = 0.1$, $\delta = 0.01$, $\delta_u = 1$, $U_0 = 1$. (a,b) $A = -0.5$, $Pe = 1000$ and $Pe = \infty$ (lines marked by $\circ$ symbols). (c,d) $A = 0.5$, $Pe = 2500$ and $Pe = \infty$ (lines marked by $\circ$ symbols).

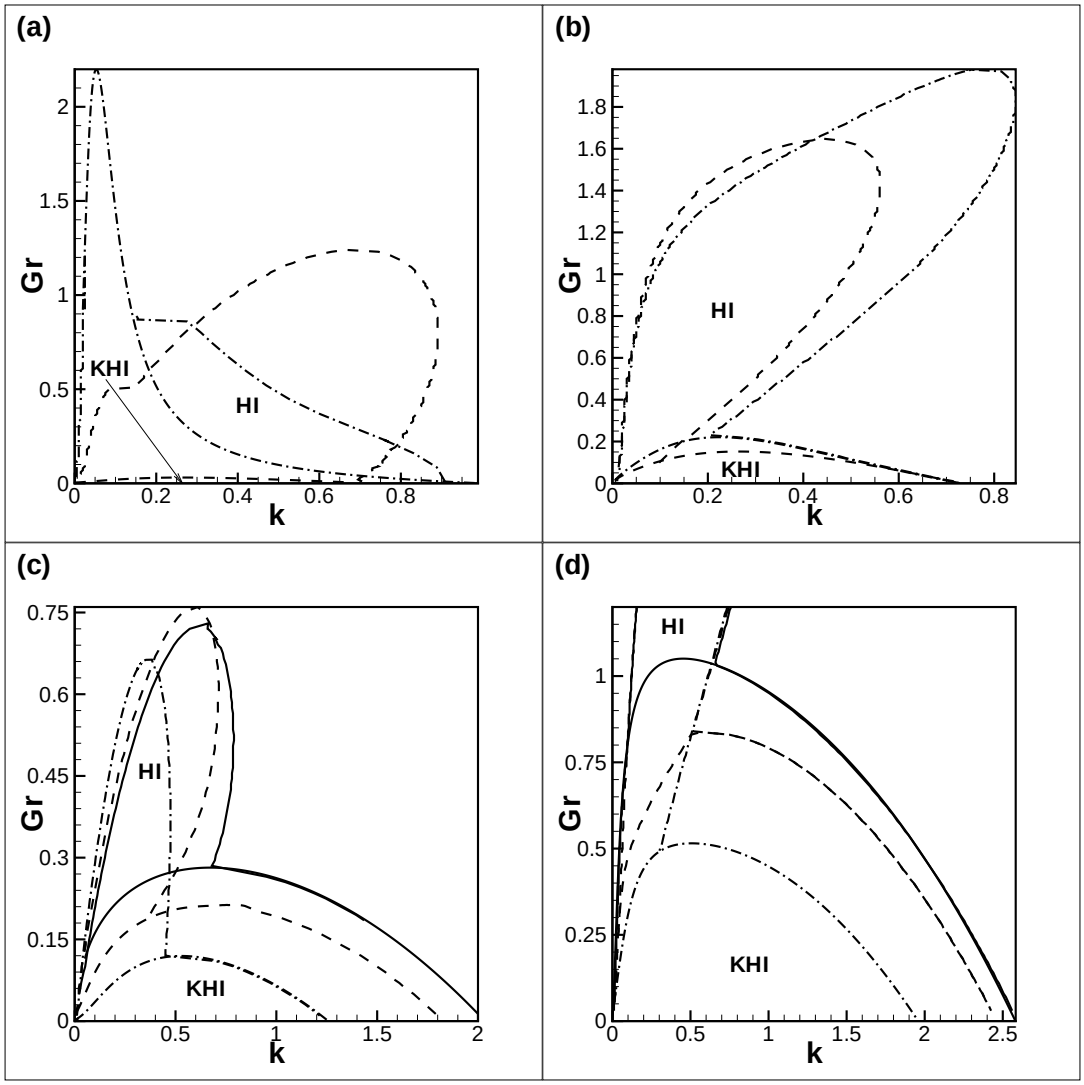

Figure 7.11: The neutral curves are plotted for a miscible interface between two liquids with the heavier one underneath. (a) The curves are obtained for $U_0 = 1$, $\delta_u = 1$ and $Gr = 1$; and (a) $Ca = 0$, $\delta = 0.1$, $A = 0.5$ and different values of Re and Pe: $Pe = 60$ and $Re = \infty$ (dash-dot line), $Re = 15$ and $Pe = \infty$ (dash line). (b) $Ca = 0$, $Re = 15$, $Pe = 60$, $A = 0.5$ and different values of δ: $\delta = 0.1$ (dash-dot line) and $\delta = 0.5$ (dash line). (c) $Pe = 100$, $\delta = 0.3$, $A = -0.5$, $Ca = 0.05$ and different values of Re: $Re = \infty$ (solid lines), $Re = 250$ (dash lines), and $Re = 25$ (dash-dot lines). (d) the same parameters in (c) but $A = 0.5$, $Ca = 0.08$.

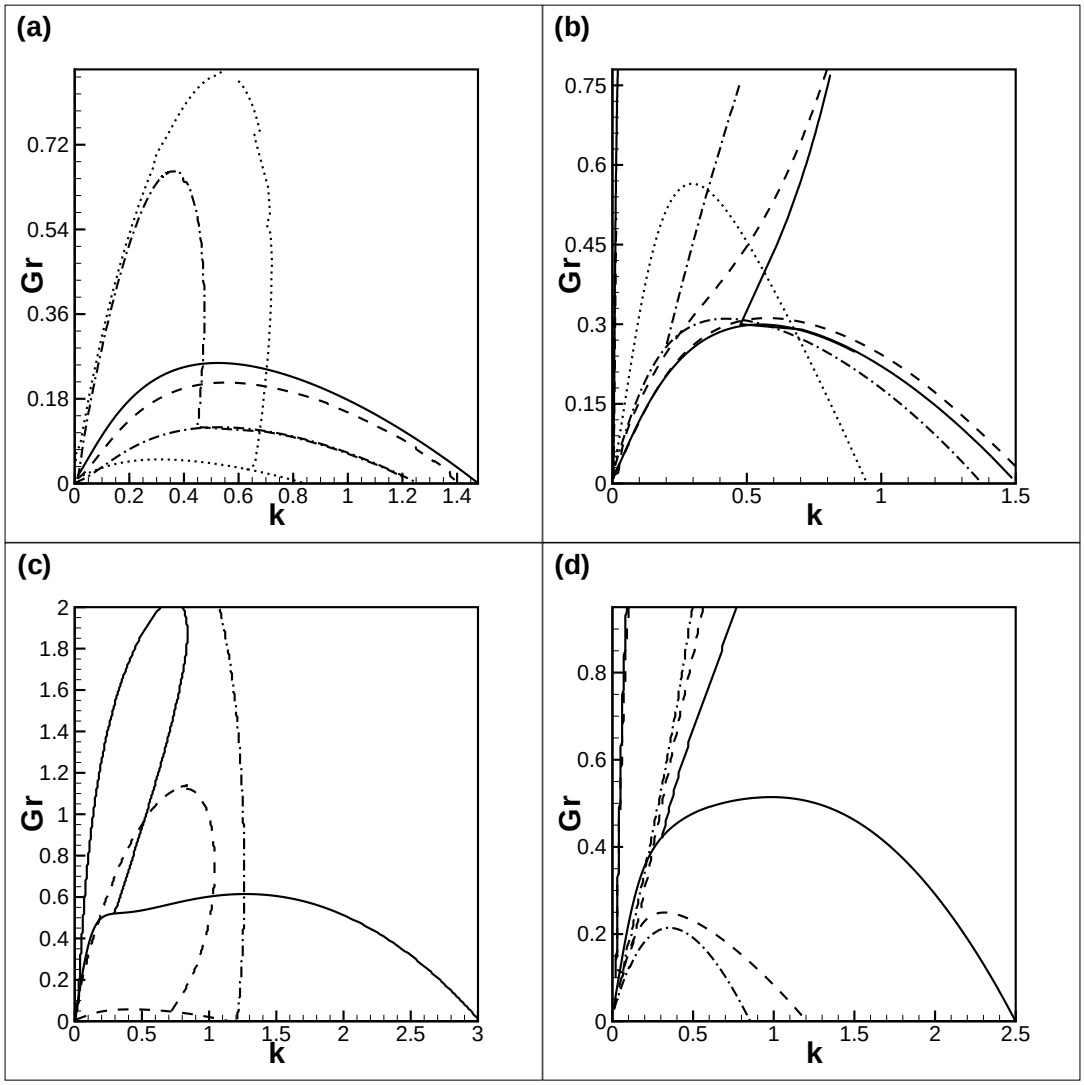

Figure 7.12: The neutral curves are plotted for a miscible interface between two liquids with the heavier one underneath. The curves are obtained for $U_0 = 1$, $\delta_u = 1$. (a) $Re = 25$, $\delta = 0.3$, $A = -0.5$, $Ca = 0.05$ and different values of Pe: $Pe = \infty$ (solid line), $Pe = 1000$ (dash lines), $Pe = 100$ (dash-dot lines), and $Pe = 10$ (dot lines). (b) $A = 0.5$, other parameters and lines as in (a). (c) $Pe = 20$, $Re = 100$, $A = 0.5$, $Ca = 0.05$ and different values of δ: $\delta = \delta_0/2 \sim 0.158$ (solid lines), $\delta = \delta_0 \sim 0.316$ (dash lines), $\delta = 2\delta_0 \sim 0.632$ (dash-dot line). (d) $Pe = 100$, $Re = 25$, $A = 0.5$, $Ca = 0.05$ and different values of δ: $\delta = 0.1$ (solid lines), $\delta = 0.3$ (dash lines), and $\delta = 0.6$ (dash-dot lines)

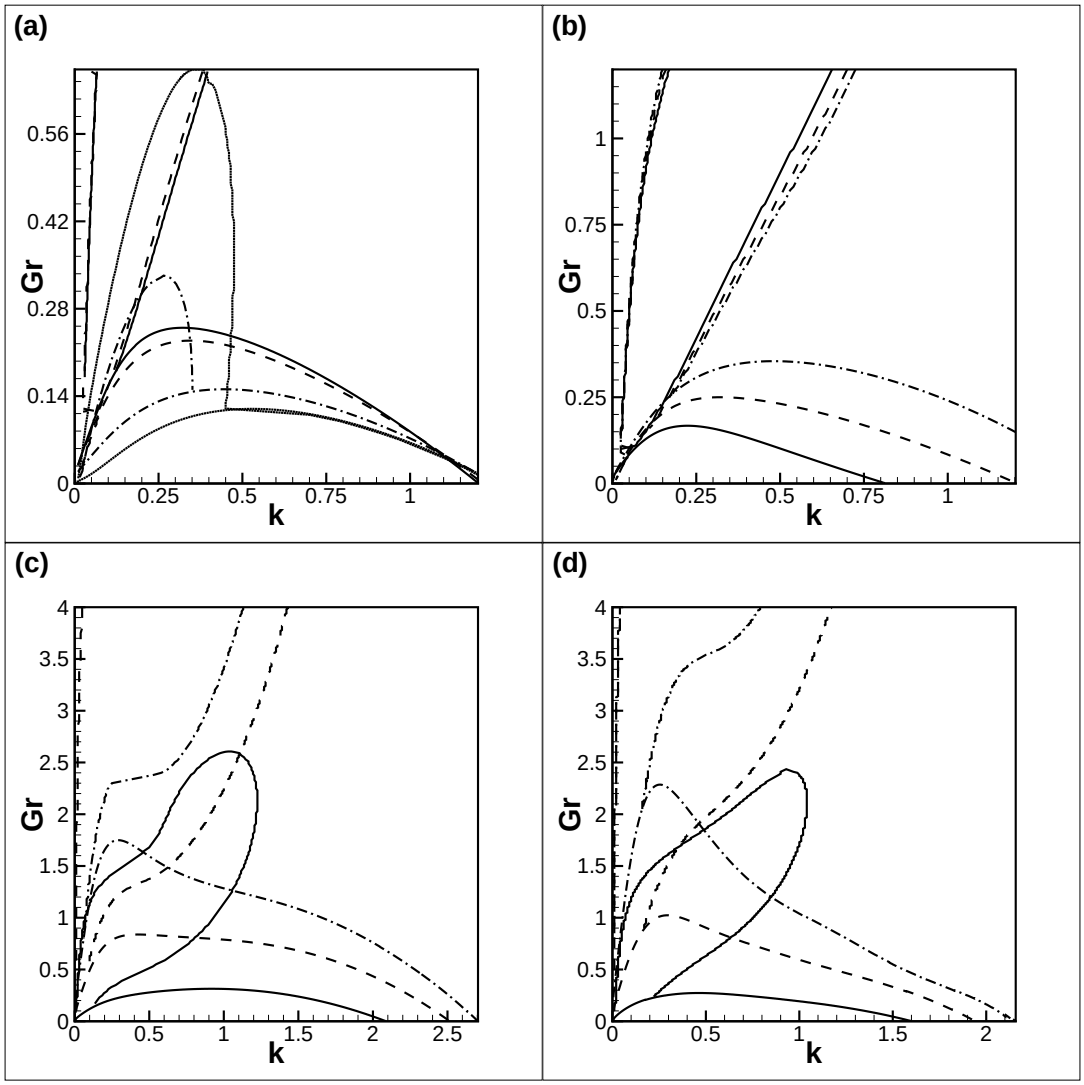

Figure 7.13: The neutral curves are plotted for a miscible interface between two liquids with the heavier liquid underneath. The curves are obtained for $\delta_u = 1$, $Pe = 100$. (a) $Re = 25$, $\delta = 0.3$, $Ca = 0.05$ and different values of A: $A = -0.5$ (solid lines), $A = -0.3$ (dash lines), $A = 0.3$ (dash-dot lines), and $A = 0.5$ (dot lines). (b) $Re = 25$, $\delta = 0.3$, $A = 0.5$ and different values of Ca: $Ca = 0$ (solid lines), $Ca = 0.05$ (dash lines), and $Ca = 0.1$ (dash-dot lines). In (c,d) data is obtained for $Re = 10$, $Ca = 0.05$, $\delta = 0.05$ and different values of U_0: $U_0 = 1$ (solid lines), $U_0 = 2$ (dash lines), and $U_0 = 3$ (dash-dot lines), $A = -0.5$ in (c) and $A = 0.5$ in (d).

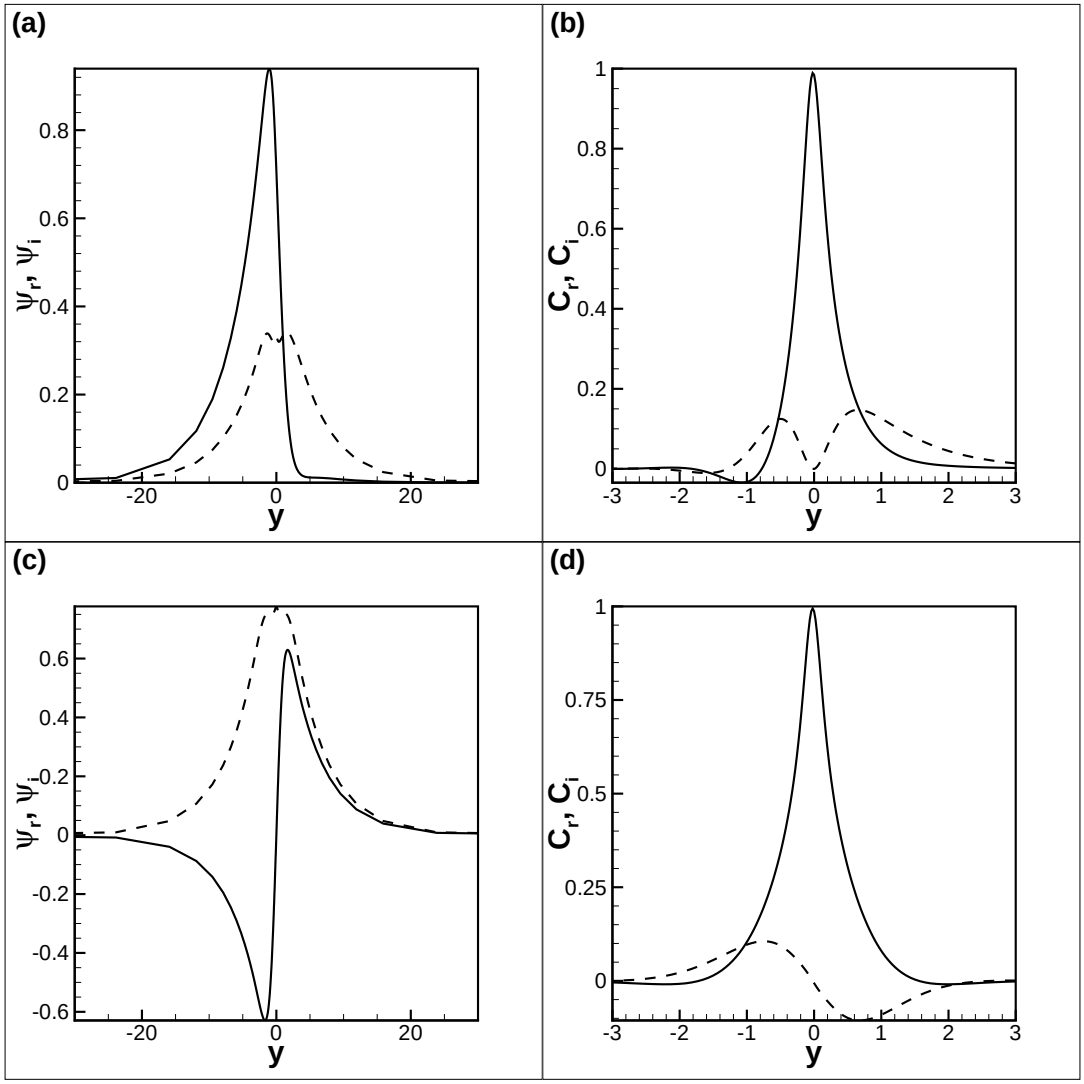

Figure 7.14: The eigenfunctions, namely the profiles of stream function (a,c) and concentration (b,d) are shown for perturbations developing at a miscible interface that separates two liquids in relative shear motion with the heavier liquid underneath. The functions are plotted for $k = 0.2$, $Pe = 100$, $Ca = 0.05$, $\delta = 0.1$, $Re = 25$, $A = 0.5$ and for (a,b) $Gr = 0.1$ (the range of the Kelvin-Helmholtz instability) and (c,d) $Gr = 1$ (the range of Holmboe instability). The solid lines depict the real parts, and the dashed lines show the imaginary parts. The eigenvalues are $\omega_i = (0, 0.087)$ (for a,b) and $\omega_i = (0.283, 0.011)$ (for c,d).

higher values of Re, but ceases to exist for small values of Grashof number (Gr) if the viscosity is stronger.

Figure 7.11 (a,b) show the effects of diffusivity and viscosity acting separately and simultaneously on the stability of the sharp interface δ. Although the effect of diffusivity and viscosity are the same for stationary liquids if $\delta \to 0$, Figure 7.11 (a) shows that diffusivity enhances the Kelvin-Helmholtz instability, especially at the modes concentrated around $k \sim 0.1$ with the highest Gr. In contrast, the effect of viscosity dramatically reduces the zone of Kelvin-Helmholtz instability to the lowest values of Gr. The other interesting observation, in immiscible viscous liquids, is that the Holmboe instability zone is larger than the zone of the case of miscible inviscid liquids. Figure 7.11 (b) shows the zones of KHI and HI are also dependent on the interface thickness δ if both diffusivity and viscosity acting together on the phase boundary. The characteristics of neutral curves are similar to the observed curves plotted for immiscible viscous liquids. However, the development of both instabilities does not depend on the interface thickness δ, e.g, HI develops even if $\delta > 0.427$ for which can not develop if the liquids are immiscible.

Figures 7.11 (c,d), 7.12 and 7.13 show the neutral curves for miscible interfaces taking the full account of the capillary terms. As expected, the interface is stable for higher Grashof numbers. At lower values of the Grashof number the interface is subject to either the Kelvin-Helmhotz or Holmboe instabilities. The effect of interfacial diffusion on the interface stability is illustrated by Figure 7.12 (a,b). The influence of diffusivity is different for the negative and positive values of the parameter A. If $A < 0$, even though the diffusion through the interface suppresses the development of the Kelvin-Helmoltz instability, the zone of the Holmboe instability gets even larger. The Holmboe instability does not exist for the cases of weak diffusivity (large Pe numbers). If $A > 0$, the range of Gr for which the instability can be observed is much larger. The presence of interfacial diffusion does not significantly change the zone of the Kelvin-Helmholtz instability until diffusion is too strong ($Pe = 10$) (see Figure 7.12 (b)). The increase in diffusivity makes the region of the Holmboe instability smaller, and the Holmboe instability is not observed for low Peclet numbers (e.g. $Pe = 10$).

Figures 7.12 (c,d) show the neutral curves for the interfaces of various thick-

nesses. Similar to Figures 7.9 (c,d) thinner interfaces are more prone to the Kelvin-Helmholtz instability. In chapter 6.2, it was shown that the configuration with the heavier liquid below the lighter one is thermodynamically unstable with the exponential growth of perturbations for interfaces thicker than the equilibrium value $\delta_0 \equiv \sqrt{Ca/A}$. This result is confirmed in the current work and is illustrated in Figure 7.12 (c), where the neutral curve for $\delta = 2\delta_0$ splits the plot into two parts. The longwave modes are thermodynamically unstable (almost independent on the value of the Grashof number) and the shortwave modes are stable. In contrast to the cases of stationary liquids, because of the continuous velocity profile, we did not observe convergence to the results for the sharp interface. Figures 7.11 (c,d) show the influence of viscosity, and, as expected, viscosity introduces additional damping thus reducing the range of unstable modes.

Figure 7.13 (a) depicts the neutral curves for different values of A. The more positive values of A (stronger diffusion) correspond to a larger zone of the Kelvin-Helmholtz instability, which agrees with Figures 7.12 (a,b). Correspondingly, for negative values of A, the zones of instability are significantly reduced. Figure 7.13 (b) illustrates that the capillary terms enlarge the zones of instability, similar to the immiscible case (Figure 7.2 (a)). Figures 7.13 (c,d) show the neutral curves for the imposed flows of different amplitudes. Obviously, the increase in the flow intensity expands the zones of the Kelvin-Helmholtz and Holmboe instabilities.

Finally, Figures 7.14 depict the eigenfunctions plotted for the parameters of Figure 7.12 (d), for $k = 0.2$ and for two different levels of Grashof numbers. These correspond to the Kelvin-Helmoltz and Holmboe disturbances. The streamfunction profiles look very similar to the curves plotted in Figures 7.3 (c,d) for the immiscible results. In the miscible case, the concentration profiles are added. The concentration profiles are much narrower, with the width similar to the case of $Gr < 0$ (Figures 7.8 (a,c)).

7.3 Conclusion

In this part, we used the phase-field approach to investigate the linear instability of a horizontal interface that separates two slowly miscible liquids. The liquids

are in relative shear motion. The obtained results were validated against the data available for immiscible interfaces that are subject to either the Rayleigh-Taylor, or Kelvin-Helmholtz, or Holmboe instabilities. The results are obviously different for the gravitationally stable and unstable configurations.

In the case of the heavier liquid lying above the lighter liquid, the interface is unconditionally unstable. The addition of the flow does not make the interface more unstable, in the sense that some of the modes (with longer wavelengths) start growing faster in the presence of the flows, but the growth of short wave modes is slowed down. Diffusivity introduces an additional mechanism of dissipation, and its action is similar to the influence of the viscous force. Capillarity reduces the growth rates, primarily affecting the development of the modes of shorter wavelengths. If the capillary forces are neglected, then the gradual decrease of the interface thickness can reveal the sharp-interface behaviour. If however the capillary terms are non-negligible, then the decrease in the interface thickness does not produce convergence to any limiting curve. When Ca and δ were both simultaneously decreased at the same rate, the limiting behaviour was not revealed either.

The configuration with the heavier liquid placed underneath the lighter one is stable if no flow is imposed. The flow driven along the interface surface destabilises the interface by introducing the Kelvin-Helmholtz and Holmboe instabilities. The interface would remain stable at very high Grashof number values, but at low Grashof number the flow makes the interface unstable. Usually, both the zones of the Kelvin-Helmholtz and Holmboe instabilities can be identified. The zone of the Kelvin-Helmholtz instability lies at lower Grashof number values, and the zone of the Holmboe instability is attached to the zone of the Kelvin-Helmholtz instability and usually extends to significantly higher Grashof number values. As expected, the zones of instability are significantly enlarged for the flows with higher amplitudes of base velocity (U_0). Surprisingly, we found that interfacial diffusion also expands the zones of instability. The interface is also more unstable if its thickness is small. However, in the case of $A < 0$ and very thick interfaces, with thicknesses exceeding the equilibrium value δ_0, the interface is unconditionally unstable due to the thermodynamic instability. In addition, the instability zones are increased if the capillary effects are added. Viscosity

however suppresses the instability, reducing the range of unstable modes.

Chapter 8

Summary and further work

We used the linear stability analysis to investigate how an interface separating two miscible liquids evolves when adding diffusivity with viscosity, capillarity and body forces. The normal modes method is used and the perturbations were assumed to grow or decay faster than the mixing region (boundary phase). The perturbations were also assumed to vanish at infinity as we wished to eliminate the effect of the boundaries on the interface. First, we considered the stability of an interface between two stationary liquids. Next, we assumed that the liquids participate in the relative motion. The main conclusions of the work are summarised below.

8.1 Summary

The main aim of our work has been to investigate the dynamics of an interface separating two miscible liquids using linear stability analysis. The phase-field approach was employed to model the evolution of a miscible liquid-liquid binary mixture. Two different configurations were adopted using two superposed liquids that can be stationary or in relative shear motion. The development of gravity-capillary waves, RTI, KHI, and Holmboe instabilities were assessed.

Firstly, the classical sharp interface model was used to extract data that later was used to validate the capability of the phase-field approach in recovering the dispersion relations of RTI and GCW. Within the framework of the Boussinesq approximation, we have reproduced the analytical data of the Rayleigh-Taylor in-

stability and gravity-capillary waves. For $\delta_u = \delta = 0$, it was also shown that the combined Rayleigh-Taylor and Kelvin-Helmholtz instabilities increase the instability of the interface more than in the case of a single instability, i.e either RTI or KHI. Sharp interface results showed that the unconditionally stable interface may become unstable in the form of the Kelvin-Helmholtz instability if a shear motion is imposed on the sharp interface. Furthermore, Holmboe instability develops if viscous liquids were considered.

Secondly, the phase-field approach was used to investigate the behavior of the phase boundary separating two superposed liquids, which are initially motionless. For immiscible liquids, the data showed that the phase-field approach is capable of reproducing the sharp interface limits if $\lambda < \delta$. It was found that viscosity always has a dissipation effect on the interface instability regardless whether the heavier liquid overlies or underlies a lighter one. It was also found that the capillarity becomes prominent for sharper interfaces if the heavier liquid sits on top of the lighter one. When the lighter liquid overlays the heavier one, gravity-capillary waves are expanded to the short wavelengths region. It was also found that the damping is mainly defined by the viscous effects that reduce the range of the modes that exhibit the wave-like behaviour (GCW). Furthermore, the purely thermodynamic instability was also investigated. Based on a fourth order differential equation, which includes the capillarity effects, we found that the phase boundary is unstable if the interface width exceeds the value of the thickness at equilibrium and the binary system is far from its critical point.

In miscible system, both thermodynamics and hydrodynamics may play a role in determining the decay or growth of perturbations at a diffuse (or sharp) interface. When combining thermo- and hydrodynamic stability, we found that the diffusivity introduces an additional dissipation, and its influence is very similar to the effects produced by the viscous force. The introduction of diffusivity slows the growth of the Rayleigh-Taylor instability, reducing the propagation speeds of the gravity-capillary waves and enhancing the damping of the waves.

In general, diffusivity and capillarity, dampen perturbations, but these effects interplay and hence can emphasize or suppress each other. The cumulative viscous and diffusive all damping is able to completely suppress the growth of the short wavelength modes, which is not observed when these effects act separately. The

strong viscous or diffusive damping can make the effect of capillarity practically non-existent. That means that the use of the phase-field approach as a numerical method for describing the evolution of immiscible interfaces should in general take into account the correlations between the Reynolds, Péclet, capillary numbers, and the interface thickness.

We also found qualitative difference in the results obtained for $Ca = 0$ and $Ca \neq 0$. For the case of negligible capillary effects, the evolution of small perturbations is totally determined by hydrodynamics. The diffusion is included by the diffusive flux defined by the Fickian law, but we found that the concentration field in this case mostly adjusts the variations of the velocity field. If however $Ca \neq 0$, then the evolution of perturbations is dominated by the thermodynamic part of the mathematical problem. The difference in the results is even stronger for the gravity-capillary waves. In the case of non-negligible capillary effects and when $A < 0$ and $\delta > \delta_0$, the thermodynamic longwave instability makes the layer unstable even if the lighter liquid overlays the heavier one.

Thirdly, we studied the effect of shear flow on the instability of the phase boundary separating two miscible liquids. The investigations were divided into a number of cases: immiscible liquids, miscible inviscid and viscous liquids for $Ca = 0$ and $Ca \neq 0$. For immiscible liquids, it was found that by adding a strong external shear motion to the Rayleigh-Taylor instability, the instability of the interface increases in the limit of long wavelengths. However, the short wavelengths are completely stabilised. In this case, it was found that the viscosity and capillarity retain their dampening roles. It was also found that the sharp interface limits can be recovered, however, we did not observe any convergence of the data if the capillary forces are retained.

In addition, the unconditionally stable interface between two immiscible liquids (gravity-capillary waves) were found to be unstable if the shear motion is introduced. In this case, the interface is subjected to both Kelvin-Helmholtz and Holmboe instabilities, which are determined by the Grashof number, the shear motion and the ratio thickness of shear layer to the concentration. We found that the Kelvin-Helmholtz instability is enhanced by a strong shear motion and capillarity, however, it is dampened through the viscosity and Grashof number. Meanwhile the Holmboe instability is enhanced by the reduction in the width of

the concentration thickness and the increase in the Grashof number values. In contrast, the capillarity and the shear motion dampen the Holmboe instability.

We also investigated the effect of the shear motion on the stability of the phase boundary separating two miscible liquids. When the capillarity was neglected, we found that the diffusivity is similar to the role of the viscosity. They introduce further dissipation in dampening the instability resulting from the combination of the Kelvin-Helmholtz and Rayleigh-Taylor instabilities. By including the capillarity, further unstable modes can be completely cut off. Moreover, for miscible inviacid liquids, we have found that the diffusivity enhances the Kelvin-Helmholtz instability and dampen the long wavelengths of the Holmboe instability, which can be diminished for strong diffusivity. If, however, viscosity is included, the Kelvin-Helmholtz instability only develops for small values of Grashof number, and the Holmboe instability develops for large values of Grashof number. The main findings in the study of stratified shear flow is that the behavior of the interface can be altered if capillarity and diffusivity simultaneously act on the interface.

8.2 Further work

Throughout the current fundamental study, we focused on the use of the linear stability analysis to investigate the evolution of the phase boundary between two miscible liquids. When the liquids are stationary, we found that the perturbations are initially $2D$, however, if the liquids are in relative shear motion the perturbations might initially be $3D$. Therefore, a further study can be conducted to identify when $3D$ perturbations are more dangerous. In such a case, it would be interesting to investigate how the behaviour of the interface will be changed.

It is known that if there is a strong viscosity gradient, the interface between two immiscible liquids would behave differently to the case of assuming the kinematic viscosity constant everywhere in the system. So for a better understanding of the behaviour of the interface in more practical problems, the current study can be extended to consider the linear theory within the framework of phase-field approach for further investigation of the evolution of interface separating two

miscible liquids endowed with strong viscosity gradients. The development of the governing equations may need to be reconsidered, where the current study can be used as a limiting case for validation.

The Marongoni effect can play an important role in mass transfer, which is generally induced by a strong gradient of capillary forces. The phase-field approach represents the surface tension by a Korteweg stress, which is represented by gradient of concentration. This means that Marongoni effects are already present in the current phase-field approach. As further investigation, one can consider both micro-gravity and very sharp interfaces in order to identify Marongoni effects.

The study could be extended to include the effect of nonlinearity on the evolution of phase boundary separating two miscible liquids. For this purpose, direct numerical simulation (DNS) would be an appropriate choice in order to capture the full scale of a flow allowing us to predict the full mixing process in miscible liquids. We could proceed by considering a 2D problem of two superposed liquids, in which either RTI and GCW can result. Also, when the liquids are in relative parallel shear motion, it is important to understand whether the diffusivity enhances the mixing in the form of KHI as was shown in the current linear stability analysis. Also, shear flow between miscible liquids with strong viscosity gradients would be great of importance, since it is relevant to a number of engineering applications such as: transportation of crude oil in pipelines, mixing liquids in chemical industry processes and cleaning in food industry where a highly viscous liquids removed by other less viscous liquids.

Appendix A

The effect of diffusivity on the evolution of the interface

Here, we investigate the evolution of the width of the interface between two miscible liquids by considering only the effect of pure diffusivity. We assume that the change in the concentration profile is in the direction of the y coordinate as depicted in Figure 1. Thus, the full nonlinear numerical analysis of $1D$ system is conducted for the early time of interface evolution, which can be compared against the growth of the normal modes used in the current work. So, in order for the linear stability analysis to be valid, we have to show that the growth of these modes is faster that the growth of the interface width due to the diffusivity. In fact we just need to show that interface width grows slower in a non-exponential function. This allows us to consider the basic concentration C_0 unchanged in front of the evolution of the perturbations.

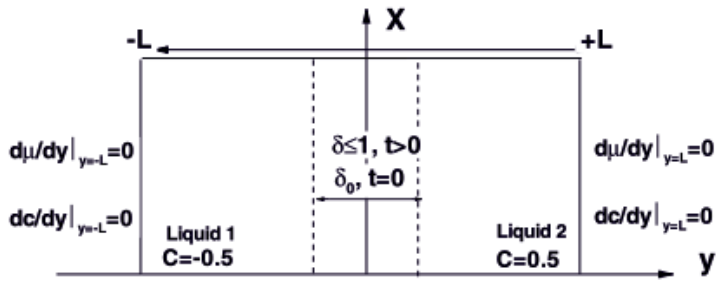

Figure 1: The basic state of two miscible liquids disposed initially in horizontal contact with different concentration $C = -0.5$ for $y < 0$ and $C = 0.5$ for $y > 0$.

Let consider a plane layer contains two miscible liquids. Initially the liquids are stationary and assuming that the evolution of the liquids is purely diffusive in the direction y. The governing equations describe the dynamics of such system are given by

$$\frac{\partial C}{\partial t} = \frac{1}{Pe}\nabla^2 \mu, \tag{1}$$

$$\mu = 2AC + 4C^3 - Ca\nabla^2 C. \tag{2}$$

This equation is solved numerically through the finite difference method and using second-order accurate explicit scheme. We assume that the thickness of the interface is $\delta << L$ and the gravity effect is neglected. The equation is discretised as follows

$$C_i^{n+1} = C_i^n + \frac{\triangle t}{\triangle y^2}\left(\mu_{i+1}^n - 2\mu_i^n + \mu_{i-1}^n\right), \tag{3}$$

where the Peclet number Pe is absorbed in time step Δt, whilst the chemical potential is written as

$$\mu_i^n = 2AC_i^n + 4C_i^n - \frac{Ca}{\triangle y^2}\left(C_{i+1}^n - 2C_i^n + C_{i-1}^n\right). \tag{4}$$

The boundary conditions applied to the concentration and the chemical potential at the boundaries ($y \to \pm L$) are

$$\frac{\partial C}{\partial y} = 0, \tag{5}$$

$$\frac{\partial \mu}{\partial y} = 0, \tag{6}$$

and by using the Taylor expansion we obtain the expressions of the values of C and μ at $y \to \pm L$, which are given by the following expressions

$$C_N = \frac{4\,C_{N-1} - C_{N-2}}{3}, \tag{7}$$

$$C_0 = \frac{4\,C_1 - C_2}{3}, \tag{8}$$

$$\mu_N = \frac{4\,\mu_{N-1} - \mu_{N-2}}{3}, \tag{9}$$

$$\mu_0 = \frac{4\,\mu_1 - \mu_2}{3}, \tag{10}$$

where N is the total number of grid points. In order to obtain the numerical results that suit our purpose in the current study, we assume that the thickness of the interface δ must always remain much less than the total length of the plan layer $2L = 6$, therefore we specified $\delta \leq 1$. The initial concentration is given by

$$C_0 = 0.5 \tanh\left(\frac{y}{\delta_0}\right), \tag{11}$$

where δ_0 is the initial thickness, its values were varied until we have found that the influence of the initial thickness is not important. The calculations are initialized for the thickness $\delta_0 = 10^{-3}$ and the results are presented in the following section.

Numerical Results

The numerical results presented in the Figure A. 2 show the effect of the phase parameter A and the capillary number Ca on the evolution of the thickness δ of the interface separating two miscible liquids. Figure 2 (a) shows three different profiles of the concentration at different time steps. Figure 2 (b) and (c) show that the thickness evolves according to the theoretical expression $\delta(t) = \alpha\sqrt{t}$ for all values of the parameter A ($-0.5 \leq A \leq 0.5$). When $A > 0$ the thickness of the interface evolves faster than in the case the values of $A < 0$ as Figure 2 (d) indicates. The diffusion coefficient follows the expression $\delta(t) = \sqrt{D\,t}$, here we used $\alpha = \sqrt{D}$.

In the early stage of the contact, the surface tension contributes to the evolution of the thickness more than the parameter A. For strong capillarity the thickness grows faster, however, when the thickness becomes larger the surface tension seems to slow down the growth of the thickness. The influence of the capillary number becomes less apparent for $\delta > 1$ as the curves of various capillary numbers converge to the curve with lowest capillary number.

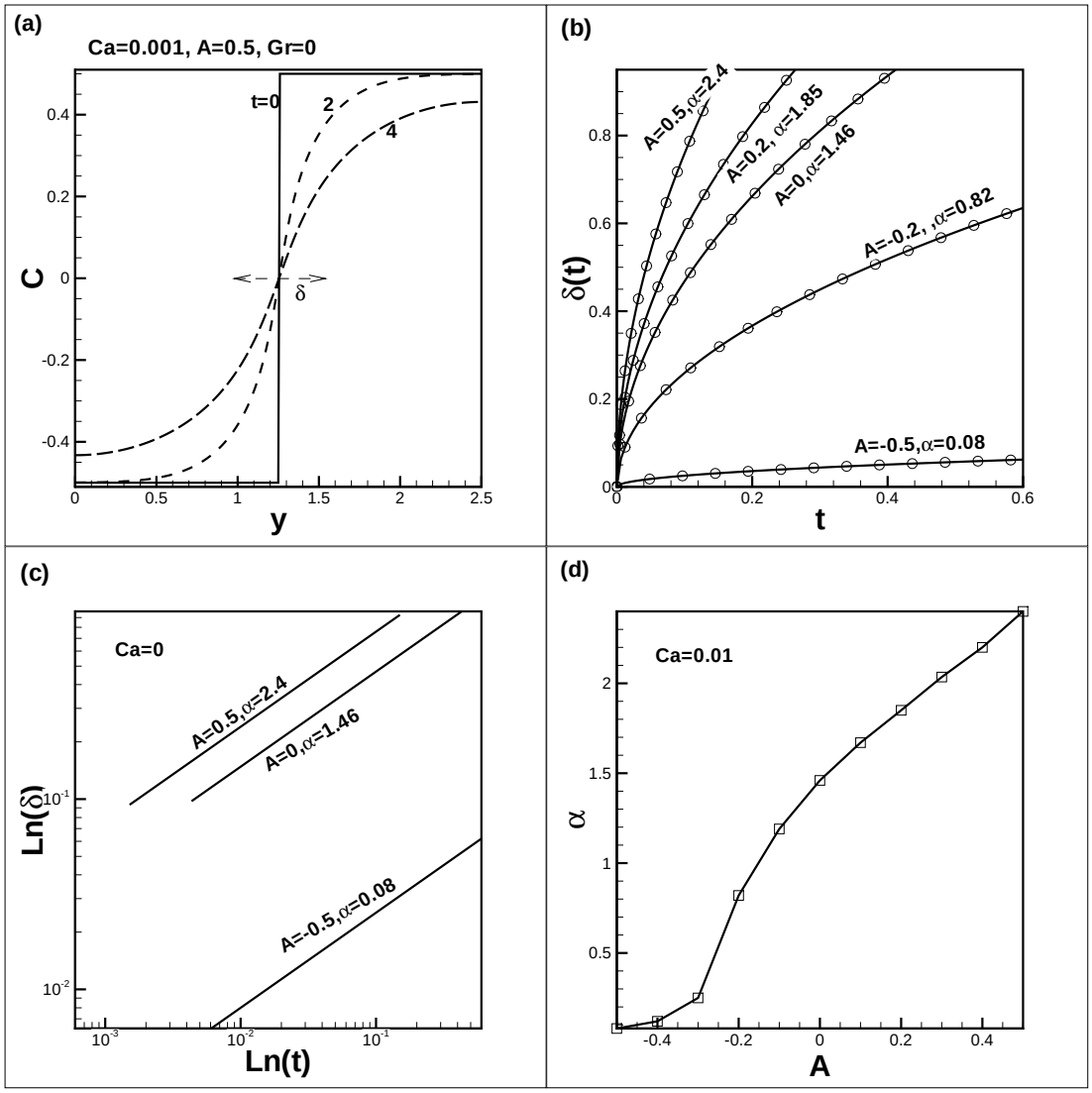

Figure 2: The evolution of the thickness of the interface δ in time; the effect of the phase parameter A and the capillary Ca is taken into account. (a) three different profiles of the concentration, the thickness δ is calculated by taking the distance between the bulks of the liquids for which the the concentration approximately is ± 0.45.(b) the curves are obtained for the thickness δ calculated numerically versus the theoretical thickness $\delta = \alpha\sqrt{t}$. (c) the logarithmic presentation of the variation of the thickness $Ln(\delta)$ versus time t for $Ca = 0$; (d) dependence of the diffusion coefficient α on the phase parameter A (solid square line). In (a) the symbol $\circ$ represents the analytic results and solid line represents the numerical data.

Conclusion

The main conclusion we may draw from this appendix is that the evolution of the thickness of the interface separating two miscible liquids, is mainly affected by the the phase parameter A and the capillary number Ca. This evolution is well fitted with the theoretical expression $\delta(t) = \sqrt{Dt}$. This indicates that the thickness of the interface remains unchangeable during the linear perturbations which grow exponentially, and hence the frozen basic state assumption is justified.

Appendix B

To avoid confusion between the dimensional and non-dimensional parameters, the latter one are written with $\overline{(.)}$.

B. 1 Non-dimensionalise the dispersion relation of inviscid immiscible liquids

Here, we attempt to write the equation (5.30) in the non-dimensional form given by the equation (5.31). Thus the dimensional form of the equation (5.30)is rewritten as follows

$$\omega^2 = gk\frac{\rho_1 - \rho_2}{\rho_2 + \rho_1} + \frac{k^3\sigma}{\rho_2 + \rho_1}, \tag{12}$$

where

$$\frac{\rho_1 - \rho_2}{\rho_2 + \rho_1} = \frac{1}{2}\phi, \tag{13}$$

then $\rho_1/(\rho_1 + \rho_2) \sim 0.5(1 - \phi/2)$ and $\rho_2/(\rho_1 + \rho_2) \sim 0.5(1 + \phi/2)$.

Using the scaling parameters of the current phase-field approach defined in equation (2.11), hence we obtain

$$\overline{\omega}^2\frac{\mu_*}{L_*^2} = \frac{1}{2}\phi gk + \frac{k^3\sigma}{2\rho_1}, \tag{14}$$

dividing by the fraction $\frac{\mu_*}{L_*^2}$ to obtain

$$\overline{\omega}^2 = \frac{1}{2}\left(\frac{\phi g L_*}{\mu_*}\right)(kL_*) + \left(k^3L_*^3\right)\left(\frac{\sigma}{\rho_1\mu_*L_*}\right), \tag{15}$$

this equation can be written in non-dimensional form as follows

$$\overline{\omega}^2 = \frac{1}{2}Gr\overline{k} + \frac{1}{2}\overline{\sigma}\overline{k}^3. \tag{16}$$

Substituting the equation (3.4) in the latter one, we obtain

$$\overline{\omega}^2 = \frac{1}{2}Gr\overline{k} + \frac{Ca}{6\delta}\overline{k}^3. \tag{17}$$

B. 2 Non-dimensionalise the dispersion relation of stationary viscous immiscible liquids

In this section we write the non-dimensional of the dispersion relation presented by the equation

$$\left(R + \nu(q^2-k^2)^2\right)\nu(q+k) - \nu^2(1+\phi/2)(1-\phi/2)(q^2-k^2)k = 0, \tag{18}$$

where $q = \sqrt{k^2 - i\omega/\nu}$ and $R = -\frac{gk}{2i\omega}\left(\frac{\phi}{2} + \frac{\sigma k^2}{(\rho_1+\rho_2)}\right)$.

Since $\phi << 1$, the equation (18) can be further simplified through dividing by $q+k$ be written as follows

$$\nu^2(q^2-k^2) - \nu^2(q-k)k = -\left(\frac{gk\phi}{2} + \frac{\sigma k^2}{(\rho_1+\rho_2)}\right)\frac{1}{-i\omega}, \tag{19}$$

by noting that $\frac{1}{-i\omega} = \frac{1}{q^2-k^2}$. Multiplying this on both sides of the equation, we obtain

$$\nu^2(q^2-k^2)(q^2-k^2) - \nu^2(q-k)(q^2-k^2)k = -\left(\frac{gk\phi}{2} + \frac{\sigma k^2}{(\rho_1+\rho_2)}\right), \tag{20}$$

for further simplification of the left hand side of this equation, we found the following

$$\nu^2(q+k)(q-k)^2 q = -\left(\frac{gk\phi}{2} - \frac{\sigma k^2}{(\rho_1+\rho_2)}\right). \tag{21}$$

Non-dimensional $q = \frac{\sqrt{\overline{k}^2 - iRe\overline{\omega}}}{L_*}$, hence $[q] = [k]$. Using this fact and scaling

parameters given in (2.11), we can write

$$\nu^2(\overline{q}-\overline{k})L_*^{-1}(\overline{q}^2-\overline{k}^2)L_*^{-2}\overline{q}L_*^{-1} = -\left(\frac{gk\phi}{2}-\frac{\sigma k^2}{(\rho_1+\rho_2)}\right). \tag{22}$$

Introducing the scaling parameter μ_* on the left hand side to obtain

$$-\left(\frac{\nu^2}{\mu_* L_*^2}\right)\left(\frac{\mu_*}{L_*^2}\right)(\overline{q}+\overline{k})(\overline{q}-\overline{k})^2\overline{q} = \left(\frac{gk\phi}{2}+\frac{\sigma k^2}{(\rho_1+\rho_2)}\right). \tag{23}$$

The equation can be written as follows

$$-\frac{(\overline{q}+\overline{k})(\overline{q}-\overline{k})^2\overline{q}}{\frac{\mu_* L_*^2}{\nu^2}} = \frac{1}{2}\frac{g\phi L_*}{\mu_*}(L_*k)+\frac{1}{2}\frac{\sigma}{\rho_1\mu_* L_*}(L_*^3k^3), \tag{24}$$

hence, the non-dimensional form is given by

$$-\frac{(\overline{q}+\overline{k})(\overline{q}-\overline{k})^2\overline{q}}{Re^2} = \frac{1}{2}Gr\overline{k}+\frac{1}{2}\overline{\sigma}\overline{k}^3, \tag{25}$$

where $\overline{\sigma}=\frac{Ca}{6\delta}$.

Appendix C

The aim of this appendix is to derive the equations for the particular cases used for producing the data in the Chapters 7 and 8, where the diffusivity, viscosity and capillarity are considered. The methods developed in this appendix are applied to explicit shooting method (ESM).

Equations used in the calculation of the data for miscible liquids

The full system of equations describing the general problem in which the phase boundary separating between two miscible liquids and subjected to shear motion. When taking into account the effects of viscosity, diffusivity, gravity and capillarity. The equations for interface subjected to shear motion, that are developed in Chpter 3, are used to explain the method used in determining the eigenvalues for the particular cases. The full equations of shear motion is rewritten as follows

$$\begin{aligned} i(U_x k-\omega)(\psi''-k^2\psi)-ikU_x'' = \frac{1}{Re}(\psi^{iv}-2k^2\psi''-k^4\psi)+ \\ Cak[(C''-k^2C)C_0'-C_0'''C]+ikGrC, \end{aligned} \tag{26}$$

$$\begin{aligned} CaC^{iv}-\left(D_0+2Cak^2\right)C''-2D_0'C'+ \\ \left(k^2\left(D_0+Cak^2\right)-D_0''-iPe(U_xk-\omega)\right)C=-ikPeC'\psi. \end{aligned} \tag{27}$$

For the cases of stationary base state, the corresponding system of equations can be obtained straightforward from the case of the equations of the case of shear motion by enforcin the velocity $U_x = 0$.

C. 3 Inviscid miscible liquids without account for capillarity effects

We present here the solution method of boundary value problem of fourth order presenting the case of inviscid miscible liquids without accounting for capillarity effects. Thus the above differential equations are reduced to the following

$$\psi'' - k^2\psi = -\frac{-kGr}{(kU_0 - \omega)D_0}\mu, \tag{28}$$

$$\mu'' - (k^2 - \frac{iPe}{(U_0k - \omega)D_0})\mu = -iPekC_0'\psi, \tag{29}$$

$$C = \frac{\mu}{D_0}. \tag{30}$$

At $y \to \infty$ the boundary conditions are given as

$$(\psi_0, \psi_1, \mu_0, \mu_1)^T = (1, \pm k, 0, 0)^T \exp(-kL), \tag{31}$$

$$(\psi_0, \psi_1, \mu_0, \mu_1)^T = (\beta, \pm q\beta, 1, \pm q)^T \exp(-qL), \tag{32}$$

where $q = \sqrt{k^2 + (U_0k - iPe\omega/D_0)}$ and $\beta = \frac{-ikGr}{Pe(k+\omega)^2}$.

The corresponding system of first differential equations needed by ESM is given by

$$\begin{pmatrix} \psi_0' \\ \psi_1' \\ \mu_0' \\ \mu_1' \end{pmatrix} = \begin{pmatrix} 0 & 1 & 0 & 0 \\ k^2 & 0 & \frac{kGr}{\omega\, D0} & 0 \\ 0 & 0 & 0 & 1 \\ -iPekC_0' & 0 & k^2 - iPe\,\omega/D_0 & 0 \end{pmatrix} \begin{pmatrix} \psi_0 \\ \psi_1 \\ \mu_0 \\ \mu_1 \end{pmatrix}, \tag{33}$$

C. 4 Miscible-inviscid liquids with $Ca \neq 0$

Here, the full boundary value problem is reduced to the problem of sixth order presents the case of inviscid miscible liquids with accounting for capillarity effect. The system of equations is given by

$$i(U_xk - \omega)(\psi'' - k^2\psi) = -Cak[(C'' - k^2C)C_0' - C_0'''C] - ikGrC, \tag{34}$$

$$CaC^{iv} - \left(D_0 + 2Cak^2\right)C'' - 2D_0'C' + \left(k^2\left(D_0 + Cak^2\right) - D_0'' + iPe(U_xk - \omega)\right)C = -ikPeC'\psi, \tag{35}$$

The exact solutions at $y \sim L_\infty$ are given by

$$(\psi_0, \psi_1, C_0, C_1, C_2, C_3)^T = (1, \pm k, 0, 0, 0, 0)^T \exp(-kL), \tag{36}$$

$$(\psi_0, \psi_1, C_0, C_1, C_2, C_3)^T = (\beta, \pm\beta q_1, 1, \pm q_1, q_1^2, \pm q_1^3)^T \exp(-q_1 L), \tag{37}$$

$$(\psi_0, \psi_1, C_0, C_1, C_2, C_3)^T = (\beta, \pm\beta q_2, 1, \pm q_2, q_2^2, \pm q_2^3)^T \exp(-q_2 L), \tag{38}$$

where

$$q_1 = \sqrt{\frac{1}{2}(2k^2 + D_0/Ca) + \frac{1}{2}\sqrt{D_0^2/Ca^2 + 4iPe(U_0 k - \omega)/Ca}}, \tag{39}$$

$$q_2 = \sqrt{\frac{1}{2}(2k^2 + D_0/Ca) - \frac{1}{2}\sqrt{D_0^2/Ca^2 + 4iPe(U_0 k - \omega)/Ca}}. \tag{40}$$

$$\beta = -\frac{kGr}{(U_0 k - \omega)(q_{1,2}^2 - k^2)}.$$

The solutions (36-38) are used as the boundary conditions for solving the following set of equations

$$\begin{pmatrix} \psi_0' \\ \psi_1' \\ C_0' \\ C_1' \\ C_2' \\ C_3' \end{pmatrix} = \begin{pmatrix} 0 & 1 & 0 & 0 & 0 & 0 \\ 0 & 0 & 1 & 0 & 0 & 0 \\ 0 & 0 & 0 & 1 & 0 & 0 \\ k^2 + \frac{ikU_x''}{U_0 k - \omega} & 0 & \frac{k^3 Ca(C_0' k^2 + C_0''')}{U_0 k - \omega} & 0 & \frac{kCaC_0'}{U_x k - \omega} & 0 \\ 0 & 0 & 0 & 0 & 0 & 1 \\ \frac{ikC'0Pe}{Ca} & 0 & A_{63} & \frac{2D_0'}{Ca} & \frac{D0 + 2Cak^2}{Ca} & 0 \end{pmatrix} \begin{pmatrix} \psi_0 \\ \psi_1 \\ C_0 \\ C_1 \\ C_2 \\ C_3 \end{pmatrix}, \tag{41}$$

where

$$A_{63} = \frac{(D_0'' - k^2 D_0 - k^4 Ca - i(U_0 k - \omega)Pe)}{Ca}.$$

C. 5 Miscible viscous liquids with $Ca = 0$

Finally, in the case of viscous miscible liquids the eigenvalues are obtained through the solution of the sixth order boundary value problem given by

$$\psi^{iv} - (2k^2 - iRe(u_x k - \omega))\psi'' + \tag{42}$$
$$k^2(k^2 - iRe(u_x k - \omega) + iRekU_x'')\psi = \frac{ikGrRe}{D_0}\mu,$$
$$\mu'' - \left(k^2 + U_x k - \frac{iPe\omega}{D_0}\right)\mu = ikPeC_0'\psi. \tag{43}$$

The exact solutions at $y \sim \infty$ are as follows

$$(\psi_0, \psi_1, \psi_2, \psi_3, \mu_0, \mu_1)^T = (1, \pm k, k^2, \pm k^3, 0, 0)^T \exp(-kL), \tag{44}$$
$$(\psi_0, \psi_1, \psi_2, \psi_3, \mu_0, \mu_1)^T = (1, \pm q_1, q_1^2 \pm q_1^3, 0, 0)^T \exp(-q_1 L), \tag{45}$$
$$(\psi_0, \psi_1, \psi_2, \psi_3, \mu_0, \mu_1)^T = \beta, \pm\beta q_2, \beta q_2^2, \pm q_2^3, 1, \pm q_2)^T \exp(-p_{1,2} L), \tag{46}$$

where $q_1 = \sqrt{k^2 + (U_0 k - iRe\omega)}$ and

$$q_2 = \sqrt{k^2 + iPe\frac{(U_0 k - \omega)}{D_0}}, \quad \beta = -\frac{ikGrRe}{Pe(U_0 k - \omega)^2(Re - \frac{Pe}{Re})}.$$

The system of first order differential equations used for linear analysis for the current case is given by

$$\begin{pmatrix} \psi_0' \\ \psi_1' \\ \psi_2' \\ \psi_3' \\ \mu_0' \\ \mu_1' \end{pmatrix} = \begin{pmatrix} 0 & 1 & 0 & 0 & 0 & 0 \\ 0 & 0 & 1 & 0 & 0 & 0 \\ 0 & 0 & 0 & 1 & 0 & 0 \\ A_{41} & 0 & A_{43} & 0 & \frac{ikReGr}{D_0} & 0 \\ 0 & 0 & 0 & 0 & 0 & 1 \\ ikPeC_0' & 0 & 0 & 0 & \frac{k^2 + iPe(U_x k - \omega)}{D_0} & 0 \end{pmatrix} \begin{pmatrix} \psi_0 \\ \psi_1 \\ \psi_2 \\ \psi_3 \\ \mu_0 \\ \mu_1 \end{pmatrix}, \tag{47}$$

where $A_{41} = -k^2(k^2 - iRe(u_x k - \omega) - iRekU_x'')$ and $A_{43} = 2k^2 - iRe(U_x k - \omega)$.

References

[1] M. Abid, J. Liu, and P. D. Ronney. Surface tension and fingering of miscible interfaces. *Physical Review Letters*, 2000. 13

[2] S. Alabduljalil and R. H. Rangel. Inviscid instability of an unbounded shear layer: effect of surface tension, density and velocity profile. *J. of Engineering Math.*, **54**:99–118, 2006. 15

[3] A. Alexakis. Stratified shear flow instabilities at large Richardson numbers. *Phys. Fluids*, **21**:054108, 2009. 15

[4] L. Allen and T. J. Bridge. Numerical exterior algebra and the compound matrix method. *Numerische Mathematik*, **92**:197–232, 2003. 37

[5] C. V. Sternling andL. E. Scriven. Interfacial turbulence: Hydrodynamic instability and the Marangoni effect. *AIChE Journal*, **5**:514–523, 1959. 11

[6] R. F. S. Andrade. Garlekin method and the solution of the Orr-Sommerfeld equation. *Revista Brasileira de Fisica*, **13**:168–182, 1983. 37

[7] L. K. Antanovskii. A phase field model of capillarity. *Phys. Fluids*, **7**:747, 1995. 18, 19

[8] D. Antrim, P. Bunton, L. L. Lewis, B. D. Zoltowski, and J. A. Pojman. Measring the mutual diffusion coefficient for dodecyl acrylate in low molecular weight poly(dodecyl acrylate) with laser line deflection (Wiener's method) and the fluorescence of pyrene. *J Phys Chem B*, **109**:11842–11849, 2005. 10

[9] T. Babadagli. Development of mature oil fields: A review. *Journal of Petroleum Science and Engineering*, **57**:221–246, 2007. 1

[10] P. G. Baines and H. Mitsudera. On the mechanism of shear flow instabilities. *Journal of Fluid Mech.*, **276**:327–342, 1994. 15

[11] D. Barkley, H. M. Blackburn, and S. J. Sherwin. Direct optimal growth analysis for timesteppers. *int. J. Numer. Meth. Fluids*, **57**:1588–1594, 2008. 26

[12] R. Barros and W. Choi. Holmboe instability in non-Boussinesq fluids. *Physics of Fluids*, **23**:124–103, 2011. 15

[13] H. J. Bart. *Reactive Extraction: Heat and Mass Transfer. Seris Editors: D. Mewes and F. Mayinger*. Springer-Verlag, 2001. 9

[14] G. Batchelor. An introduction to fluid dynamics. *Cambridge University Press*, 1967. 12

[15] R. Bellman and R. Pennington. Effects of surface tension and viscosity on Taylor instability. *Quart. Appl. Math.*, **12**, 1954. 12, 55

[16] E. S. Benilov, V. Naulin, and J. J. Rasmussen. Does a shear flow stabilize inversely stratified fluid? *Physics of Plasmas*, **2**:042106, 2005. 14

[17] R. Betchov and A. Szewczyk. Stability of shear layer between parallel streams. *Phy. Fluids*, **6**, 1963. 14, 37, 45

[18] A. Blinowski. Gradient description of capillary phenomena in multicomponent fluids. *Arch. Mech*, **27**:273–9, 1975. 18, 19

[19] P.A.M. Boomkampa, B.J. Boersmac, R.H.M. Miesena, and G.V. Beijnona. A Chebyshev collocation method for solving two-phase flow stability problems. *Journal of Computational Physics*, **132**:191–200, 1997. 37

[20] J.U. Brackbill, D.B. Kothe, and C. Zemach. A continuum method for modeling surface tension. *Journal of Computational Physics*, **100**:335–354, 1992. 17

[21] J. W. Cahn and J. E. Hilliard. Free energy of a nonuniform system. iii. nucleation in a two-component incompressible fluid. *J. Chem. Phys.*, **31**:688, 1959. 6, 17, 20, 27

[22] C. Canuto, M. Y. Hussaini, A. Quanteroni, and T. A. Zang. *Spectral methods in fluid dynamics*. Spring-Verlag Berlin, 1988. vii, 41

[23] J. R. Carpenter, N. J. Balmfoth, and G. A. Lawrence. Identifying unstable modes in stratified shear layers. *Physics of Fluids*, **22**:054104, 2010. 15

[24] J. R. Carpenter, E. W. Tedford, E. Heifetz, and G. A. Lawrence. Instability in stratified shear flow: Review of a physical interpretation based on interacting waves. *ASME, Applied Mechanics Reviews*, **64**:061001–1–17, 2012. 14, 30

[25] A. Celani, A. Mazzino, Paolo Muratore-Ginannneschi, and L. Vozella. Phase-field model for the Rayleigh-Taylor instability of immiscible liquids. *J. Fluid Mech.*, **622**:115–134, 2009. 12

[26] S. Chandrasekhar. *Hydrodynamics and Hydromagnetic Stability*. Cambridge press, 1961. 12, 14, 30, 55, 58, 78

[27] B. Chu and F. Schoenes. Diffusion coefficient of the isobutyric acid-water system in the critical region. *Physical Review Letters*, **21**:6, 1968. 9

[28] B. Chu, F. J. Schoenes, and W. P. Kao. Spatial and time dependent concentration fluctuations of isobutyric acid-water system in the neighborhood of its mixing point. *Journal of the American Chemical Society*, **90**:3042, 1968. 9

[29] D. S. Conte. The numerical solution of linear boundary value probleme. *SIAM Review*, **8**, 1966. 37, 42

[30] J. Dambrine, B. Geraud, and J. B Salmon. Interdiffusion of liquids of different viscosities in a microchannel. *New Journal of Physics*, **11**:075015, 2009. 10

[31] A. R. Davies, A. Karageorghis, and T.N. Phillips. Spectral Galerkin methods for the primary two-point boundary value problem in modelling viscoelastic flows. *J. Numer. Meth. Engng.*, **25**:273–193, 1988. 44

[32] G. D'Errico, O. Ortona, F. Capuano, and V. Vitagliano. Diffusion corfficients for binary system gylycerol+water at 25^oc. a velocity correlation study. *Journal of Chemical Engineering data*, **49**:1968–70, 2004. 9

[33] F. Dias and C. Kharif. Nonlinear gravity and capillary-gravity waves. *Annu. Rev. Fluid Mech.*, **31**:301–346, 1999. 12

[34] H. Dinga, Peter D.M. Spelta, and C. Shub. Diffuse interface model for incompressible two-phase flows with large density ratios. *J. Comput. Phys.*, **226**:2078, 2007. 12

[35] D.Jamet, D. Torres, and J.U. Brackbill. On the theory and computation of surface tension: the elimination of parasitic currents through energy conservation in the second-gradient method. *Journal of Computational Physics*, **182**:262–276, 2002. 17

[36] A. Dokoumetzidis and P. Macheras. A century of dissolution research: From noyes and whitney to the biopharmaceutics classification system. *International Journal of Pharmaceutics*, **321**:1–11, 2006. 1

[37] E. C. Donaldson, G. V. Chilingrian, and T. F. Yen. *Enhanced Oil Recovery*. New York: Elsevier, 1985. 1

[38] P. G. Drazin. The stability of a shear layer in unbounded hetergeneous inviscid fluid. *Journal of Fluid Mech.*, **4**:214–224, 1958. 15

[39] P. G. Drazin. *Introduction to hydrodynamic stability*. Cambridge University Press, 2002. 14, 15, 30, 36, 117

[40] R. E. Duff, F.H. Harlow, and C.H. Hirt. Effect of diffusion on the interface instability between gases. *Phys. Fluids*, **5**, 1962. 38

[41] H. W. Emmons, C.T. Chang, and B.C. Watson. Taylor instability of finite surface waves. *J.Fluid Mech.*, **7**, 1960. 12

[42] J.W. Evans. Nerve axon equations. iii. stability of the nerve impulse. *Indiana Univ. Math. J.*, **22**:577–594, 1972. 49

[43] J.W. Evans. Nerve axon equations. iv. The stable and unstable impulse. *Indiana Univ. Math. J.*, **24**:1169–1190, 1975. 49

[44] D. Enright R. P. Fedkiw and J. H. Ferziger. A hybrid particle level set method for improved interface capturing. *Journal of Computational Physics*, **183**:83–116, 2002. 17

[45] S. Ferreira-Dias, D. G. Valente, and J. M.F. Abreu. Comparison between ethanol and hexane for oil extraction from quercus suber l. fruits. *Journal of Grasas y Aceites*, **54**:378–383, 2003. 1

[46] A. Fick. On liquid diffusion. *Phil. Mag.*, **10**:30–39, 1855. 9

[47] R. Fjortoft. Application of integral theorems in deriving criteria for instability for laminar flows and for baroclinic circular vortex. *Geofys. Pulb. Oslo*, **17**:1–52, 1950. 14, 30

[48] H. Freundlich. *Colloid and capillary Chemistry.* Methuen, London., 1926. 7

[49] K. S. Gage. Linear viscous stability theory, for stabily stratified shear flow. *A Review, Boundary-Layer Metheorology*, **5**:3–17, 1973. 30

[50] G. Gandikota, S. Amiroudine, D. Chatain, T. Lyubimova, and D. Beynes. Rayleigh and parametric thermo-vibrational instabilities in supercritical fluids under weightlessness. *Physics of Fluids*, **100**:407–424, 2013. 11

[51] Y. Gaponenko and V. Shevtsova. Effects of vibrations on dynamics of miscible liquids. *Acta Astronautica*, **66**:174–182, 2010. 13, 22

[52] M. Gaster. A note on the relation between temporally-increasing and spatially-increasing disturbances in hydrodynamic stability. *Journal of Fluids Mechanics*, **14**:222–224, 1962. 30

[53] J.W Gibbs. On the equilibrium of heterogeneous substances. *The scientific Papers of J. Willard Gibbs*, 1876. 6, 17

[54] M. Giglio and A Vendramini. Optical measurment of gravitationally induced concentration gradients near a liquid-liquid critical point. *Physical Review Letters*, **35**:168–170, 1975. 9

[55] D. Gottlieb and S. Orszag. Numerical analysis of spectral methods. *SIAM, Philadelphia*, 1977. 37

[56] J. P. Gram. Ueber die entwickelung reeller funtionen in reihen mittelst der methode der kleinsten quadrate. *J. Reine Angew. Math.*, **94**:41–73, 1883. 42

[57] C. E. Grosch and S. A. Orszag. Numerical solution of problems in unbounded regions: Coordinate transformations. *J. Comp. Phys.*, **25**:273–295, 1977. 38

[58] M. E Gurtin, D. Polignone, and J. Vinals. Two-phase binary fluids and immiscible fluids described by an order parameter. *Math. Models Methods Appl. Sci.*, **6**:815, 1996. 18

[59] P. N. Guzdar, P. Satyanarayana, J. D. Huba, and S. L. Oskow. Influence of velocity shear on the Rayleigh-Taylor instability. *Geophysical Research Letters*, **9**:547–550, 1982. 14

[60] S. P. Haigh. *Unstable waves on a sheared density interface.* Phd. in canada, The Faculty of Graduate Studies, Department of Mathematics, The University of British Columbia, 1995. 15

[61] P. Hazel. Numerical studies of the stability of inviscid stratified shear flow. *Journal of Fluid Mech.*, **51**:39–62, 1972. 15

[62] F. B. Hicks, T. C. V. Vechten, and C. Franck. Thermally perturbed barodiffusion in a binary liquid mixture. *Physical Review E*, **55**:4158–4164, 1997. 9

[63] A. Hill and B. Straughan. A legendre spectral element method for eigenvalues in hydrodynamic stability. *J. Comp. and App. Math.*, **193**:363–381, 2006. 37

[64] C. W. Hirt and B. D. Nichols. Volume of fluid (VOF) method for the dynamics of free boundaries. *Journal of Computational Physics*, **39**:201–225, 1979. 17

[65] J. Holmboe. On the behavior of symmetric waves in stratified shear layers. *Geofys. Publ.*, **24**:67–113, 1962. 14

[66] G. Homsy. Viscous fingering in poroud-media. *Annual Review of Flui. Mechanics*, **19**:271–311, 1987. 13

[67] A. M. Hoog and G. N. Ivey. The Kelvin-Helmholtz to Holmboe instability transition in stratified exchange flows. *Journal of Fluid Mechanics*, **477**:339–362, 2003. 15

[68] A. P. Hooper and W. G. C. Boyd. Shear-flow instability at the interface between two viscous fluids. *Journal of Fluid Mechanics*, **128**:507–528, 1983. 26

[69] A. P. Hooper and W. G. C. Boyd. Shear-flow instability due to a wall and a viscosity discontinuity at the interface. *Journal of Fluid Mechanics*, **179**:201–225, 1987. 26

[70] L. Howard. Note on paper of John W. Miles. *J. Fluid Mech.*, **10**:509–512, 1961. 14

[71] L. N. Howard and S. A. Maslowe. Stability of stratified shear layers. *Boundary-Layer Met.*, **4**:511–523, 1973. 15, 119

[72] R. G. Howland, N. C. Wong, and C. M.Knobler. Experimental studies of nucleation near-critical liquid mixture. *The Journal of Chemical Physic*, **73**:522–31, 1980. 7

[73] H. Hu and D. Joseph. Miscible displacement in a Hele-Shaw cell. *Zeitschrift fr Angewandte Mathematik und Physik*, **43**:626–644, 1992. 13, 22

[74] H. Hu and D. D. Joseph. Lubricated pipelining: stability of core annualar flow. *J. Fluid Mech.*, **A 1 (10)**:359. [(v1) 396, (v2) 13,16,50–84], 1989. 26

[75] P. Huerre and P. Monkewitz. Local and global linear instabilties in spatially developing flows. *Annu. Rev. Fluid Mech.*, **22**:473–537, 1990. 25

[76] J. Humpherys, B. Standstede, and K. Zumbrun. Efficient computation of analytic basis in Evanns function analysis of large systems. *Numerische Mathematik*, 2006. 37

[77] A. j. Pearlstein. On the two-dimensionality of the critical disturbances for stratified viscous plane parallel shear flows. *Phys. Fluids*, **28**:751–753, 1985. 32

[78] D. Jacqmin. Calculation of two-phase Navier-Stokes flows using phase-field modeling. *J. Comp. Phys. Mech.*, **155**, 1999. 20

[79] D. Jacqmin. Contact-line dynamics of a diffuse fluid interface. *J. Fluid Mech.*, **402**:57–88, 2000. 12, 18

[80] K. Jamshidi-Ghaleh, M. T. Tavassoly, and N. Mansour. Diffusion coefficient measurments of transport liquid solutions using moire deflectomery. *Journal Physics Dynamics*, **37**:1993–1997, 2004. 9

[81] D. Jasnow and J. Vinals. Coarse-grained description of thermo-capillary flow. *Phys. Fluids*, **8**:660–69, 1996. 18, 19

[82] J. W. Jawitz, M. D. Annable, and P. S. C. Rao. Miscible fluid displacement stability in unconfined porous media: Two-dimensional flow

experiments and simulations . *Journal of Hazardous Materials*, **124**:224–9, 2005. 1

[83] D. D. Joseph. *Global stability of fluid motions*. 1971. 25

[84] D. D. Joseph and Y. Y. Renardy. *Fundemental of fluid dynamics. Part II: Lubricated transport, dropsand miscible liquids*. Birlin: Spriger -Verlag, 1993. 11

[85] D.D. Joseph. Fluid dynamics of two miscible liquids with diffusion and gradient stresses. *Europ. Journal of Mech. Fluids.*, 1990. 2, 18, 19

[86] D.D. Joseph. Non-solenoidal velocity effects and Korteweg stresses in simple mixtures of incompressible liquids. *Physica*, **97**:104–25, 1996. 19

[87] U. Kaatze and S. Z. Mirzaev. Slowing down in chemical reactions. *Journal of Physical Chemistry A*, **104**:5430–9, 2000. 9

[88] D. Koppel. On the stability of flow of thermally stratified fluid under the action of gravity. *Journal of Mathematical Physics*, **5**:963–982, 1964. 15, 32, 33

[89] D. J. Korteweg. Sur la forme que prennent les equations du mouvements des fluides si l'on tient compte des forces capillaires causees par des variations de densite considerables mais continues et sur la theorie de la capillarite dans l'hypothese d'une variation continue de la densite. *Arch. Neerl. Sci. Exactes Nat.*, **Ser. II, 6, 1 – 24**, 1901. 6, 9

[90] P. Kurowski, C. Misbah, and S. Tchourkine. Gravitational instability of a fictitious front during mixing of miscible fluids. *Europhys Lett.*, **29 (4)**:3099–3140, 1995. 13

[91] L. Lacaze, P. Guenoum, D. Beysens, M. Delsanti, P. Petitjeans, and P. Kurowski. Transient surface tension in miscible liquids. *Physical Review E*, **82**:041606, 2010. 7

[92] H. Lamb. *Hydrodynamics*. 6th edidtion, New york, 1945. 30

[93] L.D. Landau and E.M. Lifshitz. *Fluid mechanics*, **6. 2nd ed.** Addison-Wesley, 1987. 12, 55

[94] R. E. Langer. The stability of laminar flow of a viscous fluid. *Bull. Amer. Soc.*, **46**:257–263, 1944. 30

[95] G. A. Lawrence, S. P. Haigh, and Z. Zhu. In search of Holmboe instability. *Coastal and Estuarine Studies*, **54**:295–304, 1998. 15

[96] D.J. Lewis. The instability of liquid surfaces when accelerated in a direction perpendiculare to their planes. *Proc. Roy. Soc. A*, **202**, 1950. 12

[97] C. C. Lin. *The theory of hydrodynamic stability.* Cambridge Univeristy Press, 1955. 30

[98] W. W. Liou and P. J. Morris. A comparison of numerical methods for the Rayleigh equation in unbounded domains. *NASA Technical Memorandum*, pages 1–38, 1991. 37, 38, 45, 52

[99] J. Lowengrub and L. Truskinovsky. Quasi-incompressible Cahn-Hilliard fluids and topological transitions. *Proc. R. Soc. Lond.*, **A**:454, 1998. 2, 18, 19, 20, 21

[100] L. M. Mack. A numerical study of the temporal eigenvalue spectrum of the Blasius boundary layer. *J. Fluid Mech.*, **73**:497–520, 1976. 37

[101] S. A. Maslowe. Hydrodynamic instabilities and the transition to turbulence. *Topics in Applied Physics, SpringerLink*, **45**:181–228, 1985. 30

[102] S. A. Maslowe and R. E. Kelly. Inviscid instability of an unbounded heterogeneous shear layer. *Journal of Fluid Mech.*, **48**:405–415, 1971. 15

[103] J. C. Maxwell. Capillary action. *In Encyclopaedia Britannica,* 9^{th} *ed. Reprinted in 1952*, 1876. 16

[104] J. C. Maxwell. *The Scientific Papers of James Clerk Maxwell. W. D. Niven Editor.* New York, Dover, 1952. 9

[105] S. E. May and J. V. Maher. Capillary-wave relaxation for a meniscus between miscible liquids. *Physics Review Letters*, 1991. 7, 8, 9

[106] A. Michalke. On the spatially growing disturbances in an inviscid shear layer. *J. Fluid Mech.*, **23**:521–544, 1965. 37

[107] M. A. Monkewitz. Analytic pseudo-orthogonalization methods for linear two-point boundary value problems illustrated by the Orr-Sommerfeld equation. *Journal of Applied Mathematics and Physics*, **29**, 1978. 42

[108] M. Mukhopadhyay. *Natural extracts using supercritical carbon dioxide*. CRC Press LLC, 2000. 1

[109] B.T. Nadiga and S. Zalski. Investigations of a two-phase fluid model. *Eur. J. Mech. B Fluids*, **15**:885–96, 1996. 19

[110] B.S Ng. A numerical method for linear two-point boundary-value problems using compound matrices. *Journal of Computational Physics*, **33**:70–85, 1979. 48

[111] B.S. Ng and W. H. Reid. The compound matrix method for ordinary differential systems. *J. Comp. Phys.*, **45**:209–229, 1985. 37

[112] B. J. Olson, J. Larsson, S. K. Lee, and A. W. Cook. Nonlinear effect in the combined Rayleigh-Taylor/Kelvin-Helmholtz instability. *Physics of Plasmas*, **23**:114107, 2011. 14

[113] S. A. Orszag. Accurate solution of the Orr-Sommerfeld stability equation. *J. Fluid Mech.*, **50**:689–703, 1971. 38, 44

[114] S. Osher and J. A. Sethian. Fronts propagating with curvature dependent speed: Algorithms based on Hamilton-Jacobi formulations. *Journal of Computational Physics*, **79**:12–49, 1988. 17

[115] A. Oztekin, L.J. Cumbo, and A. Liakopoulos. Temporal stability of boundary-free shear flows: the effects of diffusion. *Theoret. Compt. Fluid Dynamics*, **13**:77–90, 1999. 44

[116] M. Payr, S. H. Vanaparthy, and E. Meiburg. Influence of variable viscosity on Betchov density-driven instabilities in capillary tubes. *J. Fluid Mech.*, **525**:333–353, 2005. 22

[117] C. Pellacani. Shear instabilities in stratified fluids; linear theory. *LA Rivista Del Nuovo Cimento*, **6**:1–26, 1983. 30

[118] M. Perlin and W. W. Schultz. Capillary effects on surface waves. *Snnu. Rev. Fluid Mech.*, **32**:241–274, 2000. 12

[119] P. Petitjeans and T. Maxworthy. Miscible displacements in capillary tubes. i. experiments. *Journal Fluids Mechanics*, **326**:37–65, 1996. 8, 9, 10

[120] S.D. Poisson. Nouvelle theorie de l' action capillaire. *Paris: Bachelier*, 1831. 6, 16

[121] J. A. Pojman, C. Whitmore, M. L. T. liveri R. Lombardo, J. Marszalek, and R. Parker. Evidence for the existence of an effective interfacial between miscible fluids: Isobutyric acid-water and 1-butanol-water in a spinning-drop tensiometer. *Langmuir*, **22**:2569–2577, 2006. 8, 11

[122] M. Prodanovic and S. L. Bryant. A level set method for determining critical curvatures for drainage and imbibition. *Journal of Colloid and Interface Science*, **304**:442–458, 2006. 17

[123] G. Quincke. Die oberfachenspannung and der grenze von alkohol mit wasserigen salzlosungen. *Ann. Phys*, **9**:338, 1902. 7

[124] M. Ratafia. Experimental investigation of Rayleigh-Taylor instability. *Phys. Fluids*, 1973. 12

[125] L. Rayleigh. On the stability of certain fluid motions. *Pro. Math. Soc. Lond.*, **11**:57–70, 1880. 14, 29

[126] L. Rayleigh. Investigation of the character of the equilibrium of an incompressible heavy fluid of varaible density. *Scientific Papers, II Cambridge press*, 1900. 11, 16

[127] E. Reverchon and I. D. Marco. Supercritical fluid extraction and fraction of natural matter. *Journal of Supercritical Fluids*, **38**:146–66, 2006. 1

[128] A. Riaz and E. Meiburg. Radial source flows in pourous media: Linear instability analysis of axial and hilecal perturbations in miscible displacements. *Physisc of Fluids*, **15**:938–946, 2003. 13

[129] R. L. Rowley and F. H. Horne. Critical exponent of the heat transport of water-isobutyric acid mixtures. *The Journal of Chemical Physic*, **71**:3841, 1979. 7

[130] S. P. Haigha and G. A. Lawrence. Symmetric and nonsymmetric Holmboe instabilities in an inviscid flow. *Phys. Fluids*, **11**:1459–1468, 1999. 15

[131] J. P. Schmid and D. S. Henningson. *Stability and transition in shear flows*. Springer, 2001. 26, 30, 36

[132] E. Schmidt. Zur theorie der linearen und nichtlinearen integralgleichungen i. teil: Entwicklung willkurlicher funktionen nach systemen vorgeschriebener. *Math. Ann.*, **63**:433–476, 1907. 42

[133] A. Silva, C. Delerue-Matos, and A. Fiuza. Use of solvent extraction to remediate soils contaminated with hydrocarbons. *Journal of Contaminant Hydology*, **31**:211–300, 1998. 1

[134] P. G. Smith, M. V. D. Ven, and S. Mason. The transient interfacial tension between two miscible fluids. *J Colloid Interface Sci*, **80**:302, 1981. 7

[135] W. D. Smyth and W. R. Peltier. The transition between Kelvin-Helmholz and Holmboe instability: An investigation of the overreflection hypothesis. *J. Atmos. Sci.*, **46**:3698–3720, 1989. 32

[136] W. D. Smyth and W. R. Peltier. Instability and transition in finite amplitude Kelvin-Helmholtz and Holmboe waves. *J. Fluid Mech.*, **228**:387–415, 1991. 15

[137] L. Sobrino. Note on capillary waves in the gradients theory of interfaces. *Can. J. Phys.*, **63**:1132–33, 1985. 19

[138] H. B. Squire. On the stability of three-dimensional of a stratified dsiturbances viscous flow between parallel walls. *Proceedings of the Royal Society A*, **142**:621–628, 1933. 32

[139] G. L. Standart, R. Taylor, and R. Krishna. The Maxwell-Stefan formulation of irreversible thermodynamics for simultaneous heat and mass transfer. *Chem. Eng. Commun.*, **3**:277–289, 1979. 9

[140] V.N. Starovoitov. Model of the motion of two-component liquid with allowance of capillary forces. *Journal Application of Mechanics Technology Physics*, **35**:891–897, 1994. 18

[141] M. S. P. Stevar and A Vorobev. Shapes and dynamics of miscible liquid/liquid interfaces in horizontal capillary tubes. *Journal of Colloid and Interface Science*, **383**:184–197, 2012. 2, 8, 10, 119

[142] M. S. P. Stevar and A Vorobev. Dissolution dynamics of liquid/liquid binary mixtures within a micromodel. *Transport in Porous Media*, **25**:064103, 2013. 2

[143] J. T. Stuart. Nonlinear stability theory. *Annual Review of Fluid Mechanics*, **2**, 1971. 26, 30

[144] G.I. Taylor. The stability of liquids surfaces when accelerated in a direction perpendicular to their planes. *Proc. Roy. Soc. A*, **201**, 1950. 11, 16

[145] V. Theofilis. Global linear instabilty analysis. *Annu. Rev. Fluid Mech.*, **43**:319–352, 2001. 25

[146] S. A. Thorp. A method of producing a shear flow in a stratified fluid. *Journal of Fluid Mechanics*, **32**:693–704, 1968. 15

[147] S. A. Thorp. Experiments on the stability of stratified shear flows. *Radio Science*, **4**:1327–1331, 1969. 15

[148] F. Torbi, A. Q. Firouz, and A. Kavousi. Comparative evaluation of immiscible near miscible and miscible co_2 huff-n-puff to enhence oil recovery from single matrix-fracrure system (experiemntal and simulation studies). *Fuel*, **93**:443–53, 2012. 1

[149] A. Tumin. The spatial stability of natural convection flow on inclined plates. *ASME J. Fluid Eng.*, **125(3)**:428–437, 2003. 37

[150] A. Vailati and M. Giglio. Nonequilibrium fluctuations in time-dependent diffusion processes. *Physical Review E*, **58**:4361–4371, 1998. 9

[151] J. D. van der Waals. The thermodynamics theory of capillary flow under hypothesis of a continuous variation of density. *(Verhandel/Konic. Akad. Weten, 193), English translation, J. Statist, Phys.*, **20**:97, 1893. 6, 9, 16, 17, 27

[152] S. H. Vanaparthy and E. Meiburg. Variable density and viscosity, miscible displacements in capillary tubes. *European Journal of Mechanics B-Fluids*, **27**:268–289, 2008. 13

[153] S. H. Vanaparthy and E. Meiburg D. Wilhelm. Density-driven instabilities of miscible liquids in a capillary tube: Linear stability analysis. *J. Fluid Mech*, **497**:99–121, 2003. 13

[154] G. Viner and J. A. Pojman. Studying diffusion of partially miscible and systems near their consolute point by laser line deflection. *Optics and Laser in Engineering*, **46**:893–899, 2008. 10

[155] R. G. Voiget, D. Gottlieb, and M. Y. Hussaini. *Spectral Methods for Partial Differential Equations*. JSIAM, 1984. 37, 38

[156] A. Vorobev. Boussinseq approximation of the Cahn-Halilliard-Navier-Stokes equation. *APS*, **123**:1–6, 2010. 19, 21, 23

[157] L. F. Wang, W. H. Ye, and Y. J. Li. Combined effect of the density and velocity gradients in the combination of Kelvin-Helmholtz and Rayleigh-Taylor instabilities. *Physics Of Plasmas*, **17**:042103, 2010. 14

[158] X. When and E. Fried. Rayleigh-Taylor problem for liquid-liquid phase interface. *Journal of Fluid Mechanics*, **560**:395–314, 2006. 33

[159] N.C. Wong and C. M. Knobler. Light-scattering studies of phase speration in isobutyric acid+water mixtures: Hydrodynamic effect. *Physical Review A*, **24**:3205–3211, 1981. 9

[160] J. C. S. Wu and E. H. Lee. Ultrafiltration of soybean oil/hexane extract by ceramic membranes. *Journal of Membrane Science*, **65**:251–9, 1999. 1

[161] W. H. Ye, L. F. Wang, C. Xue, Z. F. Fan, and X. T. He. Competitions between Rayleigh-Taylor instability and Kelvin-Helmholtz instability with continuous density and velocity profiles. *Physics of Plasmas*, **18**:022704, 2011. 14

[162] S. G. Yiantsios and B. G. Higgins. Linear instability of plane poiseuille flow of two supperposed fluids. *Phys. Fluids*, **13**:3225–3238, 1970. 32

[163] C. S. Yih. Stability of two-dimensional parallel flows for three-dimensional disturbances. *Q. Appl. Math*, **12**:434–435, 1995. 32

[164] W. Zhang, Z. Wu, and D. Li. Effect of shear flow and magnetic field on the Rayleigh-Taylor instability. *Physics of Plasmas*, **2**:042106, 2005. 14, 117

[165] B. Zoltowski, Y. Chekanov, J. Maser, J. A. Pojman, and V. Volpert. Evidence for the existence of an effective interfacial between miscible fluids:2. dodecyl acrylate-poly(dodecyl acrylate-poly) in a spinning-drop tensiometer. *Langmuir*, **23**:5522–5531, 2007. 8

Publications

- Linear stability analysis of a horizontal phase boundary separating two miscible liquids, PHYSICAL REVIEW E 88, 022404(2013)
- Linear stability of a horizontal phase boundary subjected to shear motion (Submitted to Physics of Fluids Journal)

The results also were presented in the following conferences:

- Sep 2012 UK Turbulence Consortium
- Sep 2011 UK Turbulence Consortium
- Nov 2012 1st year Postgraduate Engineering conference, University of Southampton